3rd Generation Partnership Project;
Technical Specification Group Radio Access Network;
NR;
Study on test methods;
(Release 16)

3GPP TR 38.810 V16.2.0 (2019-03)

Technical Report

Contents

Foreword

This Technical Report has been produced by the 3rd Generation Partnership Project (3GPP).

The contents of the present document are subject to continuing work within the TSG and may change following formal TSG approval. Should the TSG modify the contents of the present document, it will be re-released by the TSG with an identifying change of release date and an increase in version number as follows:

Version x.y.z

where:

- x the first digit:
  - 1 presented to TSG for information;
  - 2 presented to TSG for approval;
  - 3 or greater indicates TSG approved document under change control.
- y the second digit is incremented for all changes of substance, i.e. technical enhancements, corrections, updates, etc.
- z the third digit is incremented when editorial only changes have been incorporated in the document.

1 Scope

The objective of this study is to define the over the air (OTA) testing methodology for UE RF, UE RRM, and UE demodulation requirements for New Radio, the associated measurement uncertainty budget(s), and the related test tolerances.

The testing methodology development targets frequencies above 6 GHz, and the work is prioritized according to the frequency ranges that are included in the NR work item.

For mmWave NR UEs, RF requirements are specified as OTA requirements, using the applicable metrics. The definitions of these requirements are expected to align the spatial coverage of the requirement with the UE's working condition acceptable in expected directions. NR is expected to be used in more than one type of UEs, and different spatial coverage requirements may apply to different UE types.

2 References

The following documents contain provisions which, through reference in this text, constitute provisions of the present document.

- References are either specific (identified by date of publication, edition number, version number, etc.) or non-specific.
- For a specific reference, subsequent revisions do not apply.
- For a non-specific reference, the latest version applies. In the case of a reference to a 3GPP document (including a GSM document), a non-specific reference implicitly refers to the latest version of that document *in the same Release as the present document*.

[1] 3GPP TR 21.905: "Vocabulary for 3GPP Specifications".

[2] 3GPP TS 36.101: “Evolved Universal Terrestrial Radio Access (E-UTRA); User Equipment (UE) radio transmission and reception”.

[3] 3GPP TS 36.133: “Evolved Universal Terrestrial Radio Access (E-UTRA); Requirements for support of radio resource management”.

[4] 3GPP TS 37.144: “User Equipment (UE) and Mobile Station (MS) GSM, UTRA and E-UTRA over the air performance requirements”.

[5] 3GPP TR 37.977: "Universal Terrestrial Radio Access (UTRA) and Evolved Universal Terrestrial Radio Access (E-UTRA); Verification of radiated multi-antenna reception performance of User Equipment (UE)".

[6] 3GPP TR 37.902: "Measurements of User Equipment (UE) radio performances for LTE/UMTS terminals; Total Radiated Power (TRP) and Total Radiated Sensitivity (TRS) test methodology".

[7] 3GPP TR 38.900: “Study on channel model for frequency spectrum above 6 GHz”.

[8] 3GPP TR 38.803: “Study on New Radio Access Technology; RF and co-existence aspects”.

[9] 3GPP TR 37.842: “Radio Frequency (RF) requirement background for Active Antenna System (AAS) Base Station (BS)”

[10] 3GPP TR 38.901: “Study on channel model for frequencies from 0.5 to 100 GHz”.

[11] ETSI TR 102 273-1-1 V1.2.1 (2001-12): “Electromagnetic compatibility and Radio spectrum Matters (ERM); Improvement on Radiated Methods of Measurement (using test site) and evaluation of the corresponding measurement uncertainties; Part 1: Uncertainties in the measurement of mobile radio equipment characteristics; Sub-part 1: Introduction”.

[12] 3GPP TR 25.914: “Measurement of Radio Performances for UMTS terminals in speech mode”.

[13] 3GPP TS 34.114: “User Equipment (UE) / Mobile Station (MS) Over The Air (OTA) antenna performance; Conformance testing”.

[14] 3GPP TS 38.215: “Physical layer measurements”.

[15] CTIA OTA Test Plan version 3.7, https://www.ctia.org/

[16] 3GPP TS 38.101-2: “UE radio transmission and reception; Part 2: Range 2 Standalone”

[17] 3GPP TS 38.133: “Requirements for support of radio resource management”

[18] 3GPP TS 38.101-4: “5G; NR; User Equipment (UE) radio transmission and reception; Part 4: Performance requirements”.

[19] 3GPP TS 38.306: “NR; User Equipment (UE) radio access capabilities”.

3 Definitions, symbols and abbreviations

3.1 Definitions

For the purposes of the present document, the terms and definitions given in 3GPP TR 21.905 [1].

3.2 Symbols

For the purposes of the present document, the following symbols apply:

D DUT radiating aperture
N_{MAX_AoAs} The maximum number of simultaneously active (emulating signal) angles of arrival

3.3 Abbreviations

For the purposes of the present document, the abbreviations given in 3GPP TR 21.905 [1] and the following apply. An abbreviation defined in the present document takes precedence over the definition of the same abbreviation, if any, in 3GPP TR 21.905 [1].

AAA Active Antenna System
AoA Angle of Arrival
BW Bandwidth
CA Carrier Aggregation
CATR Compact Antenna Test Range
CDL Clustered Delay Line
CSI Channel State Information
DFF Direct Far Field
DNF Direct Near Field
DUT Device Under Test
EIS Effective Isotropic Sensitivity
EIRP Effective (or equivalent) isotropic radiated power
EPRE Energy per resource element
EVM Error Vector Magnitude
FF Far Field
FR1 Frequency Range 1
FR2 Frequency Range 2
FS Free Space
FWA Fixed Wireless Access
IBB In-band blocking
IF Intermediate Frequency
IFF Indirect Far Field
LNA Low Noise Amplifier

MU	Measurement Uncertainty
NFTF	Near Field To Far-field
NR	New Radio
NSA	Non-standalone
OTA	Over The Air
PA	Power Amplifier
RSRP	Reference signal receive power
SNR	Signal-to-Noise Ratio
SS	System Simulator
SS-RSRPB	SS reference signal received power per branch
TDL	Tapped Delay Line
TI	Test Interface
TRP	Total Radiated Power
TRxP	Transmission Reception Point
UBF	UE beam lock function
UE	User Equipment

4 General

4.1 Device types and UE power classes

In accordance to the study item objectives the following device types are considered in the scope of this study:

- Smartphone
- Laptop mounted equipment (such as plug-in devices like USB dongles)
- Laptop embedded equipment
- Tablet
- Wearable devices
- Vehicular mounted device
- Fixed Wireless Access (FWA) terminal
- Fixed mounted devices (e.g. sensors, automation etc.)
- Other UE types are not precluded for discussion as a second priority
- The development of test methodology aspects shall initially focus on the FWA, tablet, and smart phone device types

Four different FR2 UE Power Classes are defined in the Rel-15 scope in TS 38.101-2 [16]. Different UE power classes are characterized by different UE antenna design assumptions and have different UE maximum output power and reference sensitivity requirements.

The test methods defined in this document are introduced for handheld UEs and applicable to FR2 UE Power Class 3 unless otherwise stated. The test methods can be applicable for other device types such as FWA, tablets, vehicle mounted UE etc. in case they comply with UE power class 3 requirements.

The test methods can be further extended to other FR2 UE power classes (i.e. UE power classes 1, 2 and 4). At least the following test methods components are specific to different FR2 UE power classes and shall be adjusted:

- Measurement grids used for the UE RF Tx and Rx measurements.
- Noise power level (Noc) and feasible SNR range for UE demodulation and RRM test methodologies.

4.2 Testing configuration

The free space (FS) testing configuration is utilized in this study.

4.3 Test interface

A Test Interface (TI) is needed for certain control and measurement functions. Detailed functions and implementation of the TI are as follows:

- All UEs supporting NR and operating in frequency range 2 (FR2) shall support the following:
  - A mandatory UE beam lock function (UBF) to simplify the test method complexity, such that
  - The UBF can disable changes to the UE beamforming configuration when in NR_RRC_CONNECTED state
  - The measurement and reporting of synchronization signals reference signal received power per branch (SS-RSRPB) [14], such that
    - These reporting requirements apply to all FR2 UEs in the context of a test loop
    - The signalling associated with reporting SS-RSRPB is in a format which allows the UE to report a vector of values, where the number of the reported values equals to the number of receiver branches on the UE
- Additional TI functionality is not precluded

4.4 Equivalence criteria

The following 11 points have been agreed as a framework for developing OTA test to prove equivalence.

1) Multiple test methods may exist for each requirement.
2) Each test method will require its own test procedure.
3) A single conformance requirement applies for each core requirement, regardless of test procedure.
4) Common maximum accepted test system uncertainty applies for all test methods addressing the same test requirement. Test methods producing significantly worse uncertainty than others at comparable cost should not impact the common maximum accepted test system uncertainty assessment.
5) Common test tolerances apply for all test methods addressing the same test requirement.
6) A common way of establishing the uncertainty result from all test methods' individual budgets is established.
7) A common method of making an uncertainty budget (not a common uncertainty budget) is established.
8) Establish budget format examples for each addressed test method in the form of lists of uncertainty contributions. Contributions that may be negligible with some DUT and substantial with others should be in this list. For each combination of measurement method and test parameter develop a list with measurement uncertainties.
9) Describe potential OTA test methods. The description requires information about the test range architecture and test procedure. Addressing each item in each uncertainty budget with respect to the expected distribution of the errors, the mechanism creating the error and how it interacts with properties of the DUT.
10) Providing example uncertainty budgets in the TR will be useful in order to demonstrate the way a budget should be defined and how calculating its resulting measurement uncertainty is done, but the figures used in the examples will clearly be only examples and not applicable in general.
11) Each test method is required to provide technical documentation showing the equivalence of testing methodologies, justification on applicability statement and usage of same baseline metrics for the alternative methodologies.

    Each testing methodology needs to provide applicability to test the following metrics and outline the testing aspects once the metrics are properly defined:

    - EIRP and TRP based metric
    - EIS based metric

- Transmit signal quality
- Radiated Spurious Emissions
- Blocking (currently only IBB defined)

NOTE: Potential dynamic range limitations, measurement uncertainties and detailed test procedures are to be considered within UE conformance test aspects for 5G System with NR and LTE (Work Item 5GS_NR_LTE-UEConTest).

The linking of core requirements via test methods to conformance requirements is depicted in Figure 4.4-1.

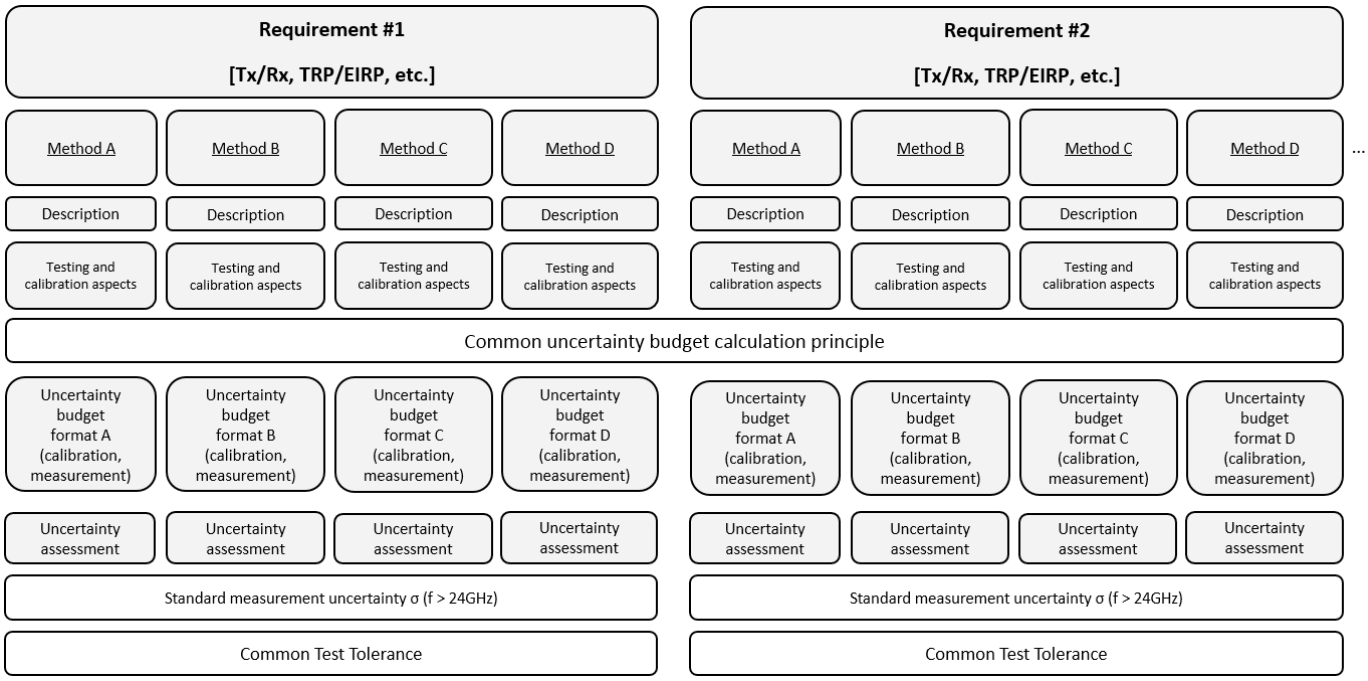

Figure 4.4-1: OTA requirement to test mapping

5 UE RF testing methodology

5.1 General

It is reasonable to expect a high level of integration of high-frequency NR devices (e.g., devices operating above 6 GHz). Such highly integrated architectures may feature innovative front-end solutions, multi-element antenna arrays, passive and active feeding networks, etc. that may not be able to physically expose a front-end cable connector to the test equipment.

For UE RF test methodology at high frequency (f > 6 GHz), the following general aspects apply:

- OTA measurement is the testing methodology for UE RF at high frequency (f > 6 GHz)
- Permitted test methods are defined in subclause 5.2 and shall demonstrate equivalence to the far field environment.

5.2 Permitted test methods

A permitted test method meets the equivalence criteria to the far field environment by having an MU less than or equal to the threshold MU for at least one test case. The applicability of methods is described in subclause 5.3.

5.2.1 Direct far field (DFF)

5.2.1.1 Description

The DFF measurement setup of UE RF characteristics for f > 6 GHz is capable of centre and off centre of beam measurements and is shown in Figure 5.2.1.1-1 below.

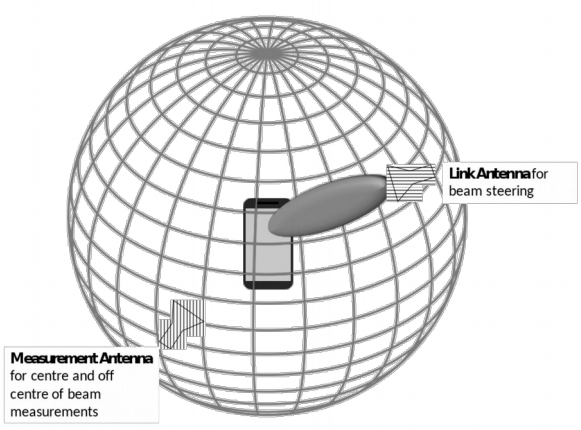

Figure 5.2.1.1-1: DFF measurement setup of UE RF characteristics

The key aspects of the DFF setup are:

- Far-field measurement system in an anechoic chamber
  - The criterion for determining the far-field distance is described in 5.2.1.2
- A positioning system such that the angle between the dual-polarized measurement antenna and the DUT has at least two axes of freedom and maintains a polarization reference.
- A positioning system such that the angle between the link antenna and the DUT has at least two axes of freedom and maintains a polarization reference; this positioning system for the link antenna is in addition to the positioning system for the measurement antenna and provides for an angular relationship independently controllable from the measurement antenna.
- For setups intended for measurements of UE RF characteristics in non-standalone (NSA) mode with 1 UL configuration, an LTE link antenna is used to provide the LTE link to the DUT. The LTE link antenna provides a stable LTE signal without precise path loss or polarization control.
- For setups intended for measurements in NR CA mode with FR1 and FR2 inter-band NR CA, test setup provides NR FR1 link to the DUT. The NR FR1 link has a stable and noise-free signal without precise path loss or polarization control.

The applicability criteria of the DFF setup are:

- The DUT radiating aperture is $D \leq 5$ cm
  - Either a single radiating aperture, multiple non-coherent apertures or multiple coherent apertures DUTs can be tested
  - If multiple antenna panels that are phase coherent are defined as a single array, the criterion on DUT radiating aperture applies to this single array
  - D is based on the MU assessment in Annex B.1.1.3
  - The measurement distance larger than the far-field criteria defined in subclause 5.2.1.2 is not precluded
  - If the uncertainties can be further optimized, the MU may be reduced or D may be increased
- A manufacturer declaration on the following elements is needed:

- Manufacturer declares antenna array size

- EIRP, TRP, EIS, EVM, spurious emissions and blocking metrics can be tested.

5.2.1.2 Far-field criteria

The minimum far-field distance R for a traditional far field anechoic chamber can be calculated based on the following equation: $R > \frac{2D^2}{\lambda}$, where D is the diameter of the smallest sphere that encloses the radiating parts of the DUT. The near/far field boundary for different antenna sizes and frequencies is shown in Table 5.2.1.2-1.

Table 5.2.1.2-1: Near field/far field boundary for different frequencies and antenna sizes for a traditional far field anechoic chamber

D(cm)	Frequency (GHz)	Near/far boundary (cm)	Path Loss (dB)	Frequency (GHz)	Near/far boundary (cm)	Path Loss (dB)
5	28	47	54.8	100	167	76.9
10	28	187	66.8	100	667	88.9
15	28	420	73.9	100	1501	96
20	28	747	78.9	100	2668	101
25	28	1167	82.7	100	4169	105
30	28	1681	85.9	100	6004	108

As can be seen in the table, the distance can be very large for larger antenna sizes and higher frequencies. This could lead to very large chambers that would be prohibitively expensive.

Generally, the exact antenna size of the DUT is unknown since the device will be in its own casing during the test and this also depends on other factors such as ground coupling effects that depend on the design. The largest device size (e.g. diagonal) could be used; however, this would lead to very large chambers even for relatively small devices. A practical way to determine the far field distance is needed.

It has been proposed to determine the testing distance based on a manufacturer declaration. One of the risks of this approach is that a distance shorter than the actual far field is chose. It should be further studied whether this could lead to underperforming devices passing the tests due to measurement inaccuracies (e.g. whether a shorter distance will lead to better measurement results than the actual far field distance).

Additionally, an experimental method was proposed to determine the far field distance based on path loss measurements. This method is based on the fact that the path loss exponent is different in the near field and the far field. By measuring the path loss gradient over a certain distance, the near/far field boundary could be found. The results of an experiment conducted on a Band 3 LTE device are shown in Figure 5.2.1.2-1. The minimum far field distance can be found at the regression intercept point.

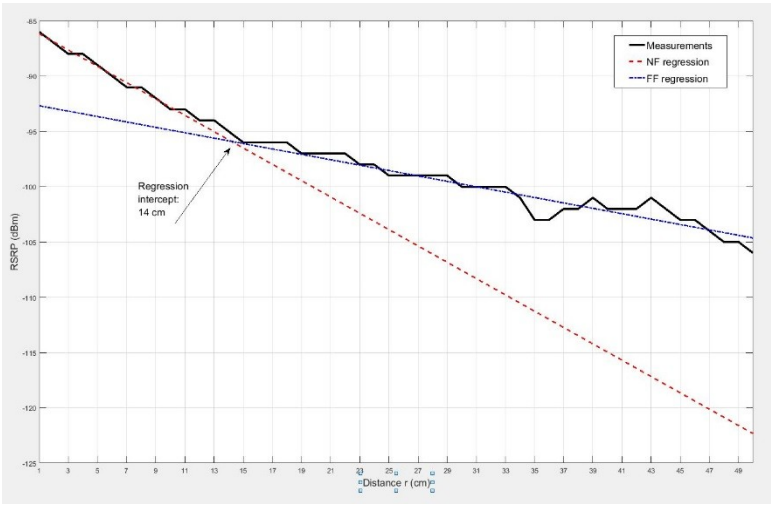

Figure 5.2.1.2-1: LTE UE FDD band 3 measurements to determine the minimum far-field distance

The figure shows an example result for the case where the frequency is 1.85 GHz. The approximate device dimensions were 13 x 8 cm. Under these conditions, the canonical minimum far-field distance would be 28.7 cm. According to this method, the minimum measurement distance would be 13.8 cm. Further work is required to determine whether this technique provides valid results for much higher frequencies and general device types.

Methods to reduce measurement distance for AAS BS are Compact Antenna Test Range, One Dimensional Compact Range, and Near Field Test Range which are all listed in TR 37.842 [9]. These may be used for NR provided they meet the equivalence criteria relative to the baseline measurement setup. Other methods are not precluded.

5.2.1.3 Testing and calibration aspects

5.2.1.3.1 Calibration Measurement Procedure

The calibration measurement is done by using a reference calibration antenna with known gain values. For the calibration measurement, the reference antenna is placed in the centre of the quiet zone. If an antenna with moving phase centre is used, a multi-segmented approach could be chosen where for multiple frequency segments the respective phase centre of the calibration antenna is placed in the centre of quiet zone. The calibration process determines the composite loss, $L_{path,pol}$, of the entire transmission and receiver chain path gains (measurement antenna, amplification) and losses (switches, combiners, cables, path loss, etc.). The calibration measurement is repeated for each measurement path (two orthogonal polarizations and each signal path). Additional details of the calibration procedure are outlined in [13].

5.2.1.3.2 Peak EIRP Measurement Procedure

The TX beam peak direction is where the maximum total component of EIRP is found, including the respective polarization of the measurement antenna used to form the TX beam, according to 5.2.1.3.7.

The measurement procedure includes the following steps:

1) Connect the SS (System Simulator) with the DUT through the measurement antenna with polarization reference Pol_{Link} to form the TX beam towards the TX beam peak direction and respective polarization.

2) Lock the beam toward that direction for the entire duration of the test.

3) Measure the mean power P_{meas} ($Pol_{Meas}=\theta$, Pol_{Link}) of the modulated signal arriving at the power measurement equipment (such as a spectrum analyser, power meter, or gNB emulator).

4) Calculate EIRP($Pol_{Meas}=\theta$, Pol_{Link}) by adding the composite loss of the entire transmission path for utilized signal path, $L_{EIRP,\theta}$, and frequency to the measured power P_{meas} ($Pol_{Meas}=\theta$, Pol_{Link}).

5) Measure the mean power P_{meas} ($Pol_{Meas}=\phi$, Pol_{Link}) of the modulated signal arriving at the power measurement equipment.

6) Calculate EIRP($Pol_{Meas}=\phi$, Pol_{Link}) by adding the composite losses of the entire transmission path for utilized signal path, $L_{EIRP,\varphi}$, and frequency to the measured power P_{meas} ($Pol_{Meas}=\phi$, Pol_{Link})

7) Calculate total EIRP (Pol_{Link}) = EIRP($Pol_{Meas}=\theta$, Pol_{Link}) + EIRP($Pol_{Meas}=\phi$, Pol_{Link})

5.2.1.3.3 TRP Measurement Procedure

The minimum number of measurement points for TRP measurement grid is outlined in Annex G.1.

The measurement procedure includes the following steps:

1) Connect the SS with the DUT through the measurement antenna with desired polarization reference Pol_{Link} to form the TX beam towards the desired TX beam direction and respective polarization.

2) Lock the beam toward that direction and polarization for the entire duration of the test.

3) For each measurement point, measure P_{meas}($Pol_{Meas}=\theta$, Pol_{Link}) and P_{meas}($Pol_{Meas}=\phi$, Pol_{Link}). The angle between the measurement antenna and the DUT (θ_{Meas}, φ_{Meas}) is achieved by rotating the measurement antenna and the DUT (based on system architecture).

4) Calculate EIRP(Pol_{Meas}=θ, Pol_{Link}) and EIRP(Pol_{Meas}=ϕ, Pol_{Link}) by adding the composite loss of the entire transmission path for utilized signal paths, $L_{EIRP,\theta}$, $L_{EIRP,\varphi}$ and frequency to the respective measured powers P_{meas}.

5) The TRP value for the uniform measurement grid is calculated using the TRP integration approaches outlined in Annex G.1.2. The TRP value for the constant density grid is calculated using the TRP integration formula in Annex G.1.3.

5.2.1.3.4 Peak EIS Measurement Procedure

The RX beam peak direction is where the minimum EIS is found according to 5.2.1.3.8.

The measurement procedure includes the following steps:

1) Establish a connection between the DUT and the SS with the downlink signal applied to the Pol_{Link}= θ-polarization of the measurement antenna

2) Position the UE so that the beam is formed towards the measurement antenna in the RX beam peak direction

3) Determine EIS(Pol_{Meas}=θ, Pol_{Link}=θ) for θ-polarization, i.e., the power level for the θ-polarization at which the throughput exceeds the requirements for the specified reference measurement channel

4) Switch the downlink to the Pol_{Link}=φ-polarization of the measurement antenna

5) Determine EIS(Pol_{Meas}=ϕ, Pol_{Link}=ϕ) for φ-polarization, i.e., the power level for the φ-polarization at which the throughput exceeds the requirements for the specified reference measurement channel

6) Calculate the resulting averaged EIS as:

$$EIS = 2*[1/EIS(Pol_{Meas}=\theta, Pol_{Link}=\theta) + 1/EIS(Pol_{Meas}=\phi, Pol_{Link}=\phi)]^{-1}$$

5.2.1.3.5 EVM Measurement Procedure

The TX beam peak direction is where the maximum total component of EIRP is found according to 5.2.1.3.7.

The measurement procedure includes the following steps:

1) Connect the SS (System Simulator) with the DUT through the measurement antenna with polarization reference Pol_{Meas} to form the TX beam towards the previously determined TX beam peak direction and respective polarization.

2) Lock the beam toward that direction for the entire duration of the test.

3) Measure EVM_θ for the θ-polarization of the modulated signal arriving at the measurement equipment (such as a signal analyser, or gNB emulator).

4) Measure EVMφ for the φ-polarization of the modulated signal arriving at the measurement equipment (such as a signal analyser, or gNB emulator).

6) Compare EVM_θ and EVMφ against the test requirement. If either EVM_θ or EVMφ meets the requirement, pass the UE.

5.2.1.3.6 Blocking Measurement Procedure

The RX beam peak direction is where the minimum EIS is found according to 5.2.1.3.8.

The measurement procedure includes the following steps:

1) Establish a connection between the DUT and the SS with the downlink signal applied to the θ-polarization of the measurement antenna

2) Position the UE so that the beam is formed towards the measurement antenna in the RX beam peak direction.

3) Apply a signal with the specified reference measurement channel on the θ-polarization, setting the power level of the signal 3dB below the EIS level stated in the requirement.

4) Apply the blocking signal with the same polarization and coming from the same direction as the downlink signal. Set the power level of the blocking signal 3dB below the level stated in the requirement.

5) Measure the throughput of the downlink signal on the θ-polarization.

6) Switch the downlink and blocking signal to the φ-polarization of the measurement antenna.

7) Repeat steps 3 to 5 on the φ-polarization.

8) Compare the results for both the θ-polarization and φ-polarization against the requirement. If both results meet the requirements, pass the UE.

5.2.1.3.7 TX Beam Peak direction search and EIRP Spherical Coverage

The beam peak search and spherical coverage test procedure apply to DUTs with different beam correspondence capability, as defined in TS38.306 [19]. The TX beam peak direction is found with a 3D EIRP scan (separately for each orthogonal downlink polarization). The TX beam peak direction search grid points for this single grid approach are defined in Annex G.2. Alternatively, a coarse and fine grid approach could be used according to the definition in Annex G.2.4.

The measurement procedure includes the following steps for each of the points in the grid:

1) Connect the SS (System Simulator) with the DUT through the measurement antenna with $Pol_{Link}=\theta$ to form the TX beam towards the measurement antenna.

2) DUT refines its TX beam toward that direction depending on DUT's beam correspondence capability which shall match OEM declaration: if DUT's beam correspondence capability is [bit-1], then DUT chooses autonomously (the corresponding TX beam) using downlink reference signals to transmit in the direction of the incoming DL signal, which is based on beam correspondence without relying on UL beam sweeping; if DUT's beam correspondence capability is [bit-0], then DUT chooses the TX beam using downlink reference signals which is based on beam correspondence with relying on uplink beam sweeping by its network-assisted uplink beam management capability, as defined in TS38.306 [19].

3) Lock the beam.

4) Measure the mean power $P_{meas}(Pol_{Meas}=\theta,Pol_{Link}=\theta)$ of the modulated signal arriving at the power measurement equipment (such as a spectrum analyser, power meter, or gNB emulator).

5) Calculate EIRP $(Pol_{Meas}=\theta,Pol_{Link}=\theta)$ by adding the composite loss of the entire transmission path for utilized signal path, $L_{EIRP,\theta}$, and frequency to the measured power $P_{meas}(Pol_{Meas}=\theta,Pol_{Link}=\theta)$

6) Measure the mean power P_{meas} $(Pol_{Meas}=\phi,Pol_{Link}=\theta)$ of the modulated signal arriving at the power measurement equipment.

7) Calculate EIRP $(Pol_{Meas}=\phi,Pol_{Link}=\theta)$ by adding the composite losses of the entire transmission path for utilized signal path, $L_{EIRP,\varphi}$, and frequency to the measured power P_{meas} $(Pol_{Meas}=\phi,Pol_{Link}=\theta)$

8) Calculate total $EIRP(Pol_{Link}=\theta)$ = $EIRP(Pol_{Meas}=\theta,Pol_{Link}=\theta)$ + $EIRP(Pol_{Meas}=\phi,Pol_{Link}=\theta)$

9) Unlock the beam.

10) Connect the SS (System Simulator) with the DUT through the measurement antenna with $Pol_{Link}=\phi$polarization to form the TX beam towards the measurement antenna.

11) Repeat steps 2) to 9).

The TX beam peak direction is where the maximum total component of $EIRP(Pol_{Link}=\theta)$ or $EIRP(Pol_{Link}=\phi)$ is found.

The EIRP results from the TX beam peak search using the minimum number of grid points as described in Annex G.2 can be re-used for EIRP spherical coverage. In case a coarse beam peak grid is used for TX beam peak search, using the minimum number of grid points defined in Annex G.3.3.2.3, the EIRP results can be re-used for EIRP spherical coverage.

In case a separate test is performed for EIRP spherical coverage, the procedure above shall be followed using the minimum number of grid points defined in Annex G.3.3.2.3 for spherical coverage.

The $EIRP_{target\text{-}CDF}$ is then obtained from the Cumulative Distribution Function (CDF) computed using [maximum($EIRP(Pol_{Link}=\theta)$, $EIRP(Pol_{Link}=\phi)$] for all grid points. When using constant step size measurement grids, a theta-dependent correction shall be applied, i.e., the PDF probability contribution for each measurement point is scaled by $\sin(\theta)$.

Editor's Note: For spherical coverage test, using maximum($EIRP(Pol_{Link}=\theta)$, $EIRP(Pol_{Link}=\phi)$) for each test point in the grid is considered as the baseline for performance evaluation and test procedure. Decision shall be made on April meeting.

5.2.1.3.8 RX Beam Peak direction search and EIS Spherical Coverage

The RX beam peak direction is found with a 3D EIS scan (separately for each orthogonal downlink polarization). The RX beam peak direction search grid points for this single grid approach are defined in Annex G.2. Alternatively, a coarse and fine grid approach could be used according to the definition in Annex G.2.4.

The measurement procedure includes the following steps for each of the points in the grid:

1) Establish a connection between the DUT and the SS with the downlink signal applied to the $Pol_{Link}=\theta$-polarization of the measurement antenna

2) Position the UE so that the beam is formed towards the measurement antenna in the desired RX beam direction.

3) Determine EIS ($Pol_{Meas}=\theta$, $Pol_{Link}=\theta$) for θ-polarization, i.e., the power level for the θ-polarization at which the throughput exceeds the requirements for the specified reference measurement channel

4) Switch the downlink to the $Pol_{Link}=\varphi$-polarization of the measurement antenna

5) Determine EIS($Pol_{Meas}=\phi$, $Pol_{Link}=\phi$) for φ-polarization, i.e., the power level for the φ-polarization at which the throughput exceeds the requirements for the specified reference measurement channel

6) Calculate the resulting averaged EIS as:

$$EIS = 2*[1/EIS(Pol_{Meas}=\theta, Pol_{Link}=\theta) + 1/EIS(Pol_{Meas}=\phi, Pol_{Link}=\phi)]^{-1}$$

The RX beam peak direction is where the minimum EIS is found.

The EIS results from the RX beam peak search using the minimum number of grid points as described in Annex G.2 can be re-used for EIS spherical coverage. In case a coarse beam peak grid is used for RX beam peak search with an EIS metric, using the minimum number of grid points defined in Annex G.3.3.2.3, the EIS results can be re-used for EIS spherical coverage. In case a separate test is performed for spherical coverage, the procedure above should be followed using the minimum number of grid points defined in Annex G.3.3.2.3 for spherical coverage.

The $EIS_{target\text{-}CDF}$ is then obtained from the Cumulative Distribution Function (CDF) computed using total EIS for all grid points. When using constant step size measurement grids, a theta-dependent correction shall be applied, i.e., the PDF probability contribution for each measurement point is scaled by $\sin(\theta)$.

5.2.1.3.9 Beam Correspondence Tolerance

The beam correspondence requirement is fulfilled if the DUT satisfies one of the following conditions, depending on the beam correspondence capability, as defined in TS38.306 [19]:

- If [bit-1], the DUT shall meet the minimum peak EIRP requirement and spherical coverage requirement with its autonomously chosen UL beams and without uplink beam sweeping. Such a DUT is considered to have met the beam correspondence tolerance requirement.

- If [bit-0], the DUT shall meet the minimum peak EIRP requirement and spherical coverage requirement with uplink beam sweeping. Such a DUT shall meet the beam correspondence tolerance requirement and shall support uplink beam management, as defined in TS38.306 [19].

Thus, the beam correspondence tolerance test is only applicable to the DUT that has beam correspondence capability as [bit-0] (which shall match OEM declaratioin), such that DUT relies on uplink beam sweeping to fulfill the minimum peak EIRP and spherical coverage requirements.

$\Delta EIRP_{BC}$ is introduced for beam correspondence tolerance based on two EIRP measurements ($EIRP_1$ and $EIRP_2$). $EIRP_1$ is the measured total EIRP based on the beam which DUT chooses autonomously (corresponding beam) to transmit in the direction of the incoming DL signal, which is based on beam correspondence without relying on UL beam sweeping. $EIRP_2$ is the measured total EIRP based on the beam yielding highest EIRP in a given direction, which is based on beam correspondence with relying on UL beam sweeping. $\Delta EIRP_{BC}$ shall be calculated over the link angles spanning a subset of the spherical coverage grid points which are corresponding to the top 50% of the $EIRP_2$ measurement.

For each of the points in the grid:

1) Follow the test procedures specified in subclause 5.2.1.3.7 with uplink beam sweeping disabled, obtain total $EIRP_1(Pol_{Link}=\theta)$ and total $EIRP_1(Pol_{Link}=\phi)$. $EIRP_1$ is calculated by [$EIRP_1$ = maximum($EIRP_1(Pol_{Link}=\theta)$, $EIRP_1(Pol_{Link}=\phi)$)]

2) Follow the test procedures specified in subclause 5.2.1.3.7, with uplink beam sweeping enabled during DUT TX beam refinement, obtain total $EIRP_2(Pol_{Link}=\theta)$ and total $EIRP_2(Pol_{Link}=\phi)$. $EIRP_2$ is calculated by [$EIRP_2$ = maximum($EIRP_2(Pol_{Link}=\theta)$, $EIRP_2(Pol_{Link}=\phi)$)]

3) Calculate the $\Delta EIRP_{BC}=EIRP_2 – EIRP_1$.

The $\Delta EIRP_{target\text{-}CDF}$ is then obtained from the Cumulative Distribution Function (CDF) computed using [$\Delta EIRP_{BC}$] for each of all top 50% of the $EIRP_2$ measurement points in the grid. When using constant step size measurement grids, a theta-dependent correction shall be applied, i.e., the PDF probability contribution for each measurement point is scaled by $\sin(\theta)$.

Editor's Note: For beam correspondence tolerance test, using maximum($EIRP_1(Pol_{Link}=\theta)$, $EIRP_1(Pol_{Link}=\phi)$) and maximum($EIRP_2(Pol_{Link}=\theta)$, $EIRP_2(Pol_{Link}=\phi)$) for each test point in the grid is considered as the baseline for performance evaluation and test procedure. Decision shall be made on April meeting

Editor's Note: The side conditions for downlink reference signals SSB and CSI-RS in beam correspondence tolearance test are FFS.

5.2.2 Direct far field (DFF) setup simplification for centre of beam measurements

5.2.2.1 Description

The DFF setup in 5.2.1 can be simplified in the following way to perform centre of the beam measurements:

- The measurement and the link antenna can be combined so that the single antenna is used to steer the beam and to perform UE RF measurements.

The measurement setup of UE RF characteristics for f > 6 GHz capable of centre of beam measurements and is shown in Figure 5.2.1.1-1 below.

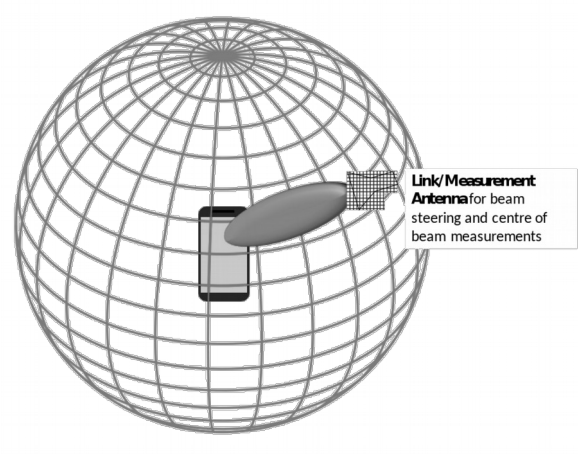

Figure 5.2.2.1-1: Centre of beam measurement setup of UE RF characteristics

The applicability criteria of the simplified DFF setup for centre of beam measurements are defined in 5.2.1.1.

5.2.2.3 Far-field criteria

The far-field criteria of the simplified DFF setup for centre of beam measurements are defined in 5.2.1.2.

5.2.2.3 Testing and calibration aspects

The same testing and calibration aspects apply as outlined in 5.2.1.3.

5.2.3 Indirect far field (IFF) method 1

The IFF method 1 creates the far field environment using a transformation with a parabolic reflector. This is also known as the compact antenna test range (CATR). Refer to Annex E for additional information.

5.2.3.1 Description

The IFF measurement setup of UE RF characteristics for f > 6 GHz is capable of centre and off centre of beam measurements and is shown in Figure 5.2.3.1-1 below.

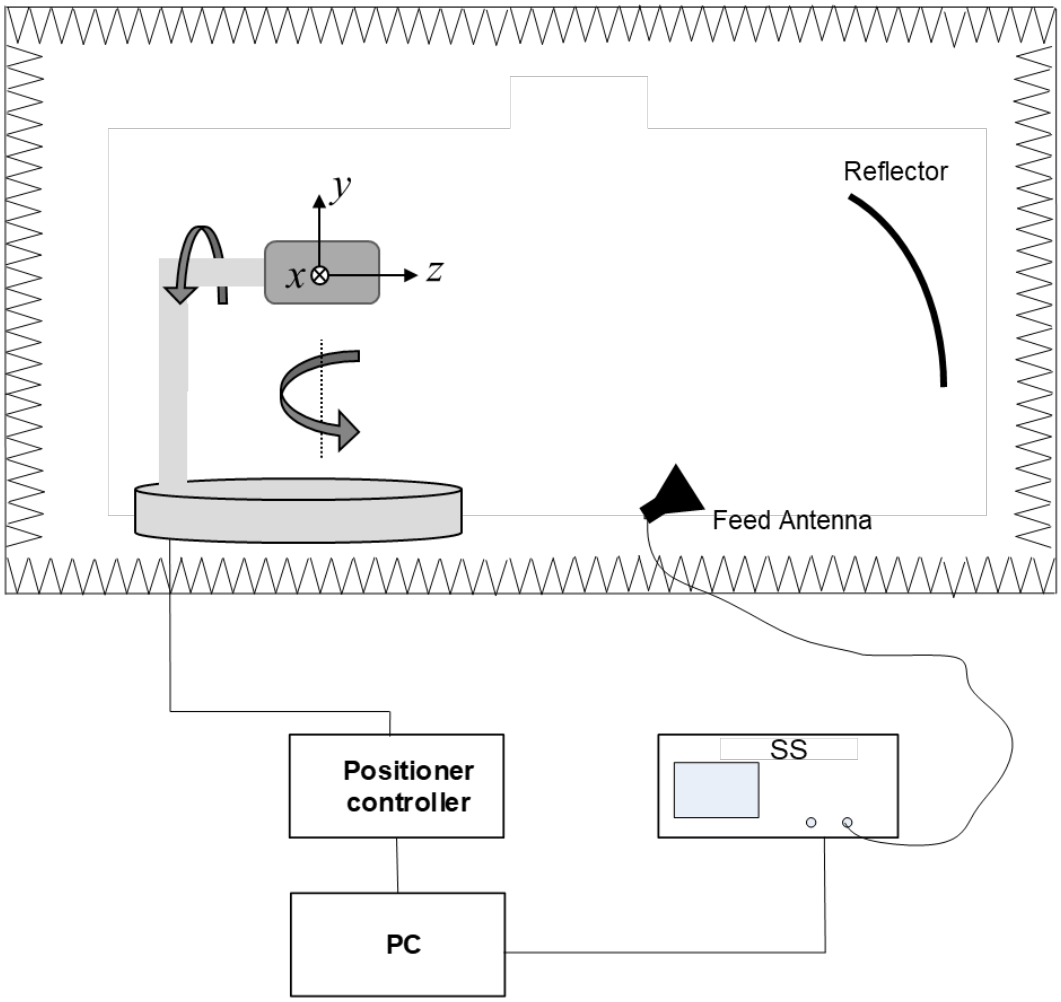

Figure 5.2.3.1-1: IFF method 1 (CATR) measurement setup of UE RF characteristic

The key aspects of this test method setup are:

- Indirect Far field of Compact Antenna Test Range as the one used in [9] with quiet zone diameter at least D.
- A positioning system such that the angle between the dual-polarized measurement antenna and the DUT has at least two axes of freedom and maintains a polarization reference.
- Before performing the UBF, the measurement probe acts as a link antenna maintaining polarization reference with respect to the DUT. Once the beam is locked then the link is to be passed to the link antenna which maintains reliable signal level with respect to the DUT.
- For setups intended for measurements of UE RF characteristics in non-standalone (NSA) mode with 1UL configuration, an LTE link antenna is used to provide the LTE link to the DUT. The LTE link antenna provides a stable LTE signal without precise path loss or polarization control.
- For setups intended for measurements in NR CA mode with FR1 and FR2 inter-band NR CA, test setup provides NR FR1 link to the DUT. The NR FR1 link has a stable and noise-free signal without precise path loss or polarization control.

The applicability criteria of this test method are:

- The total test volume is a cylinder with diameter d and height h.
- DUT must fit within the total test volume for the entire duration of the test.
- Either a single radiating aperture, multiple non-coherent apertures or multiple coherent apertures DUTs can be tested.

- EIRP, TRP, EIS, EVM, spurious emissions and blocking metrics can be tested.
- No manufacturer declaration is needed.

5.2.3.2 Far-field criteria

The CATR system does not require a measurement distance of $R > \frac{2D^2}{\lambda}$ to achieve a plane wave as in a standard far field range.

The Table 5.2.3.2-1 and Table 5.2.3.2-2 below show the paths losses which can be expected for the CATR compared to a Fraunhofer limit distance ($R > \frac{2D^2}{\lambda}$).

Table 5.2.3.2-1: Near field/far field boundary for different frequencies and antenna sizes for a traditional far field anechoic chamber

D(cm)	Frequency (GHz)	Near/far boundary (cm)	Path Loss (dB)
5	28	47	54.8
10	28	187	66.8
15	28	420	73.9
30	28	1681	85.9

Table 5.2.3.2-2: Example of CATR path losses

DUT size [cm]	Frequency (GHz)	Path Loss (dB)
5	28	52.3
10	28	58.3
15	28	61.8
30	28	67.8
NOTE 1: Final values will depend on CATR specific implementation		

For CATR, the FF distance is seen as the focal length, distance between the feed and reflector for a CATR, which can be calculated as shown below (as a rule of thumb although it can vary depending on system implementation):

- D =x [m]
- size of reflector = 2*D
- R = focal length = 3.5*size of reflector = 3.5*(2*D)

In a CATR, from the reflector to the quiet zone, there is a plane wave with no space loss.

For both direct FF and CATR, free space path loss is calculated by applying the Free Space Loss formula with R = FF distance: $\left(\frac{4\pi R}{\lambda}\right)^2$.

5.2.3.3 Testing and calibration aspects

5.2.3.3.1 Calibration Measurement Procedure

The calibration measurement is done by using a reference antenna (SGH used in Figure 5.2.3.3.1-1) with known efficiency or gain values. In the calibration measurement the reference antenna is measured in the same place as the DUT, and the attenuation of the complete transmission path (C ↔ A, as in Figure 5.2.3.3.1-1) from the DUT to the measurement receiver (EIRP), and from the RF source to DUT (EIS) is calibrated out. Figure 5.2.3.3.1-1 presents a setup of a typical compact antenna test range for EIRP calibration:

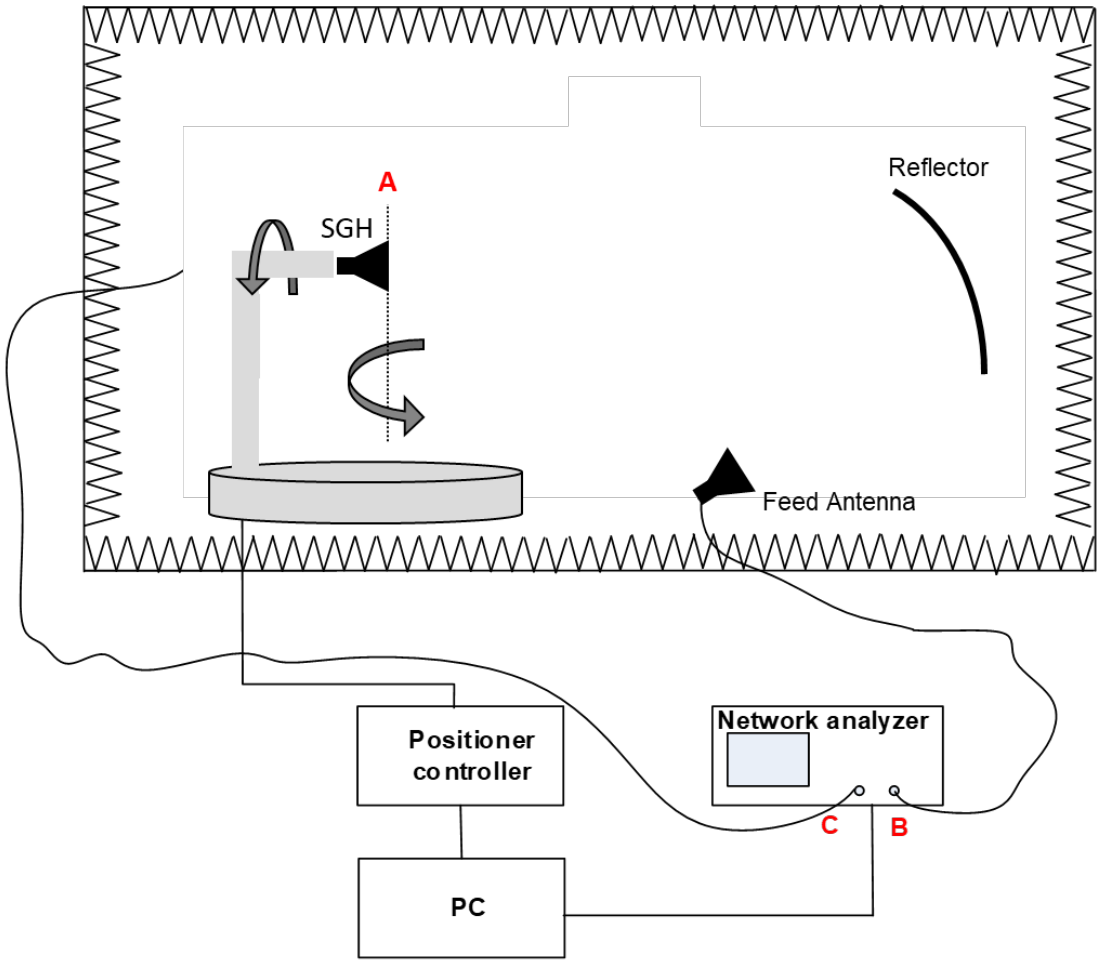

Figure 5.2.3.3.1-1. CATR calibration system setup for EIRP

5.2.3.3.2 Peak EIRP Measurement Procedure

The TX beam peak direction is where the maximum total component of EIRP is found, including the respective polarization of the measurement antenna used to form the TX beam, according to 5.2.1.3.7.

1) Connect the SS (System Simulator) with the DUT through the measurement antenna with polarization reference Pol_{Meas} to form the TX beam towards the TX beam peak direction and respective polarization.

2) Lock the beam toward that direction for the entire duration of the test.

3) Measure the mean power P_{meas} (Pol_{Meas}=θ, Pol_{Link}) of the modulated signal arriving at the power measurement equipment (such as a spectrum analyser, power meter, or gNB emulator).

4) Calculate EIRP(Pol_{Meas}=θ, Pol_{Link}) by adding the composite loss of the entire transmission path for utilized signal path, $L_{EIRP,\theta}$, and frequency to the measured power P_{meas}(Pol_{Meas}=θ, Pol_{Link})

5) Measure the mean power P_{meas} (Pol_{Meas}=ϕ, Pol_{Link}) of the modulated signal arriving at the power measurement equipment.

6) Calculate $EIRP_{\theta}$ by adding the composite losses of the entire transmission path for utilized signal path, $L_{EIRP,\varphi}$ and frequency to the measured power P_{meas} (Pol_{Meas}=ϕ, Pol_{Link}).

7) Calculate total EIRP (Pol_{Link}) = EIRP(Pol_{Meas}=θ, Pol_{Link}) + EIRP(Pol_{Meas}=ϕ, Pol_{Link})

5.2.3.3.3 TRP Measurement Procedure

The minimum number of measurement points for TRP measurement grid is outlined in Annex G.1.

The measurement procedure includes the following steps:

1) Connect the SS with the DUT through the measurement antenna with desired polarization reference Pol_{Link} to form the TX beam towards the desired TX beam direction and respective polarization.

2) Lock the beam toward that direction and polarization for the entire duration of the test.

3) For each measurement point, measure $P_{meas}(Pol_{Meas}=\theta, Pol_{Link})$ and $P_{meas}(Pol_{Meas}=\phi, Pol_{Link})$. The angle between the measurement antenna and the DUT (θ_{Meas}, φ_{Meas}) is achieved by rotating the measurement antenna and the DUT (based on system architecture).

4) Calculate $EIRP(Pol_{Meas}=\theta, Pol_{Link})$ and $EIRP(Pol_{Meas}=\phi, Pol_{Link})$ by adding the composite loss of the entire transmission path for utilized signal paths, $L_{EIRP,\theta}$, $L_{EIRP,\varphi}$ and frequency to the measured powers P_{meas}.

5) The TRP value for the uniform measurement grid is calculated using the TRP integration approaches outlined in Annex G.1.2. The TRP value for the constant density grid is calculated using the TRP integration formula in Annex G.1.3.

5.2.3.3.4 Peak EIS Measurement Procedure

The RX beam peak direction is where the minimum EIS is found according to 5.2.1.3.8.

The measurement procedure includes the following steps:

1) Establish a connection between the DUT and the SS with the downlink signal applied to the Pol_{Link}= θ-polarization of the measurement antenna

2) Position the UE so that the beam is formed towards the measurement antenna in the RX beam peak direction

3) Determine $EIS(Pol_{Meas}=\theta, Pol_{Link}=\theta)$ for θ-polarization, i.e., the power level for the θ-polarization at which the throughput exceeds the requirements for the specified reference measurement channel

4) Switch the downlink to the Pol_{Link}=φ-polarization of the measurement antenna

5) Determine $EIS(Pol_{Meas}=\phi, Pol_{Link}=\phi)$ for φ-polarization, i.e., the power level for the φ-polarization at which the throughput exceeds the requirements for the specified reference measurement channel

6) Calculate the resulting averaged EIS as

$$EIS = 2*[1/EIS(Pol_{Meas}=\theta, Pol_{Link}=\theta) + 1/EIS(Pol_{Meas}=\phi, Pol_{Link}=\phi)]^{-1}$$

5.2.3.3.5 EVM Measurement Procedure

The TX beam peak direction is where the maximum total component of EIRP is found according to 5.2.1.3.7.

The measurement procedure includes the following steps:

1) Connect the SS (System Simulator) with the DUT through the measurement antenna with polarization reference Pol_{Meas} to form the TX beam towards the previously determined TX beam peak direction and respective polarization.

2) Lock the beam toward that direction for the entire duration of the test.

3) Measure EVM_{θ} for the θ-polarization of the modulated signal arriving at the measurement equipment (such as a signal analyser, or gNB emulator).

4) Measure EVMφ for the φ-polarization of the modulated signal arriving at the measurement equipment (such as a signal analyser, or gNB emulator).

6) Compare EVM_{θ} and EVMφ against the test requirement. If either EVM_{θ} or EVMφ meets the requirement, pass the UE.

5.2.3.3.6 Blocking Measurement Procedure

The RX beam peak direction is where the minimum EIS is found according to 5.2.1.3.8.

The measurement procedure includes the following steps:

1) Establish a connection between the DUT and the SS with the downlink signal applied to the θ-polarization of the measurement antenna
2) Position the UE so that the beam is formed towards the measurement antenna in the RX beam peak direction
3) Apply a signal with the specified reference measurement channel on the θ-polarization, setting the power level of the signal 3dB below the level stated in the requirement.
4) Apply the blocking signal with the same polarization and coming from the same direction as the downlink signal. Set the power level of the blocking signal 3dB below the level stated in the requirement.
5) Measure the throughput of the downlink signal on the θ-polarization.
6) Switch the downlink and blocking signal to the φ-polarization of the measurement antenna.
7) Repeat steps 3 to 5 on the φ-polarization.
8) Compare the results for both the θ-polarization and φ-polarization against the requirement. If both results meet the requirements, pass the UE.

5.2.4 Near field to far field transform (NFTF)

The NFTF method computes the metrics defined in Far Field by using the Near Field to Far Field transformation.

5.2.4.1 Description

The NFTF measurement setup of UE RF characteristics for f > 6 GHz is capable of centre and off centre of beam measurements and is shown in Figure 5.2.4.1-1:

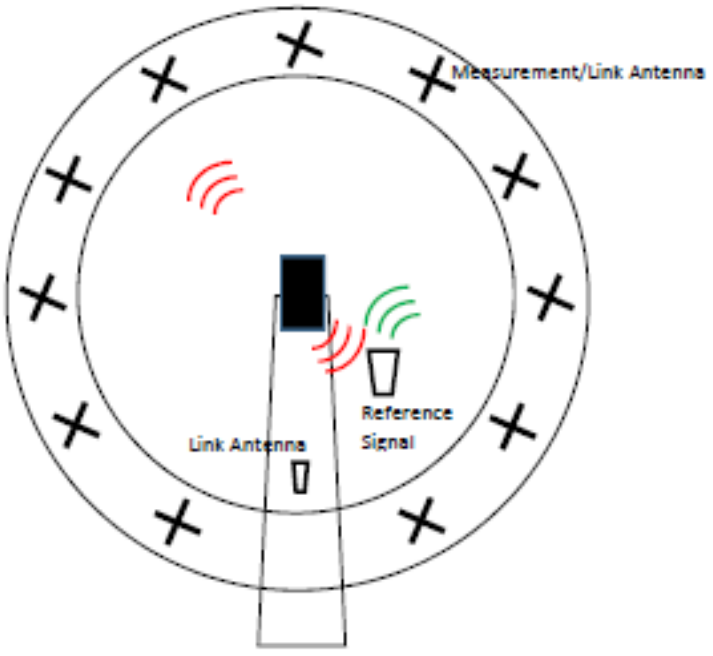

Figure 5.2.4.1-1: Typical NFTF measurement setup of EIRP/TRP measurements

The key aspects of the Near Field test range are:

- Radiated Near Field UE beam pattern are measured and based on the NFTF mathematical transform, the final metric such as EIRP is the same as the metric for the baseline setup
- A positioning system such as the angle between the dual-polarized measurement/link antenna and the DUT has at least two axes of freedom and maintains a polarization reference
- For setups intended for measurements of UE RF characteristics in non-standalone (NSA) mode with 1UL configuration, an LTE link antenna is used to provide the LTE link to the DUT. The LTE link antenna provides a stable LTE signal without precise path loss or polarization control.
- For setups intended for measurements in NR CA mode with FR1 and FR2 inter-band NR CA, test setup provides NR FR1 link to the DUT. The NR FR1 link has a stable and noise-free signal without precise path loss or polarization control.

The applicability criteria of the NFTF setup are:

- The DUT radiating aperture is $D \leq 5$ cm
  - Either a single radiating aperture, multiple non-coherent apertures or multiple coherent apertures DUTs can be tested
  - If multiple antenna panels that are phase coherent are defined as a single array, the criterion on DUT radiating aperture applies to this single array
  - D is based on the MU assessment in Annex B.1.4.3
  - If the uncertainties can be further optimized, the MU may be reduced or D may be increased
- A manufacturer declaration on the following elements is needed:
  - Manufacturer declares antenna array size
- EIRP, TRP, and spurious emissions metrics can be tested.

5.2.4.2 Testing and calibration aspects

5.2.4.2.1 Calibration Measurement Procedure

Calibration accounts for the various factors affecting the measurements of the EIRP. These factors include components such as range length path loss, cable losses, gain of the receiving antenna, etc. Each measured data point for radiated power is transformed from a relative value in dB to an absolute value in dBm. For doing that the total path loss from the DUT to the measurement receiver, named L path loss is calibrated out. The calibration measurement is usually done by using a reference antenna with known gain. This approach is based on the so called gain-comparison method. Figure 5.2.4.2-1 shows the typical configuration for measuring path loss.

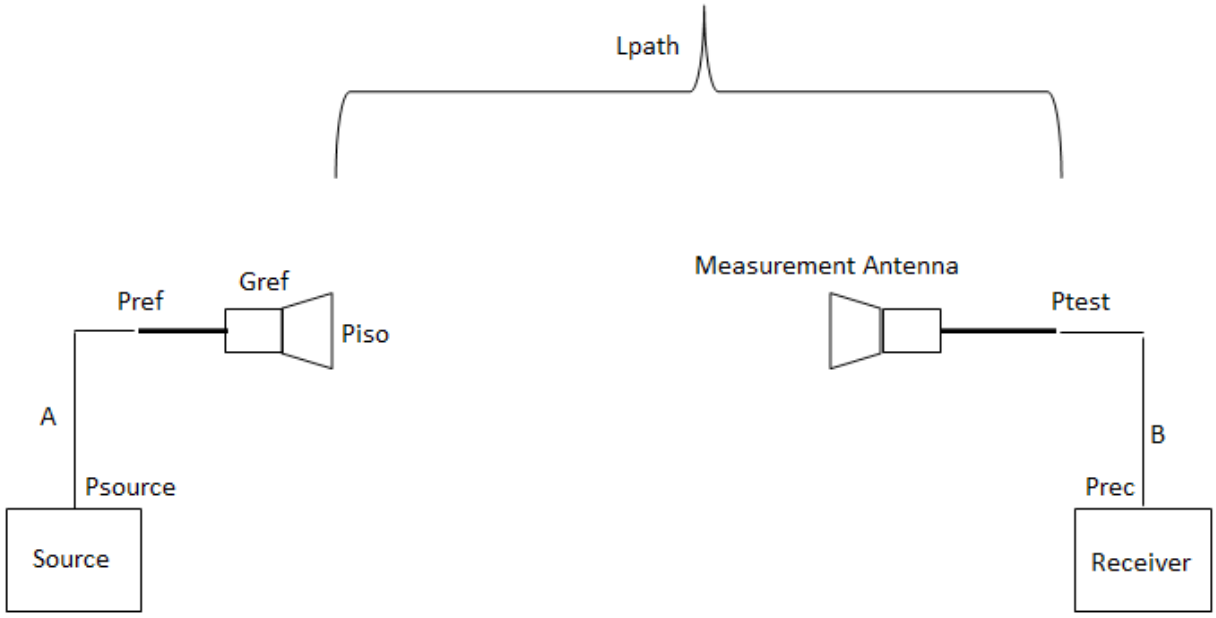

Figure 5.2.4.2-1: NFTF – Typical setup for path loss measurement

The L path loss can be determined from the power into the reference antenna by adding the gain of the reference antenna:

$$Piso = Pref + Gref$$

so that:

$$L\ path\ loss = Pref + Gref - Ptest$$

In order to determine Pref, a cable reference measurement is performed in order to calibrate out the A, and B paths. Assuming that the power at the source is fixed, it can be showed that:

$$Pref-Ptes=Prec'-Prec$$

Where Prec and Prec' are the power measured at the receiver during the calibration measurement with the reference antenna and the power measured at the receiver during the cable reference measurement respectively. L path loss is then given by:

$$L\ path\ loss = Gref + Prec' - Prec$$

5.2.4.2.2 Peak EIRP Measurement Procedure

The TX beam peak direction is where the maximum total component of EIRP is found, including the respective polarization of the measurement antenna used to form the TX beam, according to 5.2.1.3.7.

The measurement procedure includes the following steps:

1) Connect the SS (System Simulator) to the DUT through the measurement antenna with polarization reference Pol_{Meas} to form the TX beam towards the TX beam peak direction and respective polarization.
2) Lock the beam toward that direction for the entire duration of the test.
3) Perform a 3D pattern measurement (amplitude and phase) with the DUT sending a modulated signal.
4) Determine the EIRP for both polarization towards the TX beam peak direction by using a Near Field to Far Field transform.
5) Calculate total EIRP = $EIRP_{\theta}$ + $EIRP_{\phi}$

5.2.4.2.3 TRP Measurement Procedure

The minimum number of measurement points for TRP measurement grid is outlined in Annex G.1.

The measurement procedure includes the following steps:

1) Connect the SS to the DUT through the measurement antenna with polarization reference Pol_{Meas} to form the TX beam towards the previously determined TX beam peak direction and respective polarization.
2) Lock the beam toward that direction for the entire duration of the test.
3) Perform a 3D pattern measurement (amplitude and phase) with the DUT sending a modulated signal.
4) For each measurement point on the grid, determine the EIRP for both polarization by using a Near Field to Far Field transform.
5) The TRP value for the constant step size measurement grids are calculated using the TRP integration approaches outlined in Annex G.1.2. The TRP value for the constant density grid is calculated using the TRP integration formula in Annex G.1.3.

5.3 Test method applicability

The test methods in subclause 5.2 are applicable to test cases based on being less than or equal to a threshold MU.

The threshold MU for the equivalence framework will be based on direct far field (DFF) test method for D ≤ 5 cm and for indirect far field (IFF) test method for D > 5 cm.

A permitted test method will have applicability to at least one test case. Applicability is a function of DUT Antenna Configuration as defined in Table 5.3-1 DUT Antenna Configuration can be chosen by an optional declaration from a manufacturer.

Table 5.3-1: DUT Antenna Configuration

DUT Antenna Configuration	Description
1	Maximum one antenna panel with D ≤ 5 cm active at any one time
2	More than one antenna panel D ≤ 5 cm without phase coherence between panels active at any one time
3	Any phase coherent antenna panel of any size (e.g. sparse array)

Table 5.3-2 indicates the high-level applicability of test methods by DUT Antenna Configuration.

Table 5.3-2: Overview of test method applicability for permitted test methods

DUT Antenna Configuration	Direct Far Field (DFF)	Indirect Far Field (IFF)	Near Field to far field transform (NFTF)
1	Yes	Yes	Yes
2	Yes	Yes	Yes
3	No	Yes	No
NOTE: A positive indication means that applicability exists for at least one RF test cases for the given DUT Antenna Configuration			

The detailed applicability of any test method for any test will be a function of DUT Antenna Configuration, D, the actual testing distance and the resulting calculated MU. If the calculated MU is lower than the threshold MU, then that test method is applicable to the test.

6 UE RRM testing methodology

6.1 General

Testability aspects of the UE have been considered. Unless otherwise indicated below, device under test (DUT) refers to UE nodes. The exact list of RRM tests for UE can only be determined once the core requirements are settled.

For frequency bands above 6 GHz (e.g. mm-wave), conducted antenna connectors are assumed not to be available at DUT and the OTA testing is considered as the baseline approach for NR UE RRM testing methodology.

The possibility of performing conducted tests using an intermediate frequency (IF) were evaluated. It was decided that this approach would be challenging to standardise for various reasons since IF is an internal interface in the DUT and using a standardised IF (signal level, number of IF ports, IF frequency etc.) would preclude many different DUT implementations including direct conversion receivers. In addition, IF testing excludes all components which operate at the radio frequency such as RF filters, duplexers, transmit receive switch, low noise amplifier (LNA), power amplifier (PA), analogue beamforming phase shifting elements etc., and the algorithms which control such components from the test.

Further details of a suitable OTA test environment are to be discussed in the work item, and may have impact to the core requirements which are defined. For example, side conditions for the applicability of core requirements should be defined in a way in which they can be ensured in an OTA environment.

6.2 Measurement setup

6.2.1 Baseline setup

6.2.1.1 Description

The baseline measurement setup of UE RRM characteristics for frequency bands above 6 GHz is capable of establishing an OTA link between the DUT and a number of emulated gNB sources and is shown in Figure 6.2.1.1-1 below.

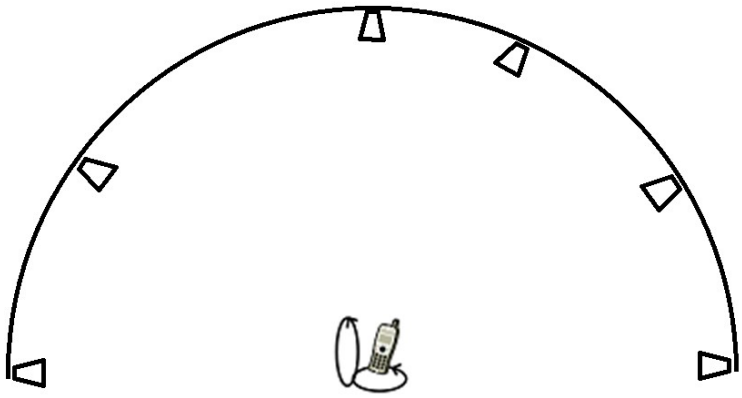

Figure 6.2.1.1-1: Baseline measurement setup of RRM characteristics

The UE RRM baseline measurement setup shall fulfil the following capabilities:

- TRxPs and Cells:
  - Up to 2 NR transmission reception points TRxPs are emulated.
  - For non-standalone (NSA) NR devices, the test setup shall emulate in addition 1 LTE cell. The emulated LTE cell provides a stable LTE signal without precise propagation modelling or path loss control between it and the DUT. No performance verification for LTE carriers is supported.

    - For setups which require NR CA mode with FR1 and FR2 inter-band NR CA, test setup shall be capable to provide NR FR1 link to the DUT. The NR FR1 link has a stable and noise-free signal without precise path loss or polarization control. No performance verification for NR FR1 carriers is supported.

- Antennas, polarization, simultaneously active AoAs:

    - N dual-polarized antennas transmitting the signals from the emulated gNB sources to the DUT.

    - The antennas transmit into the test zone in such a way that signal polarization does not prevent the DUT receiving a consistent, predictable power level.

    - $N \geq N_{MAX\_AoAs}$, where N_{MAX_AoAs} is the maximum number of simultaneously active (emulating signal) angles of arrival AoAs.

    - For the scope of Rel-15 testing $N_{MAX\_AoAs} = 2$.

        - For UE RRM baseline measurement setup based on DFF, the supported $N_{MAX\_AoAs} = 2$.

        - For UE RRM baseline measurement setup based on simplified DFF, the supported $N_{MAX\_AoAs} = 1$

        - For UE RRM baseline measurement setup based on IFF, the supported $N_{MAX\_AoAs} = 1$.

- Angular Relationship:

    - A positioning system such that an angular relationship with two axes of freedom is provided between the DUT and the test system antennas (or the setup should provide equivalent functionality).

    - For $N_{MAX\_AoAs} = 2$ the setup shall enable following relative angular relationships between the N_{MAX_AoAs} simultaneously active AoAs: 30°, 60°, 90°, 120° and 150°.

    - For single active probe scenarios, in case that step change of AoA is required, the setup shall enable following relative angular change between initial and target AoA: 30°, 60°, 90°, 120° and 150°.

- Wanted and noise (AWGN) signals can be transmitted from one or both active probes. Test description will define the exact signal/noise/SNR/SINR level per TRxP at the reference point.

- Multiple DL transmission antenna ports:

    - In case of multiple DL transmission antenna ports are required for RRM testing, the different antenna ports are mapped to different polarizations.

- Propagation Conditions

    - Test method shall allow modelling of the following propagation conditions between the DUT and the emulated gNB sources

        - Multi-path fading propagation conditions

            - Multi-path fading propagation conditions between the DUT and the emulated gNB sources are modelled as Single probe channel models as described in subclause 8.2.

            - The Single probe channel models for RRM testing adopts the same framework of Demodulation. Detailed channel parameterization should be defined in the NR WI performance part.

        - Static propagation conditions

- Measurement Uncertainty:

    - For UE RRM baseline measurement setup based on DFF, it is likely that the measurement uncertainty budget for the RRM setup may contain additional measurement uncertainty elements relative to the setup defined in subclause 5.2.1. These have been defined in Annex B.2.1.

- Applicability Criteria:

    - For UE RRM baseline measurement setup based on DFF, the applicability criteria defined for the DFF UE RF test method described in subclause 5.2.1 can be applied.

- For UE RRM baseline measurement setup based on simplified DFF, the applicability criteria defined for the DFF UE RF test method described in subclause 5.2.2 can be applied.
- For UE RRM baseline measurement setup based on IFF, the applicability criteria defined for the IFF UE RF test method described in subclause 5.2.3 can be applied.

Note: Using UE Demodulation baseline setup in subclause 7.2 to perform selected RRM metrics testing is not precluded. Feasibility and applicability of this condition should be investigated in the NR WI performance part.

6.2.1.2 Far-field criteria and Quiet Zone

For RRM baseline measurement setup based on DFF:

- The Far-field criteria defined for the DFF UE RF test method described in subclause 5.2.1 can be applied.
- A DFF measurement setup has the centre of the Quiet Zone (QZ) located at the centre of the rotational axes (of DUT and measurement antenna). For the RRM measurement baseline setup based on DFF, the vertices of the N probes have to be aligned to the resulting centre of the QZ. The centre of the QZ is taken as the reference point for MU definition for each probe. The same QZ size as for DFF UE RF test method described in subclause 5.2.1 applies.

For RRM baseline measurement setup based on simplified DFF:

- The Far-field criteria defined for the simplified DFF UE RF test method described in subclause 5.2.2 can be applied.
- The same QZ size and definition as for simplified DFF UE RF test method described in subclause 5.2.2 applies.

For RRM baseline measurement setup based on IFF:

- The Far-field criteria defined for the IFF UE RF test method described in subclause 5.2.3 can be applied.
- The Quiet Zone definition for the IFF UE RF test method described in subclause 5.2.3 can be applied.

6.2.1.3 Testing and calibration aspects

The calibration method defined for the DFF UE RF test method described in subclause 5.2.1 can be applied for UE RRM testing based on DFF [for each probe/AoA]. The calibration method defined for the IFF test method described in subclause 5.2.3 can be applied for the UE RRM testing based on IFF. The calibration method defined for the simplified DFF UE RF test method described in subclause 5.2.2 can be applied for UE RRM testing based on simplified DFF.

6.2.1.4 Test parameters and metrics

6.2.1.4.1 Test parameters and metrics required for UE RRM testing

The following test parameters and metrics need to be supported for UE RRM testing.

Test parameters for RRM testing to be controlled at the reference point:

- SNR of DL signal
- DL power level (e.g. EPRE) (from AoA)
- Relative DL power level of 2 signals
  - From intra-frequency or inter-frequency cells
  - From the same AoA or different AoAs.
- Relative DL timing of 2 signals
- Faded DL channel for each signal
- AoA for arriving signals

Metrics for RRM testing at the reference point:

- UL PRACH level transmitted by the UE
- Relative UL PRACH level transmitted by the UE
- Timing of UE UL transmission relative to DL signal
- Relative timing change of UE UL transmission relative to DL signal
- Timing measurement of UL events caused by events on the DL

6.2.1.4.2 Radiated requirements Reference point and Testing directions

For RRM baseline measurement setup based on DFF and IFF, the Reference Point is located at the centre of the QZ. From the UE perspective the reference point is the input of UE antenna array.

Calibration of power level and relative power level test parameters and RRM metrics (at the required AoAs) is required and shall be provided by the test system.

Appropriate timing and relative timing test parameters and RRM metrics (at the required AoAs) shall be provided by the test system within declared uncertainties.

The Test cases in core specification TS 38.133 [17] will be specified at the Reference point, according to the following principles:

- Specify absolute Noc level at the Reference point per angle of arrival (AoA)
  - Noc level may have different value according to operating band and UE power class
- Specify SNR at the Reference point per angle of arrival (AoA)
  - SNR is a test-specific value
- The angle(s) of arrival (AoA(s)) will be specified in each test case.

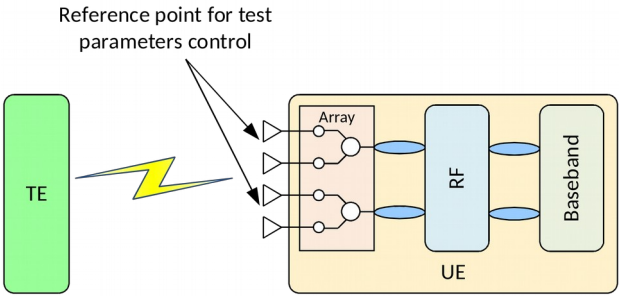

Figure 6.2.1.4.2-1: DL SNR reference point for RRM testing methodology

The following Scenarios for RRM requirements have been identified and can be supported by the NR RRM Test Methods:

Scenario 1: RRM requirement with single Angle of Arrival (1 AoA) with signal coming from RX beam peak direction.

Scenario 2: RRM requirement with single Angle of Arrival (1 AoA) with signal coming from RX non-beam peak direction.

- The test can be performed in any single direction which is covered by N^{th} percentile EIS spherical coverage of the DUT
- Value of N according to power class, as defined in TS 38.101-2 [16] clause 7.3.4.

Scenario 3: RRM requirement with two Angle of Arrivals (2 AoAs).

- Test directions:
  - Both signals come from the directions covered by the N% percentile EIS spherical coverage of the DUT

- The angle between two probes should match the relative probe spacing of 30, 60, 90, 120, 150 deg and UE is in the directions in which the UE RRM test cases can be performed.
- Value of N according to power class, as defined in TS 38.101-2 [16] clause 7.3.4.

- Case 1: TDM transmissions from 2 probes (i.e. each probe transmits both signal and/or artificial noise in TDM manner)

  Case 2: Simultaneous transmission of signals from 2 probes

The following Types of RRM requirements have been identified and can be supported by the NR RRM Test Methods:

- Type 1:
  - RRM requirements defined under the assumption that the UE is using “Fine” UE RX beams.
  - “Fine” UE RX beams are the beams used by the UE to perform PDSCH reception and used to define UE RF requirements (e.g. EIS, EIS spherical coverage)
- Type 2:
  - Requirements defined under the assumption that the UE is using “Rough” UE RX beams.
  - “Rough” UE RX beams are the beams which the UE is using for RRM measurements (e.g. for SSB measurements)

The following Modes for useful signals (S) and noise signals (N) Configuration have been identified and can be supported by the NR RRM Test Methods:

- Mode 1:
  - Test system transmits useful signals (S) and noise signals (N) to emulate target SNR condition
- Mode 2:
  - Test system transmits only useful signals (S).

For selecting the testing direction (AoA to test the requirement) fulfilling certain preconditions, two methods are feasible from the perspective of RRM baseline measurement setup, as follows:

- Method 1: Run a pretest in the RRM baseline measurement system to identify all the directions (with a given spatial granularity) at which the UE fulfils a given precondition (e.g. spherical coverage EIS). The testing directions are then chosen out of the valid directions, following a given rule. The precondition to be fulfilled, and the rule how to select the testing direction out of the valid directions, are specified in the test description.
- Method 2: For each given potential direction, test first a given precondition (e.g. minimum TP for a given power), which validates the direction as valid for testing or not. If the direction is valid, test the requirement, if not, jump to the next potential direction following a given rule. The rule how to select the potential directions and the precondition to validate them as testing direction, are specified in the test description.

6.2.1.4.3 Scenario 1 (1AoA RX beam peak) for Type 1 Requirements (“Fine” RX beams) and Mode 1 Configuration (S+N)

Conditions chosen for conducted RRM Test cases assume that the noise contribution of the UE front end is negligible. For over-the-air testing it is not feasible in practice to use signal levels high enough to make the noise of the UE front end negligible. A number of scenarios occur in the design of RRM test cases:

a) One or more side conditions are deliberately set near a lower limit, for example some RSRP reporting accuracy tests

b) A test is designed to check an event at a specific SNR, for example Radio Link Monitoring

c) The SNR is not critical provided it is high enough for the test purpose

For test cases where the SNR seen by the UE at baseband is critical:

- Set wanted noise to give a maximum of 1dB difference between Reference point SNR and Baseband SNR, so $SNR_{RP} - SNR_{BB} \leq 1dB$

Figure 6.2.1.4.3-1 shows the principle for UE Power class 3 in Band n260, with an example SNR value.

The Noc values are based on Refsens for the Operating band and on the UE Power class, and taking a baseline of UE Power class 3 in Band n260.

$$SNoc = Refsens_{PC3,\ n260,\ 50MHz} - 10Log_{10}(SCS_{Refsens} \times PRB_{Refsens} \times 12) - SNR_{Refsens} + \Delta_{thermal}$$

where:

- $Refsens_{PC3,\ n260,\ 50MHz}$ is the Refsens value in dBm specified for Power Class 3 in Band n260 for 50MHz Channel bandwidth in TS 38.101-2 [16] Table 7.3.2.3-1, [dBm/Hz]
- $SCS_{Refsens}$ is a subcarrier spacing associated with N_{RB} for 50MHz in TS 38.101-2 [16] Table 5.3.2-1, chosen as 120kHz., [Hz]
- $PRBs_{Refsens}$ is N_{RB} associated with subcarrier spacing 120 kHz for 50MHz in TS 38.101-2 [16] Table 5.3.2-1 and is 32.
- 12 is the number of subcarriers in a PRB
- $SNR_{Refsens}$ is the SNR used for simulation of Refsens, and is -1dB
- $\Delta_{thermal}$ is the amount of dB that the wanted noise is set above UE thermal noise, giving a rise in total noise of Δ_{BB}. $\Delta_{thermal}$ is chosen as 6dB, giving a rise in total noise of 1dB.

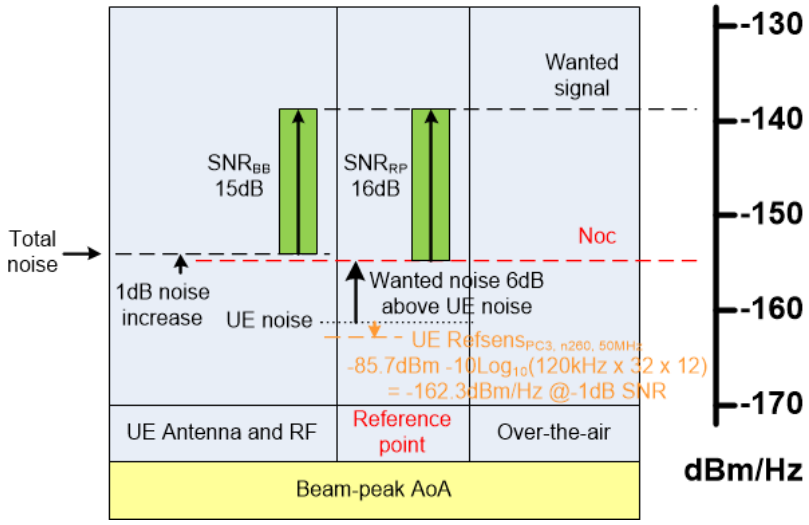

Figure 6.2.1.4.3-1: Reference point SNR_{RP} and Baseband SNR_{BB}

The following methodology to define the minimum Noc level for power class X (PC_X) and operating band Y (Band_Y) is used for the single carrier case and a single band device:

$$Noc(PC\_X, Band\_Y) = -155\ dBm/Hz + Refsens_{PC\_X,\ Band\_Y,\ 50MHz} - Refsens_{PC3,\ n260,\ 50MHz}$$

where:

- Refsens values are specified in TS 38.101-2 [16] Tables 7.3.2.1-1, 7.3.2.2-1, 7.3.2.3-1 and 7.3.2.4-1.

The Noc level for devices supporting multi-and operation and for CA cases is FFS.

The Noc values derived by the above equations are the minimum that should be used in an RRM test case to ensure that $SNR_{BB} \geq SNR_{RP}$ -1dB.

Depending on the test purpose, each RRM test case should decide whether to use a band and/or UE power class dependent Noc value, or whether a single Noc value is adequate.

6.2.1.4.4 Scenario 1 (1AoA RX beam peak) for Type 2 Requirements (“Rough” RX beams) and Mode 1 Configuration (S+N)

The Noc is derived similar as in clause 6.2.1.4.3 with the following exception:

- Noc level is increased by Y, where:
  - Value Y characterizes the antenna gain difference between the fine and rough beams in the ‘fine’ RX beam peak direction.
    - Y = 7 dB for power class 3 UE.

6.2.1.4.5 Scenario 2 (1AoA RX non-beam peak) for Type 1 Requirements (“Fine” RX beams) and Mode 1 Configuration (S+N)

The Noc is derived similar as in clause 6.2.1.4.3 with the following exception:

- Noc level is increased by X, where:
  - Value X characterizes the maximum “fine” RX beams antenna gain difference within N^{th} percentile EIS
    - X is derived based on EIS spherical coverage requirement (i.e. difference between the peak EIS and N^{th} percentile EIS values) based on TS 38.101-2 [16].
    - Value of N according to power class, as defined in TS 38.101-2 [16] clause 7.3.4.

6.2.1.4.6 Scenario 2 (1AoA RX non-beam peak) for Type 2 Requirements (“Rough” RX beams) and Mode 1 Configuration (S+N)

The Noc is derived similar as 6.2.1.4.3 with the following exception:

- Noc level is increased by X + Z, where:
  - Value X is same as defined in clause 6.2.1.4.5
  - Value Z characterizes the antenna gain difference between “fine” and “rough” RX beams within N^{th} percentile EIS directions
    - Z = [TBD] dB for power class 3 UE.
    - Value of N according to power class, as defined in TS 38.101-2 [16] clause 7.3.4.

6.2.1.4.7 Scenario 3 (2AoA) for Mode 1 Configuration (S+N)

For Scenario 3 with 2 AoA both probes transmit noise signal with same power level Noc. The Noc level is same as the value in Scenario 2 defined in section 6.2.1.4.5 for the case of using “Fine” beams and in section 6.2.1.4.6 for the case of using “Rough” beams.

6.3 Summary of initial uncertainty assessment

The detailed analysis of MU factors affecting DL SNR and power level accuracy/range is provided in Annex B.2.

7 UE demodulation and CSI testing methodology

7.1 General

This clause describes the testing methodology for NR UE demodulation and CSI reporting for FR2. Unless otherwise indicated below, device under test (DUT) refers to UE nodes. The exact list of demodulation and CSI reporting tests for

the UE can only be determined once the core requirements are settled and the test methodologies are considered in generic way to allow testing of typical UE demodulation CSI metrics.

For frequency bands above 6 GHz (e.g. mm-wave), conducted antenna connectors are assumed not to be available at DUT and the OTA testing is considered as the baseline approach for NR UE demodulation and CSI test methodology.

The possibility of performing conducted tests using an intermediate frequency (IF) were evaluated. It was decided that this approach would be challenging to standardise for various reasons since IF is an internal interface in the DUT and using a standardised IF (signal level, number of IF ports, IF frequency etc.) would preclude many different DUT implementations including direct conversion receivers. In addition, IF testing excludes all components which operate at the radio frequency such as RF filters, duplexers, transmit receive switch, low noise amplifier (LNA), power amplifier (PA), analogue beamforming phase shifting elements etc., and the algorithms which control such components from the test.

7.2 Measurement setup

7.2.1 Baseline setup

7.2.1.1 Description

The baseline measurement setup of NR UE demodulation and CSI characteristics for frequency bands above 6GHz is capable of establishing an OTA link between the DUT and a number of emulated gNB sources with one angle of arrival (AoA) to the UE, and is shown in Figure 7.2.1.1-1 below.

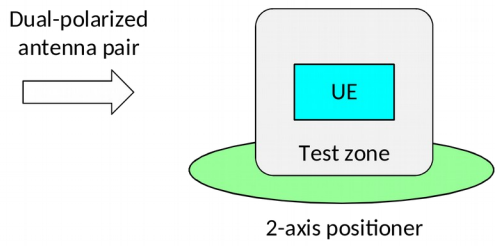

Figure 7.2.1.1-1: Baseline measurement setup for UE demodulation and CSI characteristics testing

The key aspects of the baseline setup are:

- Test is conducted in an anechoic chamber
  - The test shall be performed in the radiative near field or in the far field
  - The minimum measurement distance is described in 7.2.1.2
- The following permitted test setups are considered
  - Permitted test setups for UE RF including DFF and IFF as described in Clause 5.
  - Direct near field (DNF) test setup
    - Note: No final conclusions on the feasibility of DNF setup were made.
- One TRxP with a dual-polarized measurement antenna directed at the DUT
- Propagation Conditions
  - Test method shall allow modelling of the following propagation conditions between the DUT and the emulated gNB sources
    - Multi-path fading propagation conditions

        - Multi-path fading propagation conditions between the DUT and the emulated gNB sources are modelled as Single probe channel models as described in subclause 8.2.

    - Static propagation conditions

- A positioning system such that the angle between the dual-polarized measurement antenna and the DUT has at least two axes of freedom

- The test method shall achieve isolation between two nominally orthogonal paths from the dual-polarised TRxP to the DUT, enabling independent control of the signals reaching each baseband receiver

    - Test method supports up to DL MIMO rank 2 transmissions

    - DUTs shall support power measurement per receiver port (SS-RSRPB). Measurement equipment may use SS-RSRPB reporting from the DUT to achieve isolation and to enable independent control of the signals reaching each baseband receiver.

    - SS-RSRPB measurements and reporting are done under noise-free conditions and use static channel conditions.

    - Once established, the setup is expected to be fixed and to be used with UE Tx/Rx beamlock to allow testing of DUT baseband features under a “virtually cabled” scenario.

    - Baseline setup includes a capability to select the best UE RX beam during initial call setup.

- Support of UE demodulation and CSI requirements verification for interworking scenarios

    - For setups intended for measurements of UE demodulation and CSI characteristics in non-standalone (NSA) mode, an LTE link antenna is used to provide the LTE link to the DUT. The LTE link antenna provides a stable and noise-free LTE signal without precise path loss or polarization control. No performance verification for LTE carriers is supported.

    - For setups intended for measurements of UE demodulation and CSI characteristics in NR CA mode with FR1 and FR2 inter-band NR CA, test setup provides NR FR1 link to the DUT. The NR FR1 link has a stable and noise-free signal without precise path loss or polarization control. No performance verification for NR FR1 carriers is supported.

- The test system shall allow the following modes of noise emulation for UE demodulation testing:

    - Emulation of fixed SNR conditions at the DUT

    - Emulation of noise-free conditions at the DUT

- Measurement system shall support the TX EVM (transmit signal error vector magnitude) not worse than 6% for QPSK/16QAM/64QAM performance requirements.

- The baseline setup shall allow identification of the DUT RX beam peak direction

    - Note: RX beam peak search procedure for the DNF setup is undefined.

- Applicability Criteria:

    - In case a DNF test setup is used, the system applies at least to DUTs with a device size of $D \leq 15$cm with no manufacturer declaration and corresponding SNR calculations in Annex B.3.1 need to be used.

    - In case a DFF or IFF test system is used that leverages the permitted methods for UE RF, the same applicability criteria as in Clause 5.2 apply and corresponding SNR calculations in Annex B.3.2 and B.3.3 respectively need to be used.

7.2.1.2 Measurement distance

The test shall be performed in the radiative near field (limit of the Fresnel region) or in the far field. The minimum measurement distance *R* is defined according to the following formula:

$$R > 0.62\sqrt{\frac{D^3}{\lambda}}$$

where D is the DUT radiating aperture, and λ is the wavelength.

In case a test system is used that leverages the permitted methods for UE RF, the same measurement distance as in Clause 5 apply.

7.2.1.3 Test parameters

The following main test parameters shall be controlled by measurement equipment for UE Demodulation and CSI reporting testing.

- SNR of DL signal at reference point
- Faded DL channel

For a DNF setup the reference point for SNR of DL signal is defined as the intersection of the axes of rotation of the positioning system(s). For a DFF or IFF setups the reference point for SNR of DL signal is defined as the geometrical center of the QZ. From the UE perspective the reference point is the input of UE antenna array.

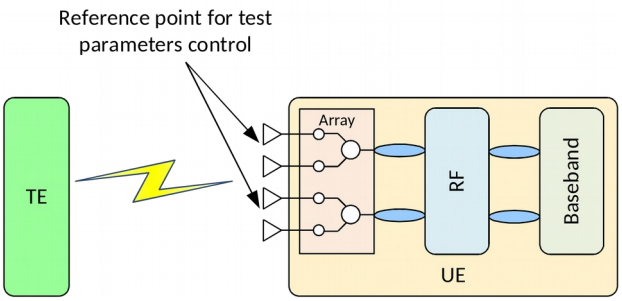

Figure 7.2.1.3-1: DL SNR reference point for UE Demodulation and CSI testing methodology

The performance requirements in TS 38.101-4 [18] will be specified at the Reference point, according to the following principles:

- Test system will transmit the useful signal and noise signals to emulate target SNR condition
- Specify absolute Noc level at the Reference point
  - Noc level may have different value according to operating band and UE Power class
- Specify SNR_{RP} at the Reference point
  - SNR_{RP} is a test-specific value
- Downlink signal and noise are aligned to the Rx beam peak direction

Simulations for UE demodulation and CSI are normally run at baseband, with results expressed as SNR_{BB}, and do not take into account the noise of the UE RF front end. For over-the-air testing it is not feasible in practice to use signal levels high enough to make the noise of the UE RF front end negligible. The approach below has been agreed:

- Set wanted noise to give 1dB difference between Reference point SNR and Baseband SNR, using agreed UE requirements, so $SNR_{RP} = SNR_{BB} + 1dB$
- Figure 7.2.1.3-2 shows the principle

The Noc values are based on Refsens for the Operating band and on the UE Power class, and taking a baseline of UE Power class 3 in Band n260.

$$Noc = Refsens_{PC3,\ n260,\ 50MHz} - 10\log_{10}(SCS_{Refsens} \times PRB_{Refsens} \times 12) - SNR_{Refsens} + \Delta_{thermal}$$

where:

- $Refsens_{PC3, n260, 50MHz}$ is the Refsens value in dBm specified for Power Class 3 in Band n260 for 50MHz Channel bandwidth in TS 38.101-2 [16] Table 7.3.2.3-1, [dBm/Hz]
- $SCS_{Refsens}$ is a subcarrier spacing associated with N_{RB} for 50MHz in TS 38.101-2 [16] Table 5.3.2-1, chosen as 120kHz.
- $PRB_{Refsens}$ is N_{RB} associated with subcarrier spacing 120kHz for 50MHz in TS 38.101-2 [16] Table 5.3.2-1 and is 32.
- 12 is the number of subcarriers in a PRB
- $SNR_{Refsens}$ is the SNR used for simulation of Refsens, and is -1dB
- $\Delta_{thermal}$ is the amount of dB that the wanted noise is set above UE thermal noise, giving a rise in total noise of Δ_{BB}. $\Delta_{thermal}$ is chosen as 6dB, giving a rise in total noise of 1dB.

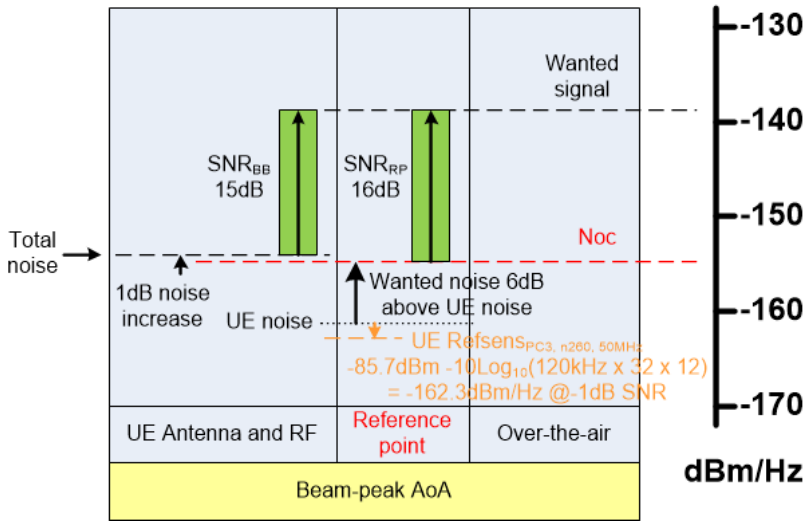

Figure 7.2.1.3-2: Reference point SNR_{RP} and Baseband SNR_{BB}

The calculated Noc value for the baseline of UE Power class 3 in Band n260 is rounded to -155dBm/Hz.

The following methodology to define the minimum Noc level for power class X (PC_X) and operating band Y (Band_Y) is used for the single carrier case and a single band device:

$$Noc(PC\_X, Band\_Y) = -155\ dBm/Hz + Refsens_{PC\_X, Band\_Y, 50MHz} - Refsens_{PC3, n260, 50MHz}$$

where Refsens values are specified in TS 38.101-2 [16] Table 7.3.2.3-1.

The following methodology to define the minimum Noc level for power class X (PC_X) and operating band Y (Band_Y) is used for the single carrier case and a multi-band device:

$$Noc(PC\_X, Band\_Y) = -155\ dBm/Hz + Refsens_{PC\_X, Band\_Y, 50MHz} - Refsens_{PC3, n260, 50MHz} + \Sigma MB_P$$

where Refsens and ΣMB_P values are specified in TS 38.101-2 [16].

7.2.1.4 Test metrics

The test method shall allow testing of typical UE Demodulation and CSI metrics similar to the metrics used of LTE, including at least:

- Absolute PDSCH throughput
- Block-error rate performance for different DL physical channels (e.g. PDCCH)
- CSI statistics (e.g. CQI accuracy, throughput ratio for different CSI or test settings, etc.)

7.3 Summary of initial uncertainty assessment

The detailed analysis of MU factors affecting DL SNR accuracy/range measurement uncertainty is provided in Annex B.3.1.

8 Propagation conditions

8.1 General

Test methods shall allow modelling of the following propagation conditions between the DUT and the emulated gNB sources:

- Multi-path fading propagation conditions
    - Fading propagation conditions between the DUT and the emulated gNB sources are modelled as Single probe channel models as described in subclause 8.2.
    - Applicable to the UE RRM testing methodology and UE Demodulation and CSI testing methodology.
- Static propagation conditions
    - Model is described in subclause 8.3.
    - Applicable to the UE RRM testing methodology and UE Demodulation and CSI testing methodology.

8.2 Multi-path fading propagation conditions

Multi-path fading propagation conditions between the DUT and the emulated gNB sources are modelled as Single probe channel models.

8.2.1 Single probe channel modelling methodology

Two options for Single probe channel modelling methodology were identified as described in subclause 8.2.1.1 and 8.2.1.2, including details on generating each single probe channel option.

Both Option 1 and Option 2 methodologies were concluded as feasible from test equipment perspective. Selection between the methodologies and the selection of specific parameters (e.g. power delay profile) are to be done in the scope of Rel. 15 NR UE performance requirements work.

FR2 measurement system is expected to support modelling of multi-path fading for single carrier scenarios with channel bandwidth of at least 200 MHz. The support of channel modelling for CA scenarios is not precluded.

8.2.1.1 Channel model Option 1

Channel model option 1 is based on the TDL methodology in the TR 38.901 [10]:

- The multi-path propagation conditions model consists of several parts:
    - A power delay profile in the form of a “tapped delay-line” (TDL), characterized by a number of taps with certain power at fixed positions on a sampling grid.
    - The channel model parameters include the Delay spread scaling factor and the maximum Doppler frequency. The test system shall allow flexible control of the respective parameters.
- Each tap is modeled based on the Jakes fading model.
- Generation of TDL channel models and power delay profiles from CDL channel models by including spatial filters to capture Tx and Rx antenna patterns is not precluded and based on the procedure described in the TR 38.901 [10].

The method to generate fading coefficients (Jakes fading model) satisfying the target parameters is not specified in [10]. Traditionally, there has been two methods to implement this type of tapped delay line models:

- The first alternative is to use the noise filtering, where the Doppler power spectrum is realized by Doppler spectrum shaping filtering of i.i.d. complex Gaussian noise sample sequences. This step is followed by generating the MIMO correlations between sequences by multiplying them with factored target MIMO correlation matrix. The matrix has dimensions US x US, where U and S denote the number of Rx and Tx antennas, respectively.

- The second alternative is the sum-of-sinusoids method, where the temporal characteristics (Doppler power spectrum) are generated by summing a number of sinusoids with specific phase, amplitude and frequency characteristics. This step is followed by generating the MIMO correlations between sequences by multiplying them with factored target MIMO correlation matrix. The matrix has dimensions US x US, where U and S denote the number of Rx and Tx antennas, respectively.

8.2.1.2 Channel model Option 2

This subclause considers channel model methodology with non-Jakes spectrum. Multi-path fading propagation conditions between the gNB emulator and test chamber probe is modelled based on Clustered Delay Line (CDL) methodology in TR 38.901 [10]. Doppler Spread and MIMO correlation related to such methodology is defined in subclauses 8.2.1.2.1 and 8.2.1.2.2 respectively.

To generate the multi-path fading propagation conditions, the following step by step procedure modified from [10] should be used to generate channel coefficients using the CDL models:

Step 1: Generate cluster delays $\tau_{n,\mathrm{scaled}}$ (from subclause 7.7.3 in [10])

The RMS delay spread values of CDL models are normalized and they must be scaled in delay so that a desired RMS delay spread can be achieved. The scaled delays can be obtained according to the following equation:

$$\tau_{n,\mathrm{scaled}} = \tau_{n,\mathrm{model}} \cdot \mathrm{DS}_{\mathrm{desired}} \qquad (8.2.1.2\text{-}1)$$

in which

- $\tau_{n,\mathrm{model}}$ is the normalized delay value of the *n*th cluster in a CDL in Tables 7.7.1.1 – 7.7.1.5 of [10]
- $\tau_{n,\mathrm{scaled}}$ is the new delay value (in [ns]) of the *n*th cluster
- $\mathrm{DS}_{\mathrm{desired}}$ is the wanted delay spread (in [ns]) and it must be specified as a channel model parameter

Step 1.1: In the case of LOS models (D and E) scale cluster the powers as specified in subclause 7.7.6 of [10]. The target Ricean K-factor values K_{desired} must be specified.

Step 2: Generate departure and arrival angles (based on subclause 7.7.1 step 1 in [10] combining 7.7-5 and part of step 7 in subclause 7.5 in [10] adding some clarifications to the parameters considered)

Generate arrival angles of azimuth using the following equation

$$\phi_{n,m,\mathrm{AOA,scaled}} = \frac{\mathrm{AS}_{\mathrm{desired}}}{\mathrm{AS}_{\mathrm{model}}}\left(\phi_{n,\mathrm{AOA}} + c_{\mathrm{ASA}}\alpha_m - \mu_{\phi,\mathrm{model}}\right) + \mu_{\phi,\mathrm{model}}, \qquad (8.2.1.2\text{-}2)$$

where

- $\phi_{n,\mathrm{AOA}}$ and c_{ASA} are the cluster AOA and the cluster-wise rms azimuth spread of arrival angles (cluster ASA), respectively, in Tables 7.7.1.1 – 7.7.1.5 of [10]

- α_m denotes the ray offset angles within a cluster given by Table 7.5-3 of [10],

- $\mu_{\phi,\mathrm{model}} = \arg\left[\sum_{n=1}^{N}\sum_{m=1}^{M}\exp\left(j\phi_{n,m}\right)P_{n,m}^{\mathrm{linear}}\right]$ is the mean angle of the original channel model table in NLOS case (equation is specified in Annex A.2 of [10]) and the LOS angle $\mu_{\phi,\mathrm{model}} = \phi_{1,AOA}$ in LOS case,

- $\mathrm{AS}_{\mathrm{model}}$ are the angular spreads. derived[1)] from the original CDL Tables 7.7.1.1 – 7.7.1.5 of [10], they are listed in Table 8.2.1.2-1

- $\mathrm{AS}_{\mathrm{desired}}$ is the wanted angular spread. It must be specified.

The angular scaling according to eq. (2) is applied to the ray angles and no further scaling is performed. The generation of AOD ($\phi_{n,m,\mathrm{AOD}}$), ZSA ($\theta_{n,m,\mathrm{ZOA}}$), and ZSD ($\theta_{n,m,\mathrm{ZOD}}$) follows a procedure similar to AOA as described above.

Note: The azimuth angles may need to be wrapped around to be within [0, 360] degrees, while the zenith angles may need to be clipped to be within [0, 180] degrees.

[1)] *The angular spread in this case is the rms angular spread without finding the minimum value over angular rotations.*

Table 8.2.1.2-1. Original (non-circular) angle spreads of CDL models.

Model	$\mathrm{AS}_{\mathrm{model}}$ [deg]			
	ASD	ASA	ZSD	ZSA
CDL-A	73.7	85.3	28.6	21.1
CDL-B	41.6	59.3	6.0	10.4
CDL-C	39.1	71.1	4.1	10.4
CDL-D	19.0	21.1	3.0	1.9
CDL-E	13.2	37.6	1.5	2.5

Table 8.2.1.2-1 contains the angle spread values of the original CDL models of 38.901 ([2]) before any angular scaling. The values are calculated for the angles AOD, AOA, ZOD, and ZOA angles after removing the mean angle $\phi_n - \mu_{\phi,\mathrm{model}}$ following the definition of rms angular spread in TR25.997, without finding the minimum over circular shifts.

Step 3: Coupling of rays within a cluster for both azimuth and elevation (based on step 2 in 7.7.1 in [10] assuming fix coupling instead of random)

Couple AOD angles $\phi_{n,m,\mathrm{AOD}}$ to AOA angles $\phi_{n,m,\mathrm{AOA}}$ within a cluster *n*. Couple ZOD angles $\theta_{n,m,\mathrm{ZOD}}$ with ZOA angles $\theta_{n,m,\mathrm{ZOA}}$ using the same procedure. Couple AOD angles $\phi_{n,m,\mathrm{AOD}}$ with ZOD angles $\theta_{n,m,\mathrm{ZOD}}$ within a cluster *n*. Instead of random procedure, the coupling is performed using the fixed coupling pattern. It must be specified.

Step 4: Generate the cross-polarization power ratios (from subclause 7.7.1 step 3 in [10])

Calculate the linear cross polarization power ratios (XPR) κ for each ray *m* of each cluster *n* as

$$\kappa_{n,m} = 10^{X/10}, \qquad (8.2.1.2\text{-}3)$$

where *X* is the per-cluster XPR in dB and must be specified.

Step 5: Specify gNB beam pattern (based on subclause 7.3 of [10] plus assumptions for gNB antenna)

With definitions and symbols of subclause 7.3 of [10] (except substitute N:=N_e, M:=M_e to avoid ambiguity), specify parameters (M_g, N_g, M_e, N_e, P) and (d_H, d_V).

Antenna element radiation patterns, including orientation of the element main polarization components as well as orientation of the antenna array should be specified.

It is assumed the co-polarized elements of the array are combined to a single RF port, i.e. they compose an antenna array that can form beams by setting certain weights per element. Weight vector for the first polarization and for the second polarization is

$$[\alpha_{1,1} \dots \alpha_{M_g,N_g}] = \left\{\frac{1}{N_g M_g}\exp\left(-j2\pi\frac{\hat{r}_{tx,max}^{T} * \bar{d}_{tx,m_g,n_g}}{\lambda_0}\right)\right\} \in \mathbb{C}^{1xN_gM_g} \quad (8.2.1.2\text{-}4)$$

where $\bar{d}_{tx,m_e,n_e}$ is the location vector of transmit antenna element $m_g = 1, \dots, M_g$ and $n_g = 1, \dots, N_g$.

Step 6: Specify initial phases

Instead of drawing initial phases $\left\{\Phi_{n,m}^{\theta\theta}, \Phi_{n,m}^{\theta\phi}, \Phi_{n,m}^{\phi\theta}, \Phi_{n,m}^{\phi\phi}\right\}$ randomly for each ray *m* of each cluster *n* and for four different polarisation combinations ($\theta\theta$, $\theta\phi$, $\phi\theta$, $\phi\phi$), initial phases must be specified.

Step 7: Coefficient generation (based on step 4 in [10])

Follow the same procedure as in Steps 10 and 11 in Subclause 7.5 in [10], with the exception that all clusters are treated as "weaker cluster", i.e. no further sub-clusters in delay should be generated[2]. Additional clusters representing delay spread of the stronger clusters are already provided in Tables 7.7.1.1 – 7.7.1.5 in [10]. Once weight vector in equation 4 is combined with eq. (7.5-22) and eq. (7.5-29) in [10], the following equations apply respectively:

$$H_{u,s,n}^{NLOS}(t) = \sqrt{\frac{P_n}{M}}\sum_{m=1}^{M}\sum_{n_e=1}^{N_e}\sum_{m_e=1}^{M_e}\begin{bmatrix}F_{rx,u,\theta}(\theta_{n,m,ZOA},\phi_{n,m,AOA})\\F_{rx,u,\phi}(\theta_{n,m,ZOA},\phi_{n,m,AOA})\end{bmatrix}^{T}\begin{bmatrix}\exp(j\Phi_{n,m}^{\theta\theta}) & \sqrt{k_{n,m}}^{-1}\exp(j\Phi_{n,m}^{\theta\phi})\\ \sqrt{k_{n,m}}^{-1}\exp(j\Phi_{n,m}^{\phi\theta}) & \exp(j\Phi_{n,m}^{\phi\phi})\end{bmatrix}\begin{bmatrix}F_{tx,s,\theta}(\theta_{n,m,ZOD},\phi_{n,m,AOD})\\F_{tx,s,\phi}(\theta_{n,m,ZOD},\phi_{n,m,AOD})\end{bmatrix}exp\left(\frac{j2\pi(\hat{r}_{rx,n,m}^{T}\cdot\bar{d}_{rx,u})}{\lambda_0}\right)exp\left(\frac{j2\pi(\hat{r}_{rx,n,m}^{T}\cdot\bar{d}_{tx,m_e,n_e})}{\lambda_0}\right)\cdot\alpha_{m_e,n_e}\cdot exp\left(j2\pi\frac{\hat{r}_{rx,n,m}^{T}\cdot\bar{v}}{\lambda_0}t\right) \quad (8.2.1.2\text{-}5)$$

$$H_{u,s,n}^{LOS}(t) = \sum_{n_e=1}^{N_e}\sum_{m_e=1}^{M_e}\begin{bmatrix}F_{rx,u,\theta}(\theta_{LOS,ZOA},\phi_{LOS,AOA})\\F_{rx,u,\phi}(\theta_{LOS,ZOA},\phi_{LOS,AOA})\end{bmatrix}^{T}\begin{bmatrix}1 & 0\\0 & -1\end{bmatrix}\begin{bmatrix}F_{tx,s,\theta}(\theta_{LOS,ZOD},\phi_{LOS,AOD})\\F_{tx,s,\phi}(\theta_{LOS,ZOD},\phi_{LOS,AOD})\end{bmatrix}\exp\left(-j2\pi\frac{d_{3D}}{\lambda_0}\right)exp\left(j2\pi\frac{\hat{r}_{rx,LOS}^{T}\cdot\bar{d}_{rx,u}}{\lambda_0}\right)exp\left(j2\pi\frac{\hat{r}_{rx,LOS}^{T}\cdot\bar{d}_{tx,m_e,n_e}}{\lambda_0}\right)\cdot\alpha_{m_e,n_e}\cdot exp\left(j2\pi\frac{\hat{r}_{rx,LOS}^{T}\cdot\bar{v}}{\lambda_0}t\right) \quad (8.2.1.2\text{-}6)$$

where s goes from 1 to S, being S the number of gNB RF ports

[2] *Note: This may need to be changed such that the three rows of CDL tables containing equal angular parameters are treated as a single cluster with three mid-paths as in Step 11 of Subclause 7.5 in [10].*

As shown above, this model is using following parameters

- Base CDL model from CDL models defined in [10, Subclause 7.7.1] characterized by normalized delay, power, AOA, AOD, ZOA and ZOD for each cluster; delay spread, angular spread and mean angle for AOA, AOD, ZOA and ZOD. Further simplification of CDL models in [10, Subclause 7.7.1] can be defined in UE demodulation performance discussion.
- Emulated gNB related parameters: gNB antenna field pattern, gNB antenna orientation and polarization
- Emulated UE related parameters: UE antenna field pattern, UE antenna orientation and polarization, UE speed and direction
- Initial phases $\left\{\Phi_{n,m}^{\theta\theta}, \Phi_{n,m}^{\theta\phi}, \Phi_{n,m}^{\phi\theta}, \Phi_{n,m}^{\phi\phi}\right\}$ for each ray *m* of each cluster *n* for NLOS paths and distance d_{3D} (explained in [10, Figure 7.4.1-1] to model LOS path loss) for LOS path.
- Tx/Rx beam selection procedure between emulated gNB and emulated UE antenna
- Ricean K factor for LOS CDL base models
- Carrier Frequency
- Fixed pairing between angles of arrival and angles of departure in Step 2 described in [10, Subclause 7.7.1].

8.2.1.2.1 MIMO Correlation

From equation 7.5-22 in [10], fading coefficients are generated per Tx per Rx for each cluster. Therefore, MIMO correlation matrix can be computed from those coefficients for each cluster. So, MIMO correlation matrix spectrum is implicit in the way we generate the fading channel coefficients and does not need to be modelled explicitly.

It is noted that the MIMO correlation can be controlled by introducing Ricean K-factor to all model scenarios and setting the K-factor properly. Alternatively, the MIMO correlation can be controlled by modifying the XPR parameter. However, this depends on the selected antenna model.

8.2.2 Path Delay grid for channel models

The path delay grid for the channel models is defined as equidistant delay grid n*ΔT with $n \in N_0$. From the test methodology perspective it is feasible to support $\Delta T \leq 1/F_{sample}$.

For single carrier scenarios with channel bandwidth up to 200MHz, the F_{sample} is defined as 200 MHz and $\Delta T \leq 5$ ns. For the channel models definition for the requirements definition a fixed quantization grid can be used (e.g. $\Delta T = 5$ns).

For intra-band CA scenarios the F_{sample} requires further studies. The F_{sample} used for these scenarios will be discussed and decided as part of the NR work item performance part.

In case multiple taps of the original delay profile end up with the same delay, the powers of the individual taps are added, resulting in a single path with the combined power.

Each tap of the scaled delay profile shall be mapped to the closest point of the delay grid defined by n*ΔT. In case a tap in the delay profile lies equidistant between two points of the delay grid, it shall be mapped to the larger delay grid point.

An example for mapping the delays for a scaled power delay profile to the equidistant delay grid is given in clause 8.2.2.1.

8.2.2.1 Example for determining the resulting delay profile

A power delay profile after delay spread scaling is given as follows in Table 8.2.2.1-1.

Table 8.2.2.1-1: Original power delay profile

Tap *k*	Power σ^{k2} (linear)	Delay τ_k [ns]
1	σ_1^2	0
2	σ_2^2	8
3	σ_3^2	23
4	σ_4^2	26
5	σ_5^2	27
6	σ_6^2	33

With the assumption of ΔT = 1/(200 MHz) = 5 ns the taps from Table 8.2.2.1-1 can be mapped onto an equidistant delay grid as shown in Table 8.2.2.1-2.

Table 8.2.2.1-2: Power delay profile after mapping to delay grid

Tap *k*	Power σ^{k2} (linear)	Delay τk [ns]
1	σ_1^2	0
2	σ_2^2	10
3	σ_3^2	25
4	σ_4^2	25
5	σ_5^2	25
6	σ_6^2	35

Since multiple taps share the same delay, those taps need to be combined into a single tap as shown in Table 8.2.2.1-3.

Table 8.2.2.1-3: Resulting delay profile

Tap k	Power σ^{k2} (linear)	Delay τk [ns]
1	σ_1^2	0
2	σ_2^2	10
3	$\sigma_3^2 + \sigma_4^2 + \sigma_5^2$	25
4	σ_6^2	35

Figure 8.2.2.1-1 shows the original and resulting delay grid.

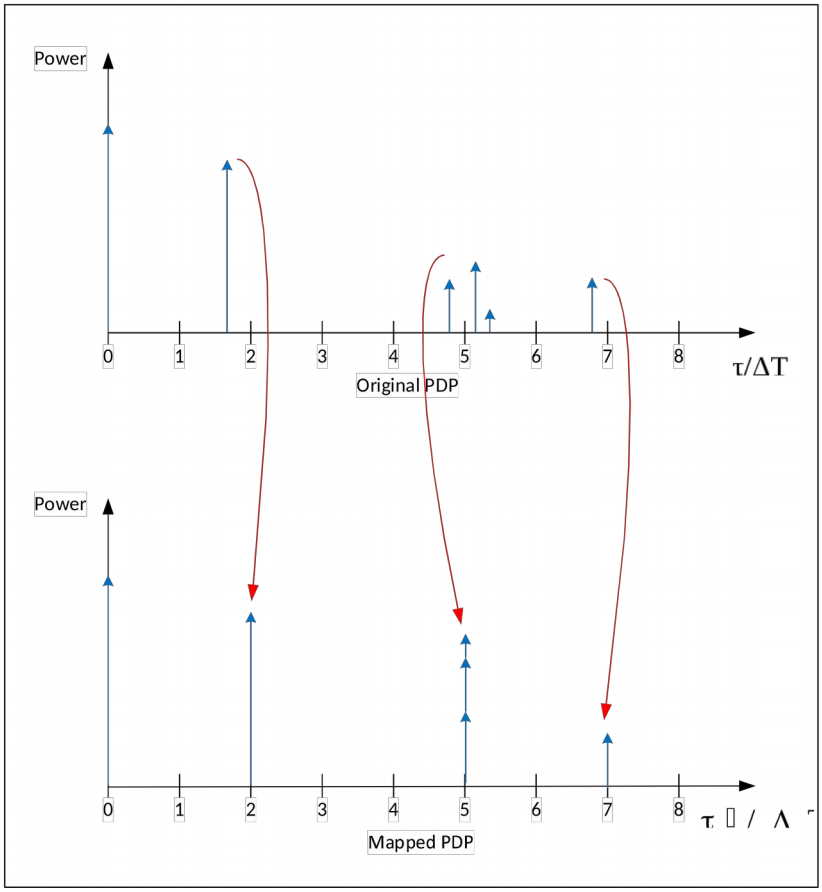

Figure 8.2.2.1-1: Original and resulting delay profile

8.3 Static propagation conditions

The test methods shall allow emulation of the following static propagation conditions for the UE with 2RX antenna port as follows.

For 1 port transmission the emulated channel matrix is defined in the frequency domain by

$$\mathbf{H} = \begin{bmatrix} 1 \\ 1 \end{bmatrix}.$$

For 2 port transmission the emulated channel matrix is defined in the frequency domain by

$$\mathbf{H} = \begin{bmatrix} 1 & j \\ 1 & -j \end{bmatrix}.$$

Note: Channel matrices above for static propagation conditions are the channel matrices generated by the channel emulator.

Annex A:
Environment conditions

A.1 Operating voltage

All nominal voltage test cases shall be performed with the DUT operated in stand-alone battery powered mode except for DUTs whose power is provided only from AC mains. For extreme voltage test cases, the UE shall fulfil all the requirements in the full voltage range, i.e. the voltage range between the extreme voltages. When those test cases require an external power source with cables connected to the DUT that could adversely affect the device performance, it shall be demonstrated that there is negligible impact to performance with the device operated in stand-alone battery powered mode compared to the device operated in external power mode first before performing the extreme voltage test cases.

Annex B:
Measurement uncertainty

B.1 Measurement uncertainty budget for UE RF testing methodology

B.1.1 Direct far field (DFF) setup

B.1.1.1 Uncertainty budget calculation principle

The uncertainty tables should be presented with two stages:

- Stage 1: the calibration of the absolute level of the DUT measurement results is performed by means of using a calibration antenna whose absolute gain is known at the frequencies of measurement
- Stage 2: the actual measurement with the DUT as either the transmitter or receiver is performed.

The MU budget should comprise of a minimum 5 headings:

1) The uncertainty source,
2) Uncertainty value,
3) Distribution of the probability,
4) Divisor based on distribution shape,
5) Calculated standard uncertainty (based on uncertainty value and divisor).

B.1.1.2 Uncertainty budget format

Table B.1.1.2-1: Uncertainty contributions for EIRP and TRP measurement

UID	Description of uncertainty contribution	Details in annex
Stage 2: DUT measurement		
1	Positioning misalignment	B.1.1.4.1
2	Measure distance uncertainty	B.1.1.4.2
3	Quality of quiet zone	B.1.1.4.3
4	Mismatch	B.1.1.4.4
5	Absolute antenna gain uncertainty of the measurement antenna	B.1.1.4.5
6	Uncertainty of the RF power measurement equipment	B.1.1.4.6
7	Phase curvature	B.1.1.4.7
8	Amplifier uncertainties	B.1.1.4.8
9	Random uncertainty	B.1.1.4.9
10	Influence of the XPD	B.1.1.4.10
Stage 1: Calibration measurement		
11	Mismatch	B.1.1.4.4
12	Reference antenna positioning misalignment	B.1.1.4.11
13	Quality of quiet zone for calibration process	B.1.1.4.18
14	Amplifier uncertainties	B.1.1.4.8
15	Uncertainty of the Network Analyzer	B.1.1.4.12
16	Reference antenna feed cable loss measurement uncertainty	B.1.1.4.13
17	Uncertainty of an absolute gain of the calibration antenna	B.1.1.4.14
18	Positioning and pointing misalignment between the reference antenna and the receiving antenna	B.1.1.4.15
19	Phase centre offset of calibration antenna	B.1.1.4.17

Table B.1.1.2-2: Uncertainty contributions for EIS measurement

UID	Description of uncertainty contribution	Details in annex
Stage 2: DUT measurement		
1	Pointing misalignment	B.1.1.4.1
2	Measure distance uncertainty	B.1.1.4.2
3	Quality of quiet zone	B.1.1.4.3
4	Mismatch	B.1.1.4.4
5	gNB emulator uncertainties	B.1.1.4.16
6	Absolute antenna gain uncertainty of the measurement antenna	B.1.1.4.5
7	Phase curvature	B.1.1.4.7
8	Influence of the XPD	B.1.1.4.10
9	Amplifier uncertainties	B.1.1.4.8
10	Random uncertainty	B.1.1.4.9
Stage 1: Calibration measurement		
11	Mismatch	B.1.1.4.4
12	Reference antenna positioning misalignment	B.1.1.4.11
13	Quality of quiet zone for calibration process	B.1.1.4.18
14	Amplifier uncertainties	B.1.1.4.8
15	Uncertainty of the Network Analyzer	B.1.1.4.12
16	Phase curvature	B.1.1.4.7
17	Uncertainty of an absolute gain of the calibration antenna	B.1.1.4.14
18	Positioning and pointing misalignment between the reference antenna and the receiving antenna	B.1.1.4.15
19	Phase centre offset of calibration antenna	B.1.1.4.17

B.1.1.3 Uncertainty assessment

The uncertainty assessment tables are organized as follows:

- For the purpose of uncertainty assessment, the radiating antenna aperture of the DUT is denoted as D, and the uncertainty assessment has been derived for the case of D = 5 cm

- The uncertainty assessment for EIRP and TRP, assuming D = 5 cm, is provided in Table B.1.1.3-1
- The uncertainty assessment for EIS, assuming D = 5 cm, is provided in Table B.1.1.3-2

Table B.1.1.3-1: Uncertainty assessment for EIRP and TRP measurement (D = 5 cm)

UID	Uncertainty source	Uncertainty value	Distribution of the probability	Divisor	Standard uncertainty (σ) [dB]
Stage 2: DUT measurement					
1	Positioning misalignment	0.50	Rectangular	1.73	[0.29]
2	Measure distance uncertainty	1.00	Rectangular	1.73	[0.58]
3	Quality of quiet zone (NOTE 2)	1.50	Actual	1.00	[1.50]
4	Mismatch (NOTE 3)	1.30	Actual	1.00	[1.30]
5	Absolute antenna gain uncertainty of the measurement antenna	0.00	Normal	2.00	0.00
6	Uncertainty of the RF power measurement equipment (NOTE 4)	2.16	Normal	2.00	[1.08]
7	Phase curvature	0.00	U-shaped	1.41	0.00
8	Amplifier uncertainties	2.00	Normal	2.00	1.00
9	Random uncertainty	0.40	Rectangular	1.73	[0.23]
10	Influence of the XPD	0.68	U-shaped	1.41	0.48
Stage 1: Calibration measurement					
11	Mismatch	0.00	U-shaped	1.41	0.00
12	Reference antenna positioning misalignment	0.29	Rectangular	1.73	0.17
13	Quality of quiet zone for calibration process (NOTE 2)	1.50	Actual	1.00	[1.50]
14	Amplifier uncertainties	0.00	Normal	2.00	0.00
15	Uncertainty of the Network Analyzer	0.40	Normal	2.00	0.20
16	Reference antenna feed cable loss measurement uncertainty	0.29	Rectangular	1.73	0.17
17	Uncertainty of an absolute gain of the calibration antenna	1.60	Normal	2.00	[0.80]
18	Positioning and pointing misalignment between the reference antenna and the receiving antenna	0.35	Rectangular	1.73	[0.20]
19	Phase centre offset of calibration antenna	0.62	Rectangular	1.73	[0.36]
EIRP Expanded uncertainty (1.96σ - confidence interval of 95 %) [dB]					[6.20]
TRP Expanded uncertainty (1.96σ - confidence interval of 95 %) [dB]					[5.37]

NOTE 1: The impact of phase variation on EIRP shall be taken into account during final MU definition for the test method.
NOTE 2: The quality of quiet zone is different for EIRP and TRP. For TRP, the standard uncertainty is [1dB]; for EIRP, the standard uncertainty of quiet zone is [1.5dB].
NOTE 3: The analysis was done only for the case of operating at max output power, in-band, non-CA.
NOTE 4: The assessment assumes maximum DUT output power.

Table B.1.1.3-2: Uncertainty assessment for EIS measurement (D = 5 cm)

UID	Uncertainty source	Uncertainty value	Distribution of the probability	Divisor	Standard uncertainty (σ) [dB]
Stage 2: DUT measurement					
1	Pointing misalignment	0.50	Rectangular	1.73	[0.29]
2	Measure distance uncertainty	1.00	Rectangular	1.73	[0.58]
3	Quality of quiet zone	1.50	Actual	1.00	[1.50]
4	Mismatch (NOTE 2)	1.30	Actual	1.00	[1.30]
5	gNB emulator uncertainties	3.34	Normal	2.00	[1.67]
6	Absolute antenna gain uncertainty of the measurement antenna	0.00	Normal	2.00	0.00
7	Phase curvature	0.00	U-shaped	1.41	0.00
8	Influence of the XPD	0.68	U-shaped	1.41	0.48
9	Amplifier uncertainties	2.00	Normal	2.00	1.00
10	Random uncertainty	0.40	Rectangular	1.73	[0.23]
Stage 1: Calibration measurement					
11	Mismatch	0.00	U-shaped	1.41	0.00
12	Reference antenna positioning misalignment	0.29	Rectangular	1.73	0.17
13	Quality of quiet zone for calibration process	1.50	Actual	1.00	[1.50]
14	Amplifier uncertainties	0.00	Normal	2.00	0.00
15	Uncertainty of the Network Analyzer	0.40	Normal	2.00	0.20
16	Phase curvature	0.00	U-shaped	1.41	0.00
17	Uncertainty of an absolute gain of the calibration antenna	1.60	Normal	2.00	[0.80]
18	Positioning and pointing misalignment between the reference antenna and the receiving antenna	0.35	Rectangular	1.73	[0.20]
19	Phase centre offset of calibration antenna	0.62	Rectangular	1.73	[0.36]
EIS Expanded uncertainty (1.96σ - confidence interval of 95 %) [dB]					[6.66]
NOTE 1: The impact of phase variation on EIS shall be taken into account during final MU definition for the test method. NOTE 2: The analysis was done only for the case of operating at max output power, in-band, non-CA.					

B.1.1.4 Measurement error contribution descriptions

B.1.1.4.1 Positioning misalignment

This contribution originates from the misalignment of the testing direction and the beam peak direction of the receiving antenna due to imperfect rotation operation. The pointing misalignment may happen in both azimuth and vertical directions and the effect of the misalignment depends highly on the beamwidth of the beam under test. The same level of misalignment results in a larger measurement error for a narrower beam.

B.1.1.4.2 Measure distance uncertainty

The cause of this uncertainty contributor is due to the reduction of distance between the measurement antenna and the DUT. If the distance of separation is $2D^2$/lambda based on D being the entire device size, then the phase variation is 22.5deg. Whether this is the minimum acceptable criteria of phase taper over the entire DUT is FFS and shall be assessed during final MU definition for the test method. Any reduction in the distance of separation increases the phase variation and creates an error which is DUT dependant. Determination of limit of the error shall be done during final MU definition for the test method.

B.1.1.4.3 Quality of quiet zone

The quality of the quiet zone procedure characterizes the quiet zone performance of the anechoic chamber, specifically the effect of reflections within the anechoic chamber including any positioners and support structures. The MU term additionally includes the amplitude variations effect of offsetting the directive antenna array inside a DUT from the centre of the quiet zone as well as the directivity MU, i.e., the variation of antenna gains in the different direct line-of-sight links. An additional MU term related to phase variation and phase ripple effects which depends on measurement distance is FFS and shall be assessed during final MU definition for the test method. This might require an augmentation of the quality of the quiet zone validation procedure.

B.1.1.4.4 Mismatch

Mismatch uncertainty occurs when;

- Changing the signal path between the measurement and calibration procedure
- Evaluating the insertion loss of a signal path

The mismatch uncertainty for a system consisting of a generator, a load and a component in between is defined as

$$\text{Mismatch contribution (standard deviation)} = \frac{|\Gamma_{generator}|\cdot|\Gamma_{load}|\cdot|S_{21}|\cdot|S_{12}|\cdot 100}{\sqrt{2}\cdot 11.5}\ \text{dB},$$

Where Γ denotes the reflection coefficient and S_{21} is the transmission coefficient, both in linear voltage ratios.

For a cascade of several components, the interactions between all components have to be evaluated. For example, for four devices in a row (shown in Figure B.1.1.4.4-1) the following contributions have to be accounted for: AB, BC, CD, ABC, BCD, ABCD. The term ABCD represents the interaction between A and D (generator and load) with the components B and C in between.

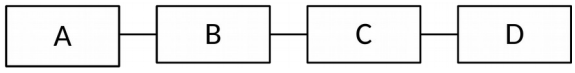

Figure B.1.1.4.4-1: Cascade of components

The combined mismatch uncertainty is given by the root sum square of the individual contributions:

$$combined\ mismatch\ uncertainty = \sqrt{(AB)^2 + (BC)^2 + (CD)^2 + (ABC)^2 + (BCD)^2 + (ABCD)^2}$$

In an optimized test procedure, the overall mismatch uncertainty is smaller when matching pairs of mismatches exist in the calibration and measurement stage since these pairs cancel each other out. Figure B.1.1.4.4-2 displays a calibration setup, where device D is replaced by device F. The mismatch contributions for this path are AB, BC, CE, ABC, BCE and ABCE. For a result based on the measurement and calibration stage, the mismatch contributions AB, BC, and ABC are matching pairs as they occur both in the measurement and calibration stage. Thus, they can be eliminated [11], and the system mismatch uncertainty is obtained as

$$\sqrt{(CD)^2 + (CE)^2 + (BCD)^2 + (BCE)^2 + (ABCD)^2 + (ABCE)^2}$$

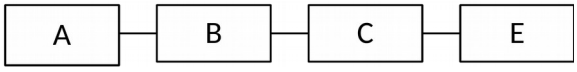

Figure B.1.1.4.4-2: Sketch of a calibration path

In the following, an example mismatch uncertainty calculation for a TX/RX patch from the measurement equipment to the measurement antenna is performed for a frequency of 43.5GHz. The example path under investigation consists of four SPDT switches, one SP6T switch and one DPDT switch and microwave cable interconnects with PC2.4 mm connectors. The attenuation and reflectance of typical components suitable for frequencies ranging up to 43.5 GHz have been considered in the calculation of the mismatch uncertainty.

Figure B1.1.4.4-3 shows a sample system setup for an EIRP/EIS test case with rather simple complexity of the switch box similar to a current sub 6GHz test setup. It should be noted that the switch unit is significantly less complex than a state-of-the-art switch unit currently used for conformance tests.

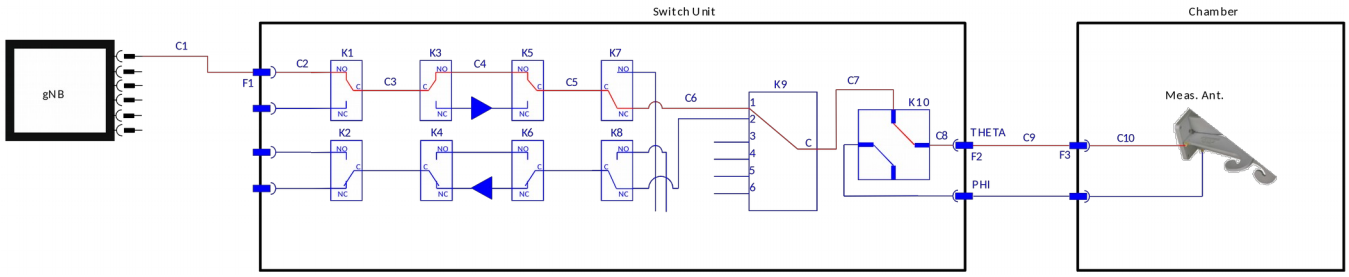

Figure B.1.1.4.4-3: Block Diagram of an EIRP/EIS test case with components from the gNB to the antenna (only portion of switch unit shown)

Table B.1.1.4.4-1 comprises the reflection and transmission properties of the components of the example path at a frequency of 43.5 GHz.

Device / Component	VSWR	Transmission (dB)	Identifier in Figure B.1.1.4.4-3	Additional Comment/ Assumption
System Simulator	3.5		gNB	
Cable	1.5	-5.38	C1	Length: 1.5m Loss: 3.59dB/m
Cable	1.5	-0.61	C2, C3, C4, C5, C6, C7, C8	Length: 0.17m Loss: 3.59dB/m
Cable	1.5	-7.18	C9, C10	Length: 2.0m Loss: 3.59dB/m
Feedthrough	1.3	-0.66	F1, F2, F3	
SPDT switch	1.9	-1.10	K1, K3, K5, K7	
SP6T switch	2.2	-1.20	K9	
Transfer switch	2.0	-1.10	K10	
Antenna	2.0		Meas. Ant.	

The calculation of the overall mismatch uncertainty for a frequency of 43.5 GHz results in a value of 2.7 dB for the standard deviation, i.e., the expanded uncertainty is 5.3 dB.

Figure B.1.1.4.4-4 depicts a possible calibration for a part of the setup.

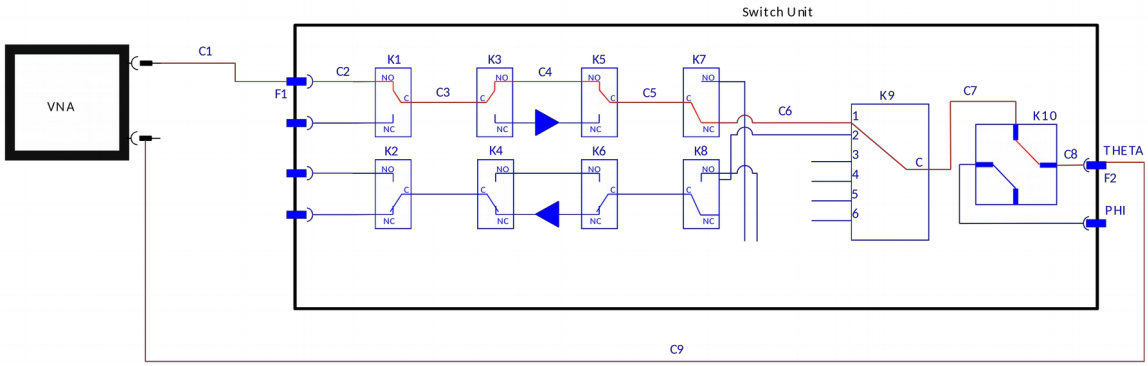

Figure B.1.1.4.4-4: Block Diagram of the calibration stage

For the VNA a return loss of 30 dB is assumed after a full two-port calibration. The calculation of the system mismatch uncertainty applying the elimination of matching pairs results in a value of 1.0 dB (standard deviation) with an expanded value of 1.9 dB.

Since the overall mismatch uncertainty value is already a standard deviation, which is RSS of values divided by the divisor (√2), the overall mismatch uncertainty value should be divided by actual divisor 1 when calculating total mismatch.

B.1.1.4.5 Absolute antenna gain uncertainty of the measurement antenna

This contribution originates from differences in gain of the calibration antenna versus the measurement antenna. In practice, the calibration antenna is used as the measurement antenna so the uncertainty contribution is 0.00.

B.1.1.4.6 Uncertainty of the RF power measurement equipment

The receiving device is used to measure the received signal level in the EIRP tests as an absolute level. These receiving devices are spectrum analysers, communication analysers, or power meters. The uncertainty value will be indicated in the manufacturer's data sheet. It needs to be ensured that appropriate manufacturer's uncertainty contributions are specified for the settings used such as bandwidth and absolute level. If a power meter is used zero offset, zero drift and measurement noise need to be included.

B.1.1.4.7 Phase curvature

This contribution originates from the finite far field measurement distance, which causes phase curvature across the antenna of UE/reference antenna. At a measurement distance of $2D^2$/lambda the phase curvature is 22.5 degrees. The impact of this factor shall be assessed during final MU definition for the test method.

B.1.1.4.8 Amplifier uncertainties

Any components in the setup can potentially introduce measurement uncertainty. It is then needed to determine the uncertainty contributors associated with the use of such components. For the case of external amplifiers, the following uncertainties should be considered but the applicability is contingent to the measurement implementation and calibration procedure.

- Stability
  - An uncertainty contribution comes from the output level stability of the amplifier. Even if the amplifier is part of the system for both measurement and calibration, the uncertainty due to the stability shall be considered. This uncertainty can be either measured or determined by the manufacturers' data sheet for the operating conditions in which the system will be required to operate.
- Linearity
  - An uncertainty contribution comes from the linearity of the amplifier since in most cases calibration and measurements are performed at two different input/output power levels. This uncertainty can be either measured or determined by the manufacturers' data sheet.
- Noise Figure
  - When the signal goes into an amplifier, noise is added so that the SNR at the output is reduced with regard to the SNR of the signal at the input. This added noise introduces error on the signal which affects the Error Rate of the receiver thus the EVM (Error Vector Magnitude). An uncertainty can be calculated through the following formula:

$$\varepsilon_{EVM} = 20\log_{10}\left(1 + 10^{\frac{-SNR}{20}}\right)$$

  - Where SNR is the signal to noise ratio in dB at the signal level used during the sensitivity measurement.
- Mismatch
  - If the external amplifier is used for both stages, measurement and calibration the uncertainty contribution associated with it can be considered systematic and constant -> 0dB. If it is not the case, the mismatch uncertainty at its input and output shall be either measured or determined by the method described in [12].
- Gain

- If the external amplifier is used for both stages, measurement and calibration the uncertainty contribution associated with it can be considered systematic and constant -> 0dB. If it is not the case, this uncertainty shall be considered.

B.1.1.4.9 Random uncertainty

This contribution is used to account for all the unknown, unquantifiable, etc. uncertainties associated with the measurements.

Random uncertainty MU contributions are normally distributed. [Note: this is different from “Miscellaneous uncertainty” or “Residual uncertainty” which can include unknown systematic errors which may not be normally distributed.]

The random uncertainty term, by definition, cannot be measured, or even isolated completely. However, past system definitions provide an empirical basis for a value. Current LTE SISO OTA measurements have random uncertainty contributions of ~0.2dB. A value of 0.5dB is suggested due to increased sensitivity to random effects in more complex, higher frequency NR test systems.

B.1.1.4.10 Influence of the XPD

This factor takes into account the uncertainty caused due to the finite cross polar discrimination (XPD) between the two polarization ports of the measurement probe. The XPD of the probe antenna shall be take into account during final MU definition for the test method..

A typical probe antenna can have XPD of 30dB.

For example if a linearly-polarized sine wave is input to the measurement antenna with a gradient of 45 degrees like the case in the following figure, then a signal level of V-antenna and H antenna are equal.

When we consider a leakage from V to H, or H to V, they can be described with the following equations.

$$ReceivedSignal@AntV = A\sin(2\pi ft) + LeakageComponentFromH \quad \text{(B.1.1.4.10-1)}$$

$$ReceivedSignal@AntH = A\sin(2\pi ft) + LeakageComponentFromV \quad \text{(B.1.1.4.10-2)}$$

Worst case can be assumed as the case that the phase of signal and leakage are same, and it can be shown as follows

$$LeakageComponentFromH = A \cdot \sin(2\pi ft) \cdot 10^{\frac{XPD}{20}} \quad \text{(B.1.1.4.10-3)}$$

$$LeakageComponentFromV = A \cdot \sin(2\pi ft) \cdot 10^{\frac{XPD}{20}} \quad \text{(B.1.1.4.10-4)}$$

If we put equations (3) in (1) and (4) in (2), we get following 2 equations.

$$ReceivedSignal@AntH = A\left(1 + 10^{\frac{XPD}{20}}\right)\sin(2\pi ft) \quad \text{(B.1.1.4.10-5)}$$

$$ReceivedSignal@AntV = A\left(1 + 10^{\frac{XPD}{20}}\right)\sin(2\pi ft) \quad \text{(B.1.1.4.10-6)}$$

Difference of amplitude between the case that there is a leakage and not can be calculated as follows.

- Amplitude when there is not the leakage: A
- Amplitude when there is the leakage (Worst): $A\left(1 + 10^{\frac{XPD}{20}}\right)$

$$MUbyXPD = 20\log_{10}\left(\frac{A\left(1 + 10^{\frac{XPD}{20}}\right)}{A}\right) = 20\log_{10}\left(1 + 10^{\frac{XPD}{20}}\right)$$

For example, if the XPD = -30dB, the calculated value can be as follows.

$$MUbyXPD = 20\log_{10}(1 + 10^{\frac{-30}{20}}) = 0.27\ dB$$

B.1.1.4.11 Reference antenna positioning misalignment

This contribution originates from reference antenna alignment and pointing error. In this measurement if the maximum gain directions of the reference antenna and the receiving antenna are aligned to each other, this contribution can be considered negligible and therefore set to zero.

B.1.1.4.12 Uncertainty of the Network Analyzer

This contribution originates from all uncertainties involved transmission magnitude measurement (including drift and frequency flatness) with a network analyser. The uncertainty value will be indicated in the manufacturer's data sheet. It needs to be ensured that appropriate manufacturer's uncertainty contribution is specified for the absolute levels measured.

B.1.1.4.13 Reference antenna feed cable loss measurement uncertainty

Before performing the calibration, the reference antenna feed cable loss have to be measured. The measurement can be done with a network analyzer to measure its S_{21} and uncertainty is introduced. This contribution should be set as zero.

B.1.1.4.14 Uncertainty of an absolute gain of the calibration antenna

The calibration antenna only appears in Stage 2. Therefore, the gain uncertainty has to be taken into account. This uncertainty will come from a calibration report with traceability to a National Metrology Institute with measurement uncertainty budgets generated following the guidelines outlined in internationally accepted standards.

B.1.1.4.15 Positioning and pointing misalignment between the reference antenna and the receiving antenna

This contribution originates from reference antenna alignment and pointing error. In this measurement if the maximum gain direction of the reference antenna and the transmitting antenna are aligned to each other, this contribution can be considered negligible and therefore set to zero.

B.1.1.4.16 gNB emulator uncertainty

gNB emulator is used to drive a signal to the horn antenna (via multiple external components such as a switch box, an amplifier and a circulator, etc.) in sensitivity tests either as an absolute level or as a relative level. Receiving device used is typically a UE/phablet/tablet/FWA. Generally there occurs uncertainty contribution from absolute level accuracy, non-linearity and frequency characteristic of the gNB emulator.

For practical reasons, in a case that a VNA is used as a calibration equipment, gNB emulator is connected to the system after the calibration measurement (Stage 2) is performed by the VNA. Hence, the uncertainty on the absolute level of gNB emulator (transmitter device) cannot be assumed as systematic. This uncertainty should be calculated from the manufacturer’s data in logs with a rectangular distribution, unless otherwise informed. Furthermore, the uncertainty of the non-linearity is included in the absolute level uncertainty.

B.1.1.4.17 Phase centre offset of calibration

Gain is defined at the phase centre of the antenna. If the phase centre of the calibration antenna is not aligned at the centre of the set up during the calibration, then there will be uncertainty related to the measurement distance.

The phase centre of a horn antenna moves with frequency along the taper length of the antenna therefore during the calibration the phase centre of all frequencies will not be aligned with the setup centre. The associated uncertainty term can be estimated using the following formula [15]:

$$\pm 20 \log_{10}\left(\frac{d_m - d_p}{d_m}\right)$$

Where d_m is the measurement distance and d_p is the maximum positional uncertainty. For a Horn antenna this is equal to 0.5 the length of the taper. This uncertainty is considered to have a rectangular distribution so the standard uncertainty is calculated by dividing the uncertainty by √3.

The same equation applies to log periodic antennas with d_m being 0.5 the length of the boom.

For a dipole antenna, given that the phase centre of the antenna is easily aligned with the centre of the set up the measurement uncertainty is zero.

If the calibration antenna (i.e. horn) is adjusted during the calibration to align the phase centre to the setup centre then this uncertainty term can be considered to be zero.

As an example a horn with a taper length of 50 mm, at 43.5 GHz and a measurement distance of 72.55 cm the uncertainty term is 0.62, with a rectangular distribution the standard uncertainty is 0.358 dB.

B.1.1.4.18 Quality of quiet zone for calibration process

During the calibration process the calibration antenna will be placed at the centre of the quiet zone. Therefore, only point P1 from the procedure outlined in B.1.1.4.3 needs to be considered for the quality of the quiet zone validation measurement.

For gain calibrations, the standard uncertainty of the EIRP results obtained following the method outlined in 2.10 shall be used. For efficiency calibrations, the standard uncertainty of the TRP result obtained following the method outlined in 2.9 shall be used.

B.1.2 Void

B.1.3 Indirect far field (IFF) method 1 setup

B.1.3.1 Uncertainty budget calculation principle

Same as in B.1.1.1.

B.1.3.2 Uncertainty budget format

Table B.1.3.2-1: IFF method 1 uncertainty contributions for EIRP and TRP measurement

UID	Description of uncertainty contribution	Details in annex
Stage 2: DUT measurement		
1	Positioning misalignment	B.1.3.4.1
2	Quality of Quiet Zone	B.1.3.4.2
3	Standing wave between DUT and measurement antenna	B.1.3.4.3
4	Mismatch	B.1.3.4.4
5	Insertion loss variation of receiver chain	B.1.3.4.5
6	RF leakage (from measurement antenna to receiver)	B.1.3.4.6
7	Uncertainty of the RF power measurement equipment	B.1.3.4.7
8	Amplifier Uncertainties	B.1.3.4.8
9	Random Uncertainty	B.1.3.4.9
10	Influence of the XPD	B.1.3.4.10
Stage 1: Calibration measurement		
11	Mismatch (RX chain)	B.1.3.4.4
12	Misalignment positioning system	B.1.3.4.11
13	Quality of the Quiet Zone for the calibration process	B.1.3.4.18
14	Amplifier Uncertainties	B.1.3.4.8
15	Uncertainty of network analyzer	B.1.3.4.12
16	Insertion loss variation of receiver chain	B.1.3.4.5
17	Mismatch (in the connection of calibration antenna)	B.1.3.4.4
18	Uncertainty of the absolute gain of the calibration antenna	B.1.3.4.13
19	Influence of the calibration antenna feed cable (Flexing cables, adapters, attenuators, connector repeatability)	B.1.3.4.14
20	RF leakage (from measurement antenna to receiver)	B.1.3.4.6
21	Positioning and pointing misalignment between the reference antenna and the receiving antenna	B.1.3.4.15
22	Standing wave between reference calibration antenna and measurement antenna	B.1.3.4.16

Table B.1.3.2-2: IFF method 1 uncertainty contributions for EIS measurement

UID	Description of uncertainty contribution	Details in annex
Stage 2: DUT measurement		
1	Positioning misalignment	B.1.3.4.1
2	Quality of Quiet Zone	B.1.3.4.2
3	Standing wave between DUT and measurement antenna	B.1.3.4.3
4	Mismatch of the transmitter chain	B.1.3.4.4
5	gNB emulator uncertainty	B.1.3.4.17
6	Insertion loss variation of transmitter chain	B.1.3.4.5
7	RF leakage (from transmitter to measurement antenna)	B.1.3.4.6
8	Influence of XPD	B.1.3.4.10
9	Amplifier Uncertainties	B.1.3.4.8
10	Random Uncertainty	B.1.3.4.9
Stage 1: Calibration measurement		
11	Mismatch RX chain	B.1.3.4.4
12	Misalignment positioning system	B.1.3.4.11
13	Quality of the Quiet Zone for the calibration process	B.1.3.4.18
14	Amplifier Uncertainties	B.1.3.4.8
15	Uncertainty of network analyzer	B.1.3.4.12
16	Insertion loss variation of receiver chain	B.1.3.4.5
17	Mismatch in the connection of calibration antenna	B.1.3.4.4
18	Uncertainty of the absolute gain of the calibration antenna	B.1.3.4.13
19	Influence of the calibration antenna feed cable: Flexing cables, adapters, attenuators, connector repeatability	B.1.3.4.14
20	RF leakage (from measurement antenna to receiver)	B.1.3.4.6
21	Positioning and pointing misalignment between the reference antenna and the receiving antenna	B.1.3.4.15
22	Standing wave between reference calibration antenna and measurement antenna	B.1.3.4.16

B.1.3.3 Uncertainty assessment

The uncertainty assessment tables are organized as follows:

- For the purpose of uncertainty assessment, the DUT size is 15 cm
- The uncertainty assessment for EIRP and TRP is provided in Table B.1.3.3-1
- The uncertainty assessment for EIS is provided in Table B.1.3.3-2

Table B.1.3.3-1: IFF method 1 measurement uncertainty for EIRP and TRP measurement

UID	Uncertainty source	Uncertainty value	Distribution of the probability	Divisor	Standard uncertainty (σ) [dB]
Stage 2: DUT measurement					
1	Positioning misalignment	0.10	Normal	2.00	0.05
2	Quality of Quiet Zone (NOTE 1)	1.50	Actual	1.00	[1.50]
3	Standing wave between DUT and measurement antenna	0.00	U-shaped	1.41	0.00
4	Mismatch (NOTE 2)	1.30	Actual	1.00	[1.30]
5	Insertion loss variation of receiver chain	0.10	Rectangular	1.73	0.06
6	RF leakage (from measurement antenna to receiver)	0.10	Actual	1.00	0.10
7	Uncertainty of the RF power measurement equipment (NOTE 3)	2.16	Normal	2.00	[1.08]
8	Amplifier Uncertainties	2.00	Normal	2.00	1.00
9	Random Uncertainty	0.40	Rectangular	1.73	0.23
10	Influence of the XPD	0.68	U-shaped	1.41	0.48
Stage 1: Calibration measurement					
11	Mismatch RX chain	0.00	U-shaped	1.41	0.00
12	Misalignment positioning system	0.00	Normal	2.00	0.00
13	Quality of the Quiet Zone for the calibration process (NOTE 1)	1.50	Actual	1.00	[1.50]
14	Amplifier Uncertainties	0.00	Normal	2.00	0.00
15	Uncertainty of network analyzer	0.40	Normal	2.00	0.20
16	Insertion As loss variation of receiver chain	0.00	Rectangular	1.73	0.00
17	Mismatch in the connection of calibration antenna	0.07	U-shaped	1.41	0.05
18	Uncertainty of the absolute gain of the calibration antenna	1.60	Normal	2.00	[0.8]
19	Influence of the calibration antenna feed cable: Flexing cables, adapters, attenuators, connector repeatability	0.00	Normal	2.00	0.00
20	RF leakage (from measurement antenna to receiver)	0.10	Actual	1.00	0.10
21	Positioning and pointing misalignment between the reference antenna and the receiving antenna	0.10	Normal	2.00	0.05
22	Standing wave between reference calibration antenna and measurement antenna	0.00	U-shaped	1.41	0.00
EIRP Expanded uncertainty (1.96σ - confidence interval of 95 %) [dB]					[5.99]
TRP Expanded uncertainty (1.96σ - confidence interval of 95 %) [dB]					[5.13]

NOTE 1: The quality of quiet zone is different for EIRP and TRP. For TRP, the standard uncertainty is [1dB]; for EIRP [1.5 dB]
NOTE 2: The analysis was done only for the case of operating at max output power, in-band, non-CA.
NOTE 3: The assessment assumes maximum DUT output power.

Table B.1.3.3-2: IFF method 1 measurement uncertainty for EIS measurement

UID	Uncertainty source	Uncertainty value	Distribution of the probability	Divisor	Standard uncertainty (σ) [dB]
Stage 2: DUT measurement					
1	Positioning misalignment	0.10	Normal	2.00	0.05
2	Quality of Quiet Zone	1.50	Actual	1.00	[1.50]
3	Standing wave between DUT and measurement antenna	0.00	U-shaped	1.41	0.00
4	Mismatch (NOTE 1)	1.30	Actual	1.00	[1.30]
5	gNB uncertainty on absolute level	[3.34]	Normal	2.00	[1.67]
6	Insertion loss variation of transmitter chain	0.10	Rectangular	1.73	0.08
7	RF leakage (from transmitter to measurement antenna)	0.10	Actual	1.00	0.10
8	Influence of XPD	0.68	U-shaped	1.41	0.48
9	Amplifier Uncertainties	2.00	Normal	2.00	1.00
10	Random Uncertainty	0.40	Rectangular	1.73	0.23
Stage 1: Calibration measurement					
11	Mismatch RX chain	0.00	U-shaped	1.41	0.00
12	Misalignment positioning system	0.00	Normal	2.00	0.00
13	Quality of the Quiet Zone for the calibration process	1.50	Actual	1.00	[1.50]
14	Amplifier Uncertainties	0.00	Normal	2.00	0.00
15	Uncertainty of network analyzer	0.40	Normal	2.00	0.20
16	Insertion loss variation of receiver chain	0.00	Rectangular	1.73	0.00
17	Mismatch in the connection of calibration antenna	0.07	U-shaped	1.41	0.05
18	Uncertainty of the absolute gain of the calibration antenna	1.60	Normal	2.00	[0.80]
19	Influence of the calibration antenna feed cable: Flexing cables, adapters, attenuators, connector repeatability	0.00	Normal	2.00	0.00
20	RF leakage (from measurement antenna to receiver)	0.10	Actual	1.00	0.10
21	Positioning and pointing misalignment between the reference antenna and the receiving antenna	0.10	Normal	2.00	0.05
22	Standing wave between reference calibration antenna and measurement antenna	0.00	U-shaped	1.41	0.00
EIS Expanded uncertainty (1.96σ - confidence interval of 95 %) [dB]					[6.49]
NOTE 1: The analysis was done only for the case of operating at max output power, in-band, non-CA.					

B.1.3.4 Measurement error contribution descriptions

B.1.3.4.1 Positioning misalignment

See B.1.1.4.1

B.1.3.4.2 Quality of Quiet Zone

See B.1.1.4.3

B.1.3.4.3 Standing wave between DUT and measurement antenna

This value is extracting the uncertainty value and standard deviation of gain ripple coming from standing waves between DUT and measurement antenna. This value can be captured by sliding (lambda/4) the DUT towards the measurement antenna as the standing waves go in and out of phase causing a ripple in measured gain. DUT scattering/interaction can also cause standing wave.

B.1.3.4.4 Mismatch

See B.1.1.4.4

B.1.3.4.5 Insertion loss variation of receiver chain

This uncertainty is the residual uncertainty contribution coming from introducing an antenna at the end of the cable. If this cable does not change/move between the calibration Stage 1 and the measurement Stage 2, the uncertainty is assumed to be systematic and negligible during the measurement stage.

B.1.3.4.6 RF leakage (from measurement antenna to receiver/transmitter)

This contribution denotes noise leaking in to connector and cable(s) between measurement antenna and receiving/transmitting equipment. The contribution also includes the noise leakage between the connector and cable(s) between reference antenna and transmitting equipment for the calibration phase.

B.1.3.4.7 Uncertainty of the RF power measurement equipment

See B.1.1.4.6

B.1.3.4.8 Amplifier Uncertainties

See B.1.1.4.8

B.1.3.4.9 Random uncertainty

See B.1.1.4.9.

B.1.3.4.10 Influence of XPD

See B.1.1.4.10

B.1.3.4.11 Misalignment positioning system

This contribution originates from uncertainty in sliding position and turn table angle accuracy. If the calibration antenna is aligned to maximum this contribution can be considered negligible and therefore set to zero.

B.1.3.4.12 Uncertainty of Network Analyzer

See B.1.1.4.12.

B.1.3.4.13 Uncertainty of the absolute gain of the calibration antenna

See B.1.1.4.14.

B.1.3.4.14 Influence of the calibration antenna feed cable (Flexing cables, adapters, attenuators, connector repeatability)

During the calibration phase this cable is used to feed the calibration antenna (SGH) and any influence it may have upon the measurements is captured. This is assessed by repeated measurements while flexing the cables and rotary joints. The largest difference between the results is recorded as the uncertainty.

B.1.3.4.15 Positioning and pointing misalignment between the reference antenna and the receiving antenna

See B.1.1.4.15

B.1.3.4.16 Standing wave between reference calibration antenna and measurement antenna

This value is extracting the uncertainty value and standard deviation of gain ripple coming from standing waves between SGH and measurement antenna. This value can be captured by sliding (lambda/4) the SGH towards the measurement antenna as the standing waves go in and out of phase causing a ripple in measured gain. SGH scattering/interaction can also cause standing wave.

B.1.3.4.17 gNB emulator uncertainty

See B.1.1.4.16.

B.1.3.4.18 Quality of the Quiet Zone for Calibration Process

See B.1.1.4.18.

B.1.4 NFTF setup

B.1.4.1 Uncertainty budget calculation principle

The uncertainty tables should be presented with two stages:

- Stage 1: the calibration of the absolute level of the DUT measurement results is performed by means of using a calibration antenna whose absolute gain is known at the frequencies of measurement
- Stage 2: the actual measurement with the DUT as either the transmitter or receiver is performed.

The MU budget should comprise of a minimum 5 headings:

1) The uncertainty source,
2) Uncertainty value,
3) Distribution of the probability,
4) Divisor based on distribution shape,
5) Calculated standard uncertainty (based on uncertainty value and divisor).

B.1.4.2 Uncertainty budget format

Table B.1.4.2-1: Uncertainty contributions for EIRP and TRP measurement

UID	Description of uncertainty contribution	Details in paragraph
	Stage 2: EIRP Near Field Radiation Pattern Measurement and EIRP Near Field DUT power measurement	
1	Axis Alignment	B.1.4.4.1
2	Probe XPD	B.1.4.4.2
3	Probe Polarization Amplitude and Phase	B.1.4.4.3
4	Probe Array Uniformity	B.1.4.4.4
5	Probe Pattern Effect	B.1.4.4.5
6	Multiple Reflections: Coupling between Measurement Antenna and DUT	B.1.4.4.6
7	Quality of the Quiet Zone	B.1.4.4.7
8	Phase curvature	B.1.4.4.24
9	Measurement Distance	B.1.4.4.8
10	NF to FF truncation	B.1.4.4.9
11	Mismatch of receiver chain	B.1.4.4.10
12	Uncertainty of the RF power measurement equipment	B.1.4.4.11
13	Amplifier uncertainties	B.1.4.4.12
14	Phase Recovery Non-Linearity over signal bandwidth	B.1.4.4.13
15	Phase Drift and Noise	B.1.4.4.14
16	Leakage and Crosstalk	B.1.4.4.15
17	Random uncertainty	B.1.4.4.16
	Stage 1: Calibration measurement	
18	Uncertainty of the Network Analyzer	B.1.4.4.17
19	Amplifier uncertainties	B.1.4.4.18
20	Mismatch of receiver chain	B.1.4.4.19
21	Mismatch in the connection of the calibration antenna	B.1.4.4.20
22	Measurement Distance	B.1.4.4.21
23	Quality of the Quiet Zone for Calibration Process	B.1.4.4.22
24	Uncertainty of the absolute gain of the calibration antenna	B.1.4.4.23

B.1.4.3 Uncertainty assessment

The uncertainty assessment table is organized as follows:

- For the purpose of uncertainty assessment, the radiating antenna aperture of the DUT is denoted as D, and the uncertainty assessment has been derived for the case of D = 5 cm
- The uncertainty assessment for EIRP and TRP, assuming D = 5 cm, is provided in Table B.1.4.3-1:

Table B.1.4.3-1: Uncertainty assessment for EIRP and TRP measurement (D = 5 cm)

UID	Description of uncertainty contribution	Uncertainty Value	Distribution of the probability	Divisor	Standard uncertainty (σ) [dB]
	Stage 2: EIRP Near Field Radiation Pattern Measurement and EIRP Near Field DUT power measurement				
1	Axis Alignment	0	Normal	2	0
2	Probe XPD	0	Normal	2	0
3	Probe Polarization Amplitude and Phase	0.11	Normal	2	0.055
4	Probe Array Uniformity (if not corrected for above)	0	Normal	2	0
5	Probe Pattern Effect (need if not pure FF)	0	Normal	2	0
6	Multiple Reflections: Coupling Measurement Antenna and DUT	0	Normal	2	0
7	Quality of the Quiet Zone (NOTE 2)	1.5	Actual	1	[1.5]
8	Phase curvature	0	Actual	1	[0]
9	Measurement Distance (no impact)	0	Rectangular	1.73	0
10	NF to FF truncation	0.006	Normal	2	[0.003]
11	Mismatch of receiver chain (NOTE 3)	1.3	Actual	1	[1.3]
12	Uncertainty of the RF power measurement equipment	2.16	Normal	2	[1.08]
13	Amplifier uncertainties	2	Normal	2	1
14	Phase Recovery Non-Linearity over signal bandwidth (NOTE 5)	0	Normal	2	[0]
15	Phase Drift and Noise	0.04	Normal	2	[0.02]
16	Leakage and Crosstalk	0	Normal	2	0
17	Random uncertainty	0.4	Rectangular	1.73	[0.23]
	Stage 1: Calibration measurement				
18	Uncertainty of the Network Analyzer	0.4	Normal	2	0.21
19	Amplifier uncertainties	0	Normal	2	0
20	Mismatch of receiver chain	0	U-shaped	1.41	0
21	Mismatch in the connection of the calibration antenna	0.0987	U-shaped	1.41	0.07
22	Measurement Distance	0	Rectangular	1.73	0
23	Quality of the Quiet Zone for Calibration Process	1.5	Actual	1	[1.5]

	(NOTE 2)				
24	Uncertainty of the absolute gain of the calibration antenna	1.6	Normal	2	[0.80]
EIRP Expanded uncertainty (1.96σ - confidence interval of 95 %) [dB]					[5.92]
TRP Expanded uncertainty (1.96σ - confidence interval of 95 %) [dB]					[5.04]
NOTE 1: The impact of phase variation on EIRP shall be taken into account during final MU definition for the test method. NOTE 2: The quality of quiet zone is different for EIRP and TRP. For TRP, the standard uncertainty is [1dB]; for EIRP, the standard uncertainty of quiet zone is [1.5dB]. NOTE 3: The analysis was done only for the case of operating at max output power, in-band, non-CA NOTE 4: The assessment assumes maximum DUT output power. NOTE 5: The Phase Recovery Non-Linearity over signal bandwidth shall be taken into account during final MU definition for the test method.					

B.1.4.4 Measurement error contribution descriptions

B.1.4.4.1 Axes Alignment

Includes the following mechanical alignment errors:

- The uncertainty related with the lateral displacement between the horizontal and vertical axes of the DUT positioner.
- The differences from 90° of the angle between the horizontal and vertical axes.
- The horizontal mis-pointing of the horizontal axis to the probe reference point for Theta=0°.

These mechanical errors can result in sampling the field on a non-ideal sphere. This uncertainty can be considered to have a normal distribution.

B.1.4.4.2 Probe XPD

Refer to B.1.1.4.10 [7]. If the Probe Polarization Amplitude and Phase is measured and corrected for then this uncertainty term can be considered to be zero.

B.1.4.4.3 Probe Polarization Amplitude and Phase

The amplitude and phase of the probe polarization coefficients should be measured. This uncertainty is assumed to have a normal distribution.

B.1.4.4.4 Probe Array Uniformity (for multi -probe systems only)

This is the uncertainty due to the fact that different probes are used for each physical position. Different probes have different radiation patterns. Generally, the probe array is calibrated so that the uniformity of the probes is achieved. This uncertainty term must be considered if the amplitude and phase of each probe is not identical or corrected for. This uncertainty is assumed to have a normal distribution

B.1.4.4.5 Probe Pattern Effect

The probe/s pattern/s is assumed to be known so that the DUT measurement in near field can be corrected when performing the near field to far field transform. If the probe pattern is known, then the uncertainty term is zero. There is no direct dependence between the DUT pattern and the probe pattern in near field measurements. This uncertainty is assumed to have a normal distribution.

B.1.4.4.6 Multiple Reflections: Coupling Measurement Antenna and DUT

The multiple reflections occur when a portion of the transmitted signal is reflected form the receiving antenna back to the transmitting antenna and re-reflected by the transmitting antenna back to the receiving antenna. This uncertainty can be determined by multiple measurements of the DUT when at different distance from the probes. This uncertainty is assumed to have a normal distribution.

B.1.4.4.7 Quality of the Quiet Zone

See B.1.1.4.3

B.1.4.4.8 Measurement Distance

See B.1.1.4.2

B.1.4.4.9 NF to FF truncation

The measured near field is expanded using a finite set of spherical modes. The number of modes is linked to number of samples. The filtering effect generated by the finite number of modes can improve measurement results by removing signals from outside the physical area of the DUT. Care must be taken in order to make sure the removed signals are not from the DUT itself. This term also includes the uncertainty related to the scan area truncation. This uncertainty is usually negligible. This uncertainty is assumed to have a normal distribution.

B.1.4.4.10 Mismatch of receiver chain

See B.1.1.4.4

B.1.4.4.11 Uncertainty of the RF power measurement equipment

See B.1.1.4.6.

B.1.4.4.12 Amplifier uncertainties

See B.1.1.4.8

B.1.4.4.13 Phase Recovery Non-Linearity over signal bandwidth

This uncertainty originates from the non-linearity of the phase recovery for wide band signal. The phase recovery can be due to either phase non-linearity of the receiver and/or the DUT itself. The method to quantify the non-linarites is not defined.

B.1.4.4.14 Phase Drift and Noise

This uncertainty is due to the noise level and drift of the test range and should be determined or measured at the DUT location. The noise level is usually measured with a Spectrum Analyzer. This uncertainty is assumed to have a normal distribution.

B.1.4.4.15 Leakage and Crosstalk

This uncertainty can be addressed by measurements on the actual system setup. The leakage and crosstalk cannot be separated from the random amplitude and phase errors so that the relative importance should be determined. This uncertainty is assumed to have a normal distribution.

B.1.4.4.16 Random uncertainty

See B.1.1.4.9

B.1.4.4.17 Uncertainty of the Network Analyzer

See B.1.1.4.12

B.1.4.4.18 Amplifier Uncertainties

See B.1.1.4.8

B.1.4.4.19 Mismatch of receiver chain

See B.1.1.4.4

B.1.4.4.20 Mismatch in the connection of the calibration antenna

See B.1.1.4.4

B.1.4.4.21 Measurement Distance

See B.1.1.4.17

B.1.4.4.22 Quality of the Quiet Zone for Calibration Process

See B.1.1.4.18

B.1.4.4.23 Uncertainty of the absolute gain of the calibration antenna

See B.1.1.4.5.

B.1.4.4.24 Phase curvature

See B.1.1.4.7

B.2 Measurement uncertainty budget for UE RRM testing methodology

B.2.1 Direct far field (DFF) setup

B.2.1.1 Uncertainty budget calculation principle

The uncertainty tables cover the actual measurement using the DUT. In some cases, uncertainty may also arise from a calibration or alignment process before the measurements.

When a calibration process is used before the measurements, the uncertainty tables should be presented with two stages:

- Stage 1: the calibration of the absolute level of the DUT measurement results is performed by means of using a calibration antenna whose absolute gain is known at the frequencies of measurement
- Stage 2: the actual measurement with the DUT as either the transmitter or receiver is performed.

The MU budget should comprise of a minimum 5 headings:

1) The uncertainty source,
2) Uncertainty value,

3) Distribution of the probability,

4) Divisor based on distribution shape,

5) Calculated standard uncertainty (based on uncertainty value and divisor).

B.2.1.2 Uncertainty budget format

The uncertainty contributions depend on the parameter being controlled and/or the measurement being made. A separate table is provided for each.

Table B.2.1.2-1: Uncertainty contributions for test with defined DL SNR at reference point

UID	Description of uncertainty contribution	Details in annex
	During measurement	
1	gNB emulator SNR uncertainty	B.2.1.4.1
2	gNB emulator DL EVM	B.2.1.4.2
3	gNB emulator Fading model impairments	B.2.1.4.3
Note 1: Handling of effects related to isolation and alignment of Horizontal / Vertical polarisation is not defined Note 2: Handling of effects related to Quality of Quiet zone is not defined		

Table B.2.1.2-2: Uncertainty contributions for DL absolute power level at reference point (D = 5 cm)

UID	Description of uncertainty contribution	Details in annex
	During measurement	
1	Currently assumed to be the same as EIS measurement in Table B.1.1.2-2	B.1.1.4
Note 1: Additional uncertainty contributions may apply for faded signals Note 2: Contribution from Quality of Quiet zone may be different from EIS measurement		

B.2.1.3 Uncertainty assessment

The uncertainty assessment tables are organized as follows:

- For the purpose of uncertainty assessment, the radiating antenna aperture of the DUT is denoted as D, and the uncertainty assessment has been derived for the case of D = 5 cm

The uncertainty contributions depend on the parameter being controlled and/or the measurement being made. A separate table is provided for each.

Table B.2.1.3-1: Uncertainty assessment for test with defined DL SNR at reference point

UID	Uncertainty source	Uncertainty value	Distribution of the probability	Divisor	Standard uncertainty (σ) [dB]
		During measurement			
1	gNB emulator SNR uncertainty	0.3dB	Normal	2.00	0.15
2	gNB emulator DL EVM	-	One-sided, beneficial	-	0
3	gNB emulator Fading model impairments Note 3	[0.5dB]	Normal	2.00	[0.25]
SNR Expanded uncertainty (1.96σ - confidence interval of 95 %) [dB]					[0.57]
Note 1: Handling of effects related to isolation and alignment of Horizontal / Vertical polarisation is not defined Note 2: Handling of effects related to Quality of Quiet zone is not defined Note 3: The value is same as for LTE and shall be verified for other channel models by RAN5 during detailed MU assessment					

Table B.2.1.3-2: Uncertainty assessment for DL absolute power level at reference point (D = 5 cm)

UID	Uncertainty source	Uncertainty value	Distribution of the probability	Divisor	Standard uncertainty (σ) [dB]
During measurement					
Currently assumed to be the same as EIS measurement in Table B.1.1.3-2					
DL absolute power level Expanded uncertainty (1.96σ - confidence interval of 95 %) [dB]					[6.66]
Note 1: Additional uncertainty contributions may apply for faded signals Note 2: Contribution from Quality of Quiet zone may be different from EIS measurement					

B.2.1.4 Measurement error contribution descriptions

B.2.1.4.1 gNB emulator SNR uncertainty

See B.3.1.4.1.

B.2.1.4.2 gNB emulator Downlink EVM

See B.3.1.4.2.

B.2.1.4.3 gNB emulator fading model impairments

See B.3.1.4.3.

B.2.1.5 Assessment of testable SNR range for D=5cm

The signal and the noise provided by the test system are both attenuated by the over-the-air link loss. The UE noise then adds to the noise provided by the test system, hence degrading the SNR seen by the UE and potentially limiting the testable SNR range.

For conducted tests, the noise provided by the test system can be set much higher than the UE noise and the SNR degradation is negligible. However for over-the-air test systems, the power that can realistically be delivered into the test system probe antenna is limited, so the test point is likely to be closer to the UE noise and a small SNR degradation is allowable.

B.2.1.5.1 Method and Parameters

The initial rational in this section is elaborated for Scenario 1 (1 Angle of Arrival with signal coming from the RX beam peak direction) for Type 1 Requirements (“Fine” RX beam) and Mode 1 Configuration (TE generating S and N).

For RRM tests, DL SNR is given as a test parameter. Such SNR environment is generated by the test system by injecting both desired signal and artificial AWGN noise. To fulfil the purpose of the test, the configured SNR should be accurate enough at the UE receiver. If the absolute power level of the signal and noise from the test system is too low, then the SNR would be degraded due to the UE’s internal noise.

The calculation of Noc level is shown in clause 6.2.1.4.

The possible transmitted signal and noise strengths from the test antenna depend on the capability of the test system. The feasible transmit power depends on the conducted cable losses, the Test system transmit antenna gain and the final amplifier characteristic, especially the P1dB compression point. Considering the cable losses, probe antenna gain of 12dB and commercially available mmWave Amplifiers, and the crest factor of the downlink signal (not to cause additional EVM error from test system side), the feasible transmit power from the probe antenna is calculated below, which in turn sets the SNR range.

Table B.2.1.5.1-1: Assumed Test system parameters

	43GHz	
P1dB amplifier power	+23	dBm
Backoff from P1dB	-13	dB
Cable loss	-8	dB
Probe antenna gain	12	dB
Transmission bandwidth	100M	Hz

The third part to consider is the free space path loss between the probe antenna and the UE antenna, shown below:

Table B.2.1.5.1-2: Free Space path loss

	43GHz	
@0.725m separation	-62.3	dB

B.2.1.5.2 Void

B.2.1.5.3 Void

B.2.1.5.4 SNR range for SNR_{RP} - SNR_{BB} ≤ 1dB

The initial rational in this section is elaborated for Scenario 1 (1 Angle of Arrival with signal coming from the RX beam peak direction) for Type 1 Requirements (“Fine” RX beam) and Mode 1 Configuration (TE generating S and N).

Based on the method of setting the noise from the Test system to give a maximum of 1dB degradation in overall SNR between reference point and baseband, we can then work back through the signal chain to determine how high the SNR can be set. As the noise is set to a fixed level, the maximum SNR is set by the test system power amplifier and the channel bandwidth to be tested.

The SNR upper bound depends on the type of test system. For the Direct far field (DFF) setup the diagram below illustrates the principle, and is based on the “DFF 100MHz” tab of the accompanying spreadsheet.

The process works back through the signal chain, from left to right in the diagram.

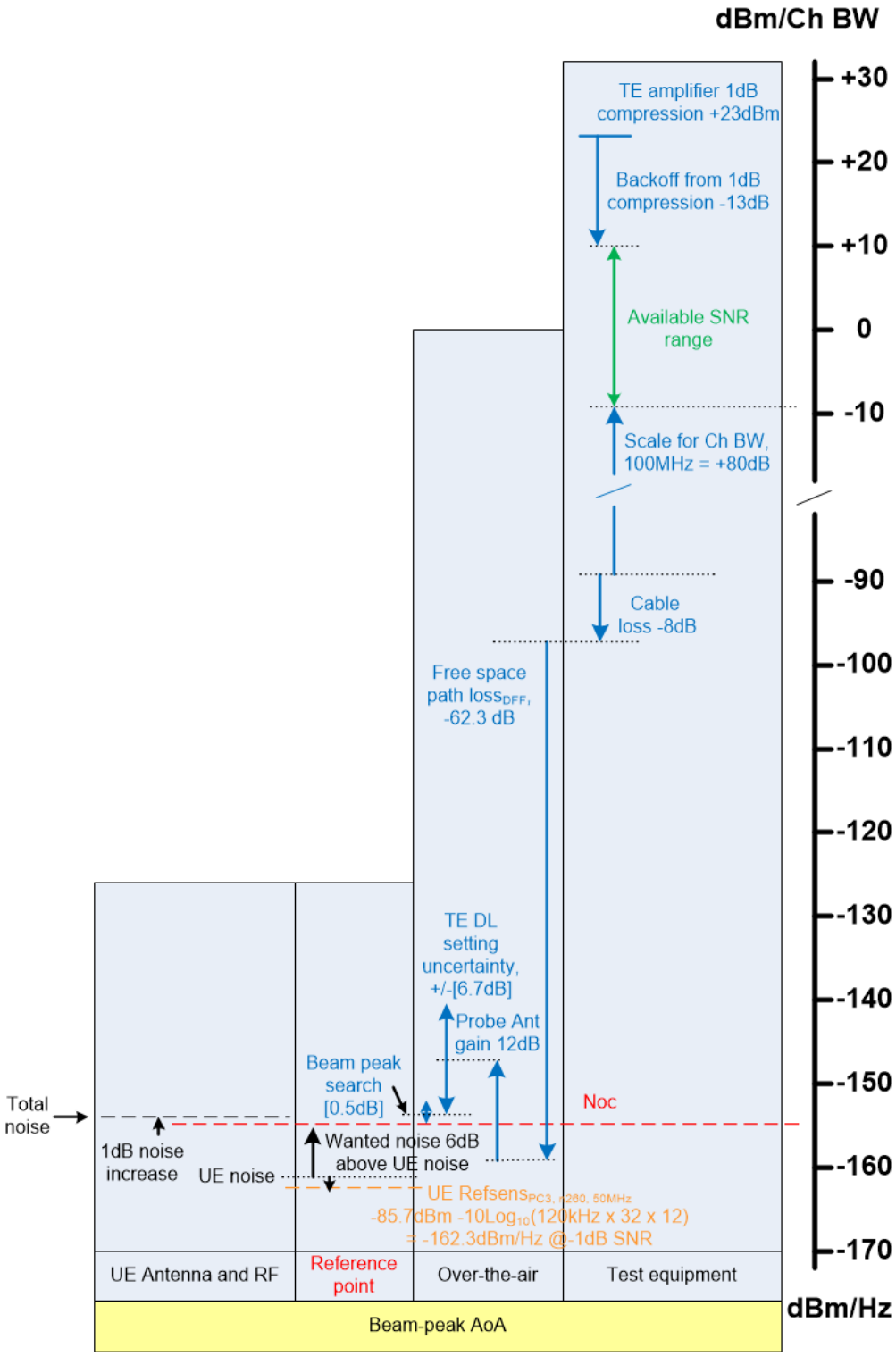

Figure B.2.1.5.4-1: Estimation of SNR range for Direct far field (DFF), Rx Beam peak direction

The test equipment must supply at least the wanted noise level at the reference point. If the noise was lower, the degradation in SNR would be greater than 1dB, and may cause a conformant UE to fail.

The accuracy of setting the signal and noise levels has been taken as +/-[6.7]dB, which is based on the Direct Far Field measurement uncertainty for EIS in Table B.1.1.3-2. It is subject to further analysis by RAN5.

During conformance test, the test system will need to find the UE Rx beam peak. At present an allowance of [0.5] dB has been included, but is subject to further analysis by RAN5.

Inclusion of these two contributions directly reduces the maximum SNR that can be measured by a test system for a given channel bandwidth. To find the maximum SNR that can be measured by a test system with a specific Channel BW, the baseband SNR in the spreadsheet is increased until the value “Wanted signal + headroom, dBm/Ch BW” is just below the “TE Power amplifier 1dB compression, dBm” value. The resulting values are given in Table B.2.1.5.4-1.

Table B.2.1.5.4-1: Predicted SNR upper bound values for Direct far field (DFF), Rx Beam peak direction

Channel Bandwidth	Maximum SNR
100MHz	[18.5dB]

Note that these are UE baseband SNR values, so the Reference point figures used in RRM test cases may be 1dB higher. Values are based on UE parameters and currently foreseen test equipment limitations, and could be improved in future.

An example of SNR calculation for DFF method is provided in “Spreadsheet 1 - RRM SNR range calculator.xls” file attached to the TR.

The feasible Noc and SNR range for other RRM scenarios, requirement types and S / N generation modes, can be assessed and given relative to the Noc and SNR range defined in the case above. Table B.2.1.5.4-2 summarizes the results.

Table B.2.1.5.4-2: Summary of SNR range and Noc feasibility for RRM DFF setup

Scenario	Requirement Type	S / N Configuration Mode	Noc	SNR Range	Notes
1	“Fine” beams	1 (S and N from TE)	Noc	SNR	Note 1
1	“Rough" beams	1 (S and N from TE)	Noc + Y	SNR - Y	Note 2
2	“Fine” beams	1 (S and N from TE)	Noc + X	SNR - X	Note 3
2	“Rough" beams	1 (S and N from TE)	Noc + X+ Z	SNR - X - Z	Note 4

Note 1: Noc as specified in section 6.2.1.4.3. Respective SNR defined as per Section B.2.1.5.4
Note 2: Y as specified in section 6.2.1.4.4.
Note 3: X as specified in section 6.2.1.4.5.
Note 4: X and Z as specified in section 6.2.1.4.6

B.2.2 Indirect far field (IFF) setup

B.2.2.1 Uncertainty budget calculation principle

Same as in B.2.1.1.

B.2.2.2 Uncertainty budget format

The uncertainty contributions depend on the parameter being controlled and/or the measurement being made. A separate table is provided for each.

Table B.2.2.2-1: Uncertainty contributions for test with defined DL SNR at reference point

UID	Description of uncertainty contribution	Details in annex
	During measurement	
1	gNB emulator SNR uncertainty	B.2.2.4.1
2	gNB emulator DL EVM	B.2.2.4.2
3	gNB emulator Fading model impairments	B.2.2.4.3
Note 1: Handling of effects related to isolation and alignment of Horizontal / Vertical polarisation is FFS Note 2: Handling of effects related to Quality of Quiet zone is FFS		

Table B.2.2.2-2: Uncertainty contributions for DL absolute power level at reference point (D = 15 cm)

UID	Description of uncertainty contribution	Details in annex
	During measurement	
1	Currently assumed to be the same as EIS measurement in Table B.1.3.2-2	B.2.1.4
Note 1: Additional uncertainty contributions may apply for faded signals Note 2: Contribution from Quality of Quiet zone may be different from EIS measurement		

B.2.2.3 Uncertainty assessment

The uncertainty assessment tables are organized as follows:

- For the purpose of uncertainty assessment, the radiating antenna aperture of the DUT is denoted as D, and the uncertainty assessment has been derived for the case of D = 15 cm

The uncertainty contributions depend on the parameter being controlled and/or the measurement being made. A separate table is provided for each.

Table B.2.2.3-1: Uncertainty assessment for test with defined DL SNR at reference point

UID	Uncertainty source	Uncertainty value	Distribution of the probability	Divisor	Standard uncertainty (σ) [dB]
		During measurement			
1	gNB emulator SNR uncertainty	0.3dB	Normal	2.00	0.15
2	gNB emulator DL EVM	-	One-sided, beneficial	-	0
3	gNB emulator Fading model impairments Note 3	[0.5dB]	Normal	2.00	[0.25]
SNR Expanded uncertainty (1.96σ - confidence interval of 95 %) [dB]					[0.57]
Note 1: Handling of effects related to isolation and alignment of Horizontal / Vertical polarisation is not defined Note 2: Handling of effects related to Quality of Quiet zone is not defined Note 3: The value is same as for LTE and shall be verified for other channel models by RAN5 during detailed MU assessment					

Table B.2.2.3-2: Uncertainty assessment for DL absolute power level at reference point (D = 15 cm)

UID	Uncertainty source	Uncertainty value	Distribution of the probability	Divisor	Standard uncertainty (σ) [dB]
		During measurement			
Currently assumed to be the same as EIS measurement in Table B.1.3.3-2					
DL absolute power level Expanded uncertainty (1.96σ - confidence interval of 95 %) [dB]					[6.49]
Note 1: Additional uncertainty contributions may apply for faded signals Note 2: Contribution from Quality of Quiet zone may be different from EIS measurement					

B.2.2.4 Measurement error contribution descriptions

B.2.2.4.1 gNB emulator SNR uncertainty

See B.3.1.4.1.

B.2.1.4.2 gNB emulator Downlink EVM

See B.3.1.4.2.

B.2.1.4.3 gNB emulator fading model impairments

See B.3.1.4.3

B.2.2.5 Assessment of testable SNR range

The signal and the noise provided by the test system are both attenuated by the over-the-air link loss. The UE noise then adds to the noise provided by the test system, hence degrading the SNR seen by the UE and potentially limiting the testable SNR range.

For conducted tests, the noise provided by the test system can be set much higher than the UE noise and the SNR degradation is negligible. However for over-the-air test systems, the power that can realistically be delivered into the test system probe antenna is limited, so the test point is likely to be closer to the UE noise and a small SNR degradation is allowable.

B.2.2.5.1 Method and Parameters

The method is the same as B.2.1.5.1, but the values related to the test system are different. The calculation of noise level is in clause 6.2.1.4.3, 6.2.1.4.4, 6.2.1.4.5 and 6.2.1.4.6.

B.2.2.5.2 Void

B.2.2.5.3 Void

B.2.2.5.4 SNR range for SNR_{RP} - SNR_{BB} ≤ 1dB

The initial rational in this section is elaborated for Scenario 1 (1 Angle of Arrival with signal coming from the RX beam peak direction) for Type 1 Requirements (“Fine” RX beam) and Mode 1 Configuration (TE generating S and N).

Based on the method of setting the noise from the Test system to give a maximum of 1dB degradation in overall SNR between reference point and baseband, we can then work back through the signal chain to determine how high the SNR can be set. As the noise is set to a fixed level, the maximum SNR is set by the test system power amplifier and the channel bandwidth to be tested.

The SNR upper bound depends on the type of test system. For the Indirect Far field (IFF) setup the diagram below illustrates the principle, and is based on the “IFF 100MHz” tab of the accompanying spreadsheet.

The process works back through the signal chain, from left to right in the diagram.

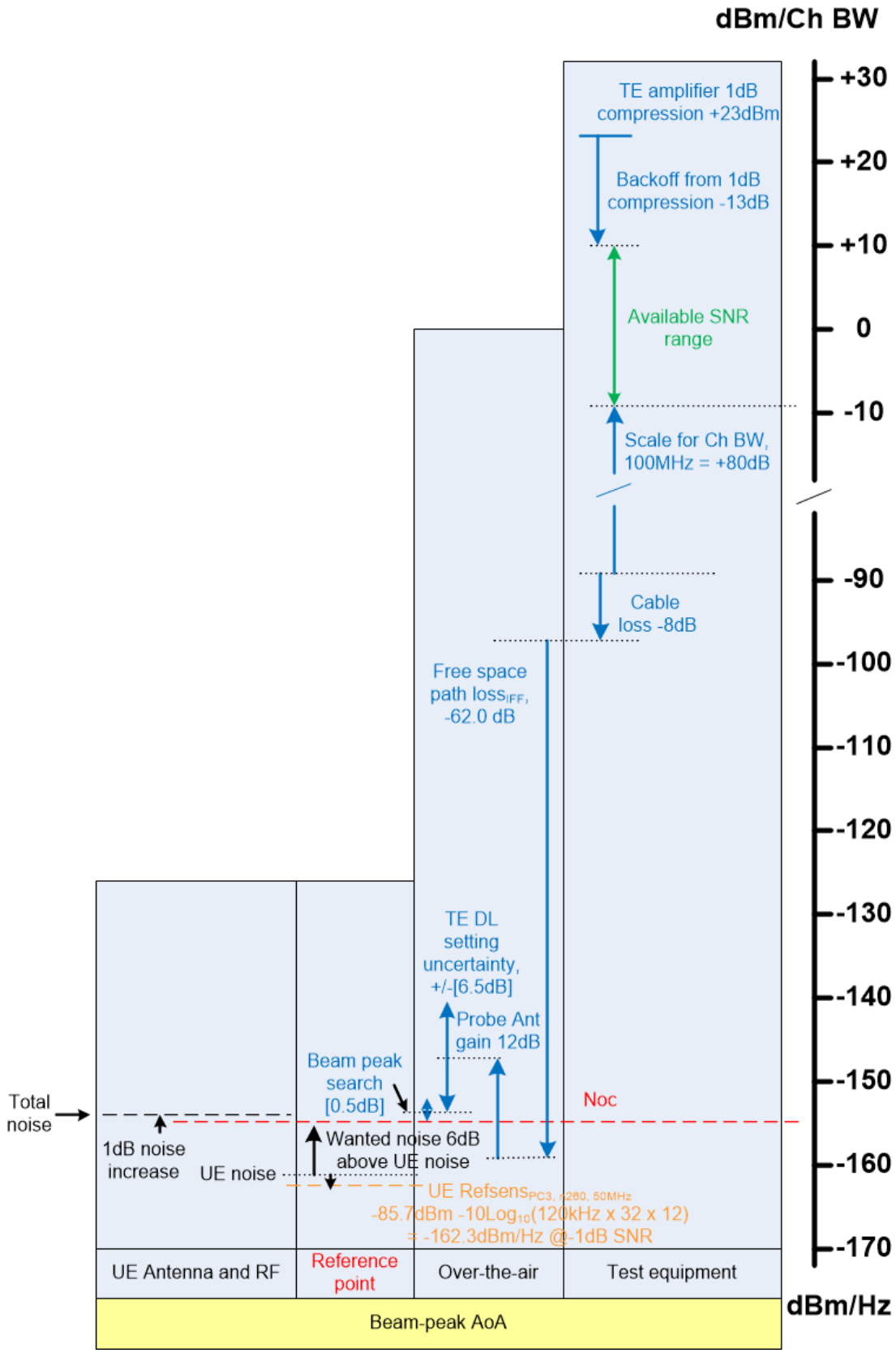

Figure B.2.2.5.4-1: Estimation of SNR range for Indirect far field (IFF)

The test equipment must supply at least the wanted noise level at the reference point. If the noise was lower, the degradation in SNR would be greater than 1dB, and may cause a conformant UE to fail.

The accuracy of setting the signal and noise levels has been taken as +/-[6.5]dB which is based on the Indirect Far Field measurement uncertainty for EIS in Table B.1.3.3-2. The uncertainty is subject to further analysis by RAN5.

During conformance test, the test system will need to find the UE Rx beam peak. At present an allowance of [0.5] dB has been included, but is subject to further analysis by RAN5.

Inclusion of these two contributions directly reduces the maximum SNR that can be measured by a test system for a given channel bandwidth. To find the maximum SNR that can be measured by a test system with a specific Channel BW, the baseband SNR in the spreadsheet is increased until the value “Wanted signal + headroom, dBm/Ch BW” is just below the “TE Power amplifier 1dB compression, dBm” value. The resulting values are given in Table B.2.2.5.4-1.

Table B.2.2.5.4-1: Predicted SNR upper bound values for Indirect far field (IFF)

Channel Bandwidth	Maximum SNR
100MHz	[19.0dB]
200MHz	[16.0dB]

Note that these are UE baseband SNR values, so the Reference point figures used in RRM test cases may be 1dB higher. Values are based on UE parameters and currently foreseen test equipment limitations, and could be improved in future.

The feasible Noc and SNR range for other RRM scenarios, requirement types and S / N generation modes, can be assessed and given relative to the Noc and SNR range defined in the case above. Table B.2.2.5.4-2 summarizes the results.

Table B.2.2.5.4-2: Summary of SNR range and Noc feasibility for RRM IFF setup

Scenario	Requirement Type	S / N Configuration Mode	Noc	SNR Range	Notes
1	“Fine” beams	1 (S and N from TE)	Noc	SNR	Note 1
1	“Rough" beams	1 (S and N from TE)	Noc + Y	SNR - Y	Note 2
2	“Fine” beams	1 (S and N from TE)	Noc + X	SNR - X	Note 3
2	“Rough" beams	1 (S and N from TE)	Noc + X+ Z	SNR - X - Z	Note 4
Note 1: Noc as specified in section 6.2.1.4.3. Respective SNR defined as per Section B.2.2.5.4 Note 2: Y as specified in section 6.2.1.4.4. Note 3: X as specified in section 6.2.1.4.5. Note 4: X and Z as specified in section 6.2.1.4.6					

B.2.3 Simplified Direct far field (DFF) setup

B.2.3.1 Uncertainty budget calculation principle

Same as in B.2.1.1.

B.2.3.2 Uncertainty budget format

The uncertainty contributions depend on the parameter being controlled and/or the measurement being made. A separate table is provided for each.

Table B.2.3.2-1: Uncertainty contributions for test with defined DL SNR at reference point

UID	Description of uncertainty contribution	Details in annex
	During measurement	
1	gNB emulator SNR uncertainty	B.2.3.4.1
2	gNB emulator DL EVM	B.2.3.4.2
3	gNB emulator Fading model impairments	B.2.3.4.3
Note 1: Handling of effects related to isolation and alignment of Horizontal / Vertical polarisation is not defined Note 2: Handling of effects related to Quality of Quiet zone is not defined		

Table B.2.3.2-2: Uncertainty contributions for DL absolute power level at reference point (D = 5 cm)

UID	Description of uncertainty contribution	Details in annex
	During measurement	
1	Currently assumed to be the same as EIS measurement in Table B.1.1.2-2	B.1.1.4
Note 1: Additional uncertainty contributions may apply for faded signals Note 2: Contribution from Quality of Quiet zone may be different from EIS measurement		

B.2.3.3 Uncertainty assessment

The uncertainty assessment tables are organized as follows:

- For the purpose of uncertainty assessment, the radiating antenna aperture of the DUT is denoted as D, and the uncertainty assessment has been derived for the case of D = 5 cm

The uncertainty contributions depend on the parameter being controlled and/or the measurement being made. A separate table is provided for each.

Table B.2.3.3-1: Uncertainty assessment for test with defined DL SNR at reference point

UID	Uncertainty source	Uncertainty value	Distribution of the probability	Divisor	Standard uncertainty (σ) [dB]
		During measurement			
1	gNB emulator SNR uncertainty	0.3dB	Normal	2.00	0.15
2	gNB emulator DL EVM	-	One-sided, beneficial	-	0
3	gNB emulator Fading model impairments Note 3	[0.5dB]	Normal	2.00	[0.25]
SNR Expanded uncertainty (1.96σ - confidence interval of 95 %) [dB]					[0.57]
Note 1: Handling of effects related to isolation and alignment of Horizontal / Vertical polarisation is not defined Note 2: Handling of effects related to Quality of Quiet zone is not defined Note 3: The value is same as for LTE and shall be verified for other channel models by RAN5 during detailed MU assessment					

Table B.2.3.3-2: Uncertainty assessment for DL absolute power level at reference point (D = 5 cm)

UID	Uncertainty source	Uncertainty value	Distribution of the probability	Divisor	Standard uncertainty (σ) [dB]
		During measurement			
Currently assumed to be the same as EIS measurement in Table B.1.1.3-2					
DL absolute power level Expanded uncertainty (1.96σ - confidence interval of 95 %) [dB]					[6.66]
Note 1: Additional uncertainty contributions may apply for faded signals Note 2: Contribution from Quality of Quiet zone may be different from EIS measurement					

B.2.3.4 Measurement error contribution descriptions

B.2.3.4.1 gNB emulator SNR uncertainty

See B.3.1.4.1.

B.2.3.4.2 gNB emulator Downlink EVM

See B.3.1.4.2.

B.2.3.4.3 gNB emulator fading model impairments

See B.3.1.4.3.

B.2.3.5 Assessment of testable SNR range for D=5cm

The signal and the noise provided by the test system are both attenuated by the over-the-air link loss. The UE noise then adds to the noise provided by the test system, hence degrading the SNR seen by the UE and potentially limiting the testable SNR range.

For conducted tests, the noise provided by the test system can be set much higher than the UE noise and the SNR degradation is negligible. However for over-the-air test systems, the power that can realistically be delivered into the test system probe antenna is limited, so the test point is likely to be closer to the UE noise and a small SNR degradation is allowable.

B.2.3.5.1 Method and Parameters

Same as B.2.1.5.1.

B.2.3.5.2 Void

B.2.3.5.3 Void

B.2.3.5.4 SNR range for SNR_{RP} - SNR_{BB} ≤ 1dB

Same as B.2.1.5.4.

B.3 Measurement uncertainty budget for UE demodulation testing methodology

B.3.1 Direct near field (DNF) setup

B.3.1.1 Uncertainty budget calculation principle

The uncertainty tables cover the actual measurement using the DUT receiver. If applicable, any uncertainty arising from a calibration or alignment process before the measurements should also be included.

The MU budget should comprise of a minimum 5 headings:

1) The uncertainty source,
2) Uncertainty value,
3) Distribution of the probability,

4) Divisor based on distribution shape,

5) Calculated standard uncertainty (based on uncertainty value and divisor).

B.3.1.2 Uncertainty budget format

Table B.3.1.2-1: Uncertainty contributions for T-put test with defined SNR at reference point

UID	Description of uncertainty contribution	Details in annex
	During T-put measurement	
1	gNB emulator SNR uncertainty	B.3.1.4.1
2	gNB emulator DL EVM	B.3.1.4.2
3	gNB emulator Fading model impairments	B.3.1.4.3
Note 1: Handling of effects related to isolation and alignment of Horizontal / Vertical polarisation is not defined Note 2: Handling of effects related to Quality of Quiet zone is not defined		

B.3.1.3 Uncertainty assessment

The uncertainty assessment tables are organized as follows:

- The uncertainty assessment for T-put measurement at defined SNR, is provided in Table B.3.1.3-1

Table B.3.1.3-1: Uncertainty assessment for T-put test with defined SNR at reference point

UID	Uncertainty source	Uncertainty value	Distribution of the probability	Divisor	Standard uncertainty (σ) [dB]
	During T-put measurement				
1	gNB emulator SNR uncertainty	0.3dB	Normal	2.00	0.15
2	gNB emulator DL EVM	-	One-sided, beneficial	-	0
3	gNB emulator Fading model impairments Note 3	[0.5dB]	Norma	2.00	[0.25]
	SNR Expanded uncertainty (1.96σ - confidence interval of 95 %) [dB]				[0.57]
Note 1: Handling of effects related to isolation and alignment of Horizontal / Vertical polarisation is not defined Note 2: Handling of effects related to Quality of Quiet zone is not defined Note 3: The value is same as for LTE and shall be verified for other channel models by RAN5 during detailed MU assessment					

B.3.1.4 Measurement error contribution descriptions

B.3.1.4.1 gNB emulator SNR uncertainty

This contribution originates from setting the ratio of signal and noise in the conducted part of the test system. It is estimated to be the same as for LTE conducted testing in TS 36.521-1 Annex F, which is ±0.3dB. The default for values in 36.521-1 Annex F is 95% confidence interval, normal distribution.

B.3.1.4.2 gNB emulator Downlink EVM

When simulations of demodulation performance are run, the downlink signal is modelled with a defined EVM, representing imperfections in the signal transmitted by the gNB. This EVM value is agreed across companies to align simulations, and is normally lower than the gNB EVM requirement, to represent “typical” conditions. The EVM used for simulations is therefore built in to the requirement points, normally specified as the SNR required to meet a specified throughput, with a defined modulation and Reference channel, under defined propagation conditions.

For a conformance test, the EVM defined for the simulations is taken as a maximum allowed value for the test system, as a worse gNB emulator EVM would make the signal harder to demodulate, and disadvantage the UE. In a test system the EVM cannot normally be set to a specific value, but is specified to be no higher than a defined value.

Following this approach, the uncertainty from gNB emulator Downlink EVM is a one-sided distribution, with beneficial effect. Without treating the positive and negative uncertainties separately, and as it would not make the SNR worse, the effective uncertainty is 0dB.

B.3.1.4.3 gNB emulator fading model impairments

This contribution originates from imperfections in the gNB emulator fading model, compared to the applied fading model. It is estimated to be the same as for LTE conducted testing in TS 36.521-1 Annex F, which is ±0.5dB. The default for values in 36.521-1 Annex F is 95% confidence interval, normal distribution.

B.3.1.5 Assessment of testable DL SNR range and accuracy for D=15cm

The signal and the noise provided by the test system are both attenuated by the over-the-air link loss. The UE noise then adds to the noise provided by the test system, hence degrading the SNR seen by the UE and potentially limiting the testable SNR range. The calculations and graphs in this subclause allow this SNR degradation to be assessed over a range of scenarios.

For conducted tests, the noise provided by the test system can be set much higher than the UE noise and the SNR degradation is negligible. However for over-the-air test systems, the power that can realistically be delivered into the test system probe antenna is limited, so the test point is likely to be closer to the UE noise and a small SNR degradation is allowable.

B.3.1.5.1 Method and Parameters

The method is the same as B.2.1.5.1, but some values related to the test system are different, and provided in Table B.3.1.5.1-1. The calculation of noise level is in clause 7.2.1.3.

Table B.3.1.5.1-1: Free Space path loss

	43GHz	
@0.5m separation	-59.1	dB

The radiative near field measurement distance is calculated for a DUT with radiating aperture D = 15cm, using the formula in clause 7.2.1.2:

Table B.3.1.5.1-2: Radiated near-field distance for D = 0.15m

	24GHz	43GHz	
Wavelength	0.0125	0.0070	m
Radiated near-field distance	0.32	0.43	m

Table B.3.1.5.1-3: Void

Table B.3.1.5.1-4: Void

B.3.1.5.2 Void

B.3.1.5.3 Void

B.3.1.5.4 SNR range for SNR_{RP} - SNR_{BB} ≤ 1dB

Based on the method of setting the noise from the Test system to give a maximum of 1dB degradation in overall SNR between reference point and baseband, we can then work back through the signal chain to determine how high the SNR

can be set. As the noise is set to a fixed level, the maximum SNR is set by the test system power amplifier and the channel bandwidth to be tested.

The SNR upper bound depends on the type of test system. For the Direct Near field (DNF) setup the diagram below illustrates the principle, and is based on the “DNF 100MHz” tab of the accompanying spreadsheet.

The process works back through the signal chain, from left to right in the diagram.

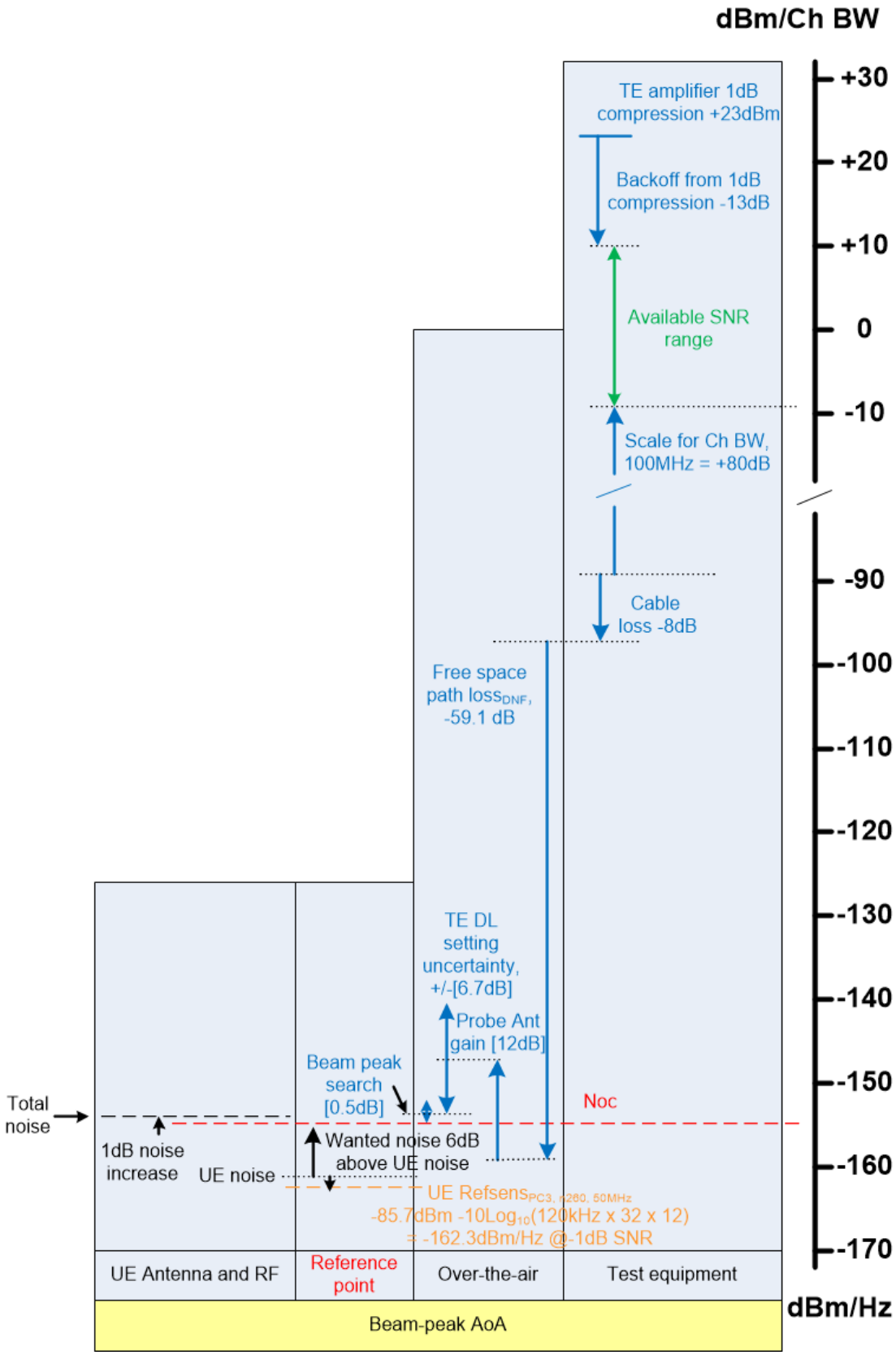

Figure B.3.1.5.4-1: Estimation of SNR range for Direct near field (DNF)

The test equipment must supply at least the wanted noise level at the reference point. If the noise was lower, the degradation in SNR would be greater than 1dB, and may cause a conformant UE to fail.

The accuracy of setting the signal and noise levels has been taken as +/-[6.7]dB, which is based on the Direct Far Field measurement uncertainty for EIS in Table B.1.1.3-2. The uncertainty is subject to further analysis by RAN5.

During conformance test, the test system will need to find the UE Rx beam peak. At present an allowance of [0.5] dB has been included, but is subject to further analysis by RAN5.

Inclusion of these two contributions directly reduces the maximum SNR that can be measured by a test system for a given channel bandwidth. To find the maximum SNR that can be measured by a test system with a specific Channel BW, the baseband SNR in the spreadsheet is increased until the value “Wanted signal + headroom, dBm/Ch BW” is just below the “TE Power amplifier 1dB compression, dBm” value. The resulting values are given in Table B.3.1.5.4-1.

Table B.3.1.5.4-1: Predicted SNR upper bound values for Direct Near field (DNF)

Channel Bandwidth	Maximum SNR
100MHz	[21.8dB]
200MHz	[18.7dB]

Note that these are UE baseband SNR values, so the Reference point figures used in TS 38.101-4 will be 1dB higher. Values are based on UE parameters and currently foreseen test equipment limitations, and could be improved in future.

Note that for the DNF method, values may need to be adjusted to take account of near-field effects.

An example of SNR calculation for DNF method is provided in “Spreadsheet 2 - Demod SNR range calculator.xls” file attached to the TR.

B.3.2 Direct far field (DFF) setup

The Measurement uncertainty contributions and uncertainty assessment are expected to be the same as for the Direct near field (DNF) setup in B.3.1.

B.3.2.1 Void

B.3.2.2 Void

B.3.2.3 Void

B.3.2.4 Void

B.3.2.5 Assessment of testable SNR range

The signal and the noise provided by the test system are both attenuated by the over-the-air link loss. The UE noise then adds to the noise provided by the test system, hence degrading the SNR seen by the UE and potentially limiting the testable SNR range.

For conducted tests, the noise provided by the test system can be set much higher than the UE noise and the SNR degradation is negligible. However for over-the-air test systems, the power that can realistically be delivered into the test system probe antenna is limited, so the test point is likely to be closer to the UE noise and a small SNR degradation is allowable.

B.3.2.5.1 Method and Parameters

The method and parameters are the same as B.2.1.5.1. The calculation of noise level is in clause 7.2.1.3.

B.3.2.5.2 Void

B.3.2.5.3 Void

B.3.2.5.4 SNR range for SNR_{RP} - SNR_{BB} ≤ 1dB

Based on the method of setting the noise from the Test system to give a maximum of 1dB degradation in overall SNR between reference point and baseband, we can then work back through the signal chain to determine how high the SNR can be set. As the noise is set to a fixed level, the maximum SNR is set by the test system power amplifier and the channel bandwidth to be tested.

The SNR upper bound depends on the type of test system. For the Direct Far field (DFF) setup the diagram below illustrates the principle, and is based on the “DFF 100MHz” tab of the accompanying spreadsheet.

The process works back through the signal chain, from left to right in the diagram.

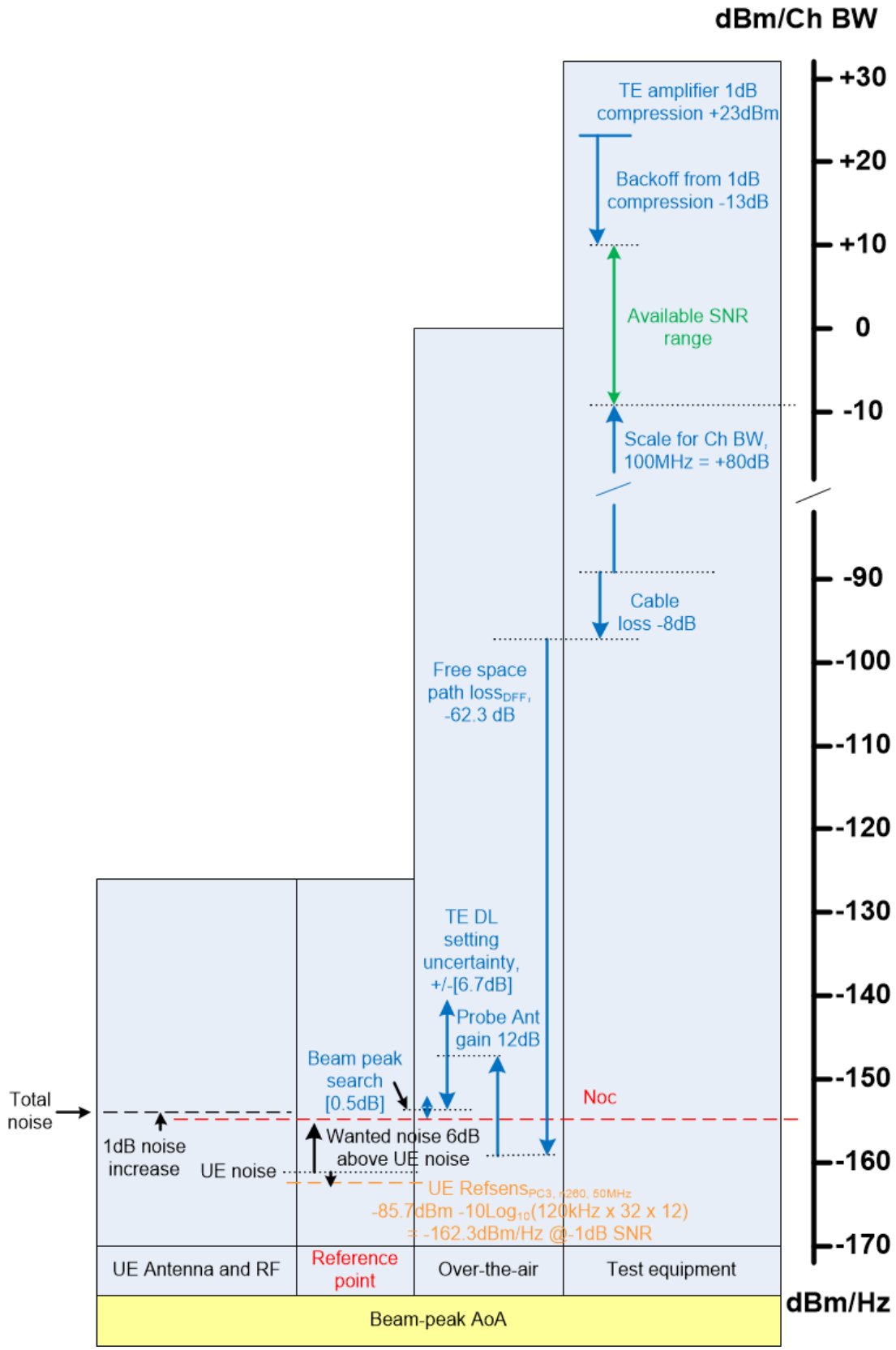

Figure B.3.2.5.4-1: Estimation of SNR range for Direct far field (DFF)

The test equipment must supply at least the wanted noise level at the reference point. If the noise was lower, the degradation in SNR would be greater than 1dB, and may cause a conformant UE to fail.

The accuracy of setting the signal and noise levels has been taken as +/-[6.7]dB, which is based on the Direct Far Field measurement uncertainty for EIS in Table B.1.1.3-2. The uncertainty is subject to further analysis by RAN5.

During conformance test, the test system will need to find the UE Rx beam peak. At present an allowance of [0.5] dB has been included, but is subject to further analysis by RAN5.

Inclusion of these two contributions directly reduces the maximum SNR that can be measured by a test system for a given channel bandwidth. To find the maximum SNR that can be measured by a test system with a specific Channel BW, the baseband SNR in the spreadsheet is increased until the value “Wanted signal + headroom, dBm/Ch BW” is just below the “TE Power amplifier 1dB compression, dBm” value. The resulting values are given in Table B.3.2.5.4-1.

Table B.3.2.5.4-1: Predicted SNR upper bound values for Direct far field (DFF)

Channel Bandwidth	Maximum SNR
100MHz	[18.5dB]
200MHz	[15.5dB]

Note that these are UE baseband SNR values, so the Reference point figures used in TS 38.101-4 will be 1dB higher. Values are based on UE parameters and currently foreseen test equipment limitations, and could be improved in future.

An example of SNR calculation for DFF method is provided in “Spreadsheet 2 - Demod SNR range calculator.xls” file attached to the TR.

B.3.3 Indirect far field (IFF) setup

B.3.3.1 Uncertainty budget calculation principle

The uncertainty tables cover the actual measurement using the DUT receiver. If applicable, any uncertainty arising from a calibration or alignment process before the measurements should also be included.

The MU budget should comprise of a minimum 5 headings:

1) The uncertainty source,
2) Uncertainty value,
3) Distribution of the probability,
4) Divisor based on distribution shape,
5) Calculated standard uncertainty (based on uncertainty value and divisor).

B.3.3.2 Uncertainty budget format

Table B.3.3.2-1: Uncertainty contributions for T-put test with defined SNR at reference point

UID	Description of uncertainty contribution	Details in annex
	During T-put measurement	
1	gNB emulator SNR uncertainty	B.3.3.4.1
2	gNB emulator DL EVM	B.3.3.4.2
3	gNB emulator fading model impairments	B.3.3.4.3
Note 1: Handling of effects related to isolation and alignment of Horizontal / Vertical polarisation is not defined Note 2: Handling of effects related to Quality of Quiet zone is not defined		

B.3.3.3 Uncertainty assessment

The uncertainty assessment tables are organized as follows:

- The uncertainty assessment for T-put measurement at defined SNR, is provided in Table B.3.3.3-1

Table B.3.3.3-1: Uncertainty assessment for T-put test with defined SNR at reference point

UID	Uncertainty source	Uncertainty value	Distribution of the probability	Divisor	Standard uncertainty (σ) [dB]
During T-put measurement					
1	gNB emulator SNR uncertainty	0.3dB	Normal	2.00	0.15
2	gNB emulator DL EVM	-	One-sided, beneficial	-	0
3	gNB emulator fading model impairments Note 3	[0.5dB]	Normal	2.00	[0.25]
SNR Expanded uncertainty (1.96σ - confidence interval of 95 %) [dB]					[0.57]
Note 1: Handling of effects related to isolation and alignment of Horizontal / Vertical polarisation is not defined Note 2: Handling of effects related to Quality of Quiet zone is not defined Note 3: The value is same as for LTE and shall be verified for other channel models by RAN5 during detailed MU assessment					

B.3.3.4 Measurement error contribution descriptions

B.3.3.4.1 gNB emulator SNR uncertainty

See B.3.1.4.1

B.3.3.4.2 gNB emulator Downlink EVM

See B.3.1.4.2

B.3.3.4.3 gNB emulator fading model impairments

See B.3.1.4.3

B.3.3.5 Assessment of testable SNR range

The Assessment of testable SNR range follows the same principle as B.3.1.5, but the values related to the test system are different and provide a different testable SNR range.

B.3.3.5.1 Method and Parameters

The method is the same as B.2.1.5.1, but the values related to the test system are different. The calculation of noise level is in clause 7.2.1.3.

B.3.3.5.2 Void

B.3.3.5.3 Void

B.3.3.5.4 SNR range for SNR_{RP} - SNR_{BB} ≤ 1dB

Based on the method of setting the noise from the Test system to give a maximum of 1dB degradation in overall SNR between reference point and baseband, we can then work back through the signal chain to determine how high the SNR can be set. As the noise is set to a fixed level, the maximum SNR is set by the test system power amplifier and the channel bandwidth to be tested.

The SNR upper bound depends on the type of test system. For the Indirect Far field (IFF) setup the diagram below illustrates the principle, and is based on the “IFF 100MHz” tab of the accompanying spreadsheet.

The process works back through the signal chain, from left to right in the diagram.

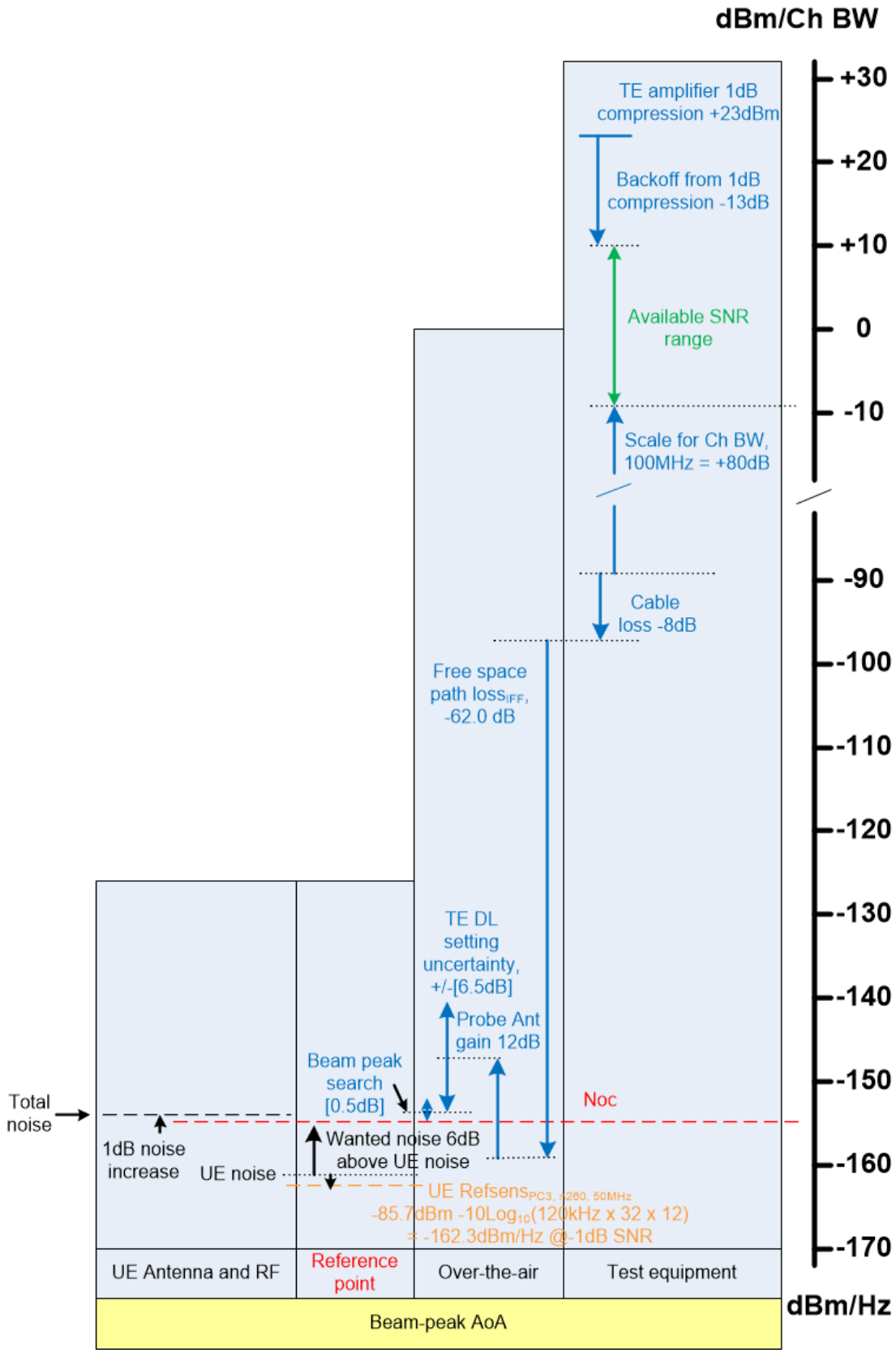

Figure B.3.3.5.4-1: Estimation of SNR range for Indirect far field (IFF)

The test equipment must supply at least the wanted noise level at the reference point. If the noise was lower, the degradation in SNR would be greater than 1dB, and may cause a conformant UE to fail.

The accuracy of setting the signal and noise levels has been taken as +/-[6.5]dB which is based on the Indirect Far Field measurement uncertainty for EIS in Table B.1.3.3-2. The uncertainty is subject to further analysis by RAN5.

During conformance test, the test system will need to find the UE Rx beam peak. At present an allowance of [0.5] dB has been included, but is subject to further analysis by RAN5.

Inclusion of these two contributions directly reduces the maximum SNR that can be measured by a test system for a given channel bandwidth. To find the maximum SNR that can be measured by a test system with a specific Channel BW, the baseband SNR in the spreadsheet is increased until the value “Wanted signal + headroom, dBm/Ch BW” is just below the “TE Power amplifier 1dB compression, dBm” value. The resulting values are given in Table B.3.3.5.4-1.

Table B.3.3.5.4-1: Predicted SNR upper bound values for Indirect far field (IFF)

Channel Bandwidth	Maximum SNR
100MHz	[19.0dB]
200MHz	[16.0dB]

Note that these are UE baseband SNR values, so the Reference point figures used in TS 38.101-4 will be 1dB higher. Values are based on UE parameters and currently foreseen test equipment limitations, and could be improved in future.

An example of SNR calculation for IFF method is provided in “Spreadsheet 2 - Demod SNR range calculator.xls” file attached to the TR.

Annex C:
UE coordinate system

C.1 Reference coordinate system

This annex defines the measurement coordinate system for the NR UE. The reference coordinate system, reused from the LTE MIMO OTA definition in [5], is provided in Figure C.1-1 below.

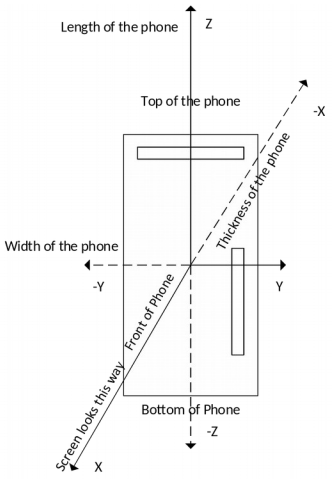

Figure C.1-1: Reference coordinate system

The following aspects are necessary:

- A basic understanding of the top and bottom of the device is needed in order to define unambiguous DUT positioning requirements for the test
- An understanding of the origin of the test system (i.e. the direction in which the x-axis points inside the test chamber) is needed in order to define unambiguous DUT orientation, DUT beam, signal, interference, and measurement angles

C.2 Test conditions and angle definitions

Table C.2-1 below provides the test conditions and angle definitions.

Table C.2-1: Test conditions and angle definitions

Test condition	DUT orientation	Link angle	Measurement angle	Diagram
Free space	Ψ=0; Θ=0; Φ=0	θ_{Link}; φ_{Link} with polarization reference Pol_{Link} = θ or ; φ	Θ_{Meas}; φ_{Meas} with polarization reference Pol_{Meas} = θ or ; φ	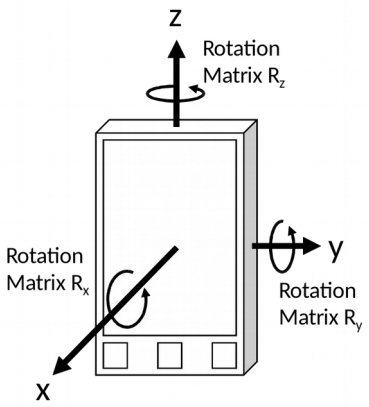
NOTE 1: A polarization reference, as defined in relation to the reference coordinate system in E.1, is maintained for each signal angle, link or interferer angle, and measurement angle				

For each UE requirement and test case, each of the parameters in Table C.2-1 are defined as single values or ranges of values, such that DUT positioning, DUT beam direction, and angles of the signal, link/interferer, and measurement are specified.

Due to the non-commutative nature of rotations, the order of rotations is important and needs to be defined when multiple DUT orientations are tested.

The rotations around the x, y, and z axes can be defined with the following rotation matrices

$$R_x(\alpha) = \begin{pmatrix} 1 & 0 & 0 & 0 \\ 0 & \cos\alpha & -\sin\alpha & 0 \\ 0 & \sin\alpha & \cos\alpha & 0 \\ 0 & 0 & 0 & 1 \end{pmatrix}$$

$$R_y(\beta) = \begin{pmatrix} \cos\beta & 0 & \sin\beta & 0 \\ 0 & 1 & 0 & 0 \\ -\sin\beta & 0 & \cos\beta & 0 \\ 0 & 0 & 0 & 1 \end{pmatrix}$$

and

$$R_z(\gamma) = \begin{pmatrix} \cos\gamma & -\sin\gamma & 0 & 0 \\ \sin\gamma & \cos\gamma & 0 & 0 \\ 0 & 0 & 1 & 0 \\ 0 & 0 & 0 & 1 \end{pmatrix}$$

with the respective angles of rotation, α, β, γ and

$$\begin{pmatrix} x' \\ y' \\ z' \\ 1 \end{pmatrix} = R \begin{pmatrix} x \\ y \\ z \\ 1 \end{pmatrix}$$

Additionally, any translation of the DUT can be defined with the translation matrix

$$T(t_x, t_y, t_z) = \begin{pmatrix} 1 & 0 & 0 & t_x \\ 0 & 1 & 0 & t_y \\ 0 & 0 & 1 & t_z \\ 0 & 0 & 0 & 1 \end{pmatrix}$$

with offsets t_x, t_y, t_z in x, y, and z, respectively and with

$$\begin{pmatrix} x' \\ y' \\ z' \\ 1 \end{pmatrix} = T \begin{pmatrix} x \\ y \\ z \\ 1 \end{pmatrix}$$

The combination of rotations and translation is captured by the multiplication of rotation and translation matrices.

For instance, the matrix M

$$M = T(t_x, t_y, t_z) R_x(\alpha) R_y(\beta) R_z(\gamma)$$

describes an initial rotation of the DUT around the z axis with angle γ, a subsequent rotation around the y axis with angle β, and a final rotation around the x axis with angle α. After those rotations, the DUT is translated by t_x, t_y, t_z in x, y, and z, respectively.

C.3 DUT positioning guidelines

The centre of the reference coordinate system shall be aligned with the geometric centre of the DUT in order to minimize the offset between antenna arrays integrated at any position of the UE and the centre of the quiet zone.

Near-field coupling effects between the antenna and the pedestals/positioners/fixtures generally cause increased signal ripples. Re-positioning the DUT by directing the beam peak away from those areas can reduce the effect of signal ripple on EIRP/EIS measurements. Figure C.3-1 and C.3-2 illustrate how to reposition the DUT in a distributed axes and combined axes system, when the beam peak is directed to the DUTs upper hemisphere (DUT orientation 1) or the DUTs lower hemisphere (DUT orientation 2).

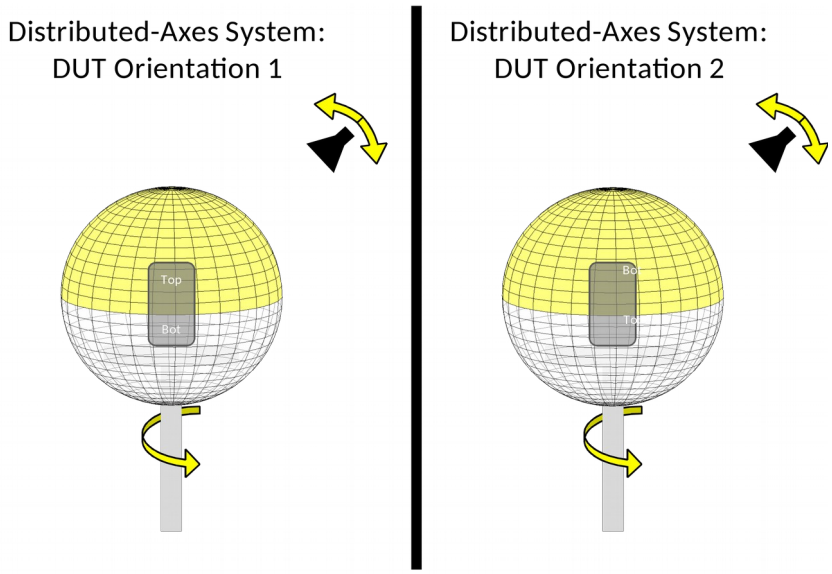

Figure C.3-1: DUT re-positioning for distributed-axes system

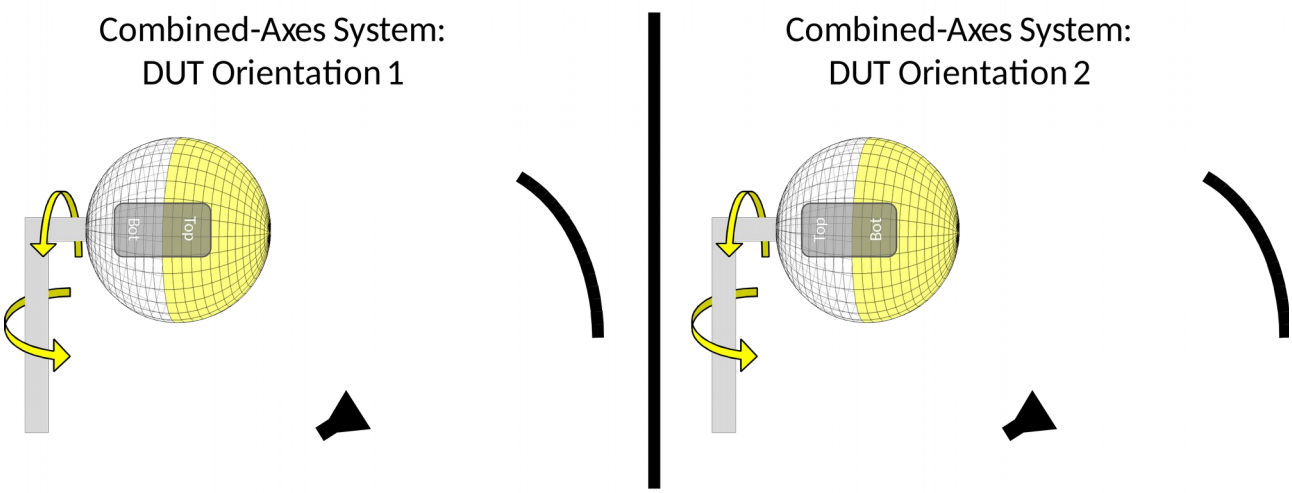

Figure C.3-2: DUT re-positioning for combined-axes system

For EIRP/EIS measurements, re-positioning the DUT makes sure the pedestal is not obstructing the beam path and that the pedestal is not in closer proximity to the measurement antenna/reflector than the DUT. For TRP measurements, re-positioning the DUT makes sure that the beam peak direction is not obstructed by the pedestal and the pedestal is in the measurement path only when measuring the back-hemisphere. No re-positioning during the TRP measurement is required.

Annex D:
Quality of the quiet zone validation

D.1 General

This annex describes the procedures for validating the quality of the quiet zone for the permitted far-field methods outlined in subclause 5.2.1 (DFF), in subclause 5.2.2 (simplified DFF), and in subclause 5.2.3 (IFF).

D.2 Procedure to characterize the quality of the quiet zone for the permitted far field methods

This procedure is mandatory before the test system is commissioned for certification tests and characterizes the quiet zone performance of the anechoic chamber, specifically the effect of reflections within the anechoic chamber including any positioners and support structures. Additionally, it includes the effect of offsetting the directive antenna array inside a DUT from the centre of the quiet zone, i.e., the centre of rotation of the DUT and measurement antenna positioning systems as well as the directivity MU, i.e., the variation of antenna gains in the different direct line-of-sight links.

The quiet zone is illustrated in Figure D.2-1 which includes the definitions of centre of quiet zone range, i.e., the geometric centre of the positioning systems, and the range length, i.e., the distance between the centre of the quiet zone and the aperture of the measurement antenna.

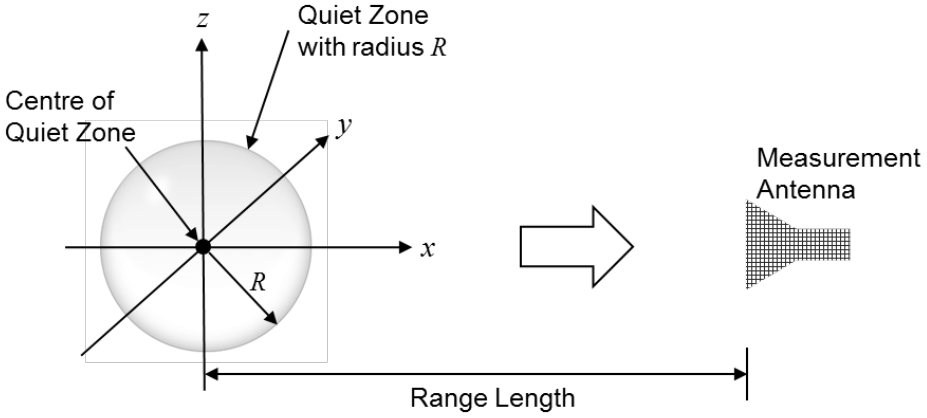

Figure D.2-1: Quiet Zone Illustration

The outcome of the procedures can be used to predict the

- variation of the TRP measurements, spherical surface integrals of EIRP/EIS, when the DUT is placed anywhere within the quiet zone and with the beam formed in any arbitrary direction inside the chamber
- variation of the EIRP/EIS measurements when the DUT is placed anywhere within the quiet zone and with the beam formed in any arbitrary direction inside the chamber

The reference coordinate system defined in Appendix C applies to this procedure.

D.2.1 Equipment used

The reference antenna under test (AUT) that is placed at various locations within the quiet zone shall be a directive antenna with similar properties of typical antenna arrays integrated in DUTs. The characteristics in terms of Directivity and Half Power Beamwidth (HPBW) of the reference AUT are shown in Figure D.2.1-1, D.2.1-2, and D.2.1-3.

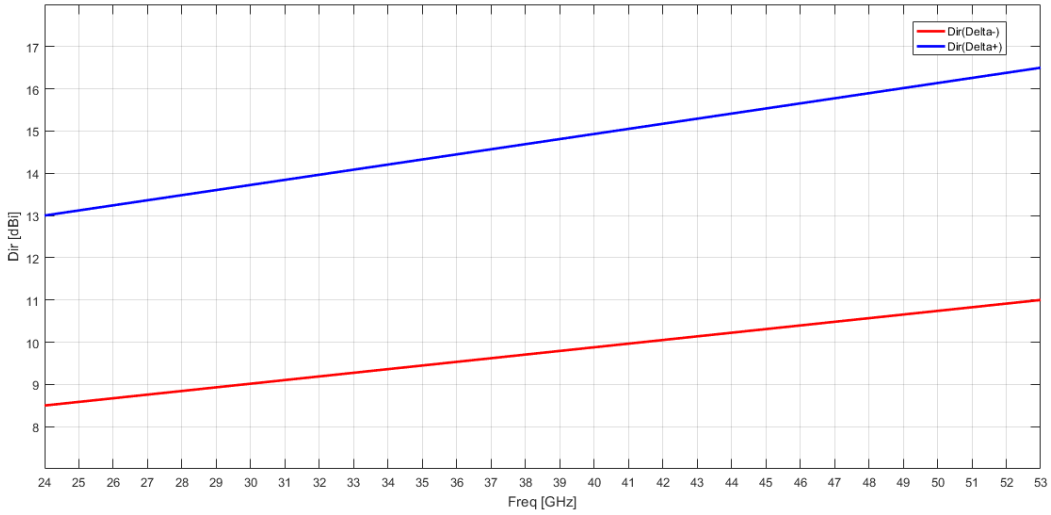

Figure D.2.1-1: Directivity mask

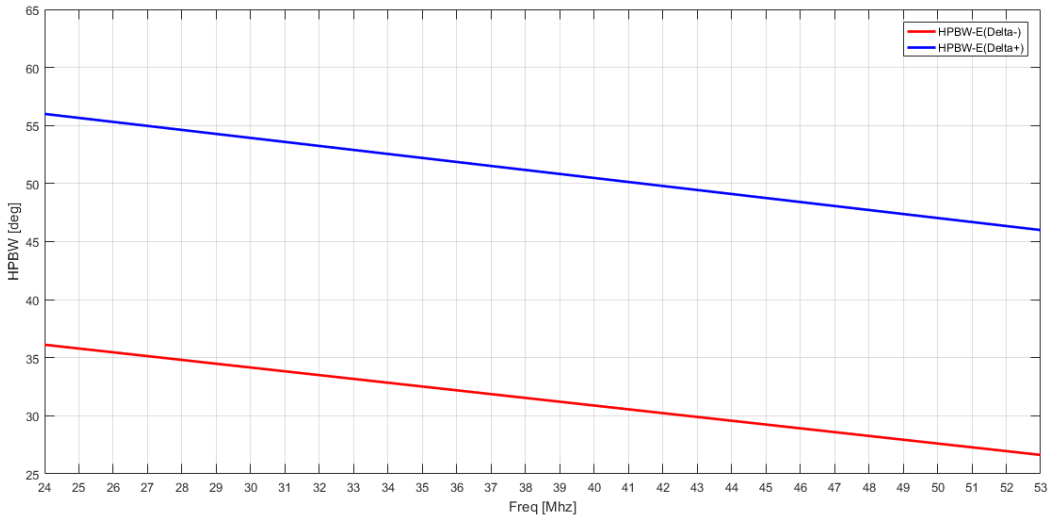

Figure D.2.1-2: 2xHPBW-E mask

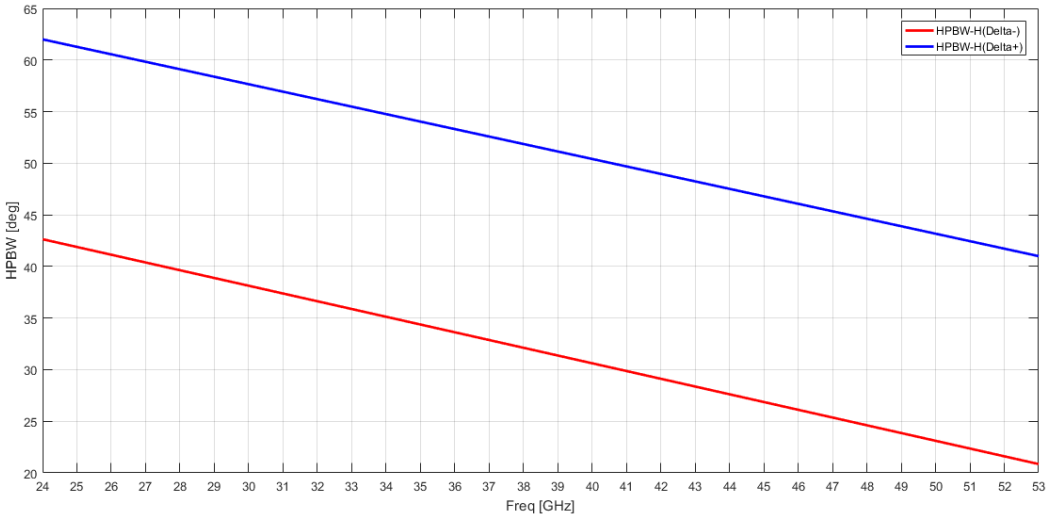

Figure D.2-3: 2xHPBW-H mask

AUT shall be symmetric on E and H planes.

The above masks for the reference antenna are met based on antenna vendors' calibration report.

For the measurement, a combination of signal generator and spectrum analyser or a network analyser can be used. The multi-port (with three ports) network analyser is most suitable to reduce test time as both polarizations of the measurement antenna can be measured simultaneously and multiple frequencies can be measured in a sweep.

D.2.2 Test frequencies

The frequencies to be used to characterize the quality of the quiet zone shall be identified during final test method definition in RAN5 WG. The quiet zone validation analysis is performed for each frequency individually.

D.2.3 Reference measurements

The quality of the quiet measurements for integrated RF parameters such as TRP shall use 3D pattern measurements of the reference antenna patterns as they most closely resemble the 3D/spherical surface measurements/integrals of EIRP or EIS. Therefore, the quality of the quiet zone measurements for TRP metrics shall be based on efficiency measurements. On the other hand, the quality of the quiet zone measurements for single-directional EIRP and EIS metrics shall be based on gain measurements of the direct line-of-sight link between the reference AUT and the measurement antenna.

D.2.4 Size of the quiet zone

The size of the quiet zone within which the variations of measurements are evaluated depends on the size of the DUT. For smartphones, the quiet zone shall be considered a sphere with radius of R=7.5cm. Alternate quiet zone sizes can be defined for larger DUTs.

D.2.5 Minimum range length

The minimum range length depends on the size of the DUT and the minimum far-field distance of typical antenna arrays integrated in DUTs.

D.2.6 Reference AUT positions

The reference AUT shall be positioned in a total of 7 different reference positions, shown in Figure D.2.6.1-1 and D.2.6.2-1

While position 1, P1, is the centre of the quiet zone, the remaining positions, 2 through 7, are off-centre positions each displaced by the radius of the quiet zone, R. The coordinates of the respective test points are shown in Table D.2.6-1.

Table D.2.6-1: Reference AUT Measurement Coordinates

Position	*x*	*y*	*z*
P1	0	0	0
P2	*R*	0	0
P3	-*R*	0	0
P4	0	*R*	0
P5	0	-*R*	0
P6	0	0	*R*
P7	0	0	-*R*

D.2.6.1 Distributed-axes system

The reference AUT shall be positioned in a total of 7 different reference positions, shown in Figure D.2.6.1-1.

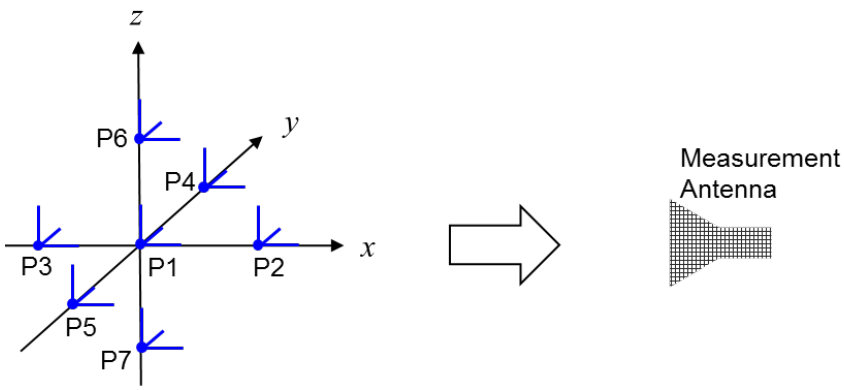

Figure D.2.6.1-1: Reference AUT Measurement Positions for distributed-axes system

The reference AUT positions inside a typical distributed-axes system are shown in Figure D.2.6.1-2.

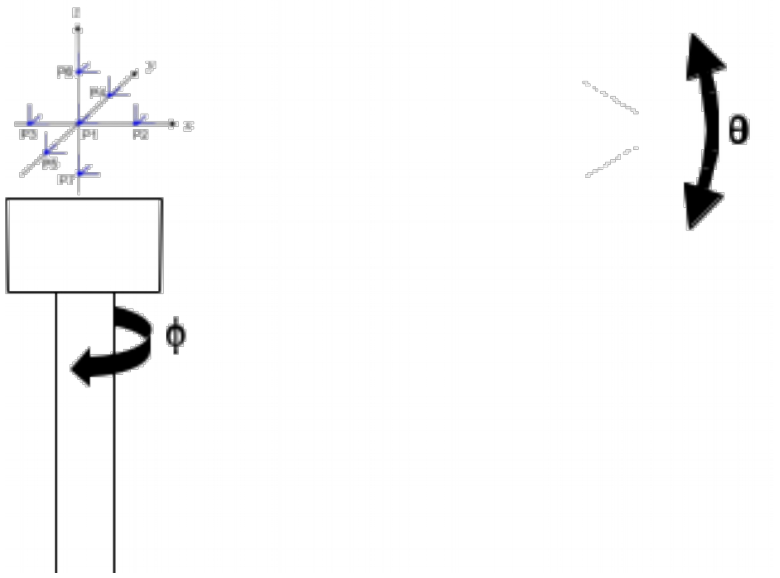

Figure D.2.6.1-2: Reference AUT Measurement Positions for distributed-axes system

D.2.6.2 Combined-axes system

The reference AUT shall be positioned in a total of 7 different reference positions, shown in Figure D.2.6.2-1.

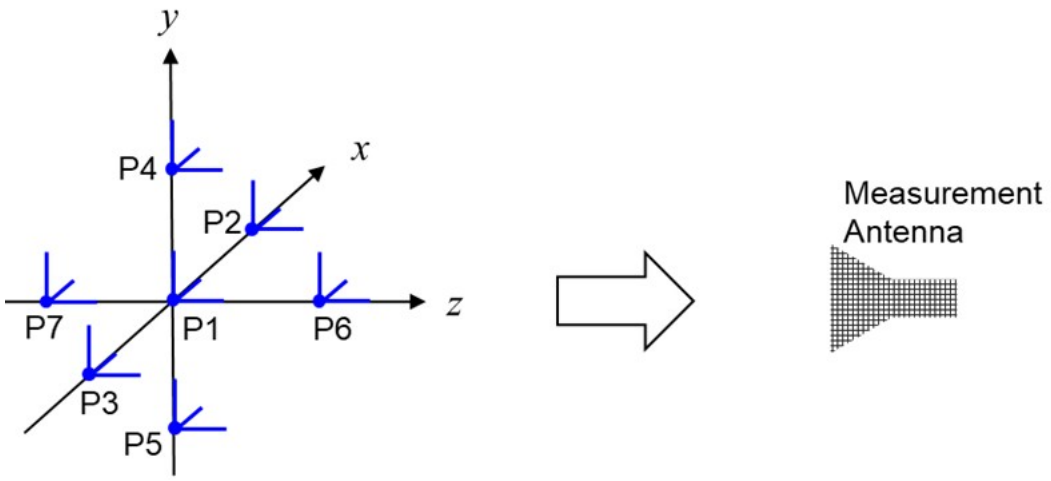

Figure D.2.6.2-1: Reference AUT Measurement Positions for combined-axes system

The reference AUT positions inside a typical combined-axes system are shown in Figure D.2.6.2-2.

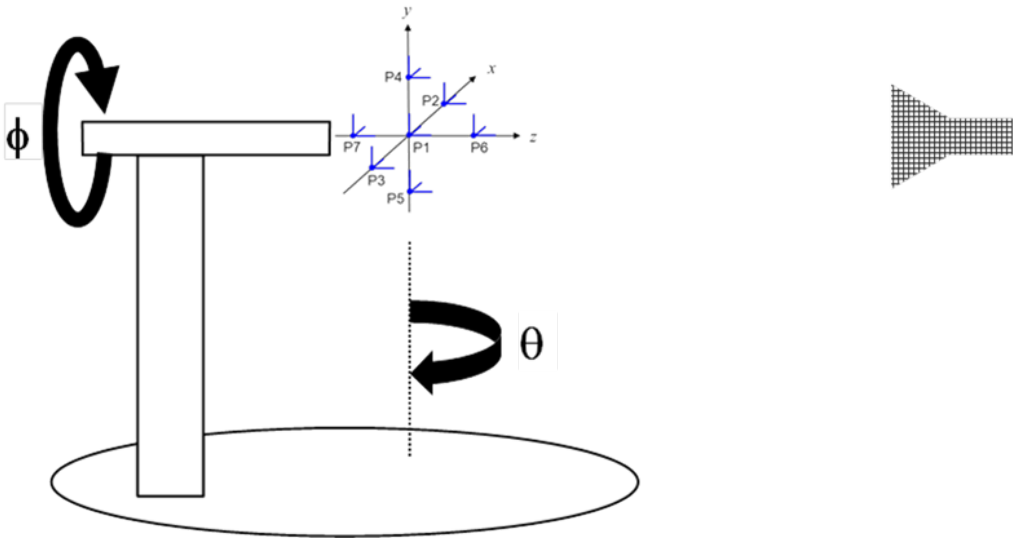

Figure D.2.6.2-2: Reference AUT Measurement Positions for combined-axes system

D.2.7 Reference AUT orientations

As different areas within the chamber could yield variations in the field uniformity inside the quiet zone caused by reflections, it is important to characterize the electromagnetic fields with the reference antennas uniformly illuminating the anechoic chamber.

D.2.7.1 Distributed-axes system

In order to keep the quality of the quiet zone characterization manageable in terms of test times, it is suggested to perform the reference measurements for the reference AUT placed at the 7 antenna positions with the antenna rotated around the y axis with 5 different angles β, i.e., $\beta = 0^o$, 45^o, 90^o, 135^o, and 180^o, and rotated around the z axis with 8 different $\gamma = 0^o$, 45^o, 90^o, 135^o, 180^o, 225^o, 270^o, and 315^o. A graphical illustration of the some sample reference AUT orientations is shown in Figure D.2.7.1-1 with a reference AUT placed at position 6, P6, for reference antenna polarization $\gamma_{pol} = 0^o$; Figure D.2.7.1-2 illustrates the reference AUT orientations for the reference polarization $\gamma_{pol} = 90^o$.

The matrix operation for the rotations and translation is defined as

$$M = T(t_x, t_y, t_z)\,\mathbf{R}_z(\gamma)\,\mathbf{R}_y(\beta)\,\mathbf{R}_{z,pol}(\gamma_{pol})$$

for the distributed-axes system.

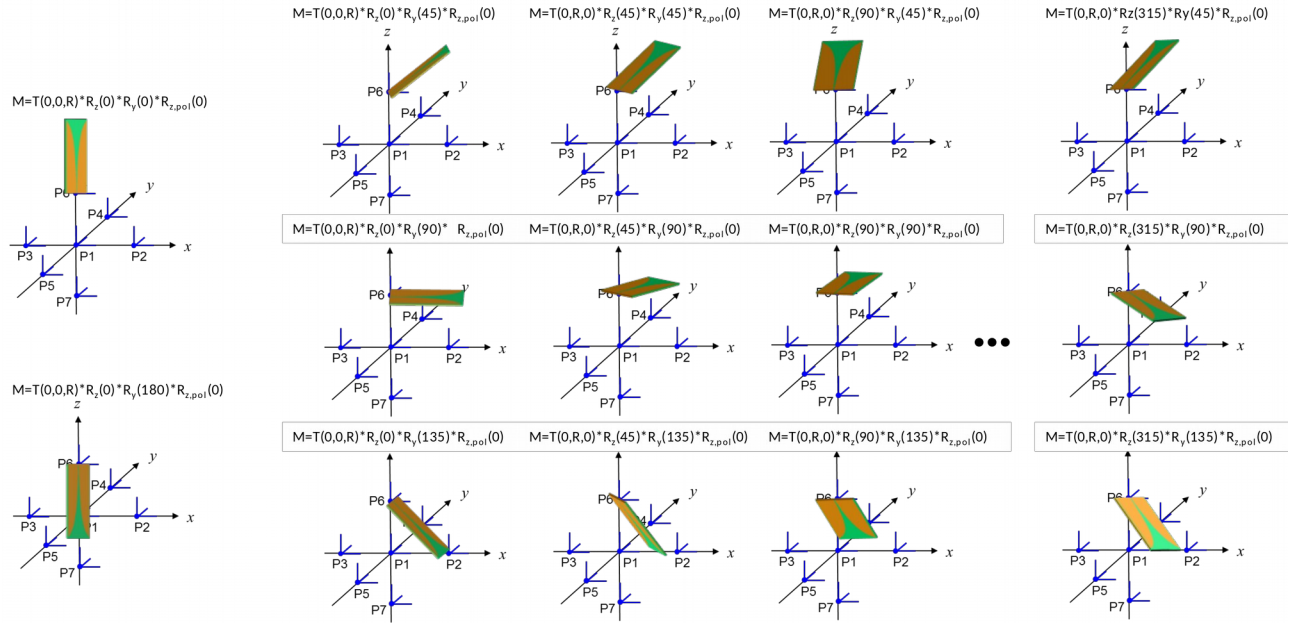

Figure D2.7.1-1: Sample reference AUT orientations for position 6, P6 for reference antenna polarization $\gamma_{pol} = 0^o$.

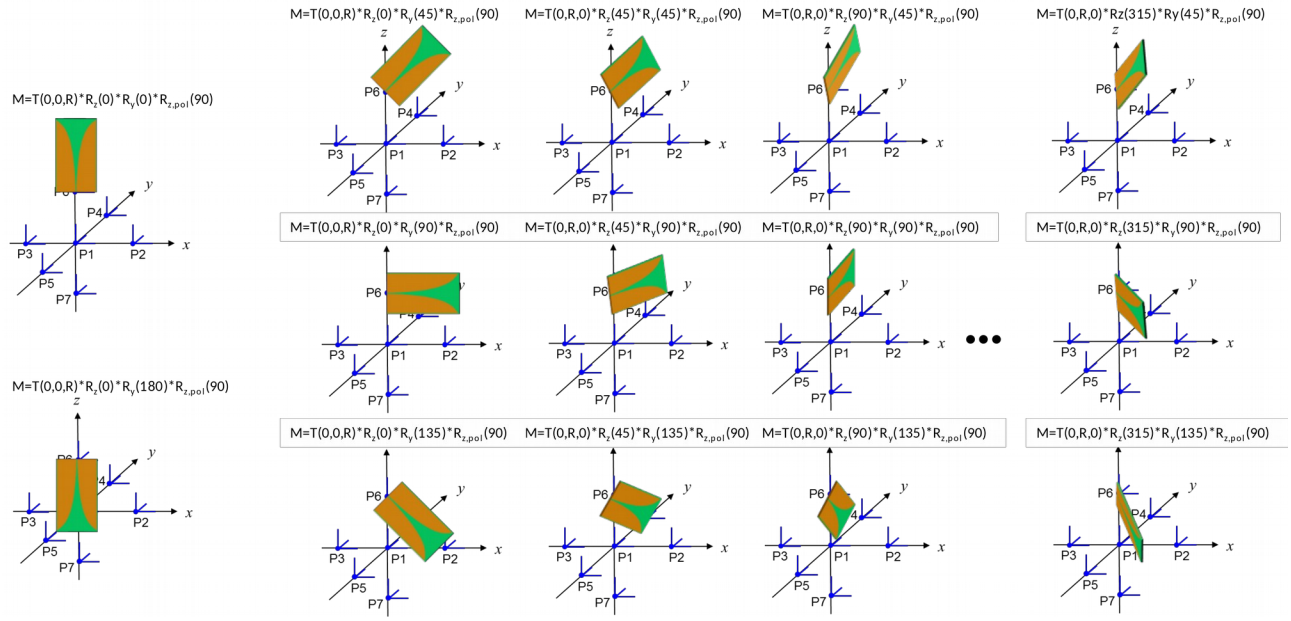

Figure D.2.7.1-2: Sample reference AUT orientations for position 6, P6, for reference antenna polarization $\gamma_{pol} = 90^o$.

When facing the z-axis, $\beta = 0^o$ and $\beta = 180^o$, the antenna does not need to be evaluated for the 8 different rotations around the z axis. A single orientation is sufficient since those orientations are unique. Due to the pedestal, distributed-axes systems are not able to measure towards the β =180º direction; for those systems, the reference measurements at this reference AUT orientation can be skipped.

If the device re-positioning approach outlined in Annex C.3 is adopted for the EIRP/EIS/TRP based conformance test cases, the quality of quiet zone analysis is sufficient only for β = 0º, 45º, 90º.

D.2.7.2 Combined-axes system

In order to keep the quality of the quiet zone characterization manageable in terms of test times, it is suggested to perform the reference measurements for the reference AUT placed at the 7 antenna positions with the antenna rotated

around the x axis with 5 different angles α, i.e., α = -90°, -45°, 0°, 45°, and 90° and rotated around the y axis with 8 different angles β = 0°, 45°, 90°, 135°, 180°, 225°, 270°, and 315°. A graphical illustration of some sample reference AUT orientations is shown in Figure D.2.7.2-1 with a reference AUT placed at position 4, P4, for reference antenna polarization γ_{pol} = 0°; Figure D.2.7.2-2 illustrates the reference AUT orientations for the reference polarization γ_{pol} = 90°.

The matrix operation for the rotations and translation is defined as

$$M = T(t_x, t_y, t_z)\,\mathcal{R}_y(\beta)\,\mathcal{R}_x(\alpha)\,\mathcal{R}_{z,pol}(\gamma_{pol})$$

for the combined-axes system.

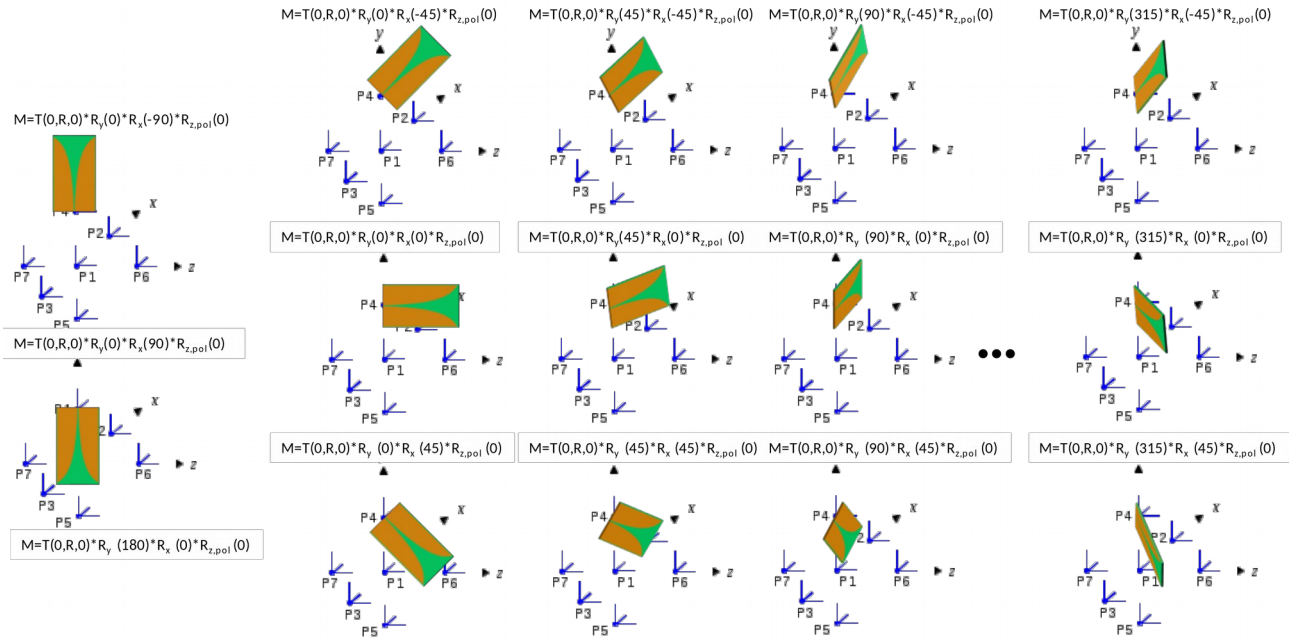

Figure D.2.7.2-1: Sample reference AUT orientations for position 4, P4, for reference antenna polarization γ_{pol} = 0°.

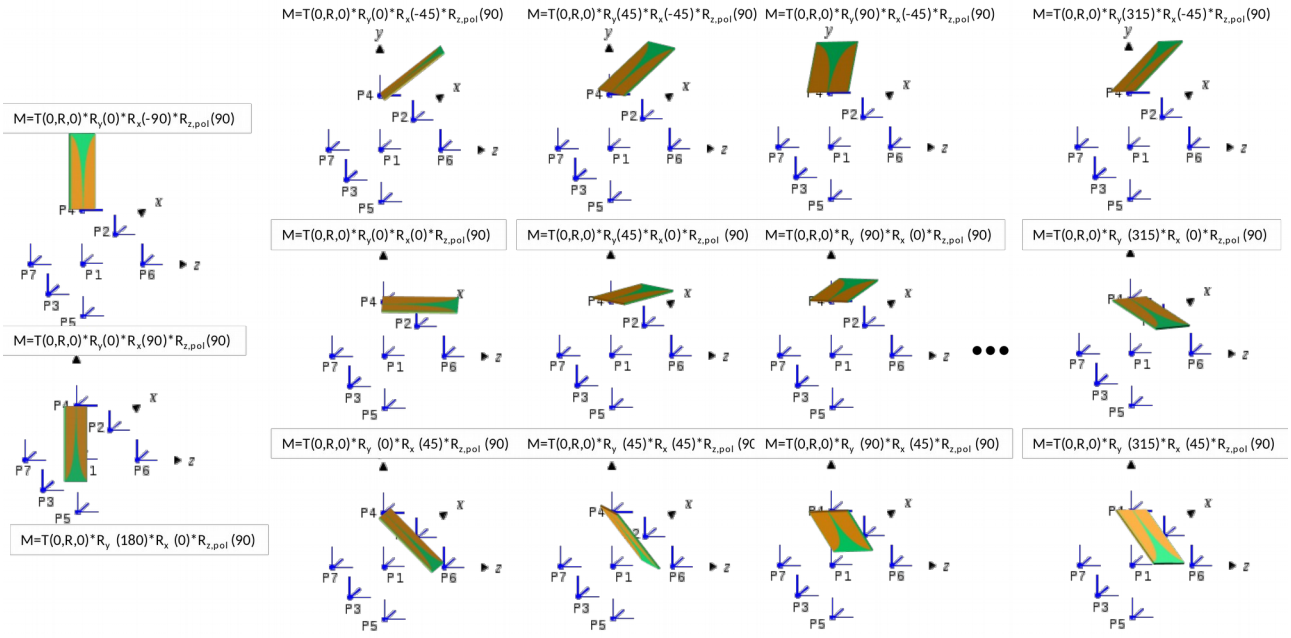

Figure D.2.7.2-2: Sample reference AUT orientations for position 4, P4, for reference antenna polarization γ_{pol} = 90°.

When facing the y axis, α = 90º and α = -90º, the antenna does not need to be evaluated for the 8 different rotations around the y axis. A single rotation is sufficient since those orientations are unique. Due to the pedestal of the 2-axis positioner, combined-axes systems are not able to measure towards the β = 180º direction; for those systems, the reference measurements at this reference AUT orientation can be skipped.

If the device re-positioning approach outlined in Annex C.3 is adopted for all EIRP/EIS/TRP based conformance test cases, the quality of quiet zone analysis is sufficient only for β = 0º, 45º, 90º, 270º, and 315º.

D.2.8 Quality of quiet zone measurement uncertainty calculations for TRP

The combined MU element related to the quality of the quiet zone for TRP and offset between UE antenna array and centre of quiet zone is the standard deviation of the various efficiency measurement results that are based on the 7 different reference AUT positions, the respective reference AUT orientations, and the two reference AUT polarization orientations..

D.2.9 Quality of quiet zone measurement uncertainty for EIRP/EIS

The MU for the quality of the quiet zone for EIRP/EIS includes the additional MU element of the directivity of the DUT and measurement antennas as shown in Figure D.2.9-1. The EIRP/EIS measurements are taking the peak gains of the respective antennas into account with the reference AUT placed in the centre of the quiet zone. Once the antenna is displaced in directions other than the measurement antenna, the direct line-of-sight link is taking reduced antenna gains into account. The type of reference AUT should therefore have similar pattern properties as typical UE antennas. For systems with very large range lengths, the directivity MU will be insignificant.

The combined MU element related to the quality of the quiet zone for EIRP/EIS, offset between UE antenna array and centre of quiet zone, and directivity is the standard deviation of the single-point gain measurement results that are based on the 7 different reference AUT positions, the respective reference AUT orientations, and the two reference AUT polarization orientations.

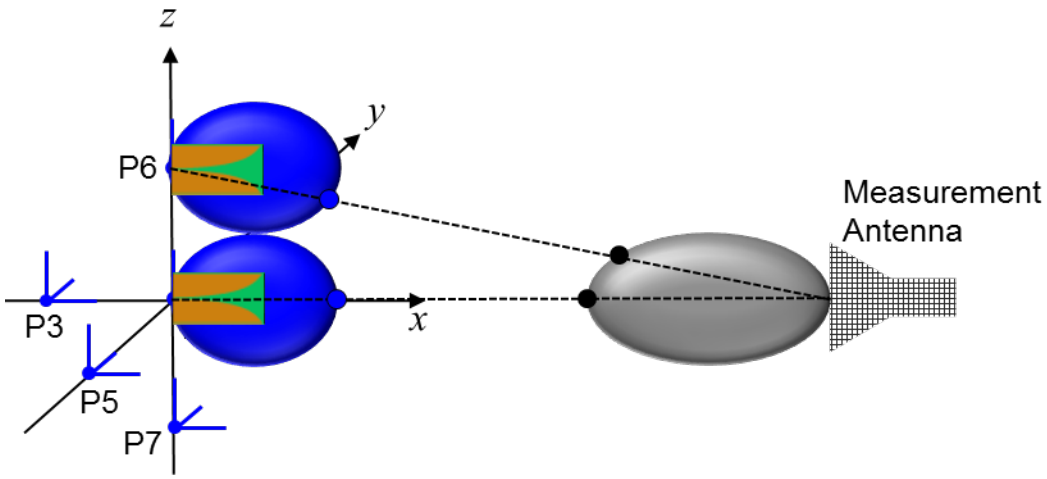

Figure D.2.9-1: Illustration of the Directivity MU Element.

Annex E:
Rationale behind IFF method 1

E.1 IFF method 1 – working principle

A CATR (Compact Antenna Test Range) is a collimator system in which the spherical wave is transformed in plane wave within the desired quiet zone (QZ). In other words, a compact range project the measurement (range) antenna infinitely far away thus making it a far-field range. Figure E.1-1 does show this concept:

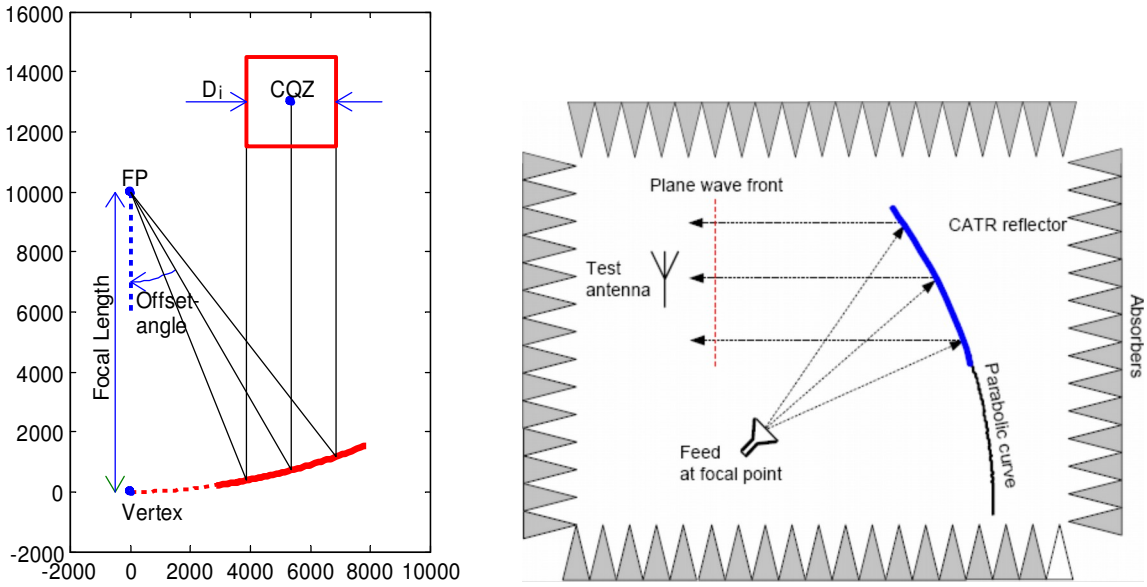

Figure E.1-1: Compact Range – working principle

This is a reciprocal system setup. For TX measurements, the device under test will radiate a spherical wavefront to the range collimator which focalises into the feed antenna only the propagation vector which matches with the boresight direction of the reflector. On the other hand, for RX measurements, the feed antenna would radiate a spherical wavefront to the range reflector which is collimated towards the DUT. In other words, the spherical wavefront is transformed into a plane wavefront when at the DUT.

In order to meet the requirements, the following parameters are mainly considered when designing a CATR:

- Quiet Zone
- Focal length
- Offset angle
- Feed location

Figure E.1-2 does introduce the concept of quiet zone (QZ). Basically, the plane wavefront (uniform amplitude and phase) is guaranteed in a certain cylinder volume:

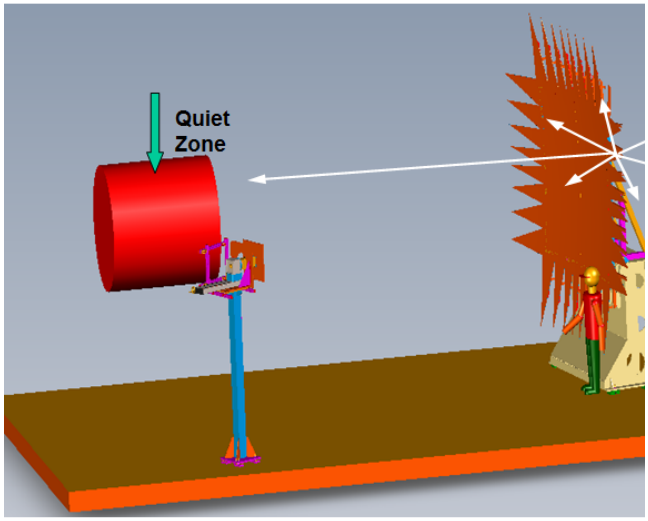

Figure E.1-2: CATR – Quiet Zone concept

Quiet Zone size would depend on mainly the reflector, feed taper, anechoic chamber design. In figure E.1-3 is shown the phase distribution in the QZ for a state of the art CATR designed for 3m QZ size at 18GHz:

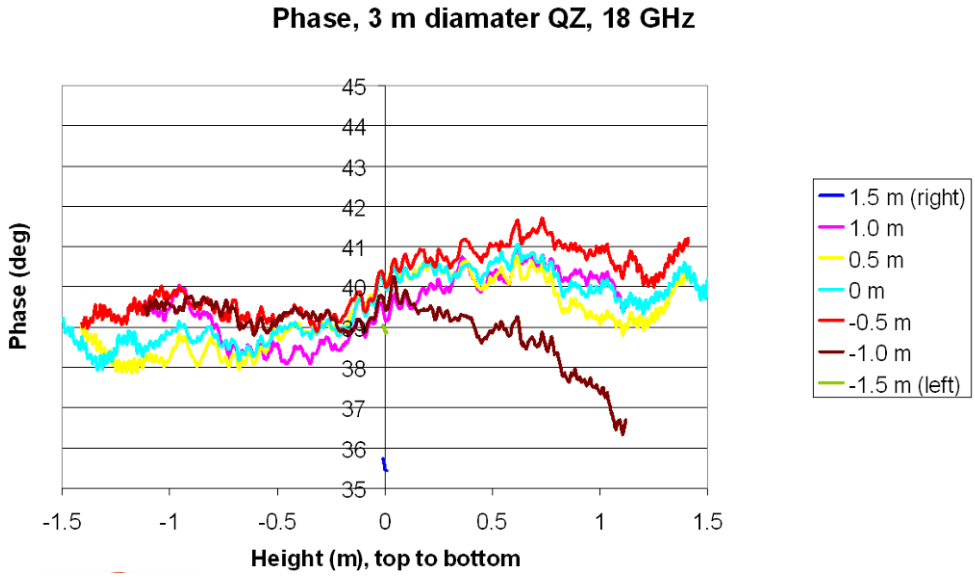

Figure E.1-3: Phase curvature within the CATR QZ

It has to be noted that the total phase variation in the QZ for a CATR is much lower than the phase variation (22.5deg) for a typical direct FF range.

E.2 IFF method 1 - a far field system

In this subclause the CATR key points are reported.

E.2.1 Quiet zone

Quiet zone quality can be impacted by amplitude uniformity, phase planarity and polarization purity.

Amplitude uniformity is mainly due to feed pattern, alignment and reflector design while phase planarity is due to feed alignment and reflector design. The polarization purity is mainly due to the parabolic system geometry considering high polarization purity feeds.

The test procedure defined in TR 38.810 Annex D.2 for determining the MU contribution from the quiet zone quality applies equally well to both direct far-field and CATR systems.

Plots in Figure E.2.1-1 and E.2.1-2 show the amplitude and phase taper plots of the in the quiet zone of a CATR system.

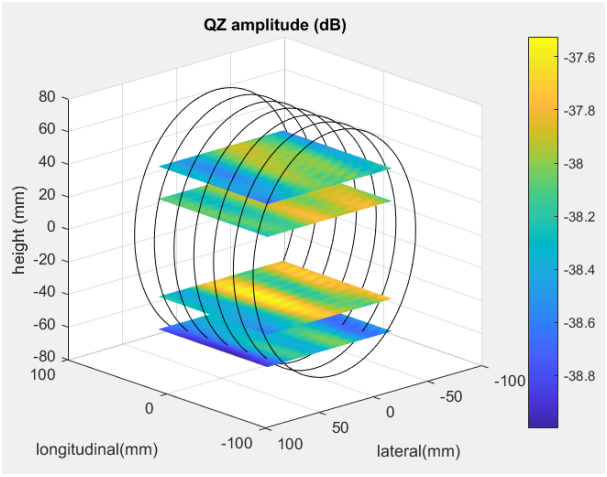

Figure E.2.1-1: Amplitude variation across the quiet zone of 15cm

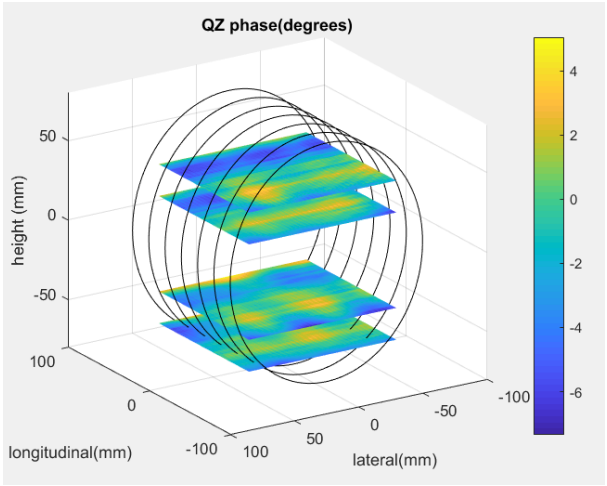

Figure E.2.1-2: Phase variation across the quiet zone of 15cm

The measurements of quiet zone in the planes shown in Figure E.2.1-1 and Figure E.2.1-2 that

- The overall amplitude variation within the quiet zone is less than 1.2 dB
- The overall phase variation within the quiet zone is less than 10˚

E.2.2 Implementation Requirements

When it comes of CATR implementations, the reflector design is one of the key point to be considered. Another important piece is the feed antenna location in the system setup. Different implementations may exist based on the test system frequency range and quite zone requirements.

E.2.2.1 Reflector(s) Type

The reflector design does play an important role when designing a CATR.

A Compact Range is a geometrical optical design, for which the reflector(s) is large in wavelength. Edges diffraction (edges are like cylindrical sources) needs to be minimized using edge treatment.

The lower frequency limit of a compact range depends on the edge treatment.

The Quality of the Quiet Zone is characterized for CATR ranges and always includes the reflections off the edges of the reflector. The example specifications for a CATR system can be seen in Table E.2.2.1-1. These specifications should show that the impact of these reflections is minor. In order to meet such specifications, the reflector must be designed in a way to reduce the reflection off the edges (the edges are either curved or have serrated edges).

Table E.2.2.1-1: Example of CATR system specifications

Frequency Range (GHz)	1.5 – 100
Quiet Zone Dimensions [H x W x L] (m)	0.5 x 0.5 x 0.5
Cross Polarization (dB)	-30

E.2.2.1.1 Serrated Edge

The direction of the edge is designed such that minimum diffraction enters the quiet zone sources. With serrations, there is a smooth transition between parabolic surface of the reflector and free space, thus reducing the diffraction effects and directing the diffracted field away from the QZ. The length of serrations defines the lowest frequency of operation. Typical serrations length is 5λ.

E.2.2.1.2 Rolled edge

The edges of the compact range reflector are no longer cut off abruptly but are smoothly bent backwards thus reducing the energy at the edges of the reflector. With well-designed rolled edge, diffraction reduces compared to serrated edge at the low and middle end of the frequency spectrum.

E.2.2.2 Feed Antenna location

The following are the feed locations most commonly used when designing a CATR:

- Side-fed
- Floor-fed
- Diagonal-fed

For a side-fed system, the feed is placed on one side of the chamber at the same height as the centre of the quiet zone so that the ray from the feed to the reflector to the centre of the quiet zone spans a horizontal plane. For a floor-fed system, the feed in placed on the floor between the reflector and the quiet zone so that the ray from the feed to reflector to the centre of the quite zone spans a vertical plane. In case of diagonal-fed (corner-fed) system, the feed is in a corner between side wall and floor so that the ray from the feed to the reflector to the centre of the quiet zone spans a diagonal plane. Typically the diagonal fed-system allows for size reduction of the anechoic chamber of approximately √2.

E.3 IFF method 1 – reciprocity

CATR systems are inherently reciprocal, i.e. they support device characterization in both transmit and receive modes and it has been already used as such within 3GPP: TR 37.842 for testing active antenna systems describes base station conformance testing for radiated transmit power (EIRP) in subclause 10.3.1 as well as for OTA sensitivity (EIS) in subclause 10.3.2.

The theoretical analysis behind this statement can be as follows:

C.A. Balanis (in his book “Antenna Theory: Analysis and Design,” Ch. 3, pp. 127-132) provides a thorough discussion of reciprocity and its consequences for radiation patterns: In brief, it shows that, due to reciprocity, the antenna patterns measured by a receiving probe antenna with the DUT transmitting will be identical to those measured by the DUT in receive mode when the probe antenna is transmitting. It is further explained that reciprocity holds whenever certain conditions are met, e.g. the device materials and propagation medium are linear.

These are the conditions met in a CATR:

As the nominally spherical wave from the feed antenna propagates toward the mirror, it's power density per area, P_{dens}, falls off with the square of the distance from the feed antenna so that at the mirror,

$$P_{\text{dens}} = \frac{P_{\text{feed}} G_{\text{feed}}}{4\pi f^2}, \quad \text{(E.3-1)}$$

where P_{feed} is the power transmitted from the feed antenna, G_{feed} is the gain of the feed antenna, and f is approximately the focal length of the mirror. The precise distance from the feed antenna to the centre of the mirror is typically slightly longer than the focal length due to the off-axis illumination and parabolic curvature of the mirror.

P_{dens} does not change as the beam propagates to the DUT since the beam is collimated. For a DUT in the quiet zone, the power received by the DUT is the product of P_{dens} and the DUT's effective aperture, A_{DUT}. This effective aperture depends on the orientation of the DUT relative to the beam, indicated by the DUT's elevation angle, θ, and its azimuth angle, ϕ. The DUT's gain, G_{DUT}, is related to this aperture according to the formula

$$A_{\text{DUT}}(\theta,\phi) = \frac{\lambda^2}{4\pi} G_{\text{DUT}}(\theta,\phi). \quad \text{(E.3-2)}$$

Thus, the ratio of received power to transmitted power, is

$$\frac{P_{\text{DUT}}}{P_{\text{feed}}} = G_{\text{DUT}}(\theta,\phi) G_{\text{feed}} \left(\frac{\lambda}{4\pi f} \right)^2 \quad \text{(E.3-3)}$$

From this derivation, it is clear that the path-loss for a CATR does not depend on the total distance between the feed antenna and the DUT but on the focal length of the mirror instead.

Less intuitive is the derivation of the path loss when the DUT is in transmit mode. In that case, the DUT's radiation pattern can be treated as a superposition of plane waves propagating in different directions. This superposition concept is valid whether the mirror is in the near or far-field of the DUT. As shown in Figure E.3.1-1, the mirror captures plane waves propagating in a range of directions, but the different directions are focused to different points by the mirror. Only those plane waves propagating along the optical axis of the mirror (indicated in pink) are focused into the feed antenna for measurement; in this mode, the feed antenna is receiving the signal from the DUT. Plane waves at larger angles not captured by the mirror are instead absorbed by the anechoic chamber. The particular angle measured by the feed antenna can be varied by rotating the DUT. For example, a rotation of the DUT in this figure could align the blue plane wave with the optical axis allowing measurement of the transmitted power in that direction.

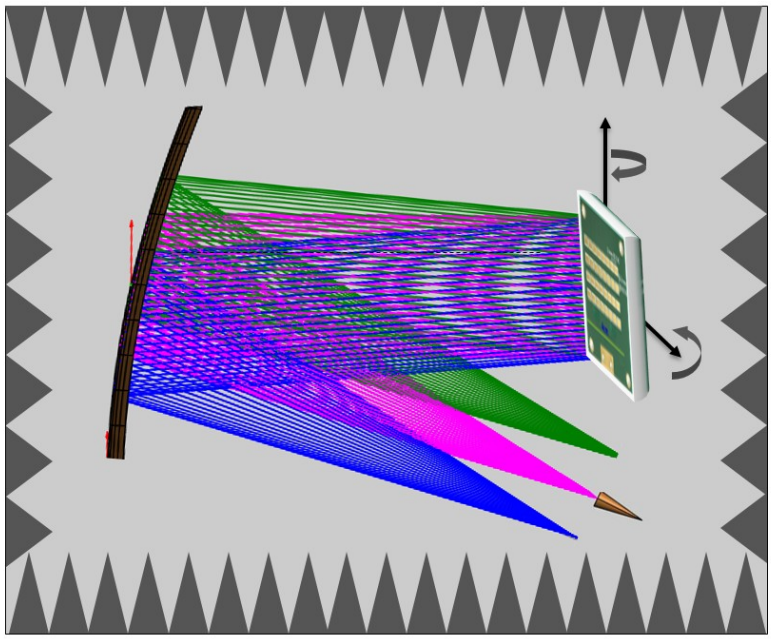

Figure E.3-1: CATR when DUT is in transmit mode

The feed antenna can only capture radiation from the relatively small range of angles that converge to a point within its aperture. The maximum angular deviation from the optical axis that can be accepted by the feed antenna is given by

$$\tan(\varphi_{max}) \approx \varphi_{max} = \frac{r}{f} \tag{E.3-4}$$

where r is the radius of the aperture, f is the focal length of the mirror, and the small angle approximation - a very good approximation for typical CATR geometries - has been invoked for simplicity.

The radiation intensity (power per unit solid angle), P_{angle}, emitted by the DUT is the total power emitted divided by 4π radians and multiplied by the gain of the DUT;

$$P_{\text{angle}} = \frac{G_{\text{DUT}}(\theta,\phi)P_{\text{DUT}}}{4\pi}. \tag{E.3-5}$$

The total power accepted by feed antenna is the integral of over the range of angles that converge within its aperture. Using the small angle approximation, the integral gives

$$P_{\text{feed}} = \frac{G_{\text{DUT}}(\theta,\phi)P_{\text{DUT}}}{4\pi}\left(\pi\varphi_{\text{max}}^2\right). \tag{E.3-6}$$

Substituting for φ_{max} using (4), and with the aperture of the feed antenna as $A_{\text{feed}} = \pi r^2 = \frac{\lambda^2}{4\pi}G_{\text{feed}}$, the ratio of power received by the feed antenna to power transmitted by the DUT is

$$\frac{P_{\text{feed}}}{P_{\text{DUT}}} = G_{\text{DUT}}(\theta,\phi)G_{\text{feed}}\left(\frac{\lambda}{4\pi f}\right)^2 \tag{E.3-7}$$

Equation (7) shows that the transmission losses from the DUT to the feed are identical to the transmission losses from the feed to the DUT, given by Eq. (3), thus proving reciprocity.

This reciprocity result, which holds true regardless of DUT orientation, assures identical antenna pattern measurements for DUTs in both transmit and receive modes. Beyond pattern measurements, this result also has implications for other device tests. EIRP and EIS tests are both possible in a CATR system as the same path losses are present in both

directions. Likewise, EVM in transmit and receive are supported since both will experience the same predicted path losses given in Eqs. (7) and (3).

Reporting measurement results in order to further detail the reciprocity of a CATR by showing the comparison between the s12, and s21 coefficients of the scattering matrix have been obtained as follows:

- Measurement results are from a commercial CATR at mmWave. This range is capable of measuring DUTs within 24GHz to 40GHz frequency range. The CATR is designed for a 1.5m QZ and the results are from a QZ ripple test (field distribution) activity done on the setup. In figure E.3-2 the QZ ripple test setup is shown:

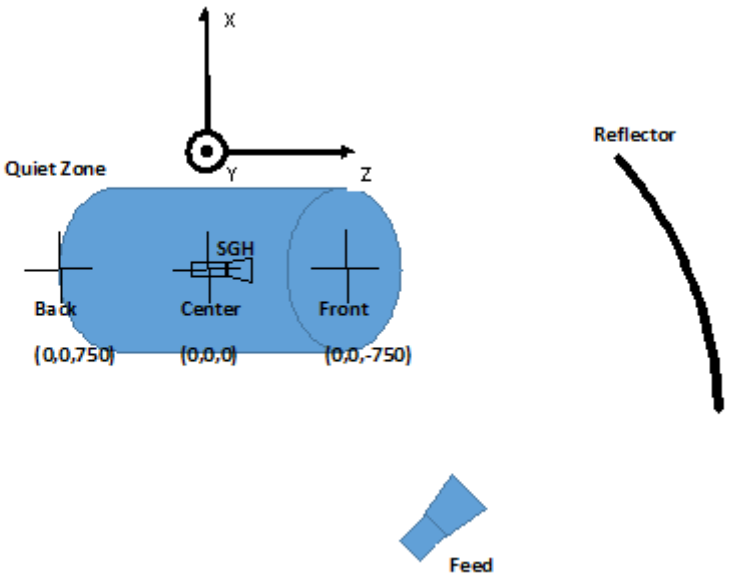

Figure E.3-2: CATR- QZ ripple test (field distribution) set up

- A Standard Gain Horn (SGH) is used as reference antenna. Since it is a field distribution measurement where the ability of the CATR to emulate a plane wave in the QZ is tested, for all the measurements the SGH aperture was pointing the CATR's reflector. The reference antenna has been swept on the X and Y-axis when at different Z positions. Especially, Vertical cut means that the scan is done long the Y-axis while Horizontal Cut means that the scan is long the X-axis. In both cases, Vertical and Horizontal components of the field are measured in amplitude, and phase (complex quantity). The aim is to define the amplitude and phase taper in the QZ. For our measurements, s21 and s12 coefficients have been measured and compared for each Y axis positions (Vertical Cut) when the SGH is at Z=0, centre of the QZ.

- Comparison between s21 and s12 complex coefficients (amplitude and phase) is reported for 26.5GHz and Vertical Cut. Figure E.3.1-3 and E.3.1-4 show the reciprocity in terms of amplitude and phase

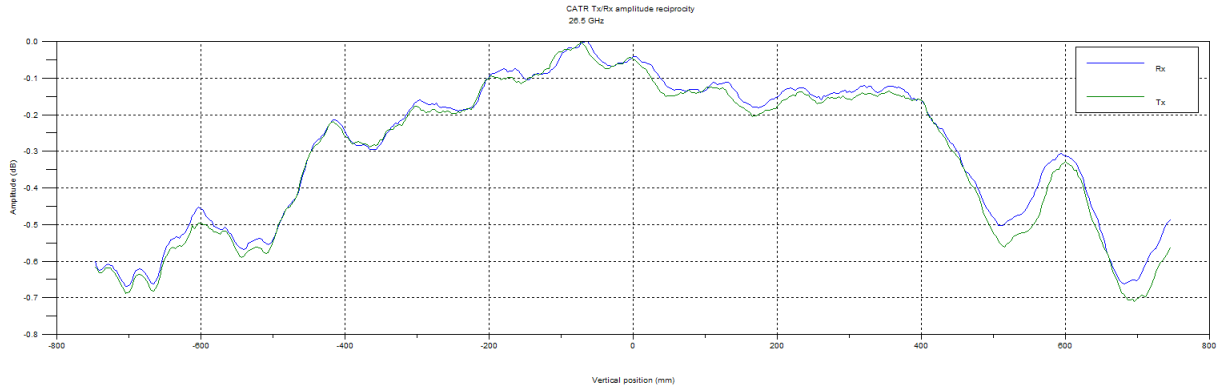

Figure E.3-3: CATR- Amplitude Reciprocity (Vertical cut)

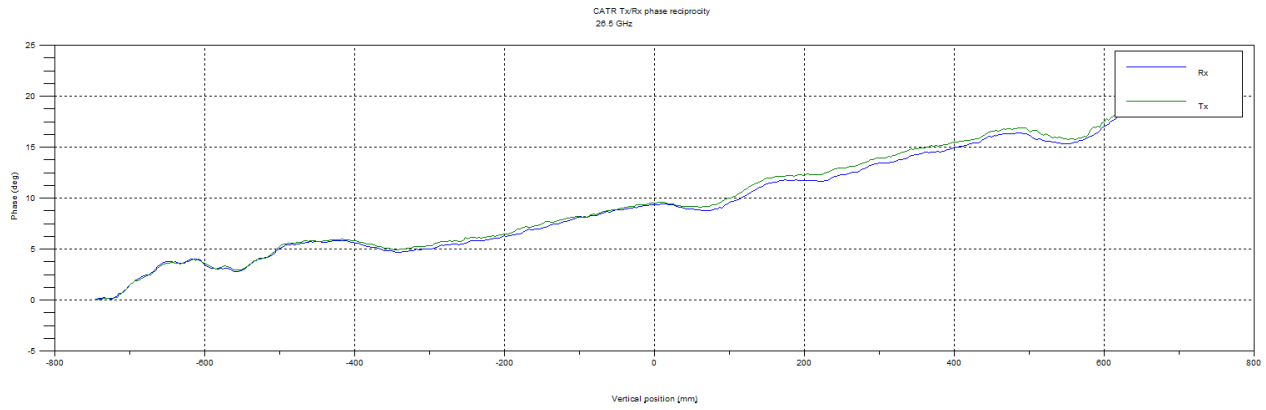

Figure E.3-4: CATR- Phase Reciprocity (Vertical Cut)

E.4 IFF method 1 – DUT offset from the QZ centre

The uncertainty due to the DUT offset from the QZ centre can vary based on the knowledge of antenna array position embedded in the DUT. In this subclause, an analysis of the impact of this uncertainty for CATR is provided when measuring single points quantities such as both EIRP (TX measurements) and EIS (RX measurements).

In figure E.4-1, and E.4-2 the test scenarios A1 and A2 are reported for RX tests and TX tests respectively:

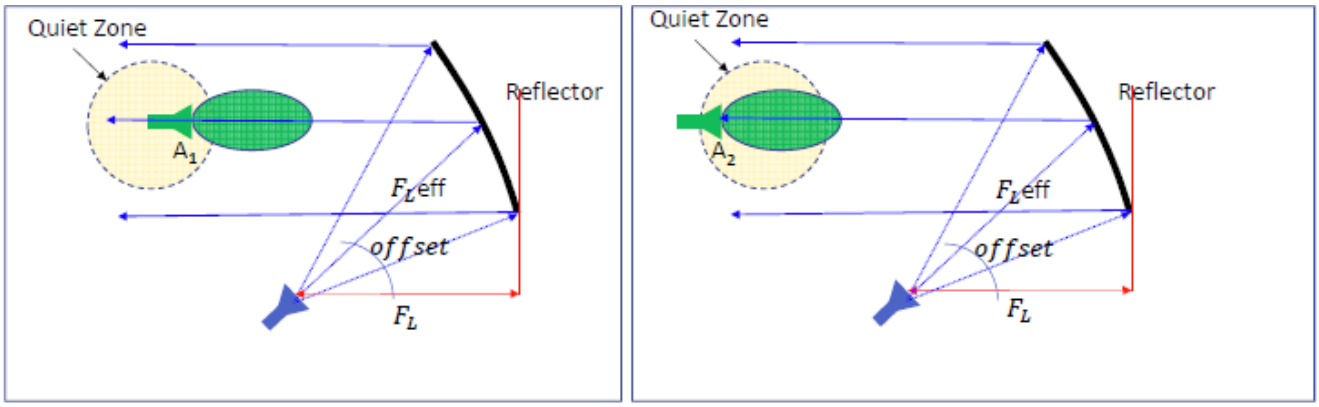

Figure E.4-1: CATR – RX tests scenarios A1 and A2

The QZ is within the collimated beam. There are no free space losses between the reflector and DUT. The only path loss is between the feed and the reflector so since this distance is fixed, this path loss can be easily calibrated. The final spatial attenuation is equal to $1/F_{L,eff}\text{^}2$, where $F_{L,eff}$=effective focal length =$(2*F_L)/(1+\cos(\text{offset}))$. It means that the distance from the QZ to the reflector is longer than the F_L=focal length. In a state of the art CATR, the offset is typically set to 27deg by design, so that the $F_{L,eff}=1.058*F_L$.

As a consequence of this, if DUT is moved within the QZ, there is no change in the path loss so the power received in A1 is equal to power received in A2. The associated uncertainty is then 0dB.

However, due to diffraction from the reflector, the field distribution in the Quiet Zone is not perfectly uniform. Therefore, there will be some variation for the amplitude and phase of the received field. Typical amplitude variations are less than 1 dB within the Quiet Zone and can be estimated by the QZ characterization process.

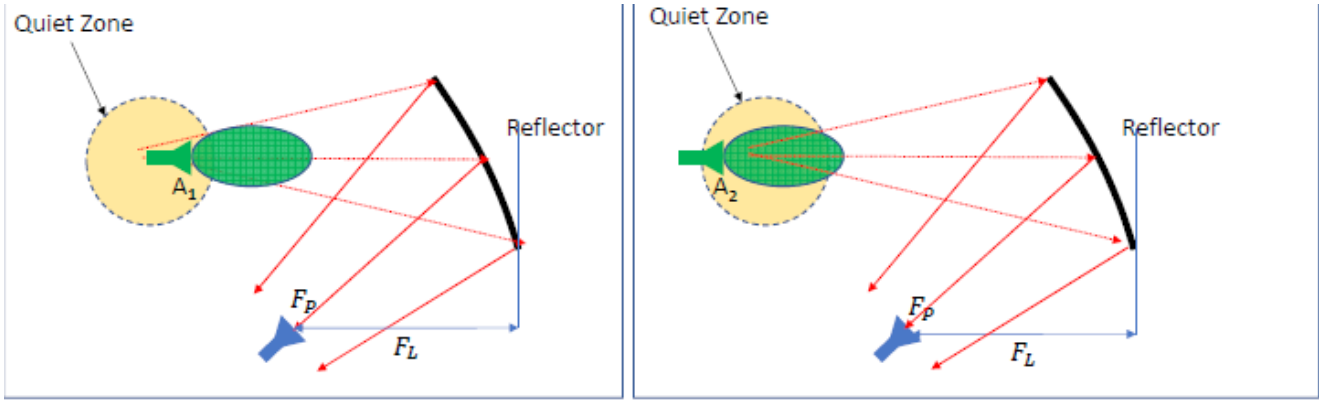

Figure E.4-2: CATR – TX tests scenarios A1 and A2

The following assumptions can be considered:

- Reciprocity
  - For a CATR the reciprocity is valid
  - Path loss calculation is identical to the RX case
- DUT will have a radiation pattern which can be described as a series of plane wave propagating in different directions. The particular plane wave propagating along the reflector centreline will be focused on the reflector feed. Figure E.4-3 does show this:

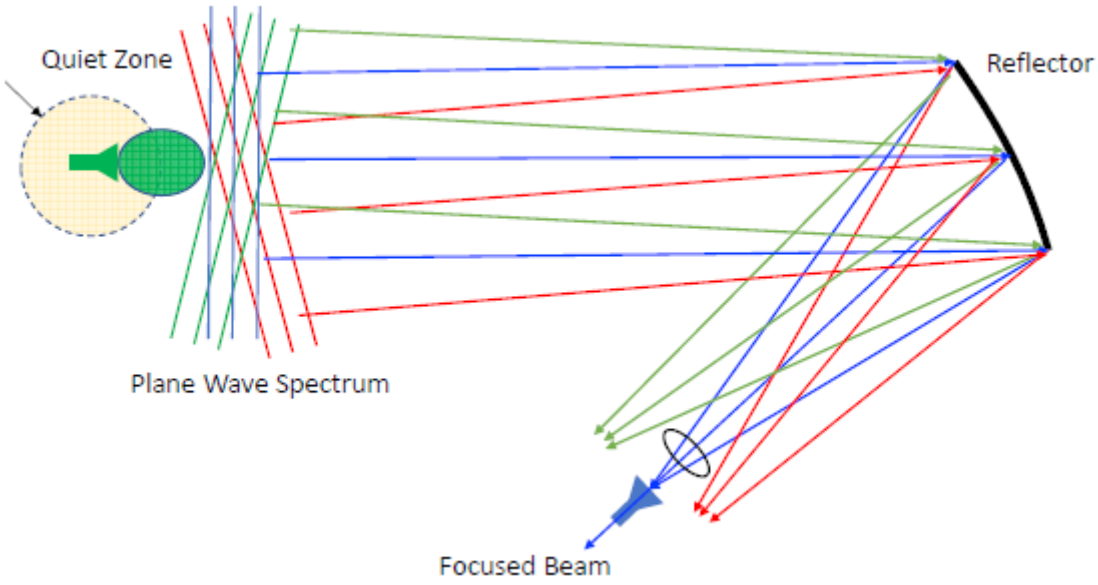

Figure E.4-3: CATR – Radiation Pattern measurement when TX by DUT

- By rotating the DUT in the QZ, the reflector moves a particular point of the FF pattern along the CATR feed
- No matter what the distances from the reflector are, the power received from the feed is the same.
  - The final spatial attenuation at the feed is equal to $1/F_{L,eff}\text{^}2$, where $F_{L,eff}$=effective focal length.

Based on the above assumptions the associated uncertainty is 0dB.

To better understand the above, mainly for the TX case – DUT transmitting, in Figure E.4-4 the CATR power transfer function is given:

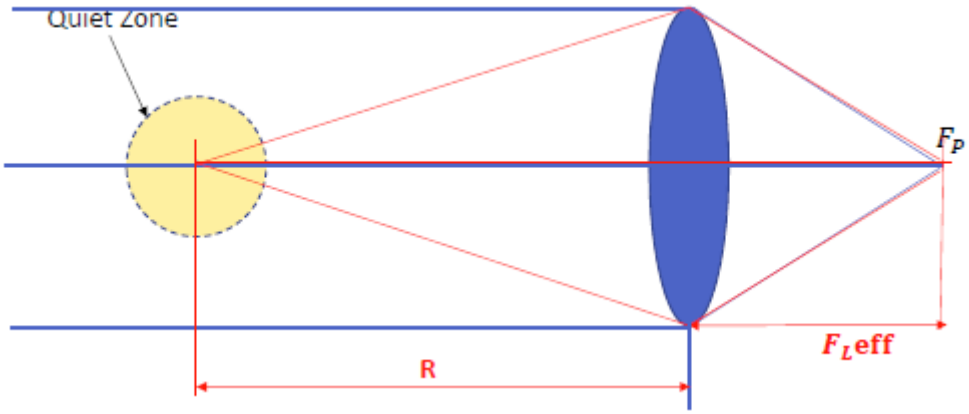

Figure E.4-4: CATR – Power Transfer Function

Blue and Red lines are representing the DUT receiving and transmitting respectively. It is assumed that all sources are isotropic point sources. This assumption can be generalized to real sources since any real source can be expanded in a number of isotropic sources.

When transmitting from the QZ (TX case – DUT transmitting) the spherical wavefront is imaged by the lens/reflector in the focal point with the general magnification factor so that the below equations are valid:

- Loss up to the reflector -> 1/R^2
- Gain up to the reflector -> $(R/F_{L,eff})^2$ -> magnification factor $(R/F_{L,eff})$ where $F_{L,eff}$=effective focal length
- Total gain -> $1/R^2*(R/F_{L,eff})^2=1/F_{L,eff}^2$

When transmitting from the focal point – Fp (RX case – DUT receiving) the spherical wavefront from the feed is become a “perfect” plane wave after the lens/reflector. The final attenuation is equal to $1/F_{L,eff}^2$.

It was shown that in both cases the attenuation in the system is proportional to the free space path loss provided by the distance from the feed and lens/reflector. The attenuation is independent from the distance to the QZ.

E.5 IFF method 1 – operating frequency range

Compact Antenna Test Range solution can cope with all frequencies defined for FR2.

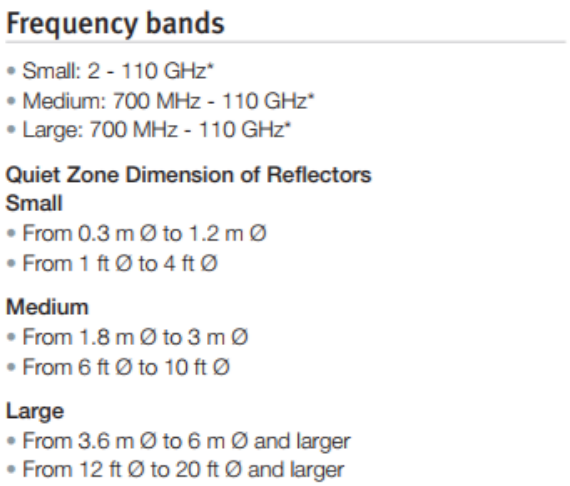

Figure E.5-1. Example frequency specification for a CATR

E.6 IFF method 1 – positioning system

CATR is provided with a positioning system such that the angle between the dual-polarized measurement antenna and the DUT has at least two axes of freedom and maintains a polarization reference. In the CATR case, positioner is placed at the quiet zone area where the DUT is.

E.7 IFF method 1 – link antennas

CATR for NR RF FR2 requirements includes a NR link antenna to allow off centre beam measurements. Together with the UE beam lock test function, this link antenna allows to measure the whole radiation pattern.

The way it is used is described below:

- Before performing the UE beam lock test function, the measurement probe acts as a link antenna maintaining polarization reference with respect to the DUT. Once the beam is locked then the link is to be passed to the link antenna which maintains reliable signal level with respect to the DUT. Then UE can be rotated to measure the whole radiation pattern without losing the connection with the system simulator.

Hence, thanks to the link antennas and the UE Beam lock test function, CATR is capable of centre and off centre of beam measurements.

Additionally, for setups intended for measurements of UE RF characteristics in non-standalone (NSA) mode with 1UL configuration, an LTE link antenna is used to provide the LTE link to the DUT

- The LTE link antenna provides a stable LTE signal without precise path loss or polarization control

CATR is provided with such LTE link antenna.

Annex F:
Rationale behind NFTF method

F.1 NFTF method – working principle

A NFTF (Near Field to Far Field Transform) system measures the amplitude and phase on a surface (spherical in this case) around he DUT. The 3D far field pattern is obtained by using a modal spherical wave expansion. The Near Field to Far Field Transform is based on the Huygen's principle. A direct solution of the Helmholtz equations is found by applying boundary conditions on the surface at an infinite distance away from the DUT. From the tangential fields over the surface, the modal coefficients can be determined using the orthogonality of the modal expansion.

The Near to Far field transform is performed in two steps:

- Expansion (or projection) of the measured Near Field over a set of orthogonal basis functions to evaluate the transformed spectrum

  $E_{meas}(r) = Spectrum * F_{basis}(r)$

- FF (EFF) computation using a the previously calculated spectrum and with the basis functions evaluated at $r \rightarrow \infty$:

  $E_{FF} = Spectrum * F_{basis}(r \rightarrow \infty)$

The Nyquist sampling criterion must be met to obtain enough measurement points for the near field to far field transform to be valid. The equations for the sampling criterion are below:

$\Delta\phi.r<\lambda/2$

$\Delta\theta.r<\lambda/2$

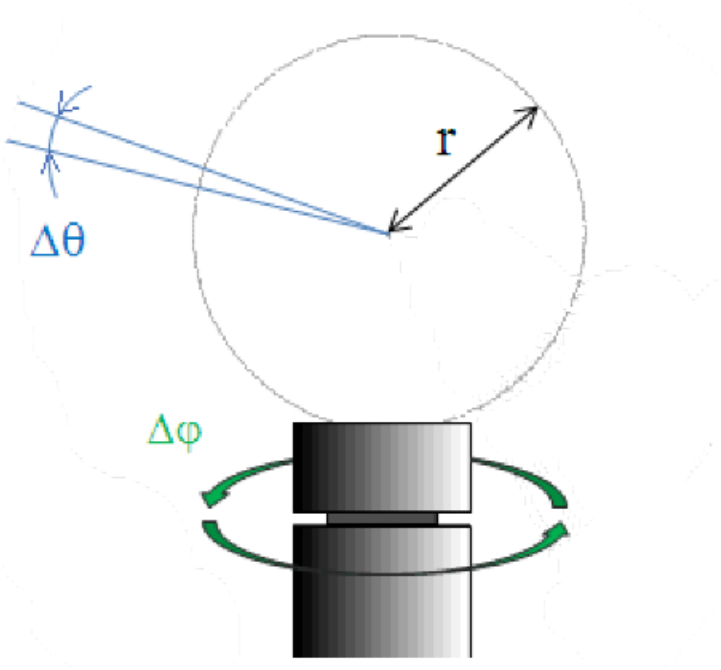

Figure F.1-1: Sampling Criterion

The method outlined above is normally performed on antennas which are fed from a signal source but can also apply to DUTs which are transmitting by using the phase recovery technique.

F.2 NFTF – Spherical Scan

A circular probe array as shown in Figure F.3-1 can measure the full 3D pattern with a rotation in azimuth only. Through use of electronic switching between the probe array elements the points in elevation can be measured without rotating the DUT in the elevation plane.

F.3 NFTF – Implementation for Self-Transmitting DUTs

F.3.1 Phase Recovery Technique

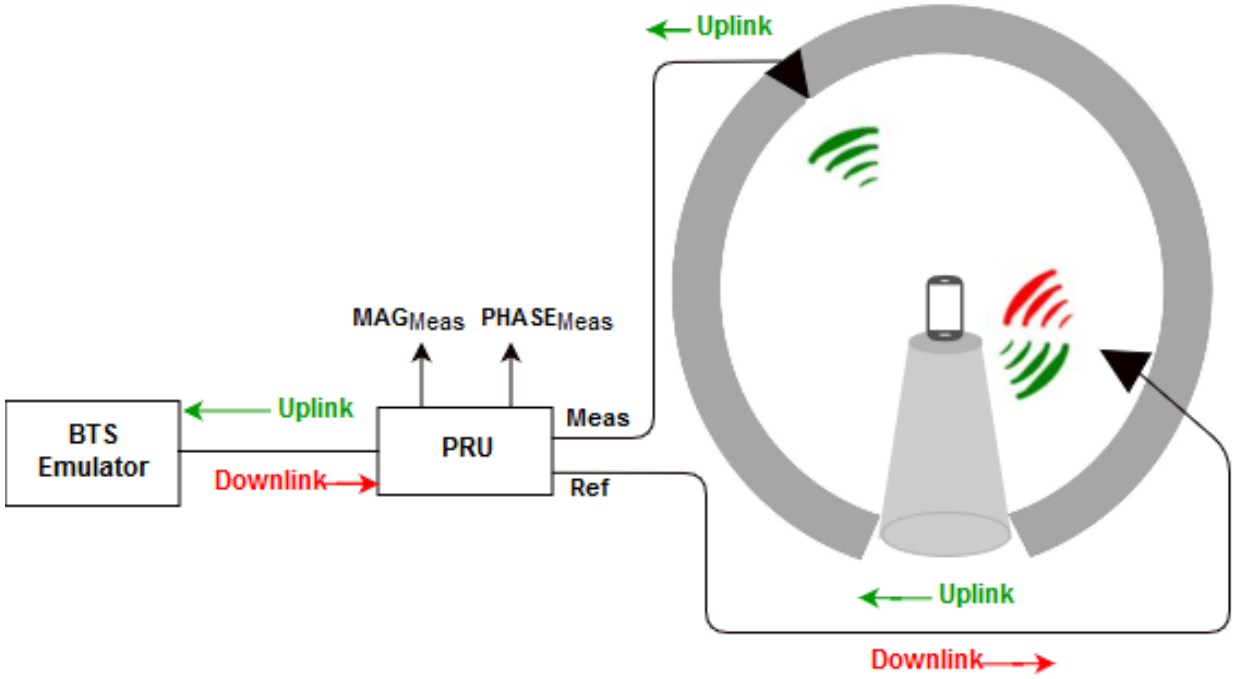

Figure F.3-1: Typical Test System using Phase Recovery Technique

Figure F.3-1 shows the block diagram of a Near Field Range with the Phase Recovery Unit.

The technique is based on the synchronous reception of two signals, the measurement and reference. The signal transmitted by the DUT is measured simultaneously with two probes, one being the measurement probe and the other being the reference probe. These two signals are fed into the PRU (Phase Recovery Unit) and the amplitude and absolute phase are acquired.

F.3.2 Obtaining EIRP and TRP

During the near field to far field transformation process, the calibration is applied so that the transmitted power (EIRP) is transformed from dB to dBm. Because the full 3D pattern is measured the TRP can be calculated using the EIRP results. The EIRP results at beam peak can be also easily obtained.

F.4 NFTF – Measurement Uncertainty due to Phase Variation

During the near field to far field transform the DUT's offset from the reference coordinate system is corrected for. This is can be achieved because the absolute phase is measured.

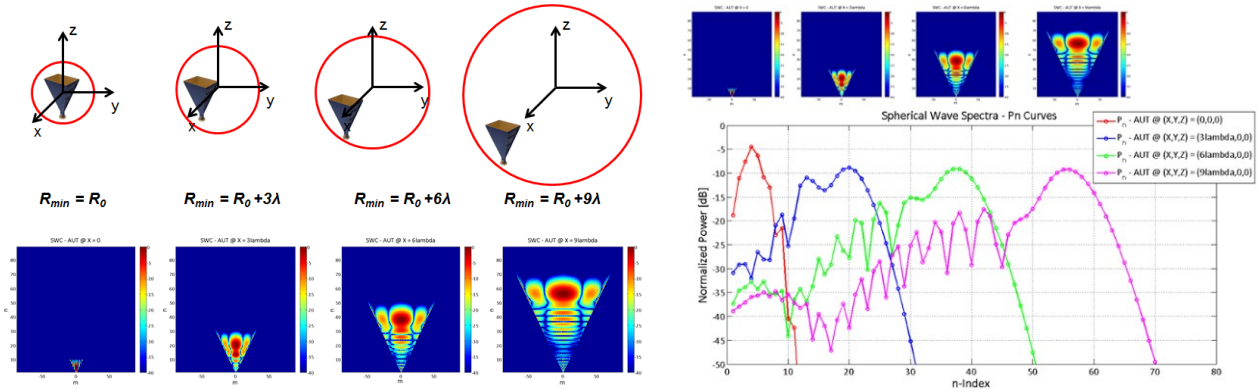

Figure F.4-1: Spherical Wave Coefficients (SWC) graphical representation

Figure 4.1 shows the Spherical Wave Coefficients of a horn measured at three different distances away from the center of the reference coordinate system. As can be seen in the figures:

- The DUT far field pattern remains the same
- The DUT far field phase changes with a vector component defined by the displacement of the reference coordinate system
- The number of spherical wave that are needed to fully represent the antenna increases as the DUT moves further away from the center of the reference coordinate system.
- As the minimum sphere increases ⇔ the number of field samples increases.

If the criteria above are respected during the near field acquisition, there is no uncertainty due to the DUT offset from the reference coordinate system (center of the QZ).

Annex G: Measurement Grids

This appendix describes the assumptions and definition of the minimum number of measurement grid points for various grid types.

A total of three measurement grids are considered:

- Beam Peak Search Grid: using this grid, the TX and RX beam peak direction will be determined. 3D EIRP scans are used to determine the TX beam peak direction and 3D Throughput/RSRP/EIS scans for RX beam peak directions.
- Spherical Coverage Grid: using this grid, the CDF of the EIRP/EIS distribution in 3D is calculated to determine the spherical coverage performance.
- TRP Measurement Grid: using this grid, the total power radiated by the DUT in the TX beam peak direction is determined by integrating the EIRP measurements taken on the sampling grid.

G.1 TRP Measurement Grids

This sub-clause describes the assumptions and derives the minimum number of TRP measurement grid points for various grid types.

G.1.1 Assumptions

For non-sparse antenna arrays used for smartphone UEs, an 8 x 2 antenna array was used for the measurement grid analyses. Table G.1.1-1 and Table G.1.1-2 outline the adapted equations from [9] that are used to simulate the UE antenna patterns for in-band measurements.

Table G.1.1-1: Single Antenna Element Radiation Pattern

Antenna element horizontal radiation pattern	$A_{E,H}(\varphi) = -\min\left[12\left(\frac{\varphi}{\varphi_{3dB}}\right)^2, A_m\right] dB$, A_m =30 dB
Horizontal half-power beamwidth of single element	260°
Antenna element vertical radiation pattern	$A_{E,V}(\theta) = -\min\left[12\left(\frac{\theta - 90}{\theta_{3dB}}\right)^2, SLA_v\right]$, SLAv =30 dB
Vertical half-power beamwidth of single array element	130º
Array element radiation pattern	$A_E(\varphi,\theta) = G_{E,\max} - \min\left\{-\left[A_{E,H}(\varphi) + A_{E,V}(\theta)\right], A_m\right\}$
Element gain without antenna losses	$G_{E,max}$ = 1.5 dBi

Table G.1.1-2: Composite Antenna Array Radiation Pattern

Composite array radiation pattern in dB $A_A(\theta,\varphi)$	$A_{A,Beami}(\theta,\varphi) = A_E(\theta,\varphi) + 10\log_{10}\left[\left\|\sum_{m=1}^{N_H}\sum_{n=1}^{N_V} w_{i,n,m} \cdot v_{n,m}\right|^2\right]$ the super position vector is given by: $v_{n,m} = \exp\left[i \cdot 2\pi\left[(n-1)\cdot\frac{d_V}{\lambda}\cdot\cos(\theta) + (m-1)\cdot\frac{d_H}{\lambda}\cdot\sin(\theta)\cdot\sin(\varphi)\right]\right]$, $n = 1,2,\ldots N_V; m = 1,2,\ldots N_H;$ the weighting is given by: $w_{i,n,m} = \frac{1}{\sqrt{N_H N_V}}\exp\left[i \cdot 2\pi\left[(n-1)\cdot\frac{d_V}{\lambda}\cdot\sin(\theta_{i,etilt}) - (m-1)\cdot\frac{d_H}{\lambda}\cdot\cos(\theta_{i,etilt})\right]\right]$
Antenna array configuration (Row×Column)	8 × 2
Horizontal radiating element spacing d_h/λ	0.5
Vertical radiating element spacing d_v/λ	0.5

The reference/baseline antenna pattern is shown in Figure G.1.1-1

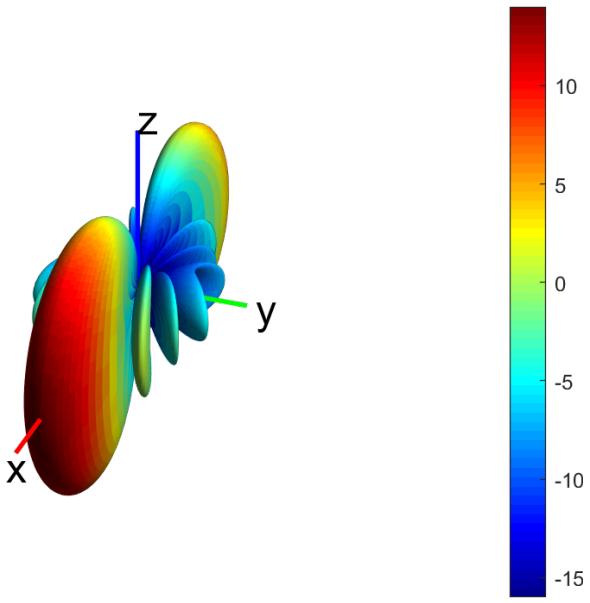

Figure G.1.1-1: Reference 8x2 Antenna Pattern

The relative orientation of the simulated antenna array and the measurement grid is altered randomly and the standard deviation between TRPs for each measurement grid is derived from a set of 10000 random orientations.

In Figure G.1.1-2, three rotations used for the simulation analyses are illustrated, i.e., the antenna pattern are rotated in ϕ and θ but also along its beam peak axis.

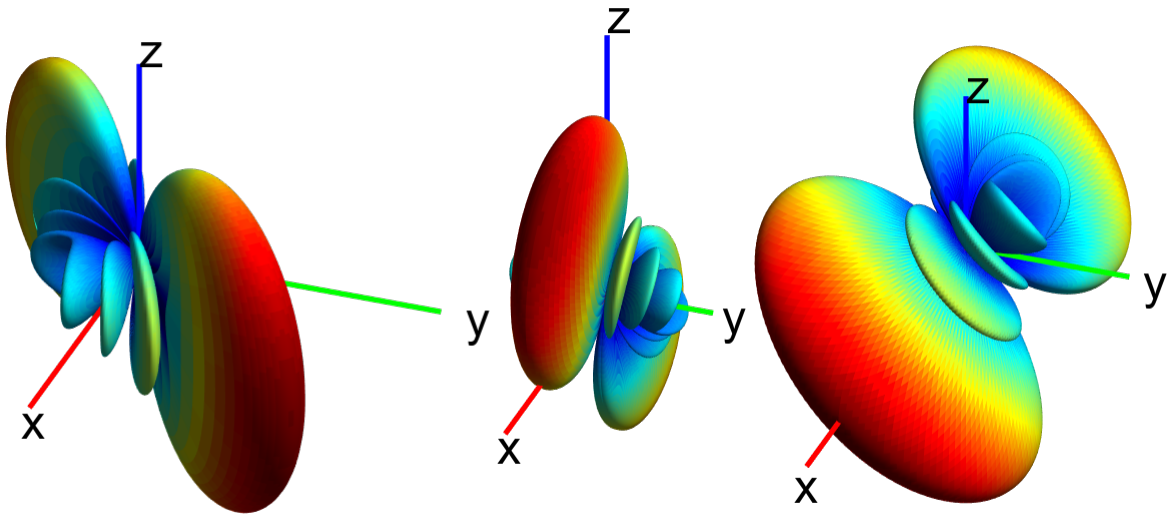

Figure G.1.1-2: Sample Rotations of 8x2 antenna pattern, left: 45° in ϕ, centre: 45° in θ (instead of 90° as shown in Figure G.1.1-1), right: rotation of 45° along the beam peak axis (angle α)

The randomization of the various rotations is illustrated in Figure G.1.1-3. The rotations in ϕ and α can be handled in a completely random fashion, e.g., phi_rot = 360*rand(10000,1). For the rotations around θ, the number of rotations near the poles should be the same compared to the equator since the surface area near the poles is much smaller than around the equator, i.e., the distribution needs to be scaled by sin(θ).

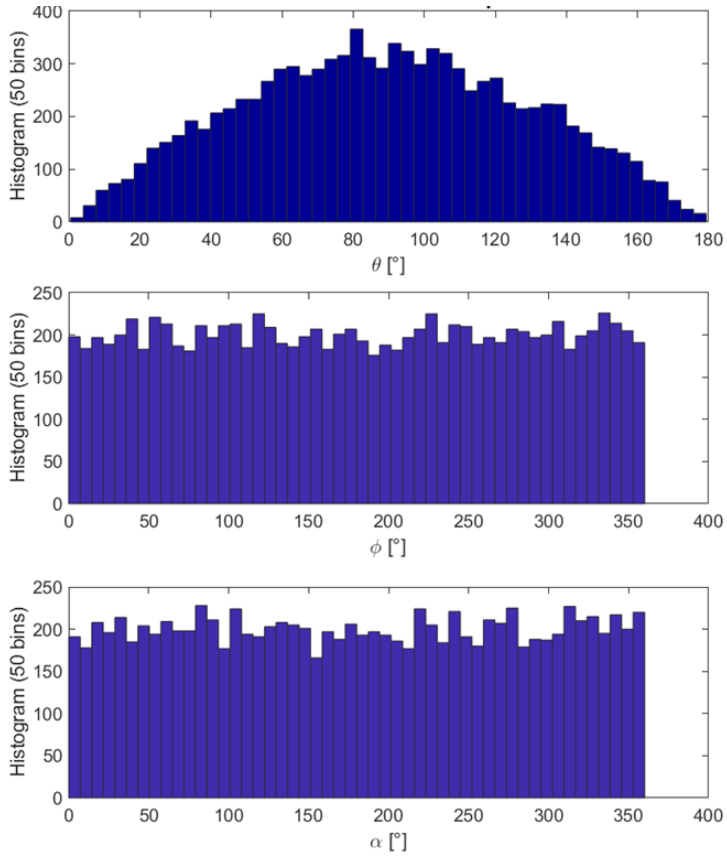

Figure G.1.1-3: Histogram of random distribution of θ, ϕ and α rotations

The minimum number of measurements points shall guarantee that the standard deviation for the TRP measurement grid shall not exceed 0.25dB for all DUT types.

G.1.2 Grid Types

Two different measurement grid types are considered.

The constant step size grid type has the azimuth and elevation angles uniformly distributed as illustrated in Figures G.1.2-1 in 2D and G.1.2-2 in 3D.

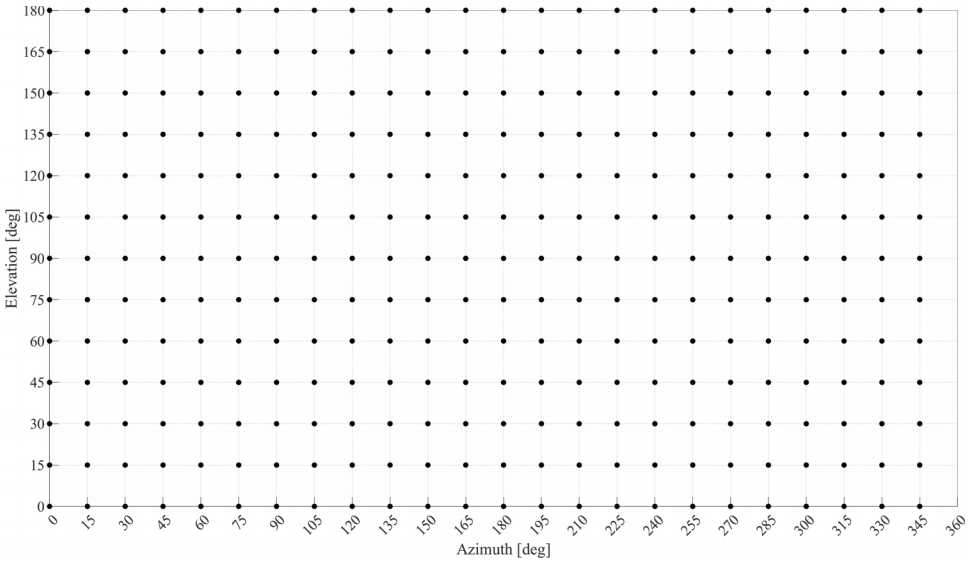

Figure G.1.2-1: Distribution of measurement grid points in 2D for a constant step size grid with Δθ=Δϕ=15° (266 unique measurement points)

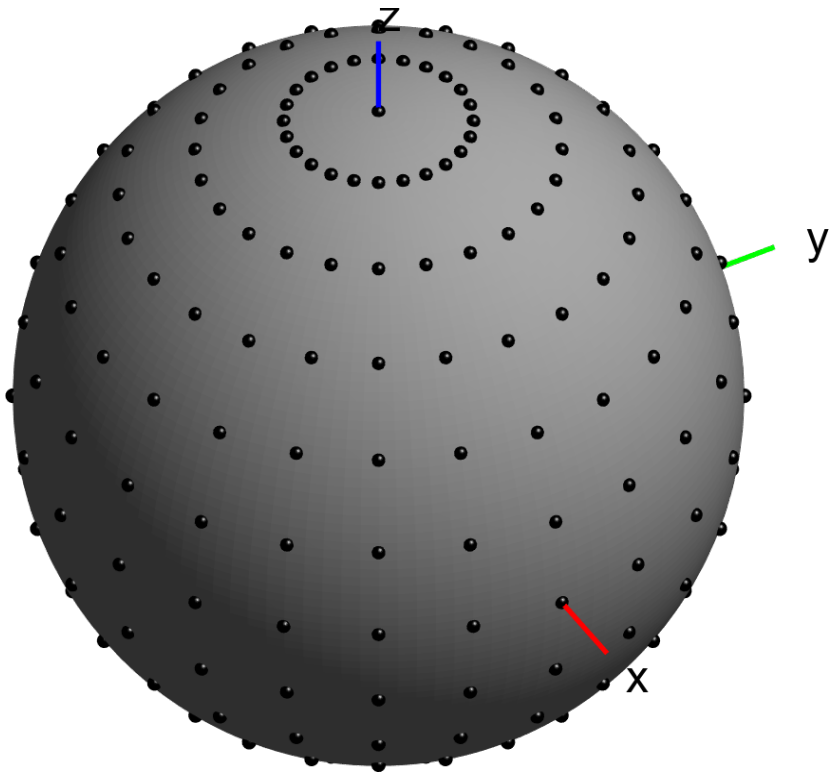

Figure G.1.2-2: Distribution of measurement grid points in 3D for a constant step size grid with Δθ=Δϕ=15° (266 unique measurement points)

Constant density grid types have measurement points that are evenly distributed on the surface of the sphere with a constant density as illustrated in Figures G.1.2-3 in 2D and G.1.2-4 in 3D.

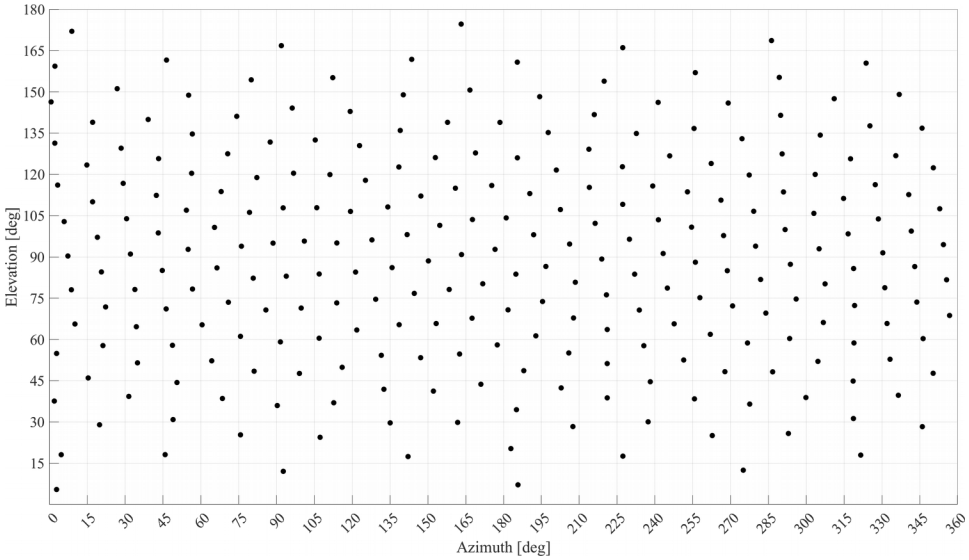

Figure G.1.2-3: Distribution of measurement grid points in 2D for a constant density grid with 266 unique measurement points

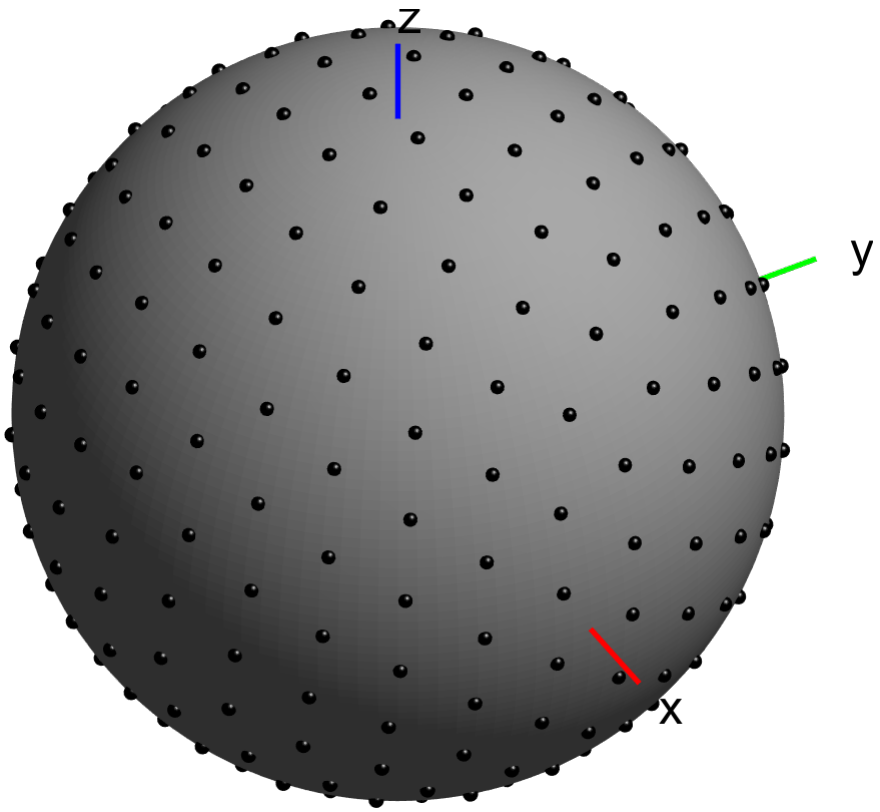

Figure G.1.2-4: Distribution of measurement grid points in 3D for a constant density grid type with 266 unique measurement points

Simulations of the Voronoi regions for different constant density implementations show that grid points are not always surrounded by 6 equidistant grid points as illustrated in Figure G.1.2-5 for the charged particle implementation and in Figure G.1.2-6 for the Golden Spiral implementation

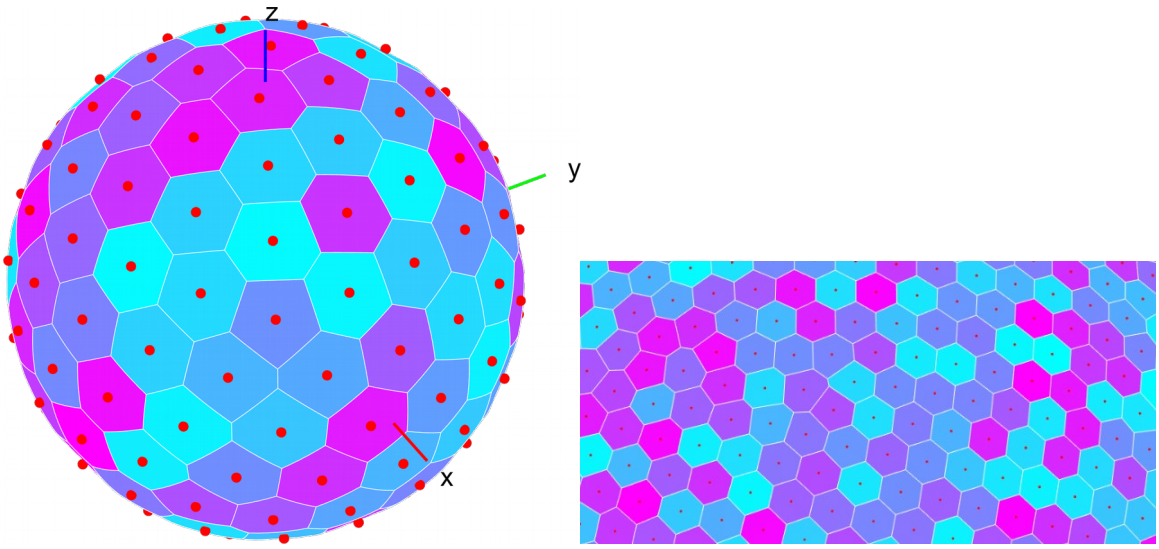

Figure G.1.2-5: Voronoi regions for the Charged Particle Grid implementation with 140 measurement points on left and with 3000 measurement points on right (excerpt shown)

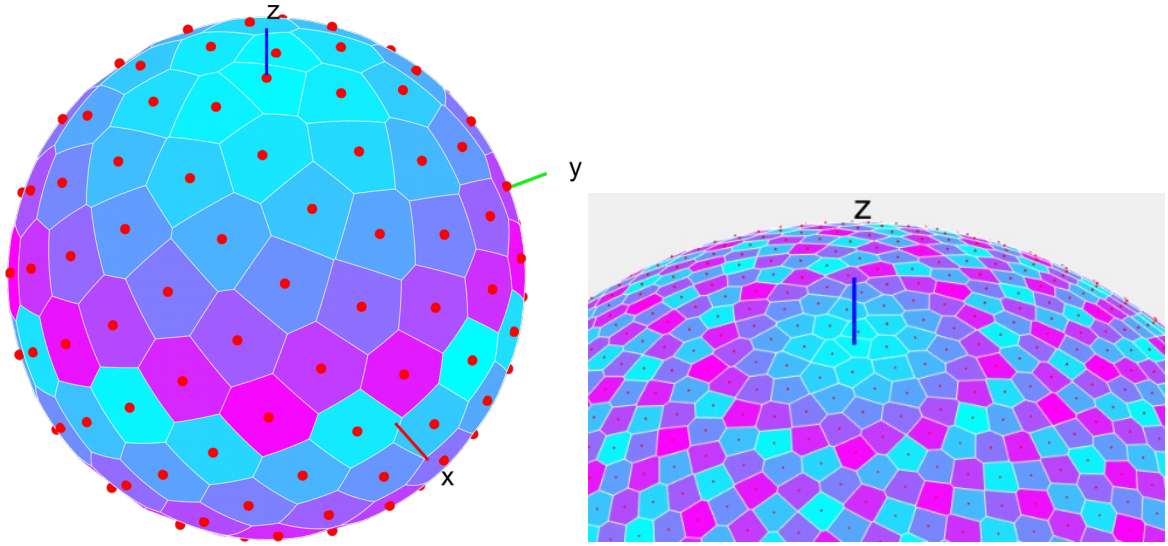

Figure G.1.2-6: Voronoi regions for the Golden Spiral Grid implementation with 140 measurement points on left and with 3000 measurement points on right (excerpt shown)

G.1.2 TRP Integration for Constant Step Size Grid Type

Different approaches to perform the TRP integration from the respective EIRP measurements are outlined in the next sub clauses for the constant step size grid type.

G.1.2.1 TRP Integration using Weights

In many engineering disciplines, the integral of a function needs to be solved using numerical integration techniques, commonly referred to as “quadrature”. Here, the approximation of the integral of a function is usually stated as a weighted sum of function values at specified points within the domain of integration. The derivation from the closed surface TRP integral

$$TRP = \int_S \frac{EIRP(\theta,\phi)}{4\pi} \bullet \sin\theta \bullet d\theta\, d\phi$$

to the classical discretized summation equation used for OTA

$$TRP \approx \frac{\pi}{2NM} \sum_{i=1}^{N-1} \sum_{j=0}^{M-1} \left[EIRP_\theta(\theta_i, \phi_j) + EIRP_\phi(\theta_i, \phi_j) \right] \sin(\theta_i)$$

has been derived in [15]. The weights for this integral are based on the sinθ·Δθ weights. More accurate implementations are based on the Clenshaw-Curtis quadrature integral approximation based on an expansion of the integrand in terms of Chebyshev polynomials. This implementation does not ignore the measurement points at the poles (θ=0° and 180°) where sinθ = 0. The discretized TRP can be expressed as

$$TRP \approx \frac{1}{2M} \sum_{i=0}^{N} \sum_{j=0}^{M-1} \left[EIRP_\theta(\theta_i, \phi_j) + EIRP_\phi(\theta_i, \phi_j) \right] W(\theta_i)$$

which the sinθ·Δθ weights replaced by a weight function W(θ) and extends the sum over I to include the poles. The Clenshaw-Curtis weights are compared to the classical sin θ·Δθ weights in Tables G.1.2.1-1 and G.1.2.1-2 for two different numbers of latitudes. The TRP measurement grid consists of N+1 latitudes and M longitudes with

$$\theta_i = i\Delta\theta \text{ where } \Delta\theta = \frac{\pi}{N}$$

and

$$\phi_j = j\Delta\phi \text{ where } \Delta\phi = \frac{2\pi}{M}$$

Table G.1.2.1-1: Samples and weights for the classical sin θ·Δθ weighting and Clenshaw-Curtis quadratures with 12 latitudes (Δθ=16.4°)

Classical sinθ·Δθ		Clenshaw-Curtis	
θ [deg]	Weights	θ [deg]	Weights
0	0	0	0.008
16.4	0.08	16.4	0.079
32.7	0.154	32.7	0.155
49.1	0.216	49.1	0.216
65.5	0.26	65.5	0.26
81.8	0.283	81.8	0.283
98.2	0.283	98.2	0.283
114.6	0.26	114.6	0.26
130.9	0.216	130.9	0.216
147.3	0.154	147.3	0.155
163.6	0.08	163.6	0.079
180	0	180	0.008

Table G.1.2.1-2: Samples and weights for the classical sin θ·Δθ weighting and Clenshaw-Curtis quadratures with 13 latitudes (Δθ=15°)

Classical sinθ·Δθ		Clenshaw-Curtis	
θ [deg]	Weights	θ [deg]	Weights
0	0	0	0.007
15	0.0678	15	0.0661
30	0.1309	30	0.1315
45	0.1851	45	0.1848
60	0.2267	60	0.227
75	0.2529	75	0.2527
90	0.2618	90	0.262
105	0.2529	105	0.2527
120	0.2267	120	0.227
135	0.1851	135	0.1848
150	0.1309	150	0.1315
165	0.0678	165	0.0661
180	0	180	0.007

G.1.2.2 TRP Surface Integral using the Jacobian Matrix

Total Radiated Power is given by the integral of the Effective Isotropic Radiated Power over the closed spherical surface S:

$$TRP = \oiint_S \frac{EIRP(\vec{r})}{4\pi}\, dS$$

Given any surface parameterization of

$$\vec{r}(u_1, u_2) = [x(u_1, u_2) \quad y(u_1, u_2) \quad z(u_1, u_2)]^T$$

The explicit general TRP surface integral is

$$TRP = \oiint_S \frac{EIRP(\vec{r}(u_1, u_2))}{4\pi} \cdot \sqrt{\det(J^T J)} \cdot du_1\, du_2$$

where J is the Jacobian Matrix defined at i row and j column is

$$J_{i,j} = \frac{\partial r_i}{\partial x_j}$$

The differential surface area element, in its most general form, is

$$dS = \sqrt{\det(J^T J)} \cdot du_1 du_2$$

The standard surface parameterization used in 3GPP to date is based on the definition of Spherical Coordinate System parameterization $(u_1 = \theta, u_2 = \emptyset)$ on a constant radius sphere where

$$\vec{r}(u_1 = \theta, u_2 = \emptyset) = \begin{bmatrix} x \\ y \\ z \end{bmatrix} = \begin{bmatrix} \sin\theta\cos\emptyset \\ \sin\theta\sin\emptyset \\ \cos\theta \end{bmatrix}$$

which yields the Jacobian Matrix

$$J = \begin{bmatrix} \frac{\partial x}{\partial \theta} & \frac{\partial x}{\partial \emptyset} \\ \frac{\partial y}{\partial \theta} & \frac{\partial y}{\partial \emptyset} \\ \frac{\partial z}{\partial \theta} & \frac{\partial z}{\partial \emptyset} \end{bmatrix} = \begin{bmatrix} \cos\theta\cos\emptyset & -\sin\theta\sin\emptyset \\ \cos\theta\sin\emptyset & \sin\theta\cos\emptyset \\ -\sin\theta & 0 \end{bmatrix}.$$

Hence, the differential surface area is the familiar

$$dS = \sqrt{\det(J^T J)}\, d\theta d\emptyset = \sin\theta\, d\theta d\emptyset$$

The Total Radiated Power under a Spherical Coordinate parameterization is the familiar 3GPP equation [4][5]

$$TRP = \oiint_S \frac{EIRP(\theta,\emptyset)}{4\pi} \cdot \sin\theta \cdot d\theta\, d\emptyset$$

This form of the integral is exact in the continuous case but prone to uncertainty for finite discrete uniform grid spacing

$$TRP \approx \frac{\pi}{2\,NM} \sum_{i=1}^{N-1} \sum_{j=0}^{M-1} EIRP(\theta_i, \phi_j) \sin(\theta_i)$$

The Spherical Coordinate system is not the only possible parameterization of the surface. One alternative, by definition to alleviate the sin θ = 0 problem at the sampling poles, is to consider the surface S as composed of a set of infinitesimal triangles. This triangulation method is commonly used in Finite Element Analysis and is based on Barycentric coordinates. The Barycentric parametrization $(u_1 = \xi, u_2 = \eta)$ with the domain $\xi \in [0,1]$ and $\eta \in [0,1]$ is

$$\vec{r}(u_1 = \xi, u_2 = \eta) = \begin{bmatrix} x \\ y \\ z \end{bmatrix} = \begin{bmatrix} (x_1 - x_0)\xi + (x_2 - x_0)\eta + x_0 \\ (y_1 - y_0)\xi + (y_2 - y_0)\eta + y_0 \\ (z_1 - z_0)\xi + (z_2 - z_0)\eta + z_0 \end{bmatrix}$$

The Jacobian Matrix for the Barycentric parameterization is

$$J = \begin{bmatrix} \frac{\partial x}{\partial \xi} & \frac{\partial x}{\partial \eta} \\ \frac{\partial y}{\partial \xi} & \frac{\partial y}{\partial \eta} \\ \frac{\partial z}{\partial \xi} & \frac{\partial z}{\partial \eta} \end{bmatrix} = \begin{bmatrix} \vec{J}_0 & \vec{J}_1 \end{bmatrix} = \begin{bmatrix} (x_1 - x_0) & (x_2 - x_0) \\ (y_1 - y_0) & (y_2 - y_0) \\ (z_1 - z_0) & (z_2 - z_0) \end{bmatrix} = \begin{bmatrix} (\vec{r}_1 - \vec{r}_0) & (\vec{r}_2 - \vec{r}_0) \end{bmatrix}$$

and by Lagrange's identity $\sqrt{\det(J^T J)} = \left\| \vec{J}_0 \times \vec{J}_1 \right\|$, the differential surface element is

$$dS = \sqrt{\det(J^T J)}\, d\xi d\eta = \|(\vec{r}_1 - \vec{r}_0) \times (\vec{r}_2 - \vec{r}_0)\| d\xi d\eta$$

Hence, the TRP integral expressed in Barycentric coordinates is

$$TRP = \oiint_S \frac{EIRP(\xi,\eta)}{4\pi} \cdot \|(\vec{r}_1 - \vec{r}_0) \times (\vec{r}_2 - \vec{r}_0)\| \cdot d\xi\, d\eta$$

and is approximated by the sum over all triangles Δ_i composing the closed surface S

$$4\pi TRP \approx \sum_i \int_{\eta=0}^{1} \int_{\xi=0}^{1-\eta} EIRP_i(\xi,\eta) \left\| \left(\vec{r}_{1,i} - \vec{r}_{0,i}\right) \times \left(\vec{r}_{2,i} - \vec{r}_{0,i}\right) \right\| d\xi d\eta$$

The notation of explicitly adding the subscript to the $EIRP_i(\xi,\eta)$ explicitly states the double integral of EIRP over each independent i[th] triangle has the identical bounds of integration; $\xi = [0,1-\eta]$ and $\xi = [0,1]$ which is accomplished by mapping to the standard triangle via a change of coordinates. In Barycentric coordinates, this coordinate transform is trivially accomplished knowing only the sample points at the vertices of the triangle as

$$EIRP_i(\xi,\eta) = EIRP_{0,i} + \left(EIRP_{1,i} - EIRP_{0,1}\right)\xi + \left(EIRP_{2,i} - EIRP_{0,i}\right)\eta$$

Every EIRP value in the interior of the triangle is computed as $EIRP_i(\xi,\eta)$ knowing only the three measured samples [$EIRP_{0,i}$, $EIRP_{1,i}$, $EIRP_{2,i}$] within the triangle domain $\xi = [0,1-\eta]$ and $\xi = [0,1]$ as illustrated in Figure G.1.2.2-1.

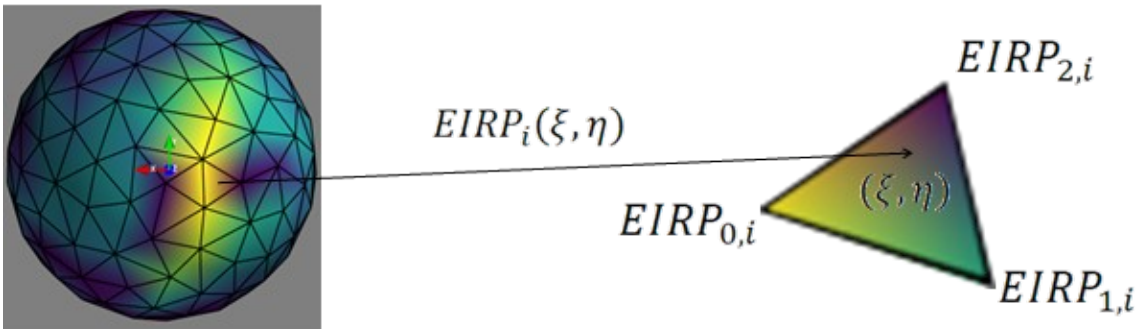

Figure G.1.2.2-1: Illustration of the triangulated sphere including the triangle formed by three measurements points

The cross product term, $2A_i \equiv \left\| \left(\vec{r}_{1,i} - \vec{r}_{0,i}\right) \times \left(\vec{r}_{2,i} - \vec{r}_{0,i}\right) \right\|$, is constant relative to the integration variables so the TRP approximation further simplifies to

$$4\pi TRP \approx \sum_i 2A_i \int_{\eta=0}^{1} \int_{\xi=0}^{1-\eta} \left[EIRP_{0,i} + \left(EIRP_{1,i} - EIRP_{0,1}\right)\xi + \left(EIRP_{2,i} - EIRP_{0,i}\right)\eta\right] d\xi d\eta$$

The double integral therefore is computed explicitly yielding

$$4\pi TRP \approx \sum_i 2A_i \cdot \left(\frac{EIRP_{0,i} + EIRP_{1,i} + EIRP_{2,i}}{6}\right)$$

The final form of the TRP approximation based on Barycentric surface parameterization is

$$TRP \approx \frac{1}{4\pi} \sum_i A_i \cdot \left(\frac{EIRP_{0,i} + EIRP_{1,i} + EIRP_{2,i}}{3}\right)$$

This yields an intuitive geometrical description of TRP approximation as simply the sum of all discrete triangle areas composing the closed spherical surface S, with each triangle scaled by the mean value of EIRP at the three measurement vertices. Guaranteed non-zero terms inside the sum mitigate possible numerical approximation issue at the poles, unlike the *sin* θ based TRP approximation. Notice that no particular definition of sample type is required for this Barycentric-based definition of TRP. This formulation can be applied to uniform grid sampling, as well as uniform density sampling, or even completely random sampling.

The mean offset can be optimized by explicitly computing the surface area of the sphere's polyhedral approximation ($4\pi \approx \sum_i A_i$) using

$$TRP \approx \frac{\sum_i A_i \cdot \left(\frac{EIRP_{0,i} + EIRP_{1,i} + EIRP_{2,i}}{3} \right)}{\sum_i A_i}$$

The Jacobian integration technique is based on subdividing the sphere into triangles and estimating the TRP integral as the sum of all triangles mean value of EIRP sampled at the triangle vertices. Given identical set of sampled points on the sphere (uniform grid spacing in both ϕ and θ), there is not a single unique representation of interconnections between the samples. In the limit as the grid spacing becomes infinitesimally small, there is no difference in TRP estimation, but the reverse is not strictly true. For small but finite angular grid sampling, there can be differences in the statistical TRP properties depending on the differences in mesh triangulation. Two different Matlab triangulations are illustrated in Figure G.1.2.2-2 on the left, Matlab's default convex hull triangulation, and on the right, a symmetric "ferromagnetic" triangulation implementation.

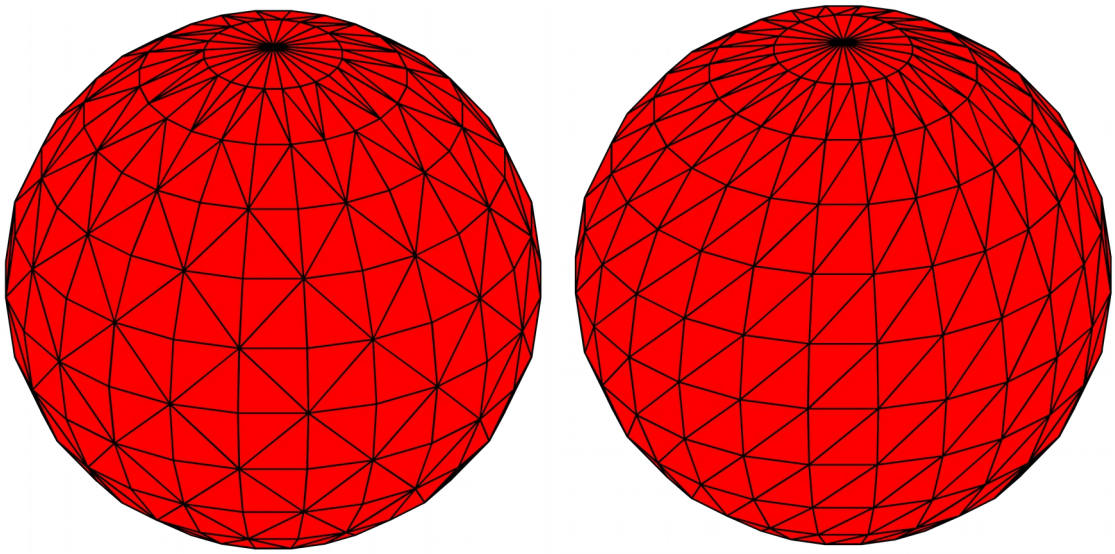

Figure G.1.2.2-2: Jacobian triangulation. On the left, Matlab's default convex hull triangulation, and on the right, a symmetric "ferromagnetic" triangulation implementation.

G.1.3 TRP Integration for Constant Density Grid Types

For constant density grid types, the TRP integration should ideally take into account the area of the Voronoi region surrounding each grid point. Assuming an ideal constant density configuration of the grid points, the TRP can be approximated using

$$TRP \approx \frac{1}{N} \sum_{i=0}^{N-1} \left(EIRP_\theta(\theta_i, \phi_i) + EIRP_\phi(\theta_i, \phi_i) \right)$$

where N is the number of grid points of the constant density grid type.

G.1.4 Simulation Results

The results for four different quadrature approaches using constant step-size measurement grids are summarized in Table G.1.4-1 for the reference 8x2 antenna array.

TABLE G.1.4-1: STATISTICS OF QUADRATURE APPROACHES FOR CONSTANT STEP SIZE MEASUREMENT GRIDS FOR THE 8X2 REFERENCE ANTENNA ARRAY.

Number of		Mean Error [dB]	STD [dB]	Min. norm. TRP [dB]	Max. norm. TRP [dB]	Integration Approach	Comment
Latitudes	Longitudes						
13	24	-0.03	0.13	-0.96	0.21	sin(theta) weights	15° step size
		0.00	0.06	-0.23	0.21	Clenshaw-Curtis weights	
		-0.01	0.22	-0.96	0.74	Jacobian integration	
		0.00	0.09	-0.24	0.32	Jacobian ferromagnetic integ.	
12	19	-0.03	0.25	-1.17	0.77	sin(theta) weights	$\Delta\theta=16.36^{o}$ & $\Delta\phi=18.95^{o}$
		-0.01	0.20	-0.92	0.76	Clenshaw-Curtis weights	
		0.00	0.26	-1.01	0.84	Jacobian integration	
		0.00	0.21	-1.00	0.73	Jacobian ferromagnetic integ.	

The following observations can be made:

- The standard deviation and the spread in TRP results is largest with the sin(θ) quadrature
- The smallest standard deviation and the smallest spread in TRP results is obtained with the Clenshaw-Curtis, and the Jacobian quadrature utilizing the ferromagnetic triangulation (from best to worst)
- The triangulation approach has an impact on the standard deviation and the spread in TRP results with the “ferromagnetic” approach outperforming the non symmetric triangulation approach
- All four quadratures meet the 0.25dB standard deviation for the 15° step size measurement grid.
- With the Clenshaw Curtis, spherical integration quadrature, and the Jacobian quadrature with ferromagnetic triangulation, a constant-step size measurement grid with 12 latitudes and 19 longitudes is sufficient to meet the maximum standard deviation of 0.25dB.

The results for two different constant-density grid implementations (charged particle and golden spiral) are summarized in Table G.1.4-2 for the 8x2 reference antenna pattern.

Table G.1.4-2: Statistics for constant density measurement grid types for the 8x2 reference antenna array

Number of Grid Points	Mean Error [dB]	STD [dB]	Min. normalized TRP [dB]	Max. normalized TRP [dB]	Implementation
130	-0.01	0.27	-1.07	0.85	Charged Particle
130	-0.02	0.37	-1.82	1.31	Golden Spiral
135	-0.01	0.23	-0.90	0.89	Charged Particle
135	-0.02	0.33	-1.64	1.27	Golden Spiral
140	0.00	0.20	-0.76	0.65	Charged Particle
140	-0.01	0.30	-1.45	1.23	Golden Spiral
145	0.00	0.18	-0.65	0.56	Charged Particle
145	-0.01	0.27	-1.32	1.20	Golden Spiral
150	0.00	0.15	-0.59	0.55	Charged Particle
150	-0.01	0.25	-1.15	1.02	Golden Spiral
155	0.00	0.12	-0.45	0.53	Charged Particle
155	0.00	0.22	-0.99	0.93	Golden Spiral
160	0.00	0.10	-0.42	0.41	Charged Particle
160	0.00	0.20	-0.82	0.95	Golden Spiral
165	0.00	0.09	-0.32	0.32	Charged Particle
165	-0.01	0.18	-0.70	1.00	Golden Spiral
170	0.00	0.08	-0.30	0.31	Charged Particle
170	0.00	0.17	-0.67	0.96	Golden Spiral
175	0.00	0.06	-0.24	0.25	Charged Particle
175	0.00	0.16	-0.56	0.91	Golden Spiral

The Charged Particle implementation requires a minimum number of 135 points and the Golden Spiral requires a minimum number of 150 points.

G.2 Beam Peak Search Measurement Grids

G.2.1 Assumptions

The simulation assumptions for the beam peak measurement grids are the same as outlined in Annex G.1.1.

G.2.2 Grid Types

Same grids as in G.1.2 are considered.

G.2.3 Simulation results

The most realistic approach is to analyse the statistical distribution of the beam peak error for a large number of random orientations.

For the simulations, the relative orientation of the simulated antenna array and the measurement grid was altered randomly. The statistical results from simulations using 50,000 random orientations are then used to determine mean error, standard deviation and percentile analysis on CDF curve of all maximum EIRPs for each measurement grid. The EIRPs are normalized by the known 8x2 antenna peak antenna gain.

Sample histograms and CDF distributions for the beam peak error for constant step-size measurement grids are shown in Figure G.2.3-1 and for the constant density measurement grid (based on the charged particle implementation) in Figure G.2.3-2. The histograms show a half-normal distribution.

Given the half-normal distribution, the MU term should be based on the determination of the offset from the beam peak that contains 95% of the distribution (alternatively, the value at which the CDF is 5%). This offset shall be considered a systematic error in the MU budget. The various statistical metrics are illustrated in Figure G.2.3-3.

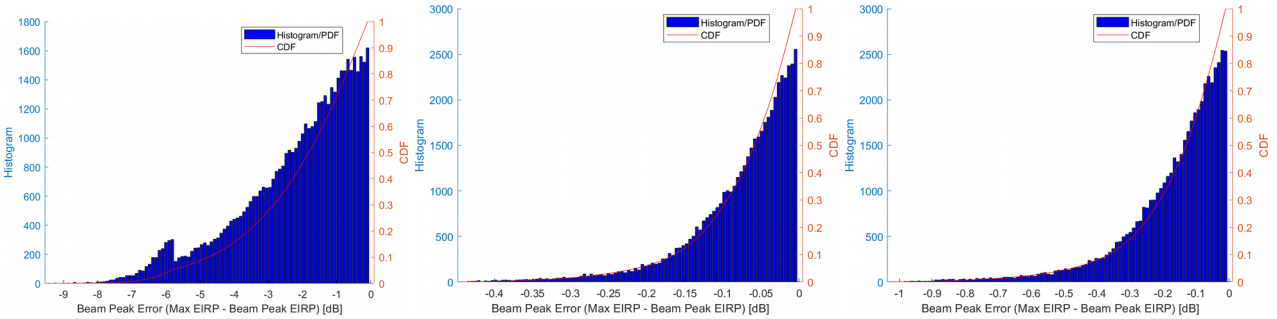

Figure G.2.3-1: Histogram of maximum beam peak errors for sample constant-step size meausurement grids (left: 2.5º, middle: 5º, right: 7.5º step size)

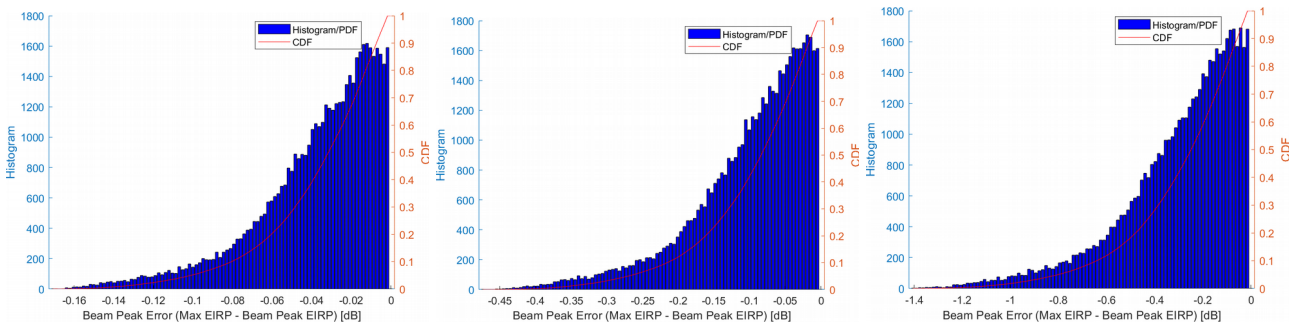

Figure G.2.3-2: Histogram of maximum beam peak errors for sample constant density measurement grids (left: 4000, middle: 1500, right: 500 grid points)

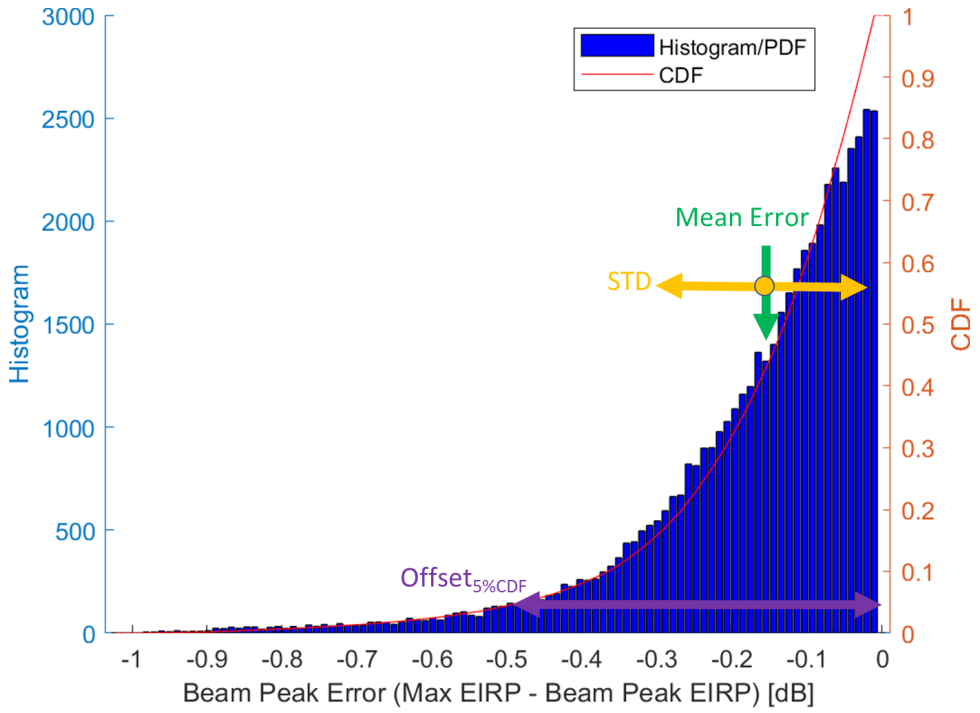

Figure G.2.3-3: Statistical metrics for a sample half-normal distribution

The mean error and the standard deviation, and the offset at which the CDF is 5% are tabulated in Table G.2.3-1 for the constant step size grids and Table G.2.3-2 for the constant density grids and plotted in Figures G.2.3-4. Figure G.2.3-5 and Figure G.2.3-6 respectively.

Table G.2.3-1: Statistical Analyses of the 50k simulations for the constant step size grids

Angular Step Size [deg]	Number of unique grid points	Mean Error [dB]	STD [dB]	$Offset_{5\%CDF}$ [dB]
2.5	10226	0.02	0.02	0.05
3.0	7082	0.02	0.02	0.08
3.6	4902	0.04	0.04	0.11
4.0	3962	0.05	0.04	0.14
4.5	3122	0.06	0.06	0.17
5.0	2522	0.07	0.07	0.21
6.0	1742	0.10	0.10	0.31
7.5	1106	0.16	0.15	0.48
9.0	762	0.23	0.22	0.69
10.0	614	0.29	0.27	0.84
12.0	422	0.42	0.39	1.21
15.0	266	0.65	0.60	1.88

Table G.2.3-2: Statistical Analyses of the 50k simulations for the constant-density grids

Number of unique grid points	Mean Error [dB]	STD [dB]	$Offset_{5\%CDF}$ [dB]
50	2.93	2.25	7.08
70	2.13	1.69	5.85
100	1.50	1.24	4.08
150	1.00	0.82	2.73
200	0.74	0.61	2.00
300	0.49	0.40	1.34
400	0.37	0.30	1.00
500	0.29	0.24	0.80
600	0.24	0.20	0.67
750	0.19	0.16	0.54
800	0.18	0.15	0.50
820	0.18	0.15	0.49
850	0.17	0.14	0.48
900	0.16	0.13	0.44
1000	0.15	0.12	0.40
1200	0.12	0.10	0.33
1400	0.10	0.09	0.29
1500	0.10	0.08	0.27
2000	0.07	0.06	0.20
3000	0.05	0.04	0.13
4000	0.04	0.03	0.10
6000	0.02	0.02	0.07
8000	0.02	0.02	0.05

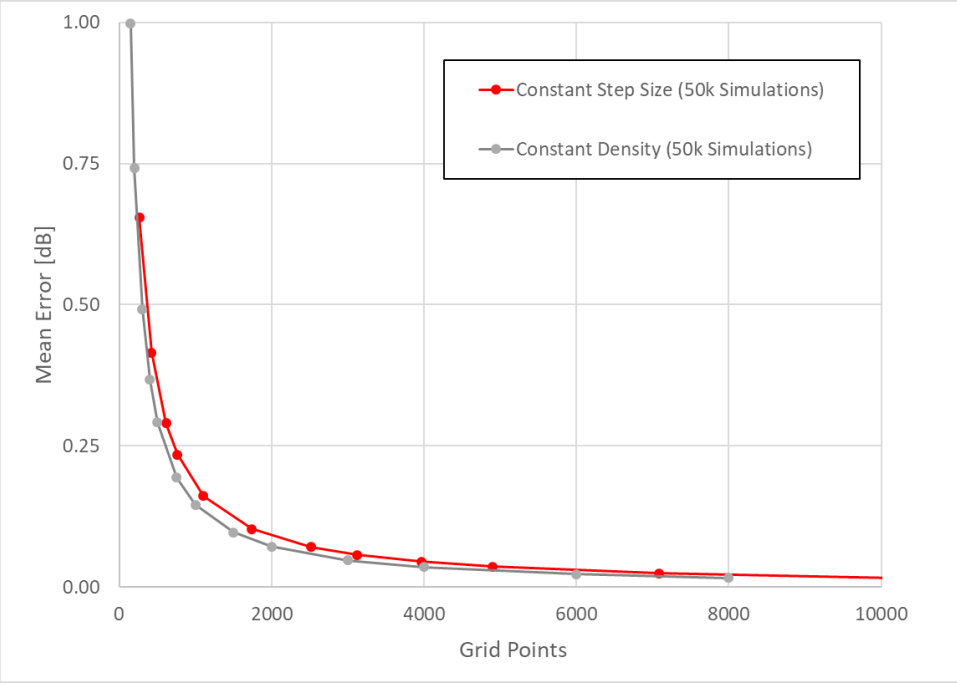

Figure G.2.3-4: Mean error of the 50k simulations

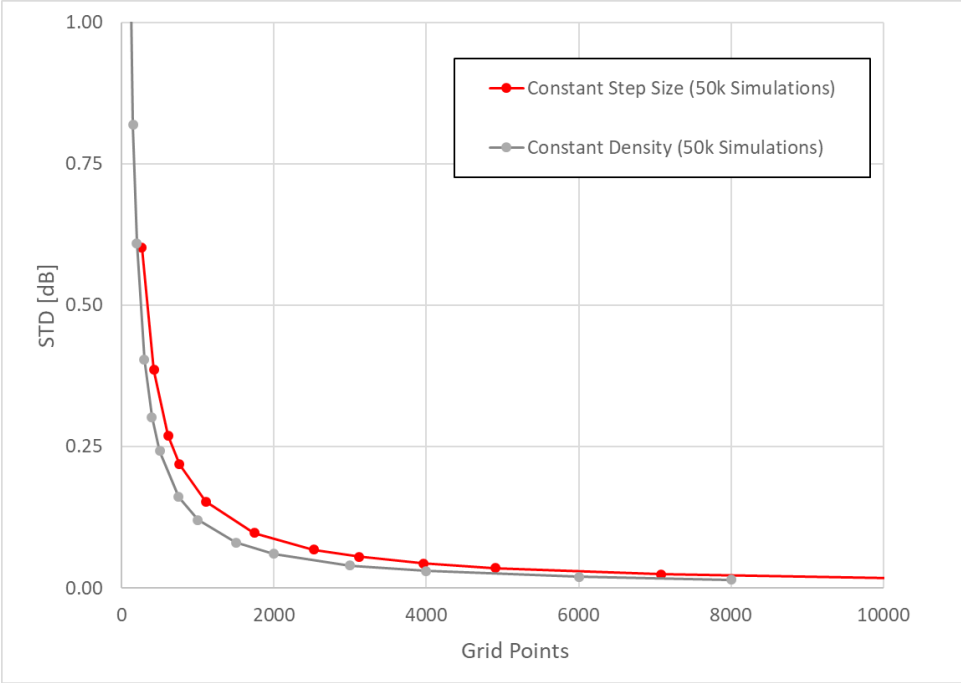

Figure G.2.3-5: Standard deviation of the 50k simulations

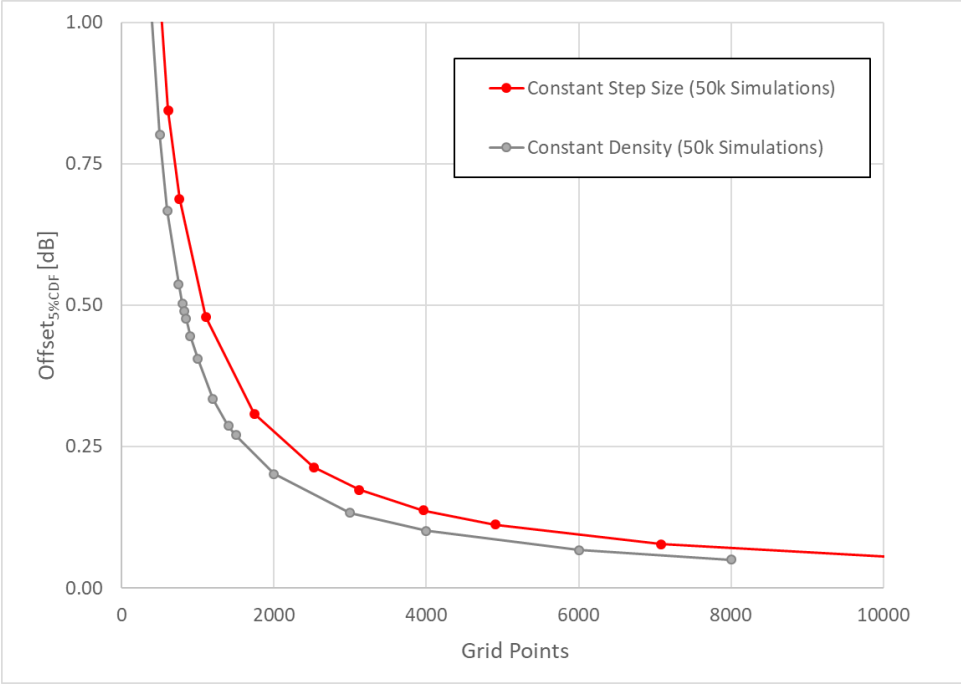

Figure G.2.3-6: Offset from the beam peak at which the CDF is 5% of the 50k simulations

It can be seen that practical measurement grids of less than 1000 unique measurement points yield mean errors of less than 0.2dB and standard deviations of less than 0.2dB, and offsets from beam peak at which CDF is 5% of less than about 0.5dB.

In Table G.2.3-3, the minimum number of unique grid points are listed for each grid type investigated for sample systematic errors of 'Beam Peak Search' of 0.2 to 0.7dB. The option with the 0.5dB seems to be best compromise in terms of MU and test points/test time.

Table G.2.3-3: Minimum number of unique grid points for sample systematic errors

Systematic Error of 'Beam Peak Search': Offset from Beam Peak at which CDF is 5%	Minimum Number of Unique Grid Points for Constant Step Size Grid	Minimum Number of Unique Grid Points for Constant Density Grid
0.2dB	2522 (5º step size)	2000
0.3dB	1742 (6º step size)	1500
0.4dB	N/A	1000
0.5dB	1106 (7.5ºstep size)	800
0.6dB	N/A	750
0.7dB	762 (9º step size)	600

Taking into account simulation results above and in order to make a reasonable trade-off with measurement uncertainties, it is recommended to use for beam peak search the following measurement grids leading to a systematic error of "Beam Peak Search" of 0.5 dB:

- Constant density grid (using the charged particle implementation) with at least 800 grid points.
- Constant step size grid with at least 1106 grid points, corresponding to an angular step size of 7.5º.

The metric using a single, fine grid for the TX beam peak search is EIRP and for the RX beam peak search it is EIS.

G.2.4 Coarse and fine measurement grids

The baseline beam peak search is based on a single and fine beam peak search grid to determine the TX/RX beam peak of the DUT in any given direction. This means that even in sectors where poor EIRP/EIS performance is observed, a very fine grid is used to search for the TX/RX beam peak.

An optimized approach, based on an initial coarse search followed by a subsequent fine search could reduce the number of beam peak search grid points significantly. The basis for this approach is to use a coarse grid with fewer number of points than the ones described in section G.2.3 in the first stage to identify candidate regions that contain the global beam peak and search for the global beam peak with the fine grid in the second stage with a minimum number of points described in section G.2.3.

As an example, Figure G.2.4-1 illustrates the coarse and fine measurement grid approach applied to TX beam search; while this illustration is for EIRP, it can easily be extended to RX beam peak search using EIS or throughput metrics For simplification purposes, 2D coarse and fine searches are illustrated but the concept can be extended to 3D easily. The UE is assumed to form a total of six beams in the 2D plane as illustrated on the left of Figure G.2.4-1. In the centre of Figure G.2.4-1, the 36 coarse beam peak search grid points in the 2D plane are illustrated. On the right, the grey circles on the respective antenna patterns illustrate the measured EIRP values towards each coarse grid point direction based on the respective beam steering directions. This illustration shows that the EIRP beam peak of the coarse search, $EIRP_{CSBP}$, is found to be the peak of the orange beam while the global TX beam peak (red beam) was not identified due to the coarse sampling of the grid points.

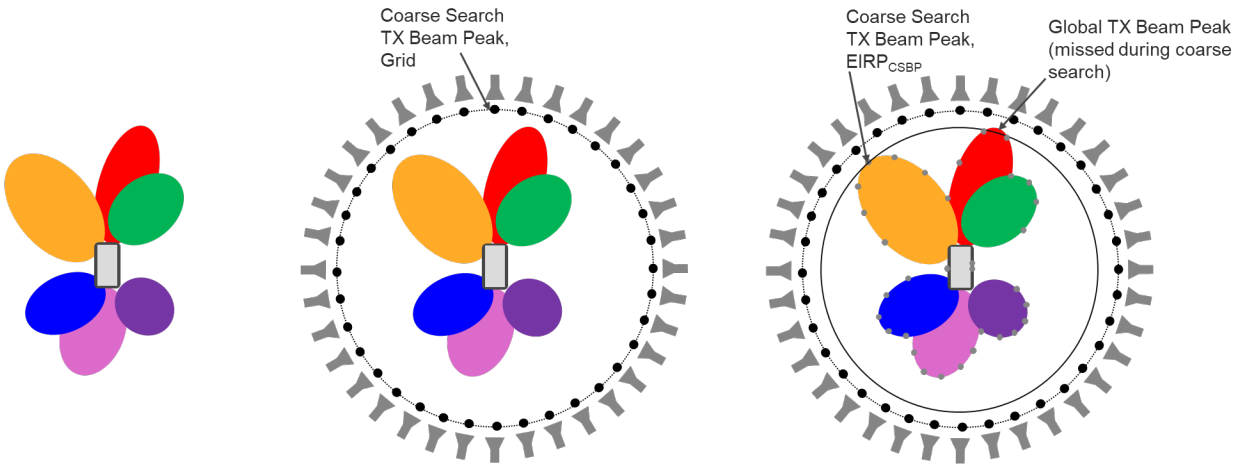

Figure G.2.4-1: Illustration of the Coarse Search Approach for TX Beam Peak Search. Left: Antenna Pattern assumptions in 2D, Centre: Coarse beam peak search grid points/discrete antenna measurement positions, Right: TX beam EIRP measurements per grid point

The proposed fine search approach is illustrated further in Figure G.2.4-2. A fine search region starting from the beam peak identified in the coarse search, $EIRP_{CSBP}$, over a range of Δ_{FS} is used to identify the regions that need to be investigated more closely with the fine search algorithm. The fine search range Δ_{FS} is a function of the angular spacing of the coarse beam peak search grid as well as the beam width of the reference antenna pattern considered for smartphone UEs.

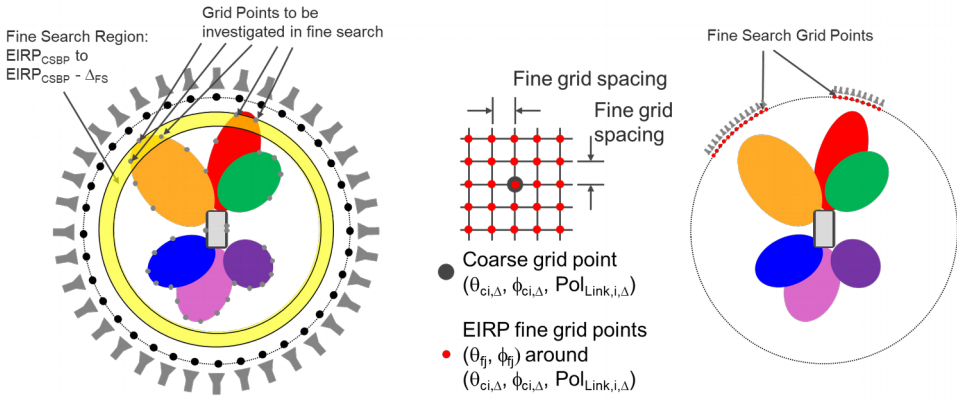

Figure G.2.4-2: Illustration of the fine beam peak search grid. Left: identify the measurement grid points that yielded EIRP values within the fine search region, right: placement of fine beam peak search grid points

Figure G.2.4-3 illustrates coarse and fine grids for constant step size measurement grids while Figure G.2.4-4 illustrates the same for constant density grid.

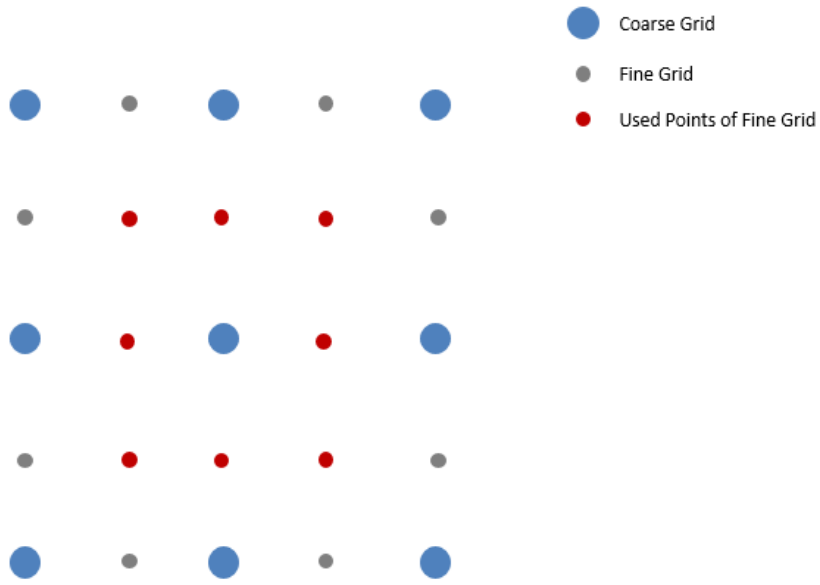

Figure G.2.4-3: Illustration: Coarse & Fine Constant Step Size Grids

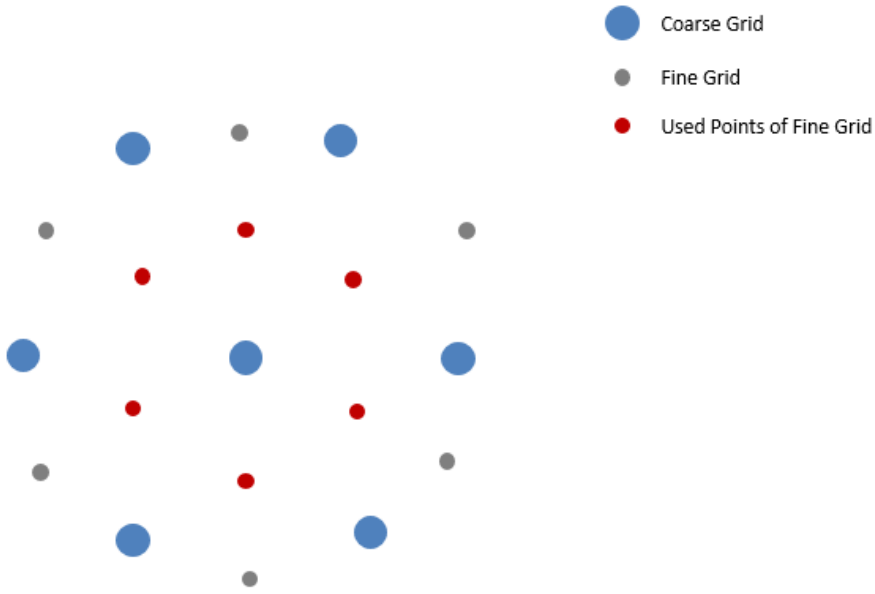

Figure G.2.4-4: Illustration: Coarse & Fine Constant Density Grids

The metric using a coarse & fine grid approach for the TX beam peak search is EIRP for both grids. For RX beam peak search either EIS or Throughput could be used for coarse grids while only EIS for fine grid,

G.3 Spherical coverage Measurement Grids

G.3.1 Assumptions

The simulation assumptions for the spherical coverage grids are the same as outlined in Annex G.1.1.

Regarding the antenna implementation and beamformer, the following assumptions have been made (refer to Figure G.3.1-1):

- Two 8x2 antenna arrays are integrated in the UE for the spherical coverage analyses

- The implementation loss for the antenna near the front is 5dB less than that for the antenna near the back
- For Beam Steering Assumptions
  - In the xz plane, 45° beam steering granularity (from 45° to 135°) has been used
  - In the xy plane, 22.5° beam steering granularity (from -90° to 90°) has been used

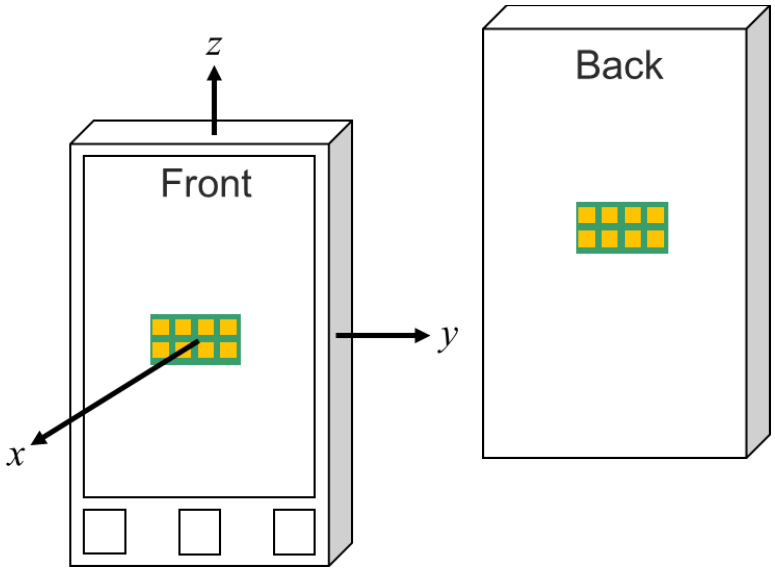

Figure G.3.1-1: Illustration of the two antenna arrays integrated in the UE.

Regarding UE Orientations/Rotations, the following assumptions were made for the analyses:

- 10000 random relative orientations between the simulated UE and the respective measurement grids
- The rotations of UE/grid will be along θ and ϕ as well as around the beam peak
- The rotations along θ will utilize a sin(θ) weighting to assume a uniform sampling on the surface.

When using constant step size measurement grids, a theta-dependent correction shall be applied, i.e., the PDF probability contribution for each measurement point is scaled by sin(theta).

G.3.2 Grid Types

Same grids as in G.1.2 are considered.

G.3.3 Simulation results

G.3.3.1 EIRP spherical coverage

The reference CDF curve was determined with a very fine constant step size measurement grid using a 1° step size in θ and ϕ. The need for scaling the PDFs by sin(θ) is highlighted in Figure G.3.3.1-1 for an EIRP spherical coverage CDF analysis based on 10000 random UE orientations with a 1° constant step size grid. While the CDF curves in Figure G.3.3.1-1a are based on the PDF scaled by sin(θ), the curves in Figure G.3.3.1-1b were not using the θ dependent scaling. Clearly, the sin(θ) scaling makes the CDF curves converge to the reference CDF curve for this very fine measurement grid, while the simulated CDFs without the sin(θ) scaling of the PDF are spread rather wide and can therefore not be used for CDF analyses.

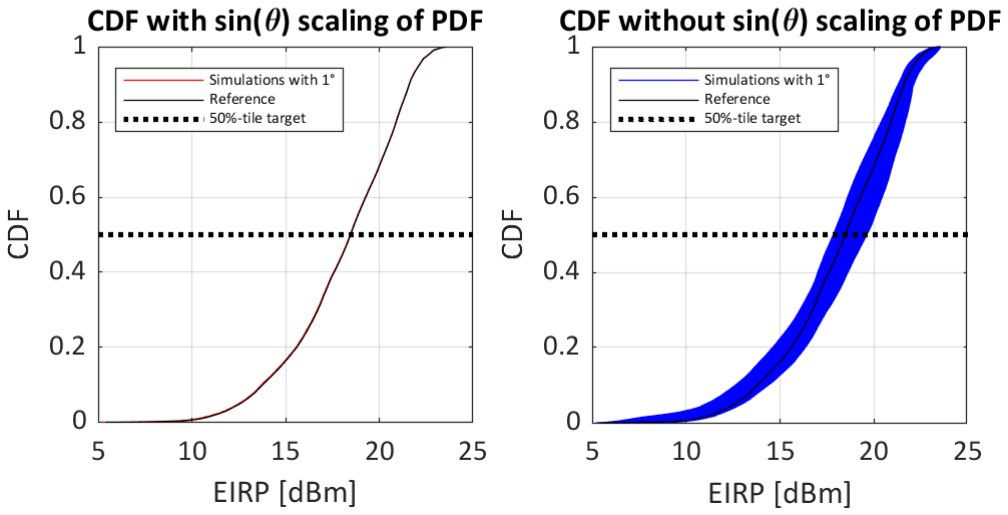

Figure G.3.3.1-1: Sample CDF Analyses for a very fine 1° constant step size measurement grid. a) with the sin(θ) scaling of the PDF and b) without the θ dependent scaling.

At the 50%-tile CDF, i.e., the target CDF for Power Class 3, statistical analyses of all 10000 EIRPs, $EIRP_{50\%CDF}$, is performed. For the example of the 1° constant step size grid, the histogram is shown in Figure G.3.3.1-2.

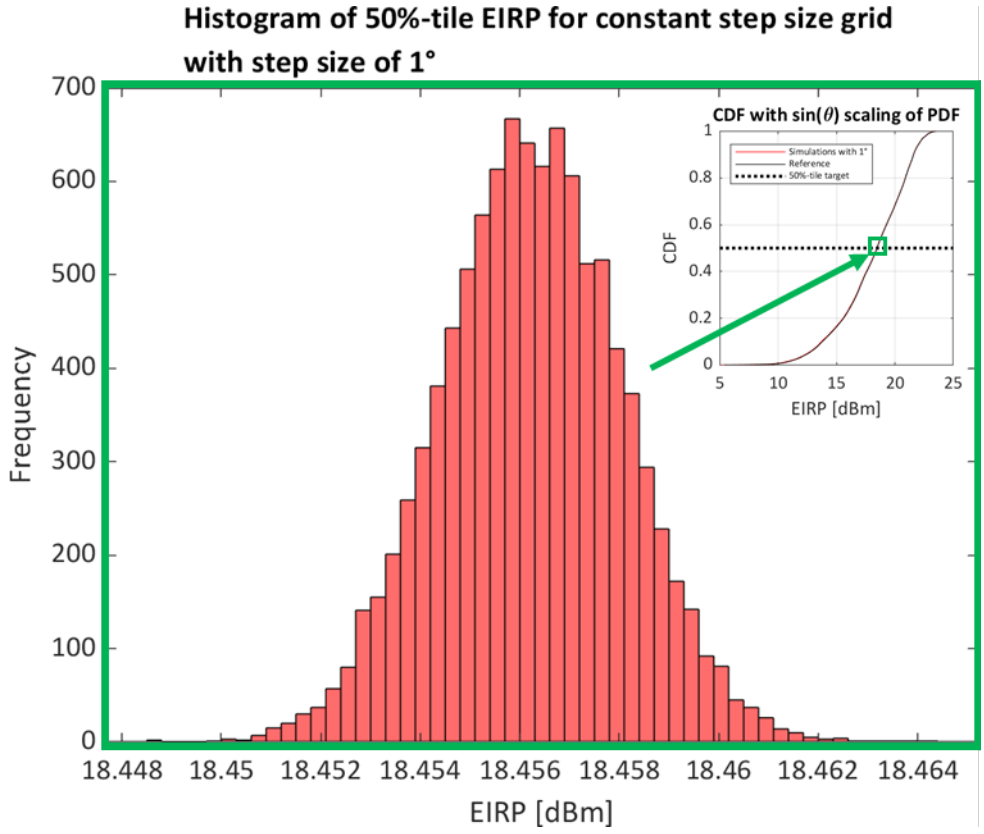

Figure G.3.3.1-2: Sample Histogram of the 10000 min EIRPs at the 50%-tile CDF for a very fine 1° constant step size measurement grid

G.3.3.1.1 Analyses with 8x2 Antenna Array with Beam Peak on the Measurement Grid

The results shown in this section are based on the 8x2 antenna array with the beam peak always aligned on a grid point. For these simulations, the completely random UE rotations in θ and ϕ were always re-adjusted to the next closest measurement grid point.

The results for various measurement grids are tabulated in Table G.3.3.1.1-1 and sample CDF curves of the $EIRP_{50\%CDF}$ for some sample grids are shown in Figure G.3.3.1.1-1.

Table G.3.3.1.1-1: Statistical results of the $EIRP_{50\%CDF}$ for the 8x2 antenna array for constant step size measurement grids and the beam peak always aligned on a grid point.

Step Size [°]	Number of unique grid points	STD [dB]	Min 50%-tile CDF Norm. EIRP [dB]	Max 50%-tile CDF Norm. EIRP [dB]	|Mean Error| [dB]
2.0	16022	0.01	-0.02	0.03	0.00
2.5	10226	0.01	-0.04	0.04	0.00
3.0	7082	0.01	-0.05	0.04	0.00
4.0	3962	0.02	-0.08	0.07	0.00
5.0	2522	0.03	-0.10	0.10	0.00
6.0	1742	0.03	-0.14	0.10	0.00
9.0	762	0.05	-0.23	0.24	0.01
10.0	614	0.06	-0.32	0.24	0.01
12.0	422	0.07	-0.26	0.22	0.01
15.0	266	0.12	-0.69	0.45	0.01
20.0	146	0.16	-0.47	0.61	0.06
22.5	114	0.27	-1.40	0.68	0.04
30.0	62	0.47	-1.65	1.10	0.09
45.0	26	0.91	-3.42	1.34	0.20

It can be observed that:

- For the 8x2 reference antenna array with the beam peak always aligned on the measurement grid, the standard deviation of the $EIRP_{50\%CDF}$ is negligible (<0.1dB) for more than ~300 unique measurement points for constant step size grids.
- For the 8x2 reference antenna array with the beam peak always aligned on the measurement grid, the mean error of the $EIRP_{50\%CDF}$ is negligible (0.1dB) for more than ~62 unique measurement points for constant step size grids.

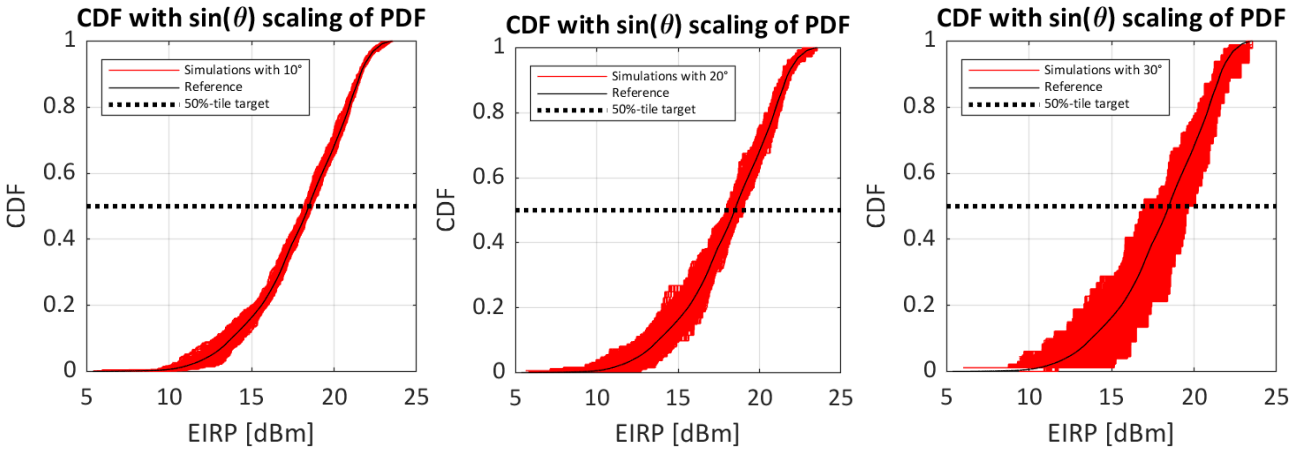

Figure G.3.3.1.1-1: CDF results for the 8x2 antenna array for constant step size measurement grids and the beam peak always aligned on a grid point.

Similar results for the constant-density measurement grids are tabulated in Table G.3.3.1.1-2 and sample CDF curves for some grids are shown in Figure G.3.3.1.1-2.

Table G.3.3.1.1-2: Statistical results of the $EIRP_{50\%CDF}$ for the 8x2 antenna array for constant density measurement grids and the beam peak always aligned on a grid point.

Number of unique grid points	STD [dB]	Min 50%-tile CDF Norm. EIRP [dB]	Max 50%-tile CDF Norm. EIRP [dB]	|Mean Error| [dB]
30	0.48	-1.74	1.72	0.01
40	0.45	-1.85	1.39	0.05
50	0.37	-1.68	1.14	0.06
70	0.25	-1.11	0.71	0.08
100	0.18	-0.82	0.69	0.04
150	0.15	-0.61	0.60	0.02
200	0.10	-0.53	0.40	0.01
300	0.08	-0.37	0.25	0.01
400	0.07	-0.28	0.33	0.01
500	0.06	-0.30	0.20	0.01

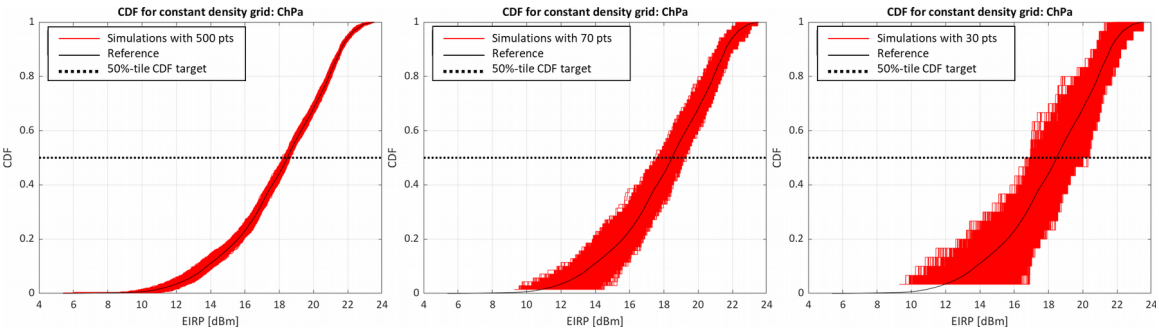

Figure G.3.3.1.1-2: CDF results for the 8x2 antenna array for constant density measurement grids and the beam peak always aligned on a grid point.

It can be observed that:

- For the 8x2 reference antenna array with the beam peak always aligned on the measurement grid, the standard deviation of the $EIRP_{50\%CDF}$ is negligible (<0.1dB) for more than ~200 unique measurement points for constant density size grids (using the charged particle implementation).

- For the 8x2 reference antenna array with the beam peak always aligned on the measurement grid, the mean error of the $EIRP_{50\%CDF}$ is always negligible (0.1dB) even for very small number of measurement points for constant density size grids.

The standard deviations between the constant step size and constant density grids is shown in Figure G.3.3.1.1-3 for the 8x2 antenna with the beam peak always placed on a grid point.

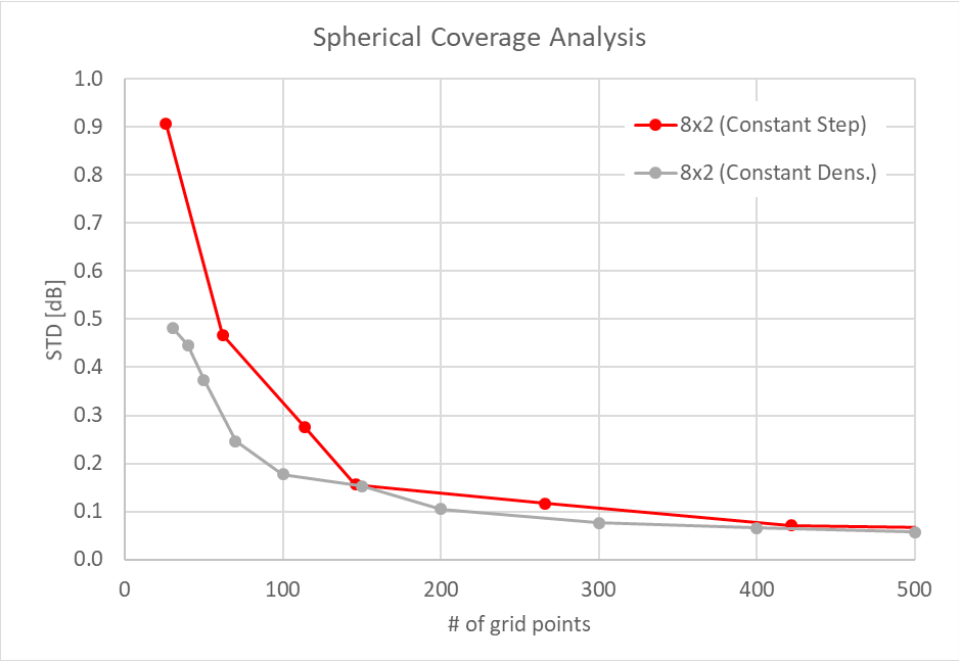

Figure G.3.3.1.1-3: Comparison of the standard deviation of $EIRP_{50\%CDF}$ for the 8x2 antenna with the beam peak always placed on a grid point.

The constant density measurement grids require fewer measurement points than the constant step size grids to achieve the same standard deviation.

G.3.3.1.2 Analyses with 8x2 Antenna Array with Beam Peak oriented completely randomly

The results in this section are based on the 8x2 antenna array with the beam peak oriented in completely random orientations, i.e., the beam peak is not always aligned to a grid point. This analysis was performed to see whether the beam peaks have to be aligned with a grid point if only the min. EIRP value at the 50%-tile CDF is of interest. It is understood that the CDF curve cannot be used to accurately determine the TX beam peak (100%-tile CDF).

The results for various constant-step size measurement grids are tabulated in Table G.3.3.1.2-1.

Table G.3.3.1.2-1: Statistical results of $EIRP_{50\%CDF}$ for the 8x2 antenna array for constant step size measurement grids and the beam peak oriented in completely random orientations.

Step Size [°]	Number of unique grid points	STD [dB]	Min 50%-tile CDF Norm. EIRP [dB]	Max 50%-tile CDF Norm. EIRP [dB]	|Mean Error| [dB]
9	762	0.05	-0.21	0.21	0.00
10	614	0.06	-0.22	0.27	0.00
12	422	0.07	-0.38	0.27	0.01
15	266	0.12	-0.61	0.45	0.01
20	146	0.17	-0.65	0.54	0.02
23	114	0.23	-1.14	0.69	0.05
30	62	0.49	-1.85	1.48	0.13
45	26	0.83	-3.60	2.11	0.27

Similar results for the constant-density measurement grids are tabulated in Table G.3.3.1.2-2.

Table G.3.3.1.2-2: Statistical results of $EIRP_{50\%CDF}$ for the 8x2 antenna array for constant density measurement grids and the beam peak oriented in completely random orientations.

Number of unique grid points	STD [dB]	Min 50%-tile CDF Norm. EIRP [dB]	Max 50%-tile CDF Norm. EIRP [dB]	|Mean Error| [dB]
30	0.56	-1.91	1.78	0.14
40	0.51	-2.14	1.80	0.15
50	0.41	-1.59	1.57	0.11
70	0.26	-1.32	1.02	0.07
100	0.19	-0.97	0.77	0.03
150	0.17	-0.80	0.62	0.02
200	0.11	-0.58	0.42	0.02
300	0.08	-0.37	0.30	0.01
400	0.07	-0.26	0.24	0.01
500	0.06	-0.28	0.23	0.01

The standard deviations and mean errors for the constant step size and constant density grids are shown in Figures G.3.3.1.2-1 and G.3.3.1.2-2 respectively, for the 8x2 antenna with the beam peak always placed on a grid point and with the beam peak placed in completely random orientations. Figure G.3.3.1.2-3 is looking at the max range of the 50%-tile CDF EIRPs which is the difference between the max and the min 50%-tile CDF EIRPs.

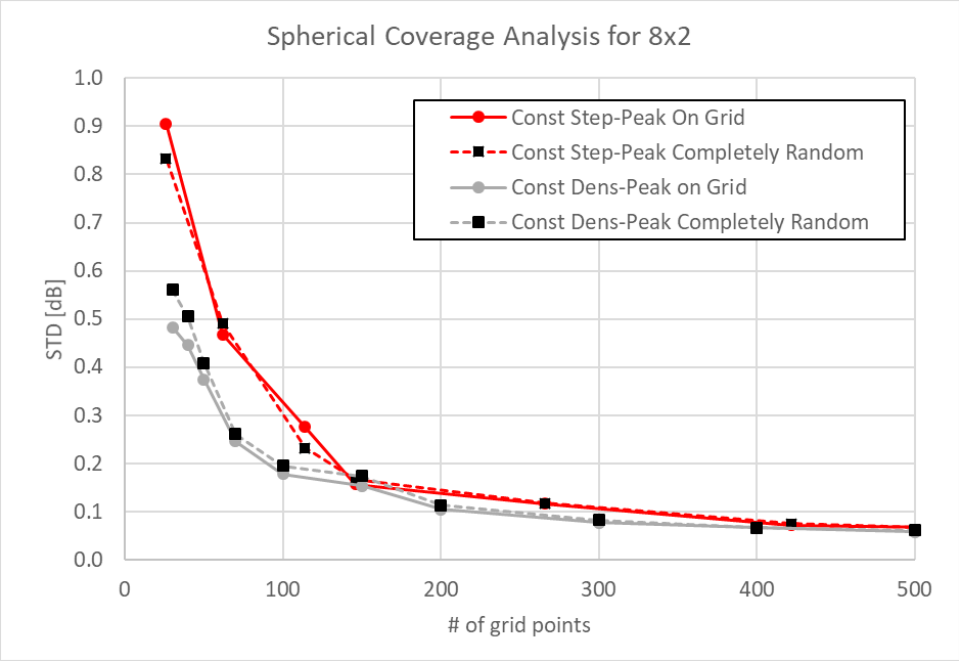

Figure G.3.3.1.2-1: Comparison of the standard deviation for the 8x2 antenna.

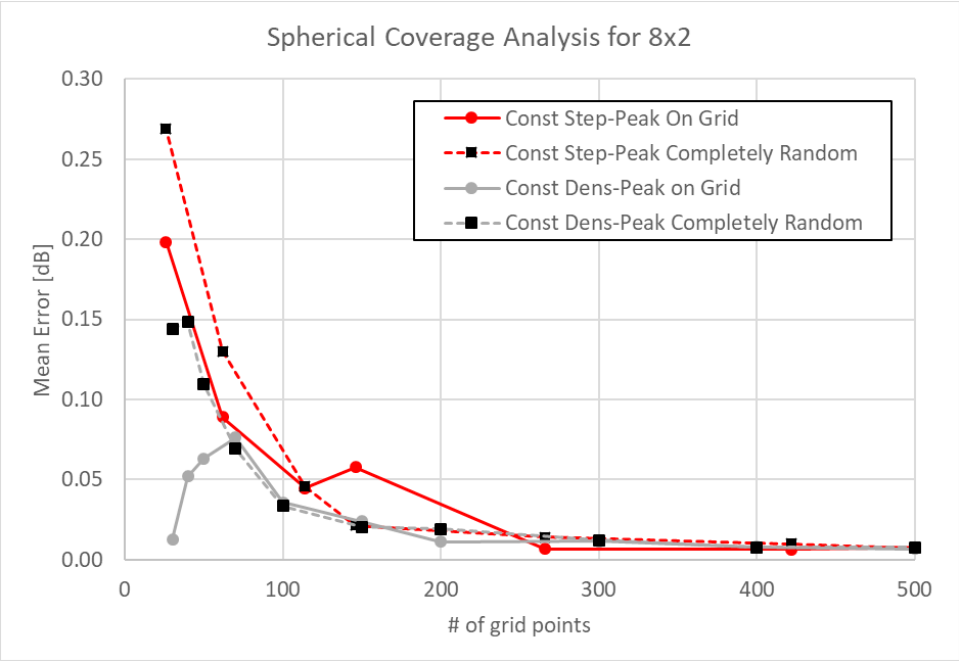

Figure G.3.3.1.2-2: Comparison of the mean error for the 8x2 antenna.

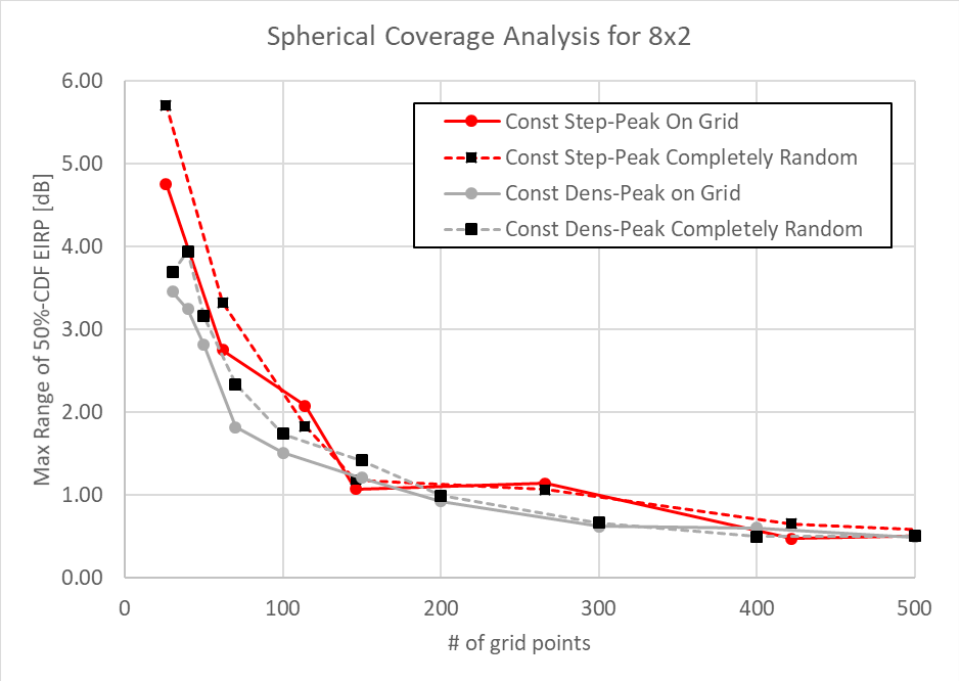

Figure G.3.3.1.2-3: Comparison of the max range of $EIRP_{50\%CDF}$ for the 8x2 antenna.

For the 8x2 reference antenna array, the standard deviation of the EIRP at the 50%-tile CDF is independent on whether the beam peak is on the measurement grid or not.

G.3.3.1.3 Conclusions

According to results in section G.3.3.1.1 and G.3.3.1.2, the following conclusions can be extracted:

- The EIRP spherical coverage measurement can be performed without having to have the beam peak having to be placed on a grid point, e.g., for coarse grids of beam peak searches.
- In order to make a reasonable trade-off with measurement uncertainties, it is recommended to use for spherical coverage grids measurement grids with at least 200 unique measurement points, i.e.,

- constant density grid (using the charged particle implementation) with at least 200 grid points: STD of 0.11dB and 0dB Mean Error
- constant step size grid with at least 266 grid points: STD of 0.12dB and 0dB Mean Error

G.3.3.2 EIS spherical coverage

The reference CDF curve was determined with a very fine constant step size measurement grid using a 1° step size in θ and ϕ. The need for scaling the PDFs by sin(θ) is highlighted in Figure G.3.3.2-1 for an EIS spherical coverage CDF analysis based on 10000 random UE orientations with a 1° constant step size grid. While the CDF curves in Figure G.3.3.2-1a are based on the PDF scaled by sin(θ), the curves in Figure G.3.3.2-1b were not using the θ dependent scaling. Clearly, the sin(θ) scaling makes the CDF curves converge to the reference CDF curve for this very fine measurement grid, while the simulated CDFs without the sin(θ) scaling of the PDF are spread rather wide and can therefore not be used for CDF analyses.

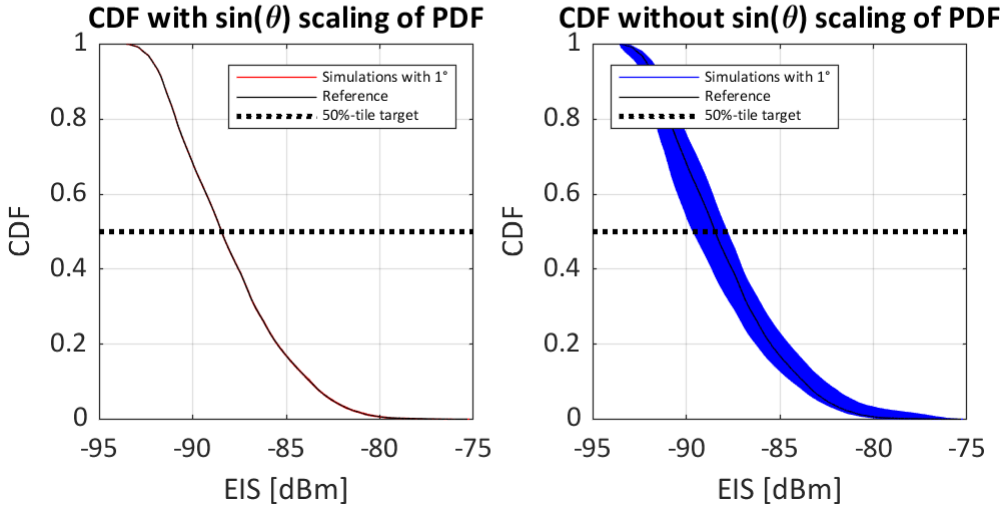

(a) (b)

Figure G.3.3.2-1: Sample CDF Analyses for a very fine 1° constant step size measurement grid. a) with the sin(θ) scaling of the PDF and b) without the θ dependent scaling.

At the 50%-tile CDF, i.e., the target CDF for PC3 [5], statistical analyses of all 10000 EISs, $EIS_{50\%CDF}$, is performed. For the example of the 1° constant step size grid, the histogram is shown in Figure G.3.3.2-2.

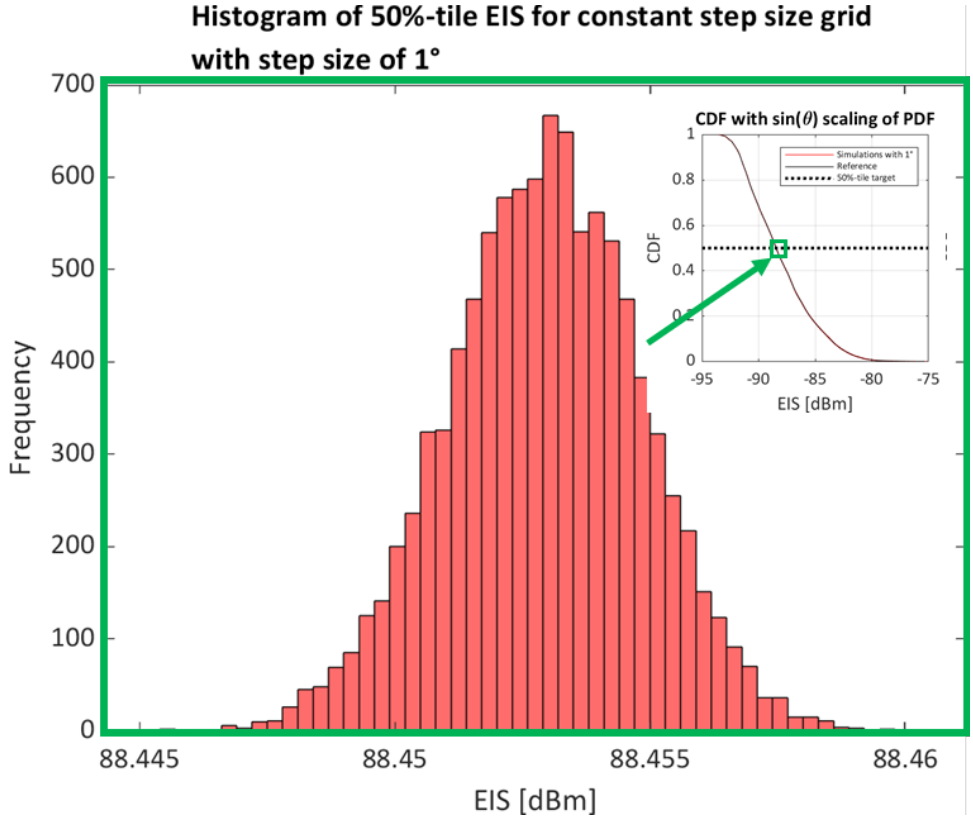

Figure G.3.3.2-2: Sample Histogram of the 10000 min EISs at the 50%-tile CDF for a very fine 1° constant step size measurement grid.

While EIRP is measured with a seemingly infinitesimal power accuracy by the test equipment, EIS is determined for finite DL power levels which has to be taken into account for the analyses. For instance, if the "true" EIS in a direction was -90.65dBm, the EIS following EIS values would be measured:

- -90.6dBm for a 0.1dB DL power step size
- -90.5dBm for a 0.5dB DL power step size
- -90dBm for a 1dB DL power step size

The analyses in this contribution are taking an unrealistic infinitesimal DL power step size as well as finite 0.1, 0.5, and 1dB step sizes into account.

G.3.3.2.1 Analyses with 8x2 Antenna Array with Beam Peak on the Measurement Grid

The results shown in this section are based on the 8x2 antenna array with the beam peak always aligned on a grid point. For these simulations, the completely random UE rotations in θ and ϕ were always re-adjusted to the next closest measurement grid point.

The results for various measurement grids are tabulated in Table G.3.3.2.1-1 and plotted in Figure G.3.3.2.1-1. Sample CDF curves of the $EIS_{50\%CDF}$ for some sample grids are shown in Figure G.3.3.2.1-2.

Table G.3.3.2.1-1: Statistical results of the $EIS_{50\%CDF}$ for the 8x2 antenna array for constant step size measurement grids and the beam peak always aligned on a grid point.

		DL Power Step Size: infinitesimal			DL Power Step Size: 0.1dB			DL Power Step Size: 0.5dB			DL Power Step Size: 1dB		
Step Size [o]	Number of unique grid points	STD [dB]	|Mean Error| [dB]	Span [dB]	STD [dB]	|Mean Error| [dB]	Span [dB]	STD [dB]	|Mean Error| [dB]	Span [dB]	STD [dB]	|Mean Error| [dB]	Span [dB]
6.0	1742	0.03	0.01	0.24	0.03	0.10	0.25	0.03	0.51	0.23	0.02	1.02	0.22
9.0	762	0.05	0.02	0.50	0.05	0.12	0.48	0.05	0.52	0.44	0.04	1.03	0.42
10.0	614	0.06	0.01	0.61	0.06	0.10	0.54	0.07	0.51	0.56	0.05	1.02	0.53
12.0	422	0.08	0.02	0.58	0.08	0.11	0.55	0.07	0.51	0.53	0.07	1.02	0.49
15.0	266	0.13	0.02	1.15	0.12	0.10	1.15	0.12	0.51	1.01	0.10	1.04	0.97
20.0	146	0.18	0.11	1.13	0.18	0.18	1.14	0.17	0.58	1.21	0.17	1.10	1.27
22.5	114	0.29	0.09	2.07	0.29	0.17	2.07	0.28	0.55	1.90	0.28	1.07	1.89
30.0	62	0.50	0.03	2.93	0.50	0.04	2.90	0.49	0.39	2.92	0.49	0.86	3.10
45.0	26	0.91	0.34	4.76	0.92	0.43	4.83	0.92	0.72	4.92	0.89	1.17	5.33

It can be observed that:

- With the beam peak always aligned on the measurement grid, the standard deviation of the $EIS_{50\%CDF}$ is negligible (<0.1dB) for more than ~350 unique measurement points for constant step size grids.
- The DL power step size has no impact on the standard deviation for constant-step size measurement grids.
- With the beam peak always aligned on the measurement grid, the mean error of the $EIS_{50\%CDF}$ roughly matches the DL power step size with more than ~200 unique measurement points for constant step size grids.

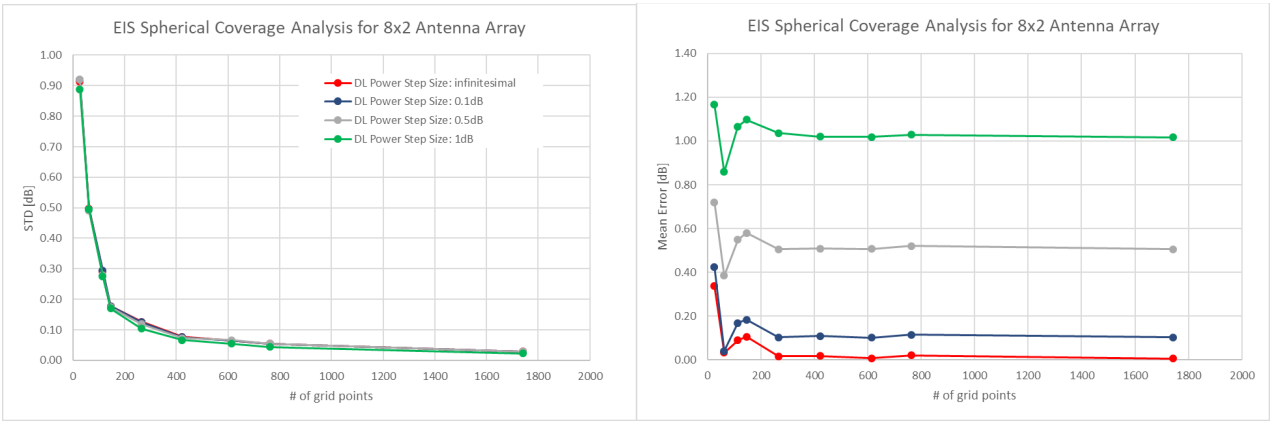

Figure G.3.3.2.1-1: Statistical results of the $EIS_{50\%CDF}$ for the 8x2 antenna array for constant step size measurement grids and the beam peak always aligned on a grid point, on the left: standard deviation, on the right: mean error

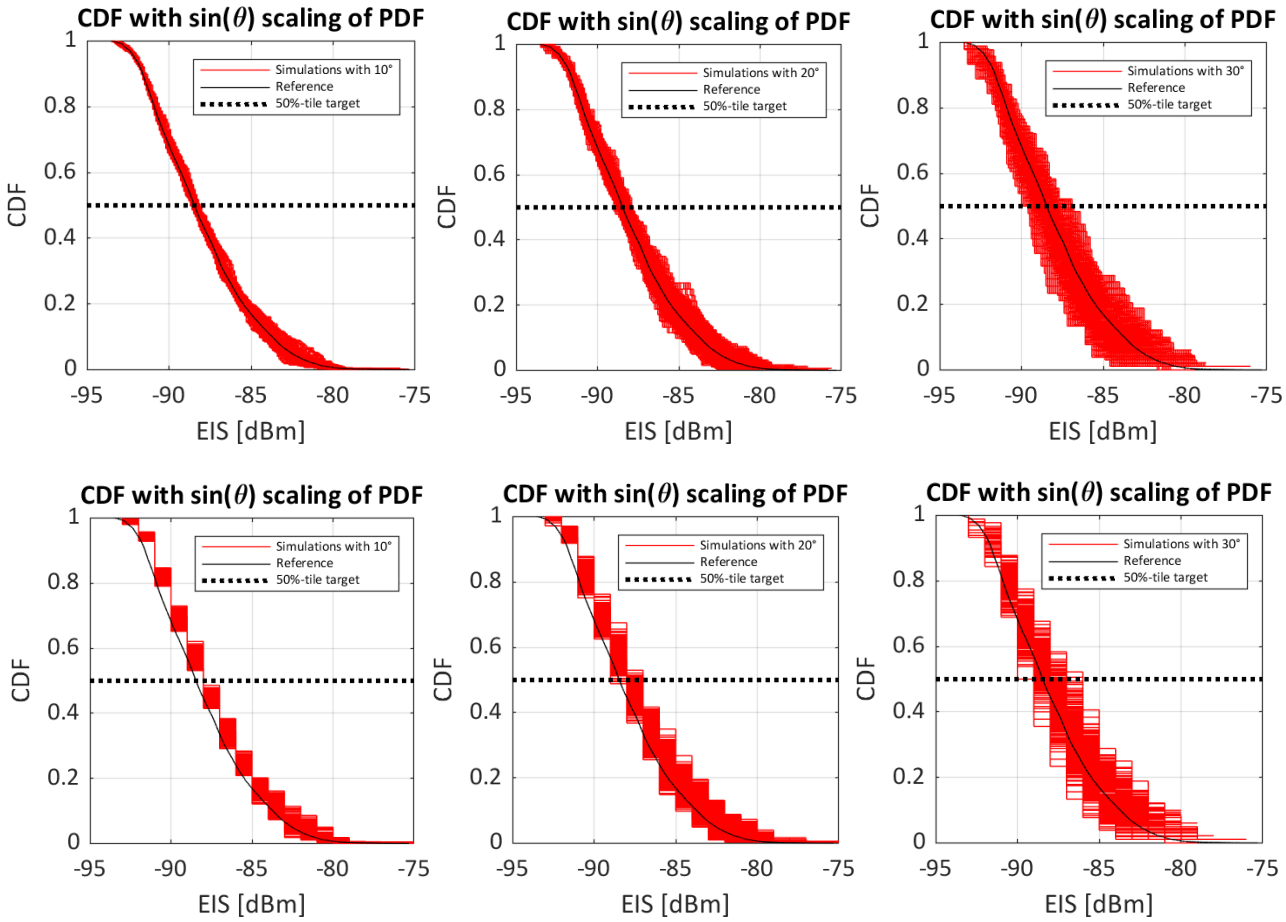

Figure G.3.3.2.1-2: CDF results for the 8x2 antenna array for constant step size measurement grids and the beam peak always aligned on a grid point. On top: DL power step size of 0.1dB, on bottom: DL power step size: 1dB.

Similar results for the constant-density measurement grids are tabulated in Table G.3.3.2.1-2 and sample CDF curves for some grids are shown in Figure G.3.3.2.1-3.

Table G.3.3.2.1-2: Statistical results of the $EIS_{50\%CDF}$ for the 8x2 antenna array for constant density measurement grids and the beam peak always aligned on a grid point.

	DL Power Step Size: infinitesimal			DL Power Step Size: 0.1dB			DL Power Step Size: 0.5dB			DL Power Step Size: 1dB		
Number of unique grid points	STD [dB]	|Mean Error| [dB]	Span [dB]	STD [dB]	|Mean Error| [dB]	Span [dB]	STD [dB]	|Mean Error| [dB]	Span [dB]	STD [dB]	|Mean Error| [dB]	Span [dB]
30	0.50	0.01	3.63	0.50	0.09	3.60	0.51	0.39	3.20	0.47	0.91	3.28
40	0.45	0.05	3.19	0.45	0.02	3.20	0.44	0.34	2.79	0.43	0.88	2.83
50	0.37	0.06	2.83	0.37	0.01	2.80	0.38	0.34	2.83	0.38	0.87	2.85
70	0.23	0.08	1.90	0.23	0.15	1.80	0.23	0.51	1.80	0.23	1.04	1.74
100	0.19	0.04	1.35	0.19	0.13	1.35	0.20	0.50	1.44	0.18	1.05	1.22
150	0.15	0.03	1.23	0.15	0.06	1.23	0.15	0.44	1.19	0.14	0.97	1.18
200	0.10	0.00	0.93	0.09	0.08	0.88	0.10	0.48	0.79	0.09	1.01	0.73
300	0.08	0.02	0.65	0.07	0.07	0.58	0.08	0.47	0.60	0.07	1.01	0.53
400	0.07	0.01	0.52	0.06	0.08	0.54	0.07	0.48	0.45	0.05	1.00	0.43
500	0.06	0.01	0.42	0.05	0.08	0.43	0.06	0.48	0.45	0.05	1.00	0.43

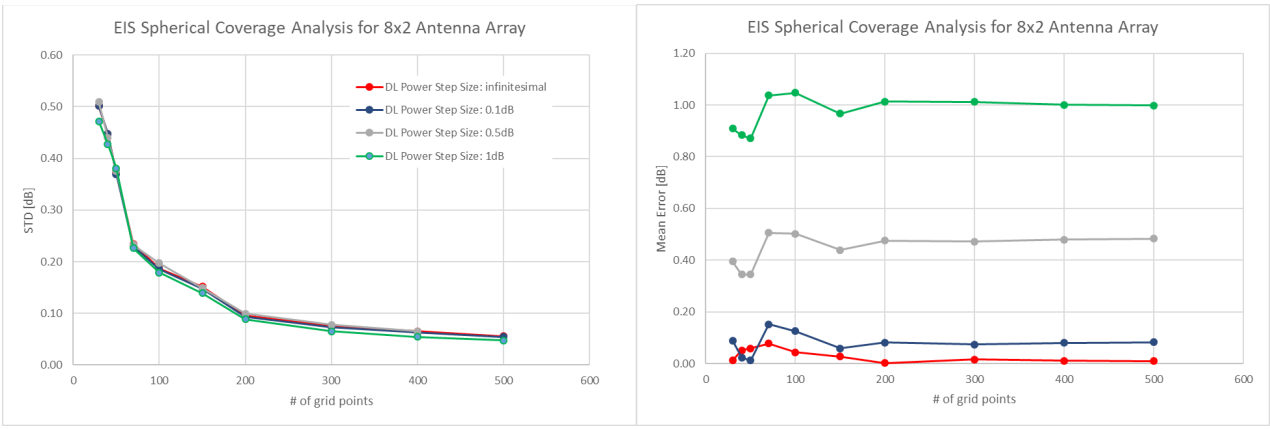

Figure G.3.3.2.1-3: Statistical results of the EIS50%CDF for the 8x2 antenna array for constant density measurement grids and the beam peak always aligned on a grid point, on the left: standard deviation, on the right: mean error

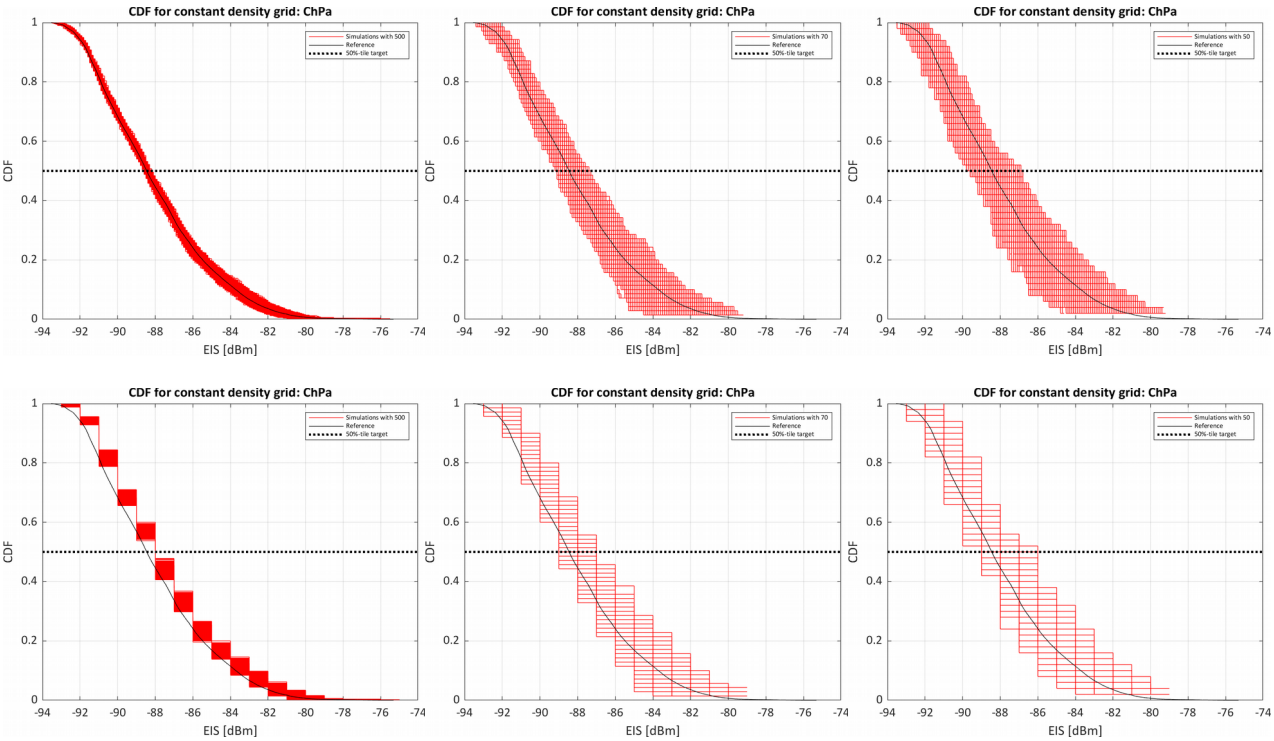

Figure G.3.3.2.1-4: CDF results for the 8x2 antenna array for constant density measurement grids and the beam peak always aligned on a grid point. From left to right: 700, 70, and 50 grid points. On top: DL power step size of 0.1dB, on bottom: DL power step size: 1dB.

It can be observed that:

- With the beam peak always aligned on the measurement grid, the standard deviation of the $EIS_{50\%CDF}$ is negligible (<0.1dB) for more than ~200 unique measurement points for constant density grids (using the charged particle implementation).
- The DL power step size has no impact on the standard deviation for constant density measurement grids.
- With the beam peak always aligned on the measurement grid, the mean error of the $EIS_{50\%CDF}$ roughly matches the DL power step size with more than ~200 unique measurement points for constant density grids.

The standard deviations between the constant step size and constant density grids is shown in Figure G.3.3.2.1-5 for the 8x2 antenna with the beam peak always placed on a grid point with a DL power step size of 0.1dB.

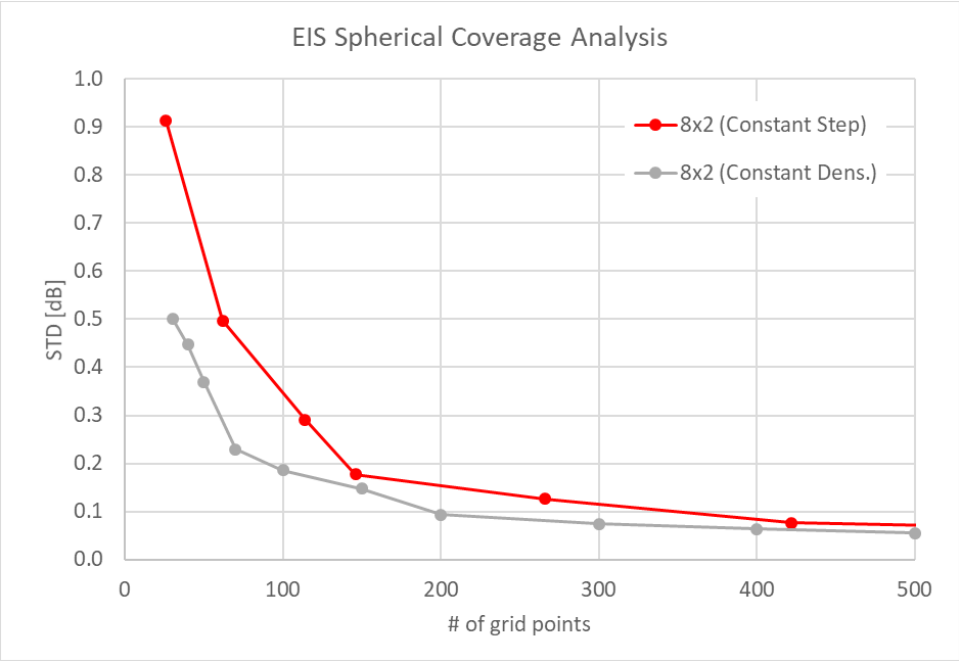

Figure G.3.3.2.1-5: Comparison of the standard deviation of $EIS_{50\%CDF}$ for the 8x2 antenna with the beam peak always placed on a grid point. DL power step size of 0.1dB.

It can be seen that the constant density measurement grids require slightly fewer measurement points than the constant step size grids to achieve the same standard deviation.

G.3.3.2.2 Analyses with 8x2 Antenna Array with Beam Peak oriented completely randomly

The results in this section are based on the 8x2 antenna array with the beam peak oriented in completely random orientations, i.e., the beam peak is not always aligned to a grid point. This analysis was performed to see whether the beam peaks have to be aligned with a grid point if only the min. EIS value at the 50%-tile CDF is of interest. It is understood that the CDF curve cannot be used to accurately determine the RX beam peak (100%-tile CDF).

The results for various constant-step size measurement grids are tabulated in Table G.3.3.2.2-1.

Table G.3.3.2.2-1: Statistical results of $EIS_{50\%CDF}$ for the 8x2 antenna array for constant step size measurement grids and the beam peak oriented in completely random orientations.

		DL Power Step Size: infinitesimal			DL Power Step Size: 0.1dB			DL Power Step Size: 0.5dB			DL Power Step Size: 1dB		
Step Size [°]	Number of unique grid points	STD [dB]	|Mean Error| [dB]	Span [dB]	STD [dB]	|Mean Error| [dB]	Span [dB]	STD [dB]	|Mean Error| [dB]	Span [dB]	STD [dB]	|Mean Error| [dB]	Span [dB]
6.0	1742	0.03	0.00	0.24	0.03	0.10	0.22	0.03	0.50	0.22	0.02	1.02	0.19
9.0	762	0.05	0.00	0.43	0.05	0.10	0.44	0.05	0.50	0.38	0.04	1.02	0.40
10.0	614	0.06	0.00	0.52	0.06	0.10	0.52	0.06	0.50	0.44	0.05	1.02	0.42
12.0	422	0.08	0.01	0.76	0.07	0.10	0.63	0.07	0.50	0.57	0.07	1.02	0.66
15.0	266	0.12	0.02	1.08	0.12	0.10	1.00	0.11	0.50	1.02	0.10	1.02	0.94
20.0	146	0.17	0.03	1.27	0.17	0.11	1.22	0.17	0.50	1.21	0.16	1.02	1.25
22.5	114	0.24	0.05	1.87	0.23	0.12	1.88	0.23	0.51	1.88	0.22	1.03	1.88
30.0	62	0.49	0.13	3.45	0.50	0.22	3.13	0.48	0.57	3.35	0.47	1.06	3.06
45.0	26	0.86	0.28	5.71	0.86	0.36	5.83	0.86	0.70	5.59	0.82	1.12	5.64

Similar results for the constant-density measurement grids are tabulated in Table G.3.3.2.2.-2.

Table G.3.3.2.2-2: Statistical results of $EIS_{50\%CDF}$ for the 8x2 antenna array for constant density measurement grids and the beam peak oriented in completely random orientations.

	DL Power Step Size: infinitesimal			DL Power Step Size: 0.1dB			DL Power Step Size: 0.5dB			DL Power Step Size: 1dB		
Number of unique grid points	STD [dB]	|Mean Error| [dB]	Span [dB]	STD [dB]	|Mean Error| [dB]	Span [dB]	STD [dB]	|Mean Error| [dB]	Span [dB]	STD [dB]	|Mean Error| [dB]	Span [dB]
30	0.56	0.16	3.85	0.56	0.23	4.20	0.55	0.57	3.50	0.53	1.03	3.63
40	0.50	0.15	3.87	0.50	0.23	3.40	0.49	0.58	3.77	0.47	1.04	3.67
50	0.41	0.11	3.25	0.41	0.18	3.10	0.39	0.54	2.87	0.38	1.03	2.83
70	0.25	0.06	2.31	0.24	0.14	2.20	0.24	0.51	2.02	0.23	1.02	2.00
100	0.20	0.03	1.50	0.20	0.11	1.58	0.19	0.50	1.41	0.18	1.00	1.35
150	0.17	0.02	1.36	0.17	0.10	1.43	0.17	0.50	1.33	0.15	1.00	1.37
200	0.10	0.02	0.80	0.10	0.10	0.86	0.10	0.50	0.79	0.09	1.01	0.74
300	0.08	0.01	0.65	0.08	0.10	0.66	0.08	0.50	0.56	0.07	1.01	0.67
400	0.06	0.01	0.54	0.06	0.10	0.49	0.06	0.50	0.44	0.05	1.01	0.48
500	0.06	0.01	0.53	0.06	0.10	0.47	0.06	0.50	0.43	0.05	1.01	0.42

The standard deviations and mean errors for the constant step size and constant density grids are shown in Figure G.3.3.2.2-1 and in Figure G.3.3.2.2-2, respectively, for the 8x2 antenna with the beam peak always placed on a grid point and with the beam peak placed in completely random orientations. Figure G.3.3.2.2-3 is looking at the max range of the 50%-tile CDF EISs which is the difference between the max and the min 50%-tile CDF EISs.

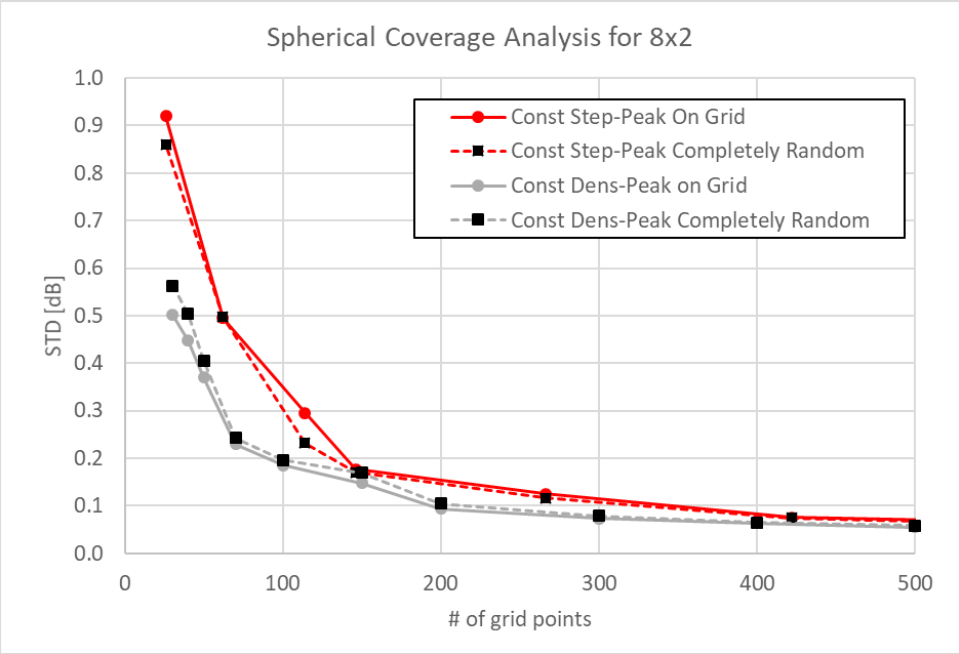

Figure G.3.3.2.2-1: Comparison of the standard deviation for the 8x2 antenna. DL power step size of 0.1dB.

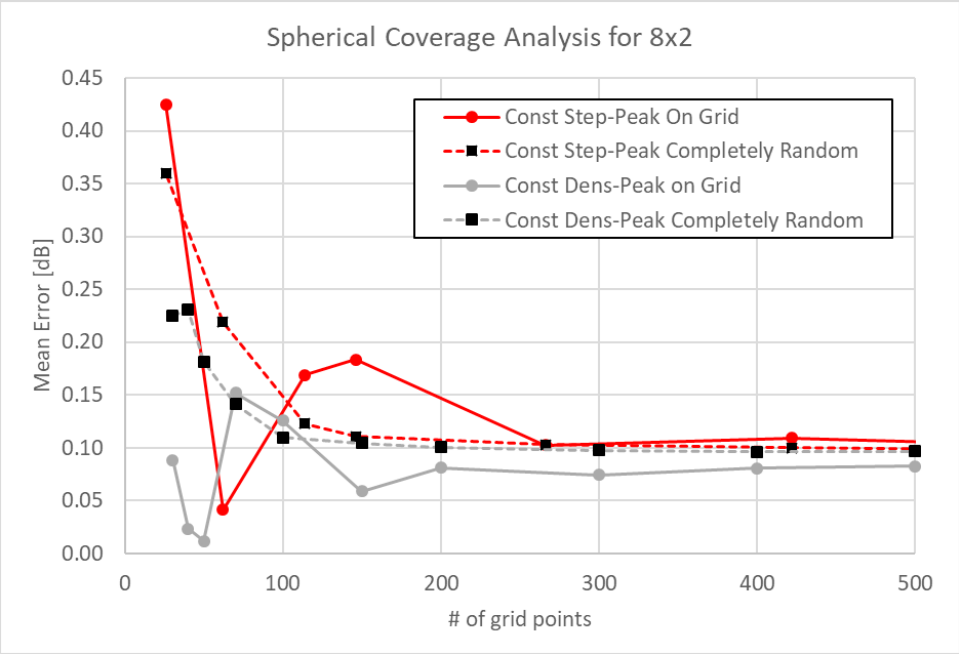

Figure G.3.3.2.2-2: Comparison of the mean error for the 8x2 antenna. DL power step size of 0.1dB.

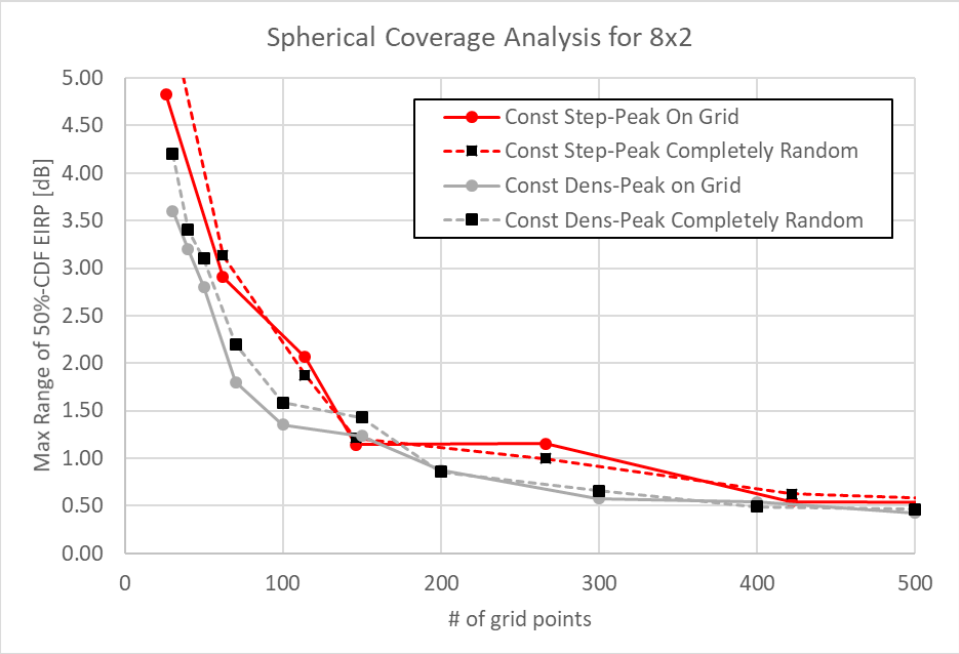

Figure G.3.3.2.2-3: Comparison of the max range of $EIS_{50\%CDF}$ for the 8x2 antenna. DL power step size of 0.1dB.

For the 8x2 reference antenna array, the standard deviation of the EIS at the 50%-tile CDF is independent on whether the beam peak is on the measurement grid or not.

G.3.3.2.3 Conclusions

According to results in section G.3.3.2.1 and G.3.3.2.2, the following conclusions can be made:

- The EIS spherical coverage measurement to be performed without having to have the beam peak placed on a grid point, e.g., for coarse grids of beam peak searches.
- In order to make a reasonable trade-off with measurement uncertainties, it is recommended to use for spherical coverage grids with at least 200 unique measurement points, i.e.,
  - constant density grid with at least 200 grid points: STD of 0.1dB and Mean Error: DL power step size
  - constant step size grid with at least 266 grid points: STD of 0.12dB and Mean Error: DL power step size

G.3.4 Clarification of Min. EIRP at fixed CDF value

For FR2, requirements have been defined for minimum EIRP at a fixed CDF percentile and similar spherical requirements are expected for maximum EIS.

Especially for coarse spherical coverage measurement grids, the number of non-zero PDF values could be very limited which causes the CDF curve to appear staggered. One sample, simulated CDF curve is shown in Figure G.3.4-1 for a coarse measurement grid (in this case, a constant step size measurement grid with angular spacing in θ and ϕ of 30°).

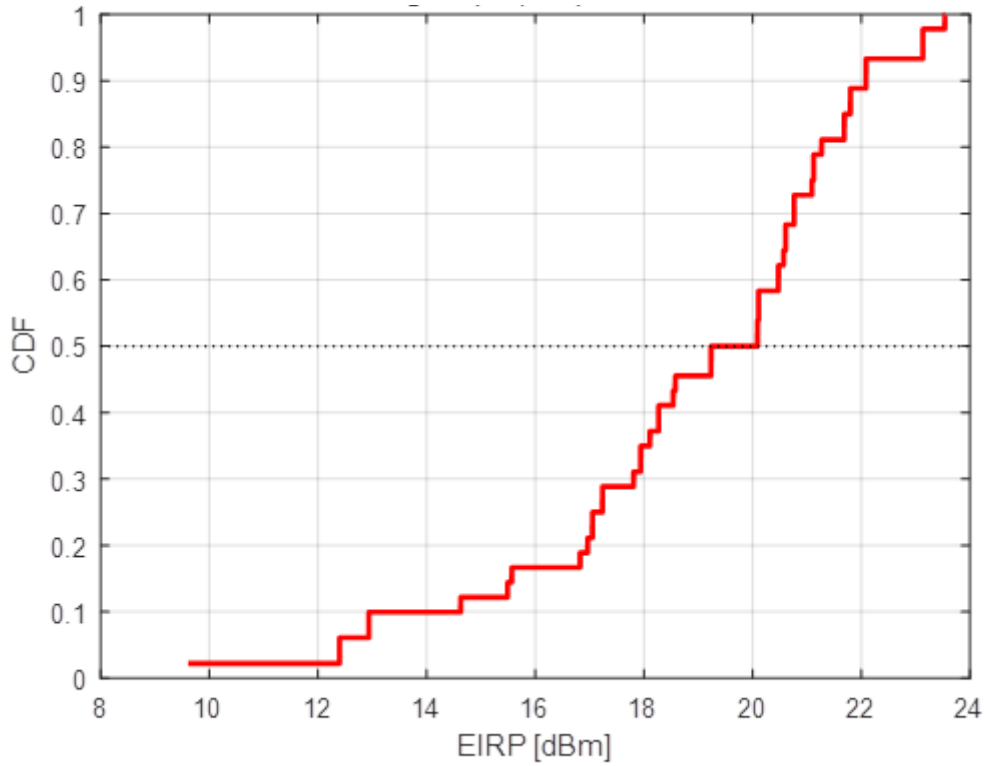

Figure G.3.4-1: Sample CDF Curve for a coarse measurement grid

While for very fine measurement grids, the definition of the min EIRP at the target CDF, $EIRP_{target\text{-}CDF,}$ is pretty clear since the CDF curve is smooth, the definition of the EIRP value at the respective CDF target should be clarified for coarse grids with staggered CDF curves. Two scenarios are outlined in Figure G.3.4-2; Figure G.3.4-2a shows the case where the CDF is not met with any EIRP value while in Figure G.3.4-2b, the target CDF is met with one (or more, as illustrated) EIRP values.

For the case shown in Figure G.3.4-2a, min. EIRP at the target CDF shall be determined based on an interpolation of the CDF curve between the top of raising edges located right above the CDF target (blue circle) and right below the target (green circle).

For the case where the target CDF is met with one or more EIRP value, as illustrated in Figure G.3.4-2b, min. EIRP at the target CDF shall be determined as the min. EIRP value that meets the CDF target.

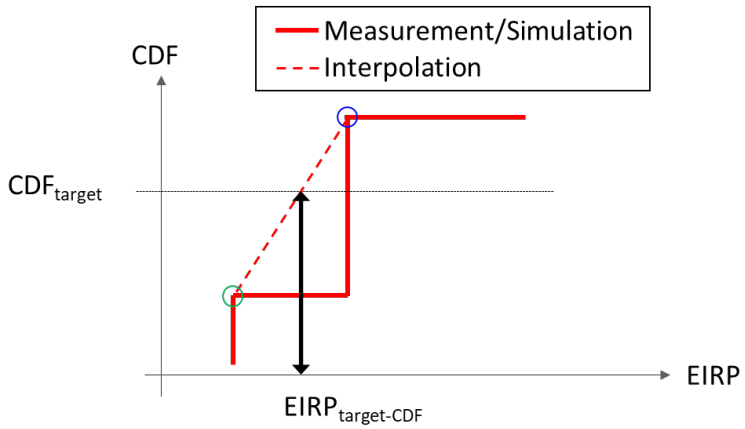

(a)

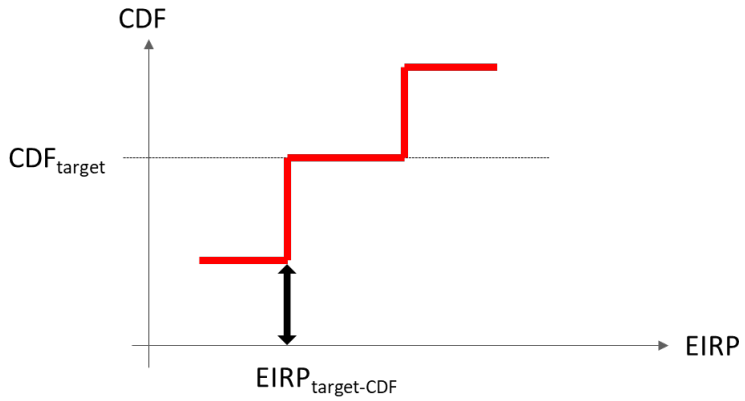

(b)

Figure G.3.4-2: Illustration of CDF scenarios, a) CDF target is not met with any EIRP value, b) CDF target is met with one or more EIRP values.

It can be concluded that, for the case when the target CDF is not met with any EIRP values, the min. EIRP at the target CDF is determined based on an interpolation of the CDF curve between the raising edges located right above the CDF target and right below the target. For the case where the target CDF is met with one more or EIRP value, define the min. EIRP at the target CDF as the min. EIRP value that meets the CDF target.

G.4 Combined Beam Peak and Spherical Coverage Analyses

Since the beam peak does not have to be aligned on the spherical coverage grid for spherical coverage analyses (as described in section G.3), the EIRP/EIS results from the EIRP/EIS beam peak search using single fine grids (as described in section G.2) could be re-used for EIRP/EIS spherical coverage which could further reduce the EIRP/EIS spherical coverage MU.

Coarse EIRP/EIS beam peak searches (as described in section G.2.3) can be used for EIRP/EIS spherical coverage analyses as long as they meet the minimum number of measurement points (200 grid points for constant density using the charged particle implementation and 266 for constant step size). As the fine grid points in the coarse & fine grid approach are localized near maximum beam peaks, only the results from the coarse search grid can be used for the CDF analyses.

Subsequent fine search approaches using constant step size grids used to determine the EIRP/EIS beam peaks require a minimum step size of 7.5º.

Subsequent fine search approaches using constant density grids used to determine the EIRP/EIS beam peaks require at least 6 points around the peak identified with the coarse grid, with a spacing corresponding to a constant density (using the charged particle implementation) over the whole sphere of at least 800 points.

Therefore, EIRP/EIS spherical coverage requirement can be verified using the results from the corresponding EIRP/EIS coarse beam peak search.

Annex H:
Change history

Change history							
Date	**meeting**	**TDoc**	**CR**	**Rev**	**Cat**	**Subject/Comment**	**New version**
2017-04	R4#82bis	R4-1702939				Skeleton of TR38.xyz on test methods for NR	0.0.1
2017-04	R4#82bis	R4-1704361				Introducing NR SI outcome on testability	0.0.2
2017-08	R4#84	R4-1708997				Corrected title, enabling measurements of NSA UEs, OTA requirement to test mapping, and RRM baseline setup	0.0.3
2017-09	NR AH#3	R4-1709525				Corrected RRM baseline setup, introduced MU budget for RF baseline setup	0.0.4
2017-10	R4#84bis	R4-1710455				Added DUT positioning guidelines	0.0.5
2017-11	R4#85	R4-1713810				Introduced description of the test interface, quality of quiet zone characterization procedures, and descriptions of measurement uncertainty elements; corrected the RRM baseline setup	0.0.6
2017-11	R4#85	R4-1713812				Preliminary measurement uncertainty values	0.1.0
2017-12	RP#78	RP-172403				Submitted for information to RAN	1.0.0
2018-01	R4 AH #1801	R4-1800341				R4-1800779 preliminary MU assessment for EIS R4-1801261 applicability criteria for the RF baseline and the MU assessment	1.0.1
2018-02	R4#86	R4-1892187				R4-1803554 TP to TR on TR structure for test method applicability R4-1802909 TP to TR 38.810 - Adding Note to EIRP MU assessment for baseline setup R4-1803414 TP to TR 38.810 - Adding AUT reference antenna masks to Annex D D.2.1 R4-1803537 TP to TR 38.810 - Characterization of Quiet Zone at mm-wave NR frequencies for Combined axis Positioner R4-1803419 TP to TR 38.810 on testing and calibration aspects for baseline system R4-1803535 TP to TR38.810 v1.0.1 on applicability of baseline setup R4-1803532 TP for TR 38.810 v1.0.0 on RRM baseline setup R4-1801808 TP to 38.810 on UE measurements for demodulation test setup in FR2 R4-1803531 TP for TR 38.810 v1.0.1 on Demodulation Baseline setup R4-1803416 Proposals for Equivalence criteria revision Removed instances of “TRS” from the text, applied stylistic corrections to clause headings, renamed the three “Summary of measurement uncertainty and test tolerances” clauses in the RF, RRM, and demodulation setups to “Summary of initial uncertainty assessment”	1.1.0
2018-03	RP#79	RP-180181				R4-1803572 TP to TR 38.810 on Measurement Uncertainty of Mismatch R4-1803571 TP to TR 38.810 - Adding MU format and MU assessment for CATR R4-1803574 TP to 38.810: Rationale behind CATR as NR RF baseline R4-1803575 TP to 38.810 addition of CATR for arbitrary device size Updated visual quality of the embedded equations Aligned clause headings with terminology agreed for permitted methods	2.0.0
2018-04	R4#86bis	R4-1804135				R4-1805062 TP to TR 38.810 Adding Appendix F - NFTF Rationale R4-1805439 Minor corrections to 38.810 Combined axes system sections R4-1805893 TP to TR 38.810 on editorial aspects R4-1805894 TP to TR 38.810 – Full package for Near Field Test Range (NFTF) Corrected clause numbering on section 5.2.3.3	2.1.0

2018-07	R4 AH1807	R4-1808774				R4-1808409 TP to TR38.810 to reflect RAN4#86bis agreements and editorial changes R4-1808412 TP to TR on OTA testing with battery R4-1806381 TP to TR 38.810 on procedure to decide applicable test methods for mmWave UE R4-1806731 TP to 38.810: Clarifications related to DUT Antenna Configurations R4-1808413 TP on RF test procedures for EVM and blocking R4-1808402 TP to TR 38.810 on open items for RRM R4-1808403 TP for TR 38.810 v2.1.0 on Demodulation and CSI Baseline setup R4-1808405 TP to TR 38.810 on Propagation model definition R4-1808518 TP to TR 38.810 on channel model generation methodology R4-1808407 TP on path delay grid for channel models Editorial corrections Updated “Definitions, symbols and abbreviations”	2.2.0
2018-08	R4#88	R4-1809982				R4-1809508 MU factors contributing to RRM parameters and metrics R4-1809509 TP for TR 38.810 on definition and feasibility of parameters and metrics for UE RRM BLS R4-1809510 TP to TR 38.810 on open items for UE Demodulation testing methodology R4-1809511 MU factors contributing to DL SNR accuracy and range R4-1809512 TP to TR 38.810 on demod measurement set-up applicability R4-1809222 TP to TR 38.810 on missing aspects for channel model option 1 R4-1809513 TP to TR 38.810 on Propagation model definition R4-1809515 TP to TR 38.810 on Channel model naming R4-1809586 TP to TR 38.810 on option 2 channel model generation methodology for FR2: parameters and procedure updates	2.3.0
2018-08	R4#88	R4-1811893				R4-1811096 TP to TR38.810 on DUT Repositioning R4-1811777 MU factors contributing to DL SNR for demodulation and CSI R4-1811778 MU factors contributing to DL SNR in RRM Test cases R4-1811779 TP to TR 38.810 on editorial corrections R4-1811780 TP to TR 38.810 on the remaining details of channel modelling methodology R4-1811782 TP to TR 38.810 on the remaining details of NR RRM testing methodology R4-1811833 Introduction of other methods for RRM baseline measurement system R4-1811835 On multiple antenna port capability for RRM baseline measurement system R4-1811836 TP to TR 38.810 on the remaining details of NR FR2 UE Demodulation and CSI testing methodology R4-1811891 TP to 38.810 on measurement grids of EIRP/EIS, TRP, Spherical Coverage R4-1810870 TP to 38.810: Update of blocking measurement procedure Editorial corrections	2.4.0
2018-09	RAN#81	RP-181710				Editorial corrections	2.5.0
2018-09	RAN#81	RP-182064				Editorial corrections - Fixed broken references in Clause 8.2.1.1 - Updated Tables 5.3-1 and 5.3-2 to align the terms	2.6.0
2018-09	RAN#81	RP-182134				Editorial corrections - Changed Release 15 to Release 16 - Changed TR title to “NR; Study on test methods”	2.6.1
2018-09	RAN#81					Approved by plenary – Rel-16 spec under change control	16.0.0
2018-12	RAN#82	RP-182363	0003	1	F	Comibned CR to TR 38.810 after RAN4 #88bis and RAN4 #89	16.1.0
2019-03	RAN#83	RP-190404	0006		F	CR to TR 38.810 (Implementation of the draft CRs endorsed in RAN4 #90)	16.2.0